Protein Kinase C α: a System of Modular Domains

by

Carter James Swanson

A dissertation submitted in partial fulfillment
of the requirements for the degree of
Doctor of Philosophy
(Biophysics)
in The University of Michigan
2016

Doctoral Committee:

Associate Professor Sivaraj Sivaramakrishnan, University of Minnesota, Co-Chair
Professor Ari Gafni, Co-Chair
Assistant Professor Ajit Joglekar
Professor John J. Tesmer
Associate Professor Margaret V. Westfall

The Protein Acrobatics Lab, circa 2014

2016

Acknowledgements

It is my pleasure to acknowledge my family, especially Vaun, Barry, Brock, Amy and Hunter who *always* empowered and encouraged me to pursue my interests.

Next, I am indebted to- and proud of- the scientific mentors and programs that have invested in me. The opportunities, training and support I received from Dr. Urs Oschner and Prof. Ben McFarland were absolutely paramount for my journey to graduate school. I am grateful to the Biophysics Program and the Program in Biomedical Sciences at the University of Michigan for the opportunity to devote the last five years to scientific training in an amazingly resource-rich environment. I am fully indebted to my thesis adviser Prof. Sivaraj Sivaramakrishnan for the support, training and scientific freedom he provided through this process. I am extremely thankful for the hours of exhilarating scientific discussions I have had with Prof. Rizal Hariadi throughout graduate school. Last, I am honored by the continued support and dedication of my distinguished committee who helped me to focus my efforts and complete this dissertation.

Finally, I could not have accomplished this work without the support of all of my friends and colleagues with whom I interacted with on a daily basis. Notably, my lab mates Rabia Malik, Mike Ritt and Dr. Ruth Sommese built a working environment where so much could be accomplished. I continue to be amazed and challenged through interactions with my fellow biophysics colleagues, especially Dr. Sam Kotler, David Rowland and Madaresh Sumit. And every day I am supported, inspired and motivated by my best friend and fiancée Colleen Carpenter.

Table of Contents

List of Figures

List of Appendices

List of Abbreviations

Abstract

Signaling proteins comprised of modular domains have evolved along with multi-cellularity as a method to facilitate increasing intra-cellular bandwidth. The effects of intra-molecular interactions between modular domains, within the context of native proteins, have been largely unexplored. Here we examine intra- and inter-molecular interactions in the multi-domain signaling protein, protein kinase C α (PKCα). We identify three circumstances in which domain-domain interactions regulate PKCα function. First, we find that an intramolecular interaction between regulatory domains and the kinase domain limit catalytic function of PKCα as anticipated from previous studies. Second, we identify an intramolecular interaction between the C1a and C2 domain of PKCα that regulates self-assembly upon calcium binding. Third, we demonstrate that the intramolecular interaction between regulatory domains and the kinase domain facilitates heterologous growth of PKCα self-assembly upon calcium binding through ring opening polymerization.

This dissertation proposes that PKCα is a system comprised of protein domain modules. We provide evidence that a network of domain-domain interactions regulate the function of PKC. Further, we provide evidence that upon binding known effectors the network of domain-domain interactions update and the function of PKCα changes. Together, this work hypothesizes that PKCα function in disparate biological phenomena can largely be attributed to internal domain-domain interactions. This work not only gives insight into PKC activation, but also provides a framework for regulatory mechanisms utilized by other kinase families and multi-domain proteins.

Chapter 1: Introduction

1.1 The role of protein kinase C structure in biological function:

1.1.1 PKC function in biology

In order to robustly communicate extracellular information into cellular and organismal phenotypes biology has evolved sophisticated signaling systems. These signal transduction systems are composed of several biomolecules including proteins, phospholipids, nucleic acids, small-molecules as well as chemical potentials that self-organize within and between cells. From a relatively constrained number of biomolecules, cells are capable of adapting to external stimuli to perform functions ranging from maintaining chemical homeostasis to movement of cells towards nutrients to hormonal communication between cells in a multi-cellular organism (1). A grand challenge in biology is understanding the physical mechanisms by which biomolecules dynamically self-organize within cells to transmit information (2-4).

Understanding how the biology of signal transduction functions has practical and contemporary consequences on human health. Pathophysiologies leading to various diseases including cancers and cardiovascular diseases often arise from dysregulation of biomolecules involved in signal transduction. Additionally, therapeutic pharmaceuticals targeting signal transduction processes have been amongst the most successful and prevalent class developed (5). As such, much of what is known of signal transduction has origins from studying when signal transduction has gone awry in diseases.

This present work focuses on a particular class of signal transduction biomolecule, the protein kinase C (PKC) superfamily, which was originally identified for its pathophysiological role in tumorigenesis and has subsequently emerged as one of the most ubiquitously critical signal transduction biomolecules (6). The PKC superfamily consists of several isoforms in multicellular organisms and has a single protein ancestor evolutionarily conserved in all eukaryotes (7, 8). The

PKC superfamily plays key regulatory roles in many cellular processes ranging from cell proliferation in yeast to memory formation in human brains and has been heavily investigated since initial discovery and characterization efforts in the early 1980s (8). Further, the PKC superfamily has been implicated in numerous chronic human diseases including heart failure, diabetes, Alzheimer's disease and cancer. To provide scale for the biological and biomedical interest of PKC, a search of the term 'protein kinase C' in the National Center for Biotechnology Information scientific literature database PubMed resulted in >59,000 unique manuscripts published since 1980 (approximately the same as 'microtubule', twice as many as 'protein kinase A', and half as many as 'actin' at time of writing). Through this body of literature both general structural/mechanistic properties of PKC as well as specific roles in biological processes have emerged. This current document will primarily focus on general structural and mechanistic properties of PKC.

The PKC superfamily functions by interacting with other biomolecules and transferring chemical information following specific extracellular signals. As the name implies, PKC is a protein which contains a kinase enzyme which catalyzes phosphorylation. Phosphorylation is a chemical reaction that is ubiquitous in biology and involves the transfer of a phosphate group from adenylyl tri-phosphate (ATP) onto a target biomolecule (9). PKC has evolved to phosphorylate proteins primarily on serine amino acid side chains (10). By phosphorylating a protein, PKC is transferring a chemical signal which alters the molecular properties of the receiving protein and in turn altering how it transmits signals (11). PKC function is typically defined by what subset of proteins it phosphorylates following a specific signal (12). In its simplest description, PKC functions analogous to a switch where only in the presence of specific signals will it phosphorylate proteins (13).

To understand how PKC functions within the context of signal transduction systems it is critical to understand what signals activate PKC and what proteins are phosphorylated by PKC. Through biochemical and physiological studies it is well documented that PKC is universally activated (ie switched on) by the lipid secondary messenger diacylglycerol (DAG) (13). DAG is a commonly employed secondary messenger in signal transduction which is typically present in the inner-leaflet of the plasma membrane following the activation of the signal transduction superfamily phospholipase C (PLC). PLC catalyzes the cleavage of the lipid phosphatidylinositol 4,5-

bisphosphate (PI(4,5)P2) into diacylglycerol and inositol 1,4,5-trisphosphate (IP3) upon activation (14). The various signals that can activate different isoforms of PLC include binding to G-proteins, calcium, being phosphorylated, or when the composition of phospholipids in the membrane is altered; these signals encompass several of the recurring modes of information transfer in signal transduction and are each highly regulated in time, space and amplitude (14). The consequence of PLC activation by so many signals is that, in-turn, many different signaling systems converge on the generation of DAG and activation of PKC **(Figure 1.1)**. This is where the 'switch' analogy of PKC becomes inadequate; activation of PKC through DAG provides insight into the instances it contributes in a signaling system, but not what functions it plays.

Even though many signaling networks converge onto the activation of PKC by DAG, the functional outcome of PKC can be very diverse. The differences often manifest through the subset of proteins that are phosphorylated by PKC which can lead to different physiological outcomes (15-17). The key question emerges: how does PKC phosphorylate different subsets of proteins? The consensus thinking in the field is that other signaling inputs, in conjunction with DAG, serve to focus the specificity of PKC phosphorylation (13, 17-21). Several additional cellular signals have been demonstrated to influence the specificity of PKC phosphorylation by directly altering the structure and catalysis of the protein. Some of these additional input signals include calcium (22), phosphatidylserine (PS) (23), $PI(4,5)P_2$ (24, 25), proteolysis (26), phosphorylation (27), de-phosphorylation (28) as well as binding interactions with several proteins (29). An updated analogy for PKC has been proposed as a micro-processor which receives a subset of signals, computes those signals through structural rearrangements, and results in a specific subset of proteins being phosphorylated (13, 21). Unfortunately, the biochemical mechanism by which PKC can 'process' information is largely unknown.

1.1.2 PKC structure background

It is hypothesized that the function of PKC is largely dependent on the structural state. Unfortunately, the full-length structure of PKC and how it changes in different functional states is poorly resolved. Despite structural detail, a large base of literature has established the connection between the structure of PKC and its ability to 'compute' signals for a specific physiological function (13, 17, 21). In the absence of structural characterization of full-length PKC, various sections of the protein termed protein domains, have been structurally

characterized in isolation. Through this approach many of the structure function relationships between signals (like calcium ions) and protein domains have been well defined. A remaining challenge is to build off of the structural knowledge of the individual protein domains to understand how functions of full-length PKC emerge.

1.1.2.1 Gene products

As referenced above, the PKC superfamily typically consists of more than one isoform in organisms. We will consider the human PKC superfamily which contains nine isoforms that fall into three classes: the classical PKCs α, β and γ; the novel PKCs δ, ε, η, θ; and the atypical PKCs ζ, ι/λ (30, 31). Each isoform of PKC has two homologous regions, an AGC kinase domain and a C1 domain which unify the superfamily. Each isoform is encoded by a different gene and expression patterns vary across cell types and cell lifetimes, and in the case of the β isoform, two different splice variants are observed (31). Each isoform is anticipated to play unique physiological roles, although it is also speculated that different isoforms are somewhat redundant for function which has partially limited the applicability of genetic approaches to studying the function of individual isoforms (32, 33). Further, because of the homology in the kinase domain, isoform specific kinase inhibitors have also had limited applicability in determining isoform specific functions (34-36). Despite striking similarity in structure between isoforms it is anticipated that each isoform contains individual regulatory mechanisms critical for biological function. Some differences in regulatory mechanisms have been thoroughly investigated including the identification of single point mutations that alter the affinity of binding calcium ions or DAG between isoforms.

A useful approach for studying the structure/function relationship of PKC is to break the roughly 70 kDa protein into discrete functional units termed protein domains (37). A protein domain is defined as a conserved peptide sequence that folds and partially functions independent of the entire protein sequence (38). Four protein domains are found in classical and novel PKCs, and three domains in atypical PKCs. For the purposes of this work we will focus on classical PKCs as they are the best structurally characterized subfamily. Further, unless otherwise noted, this study will focus on the α isoform for the same reason.

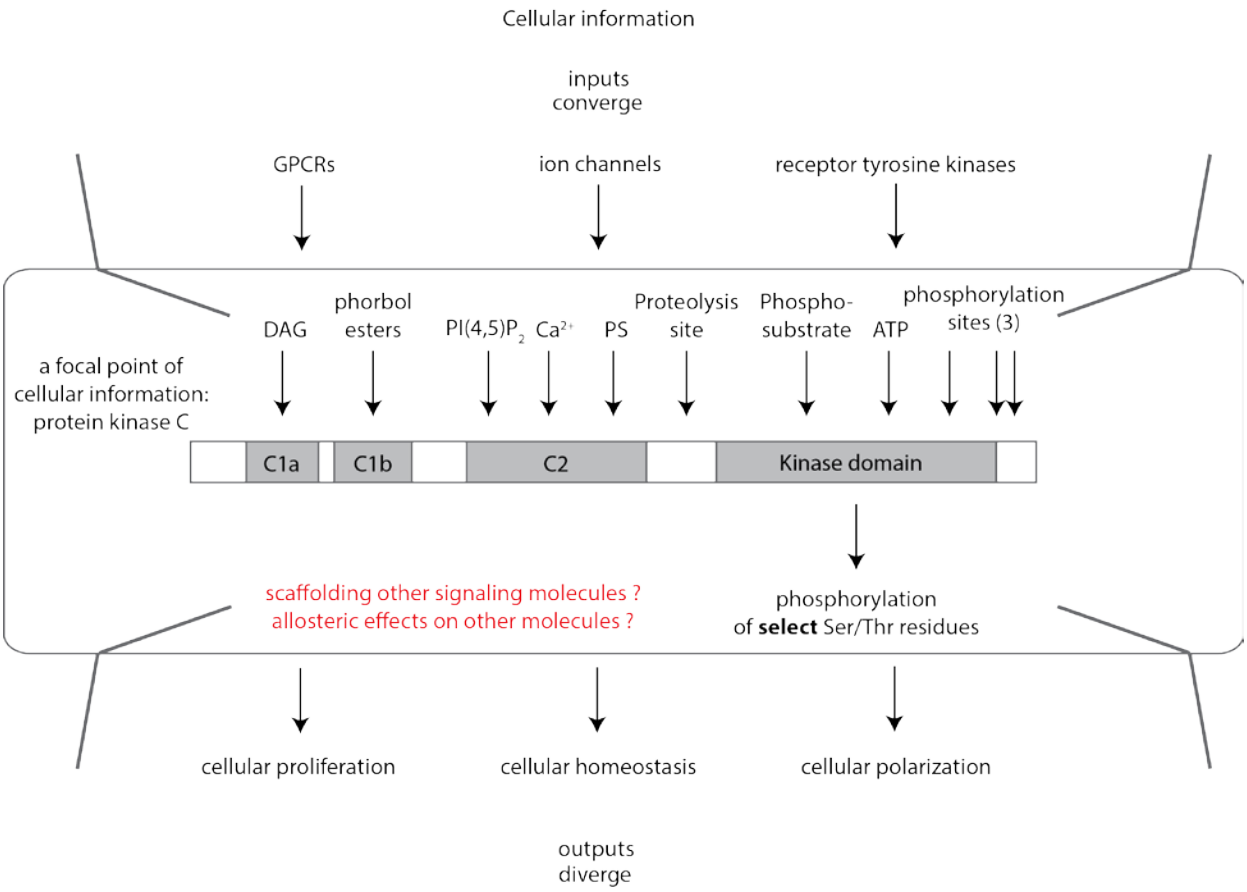

Figure 1.1. Protein kinase C is a focal point of cellular information. Multiple cellular signaling mechanisms converge onto PKC, and many different cellular responses are dependent on PKC. The top and bottom represent general sources of cellular information and various outcomes that are relevant to PKC biology. In the gray box is a more detailed model of PKC information input and output. The rectangle is a schematic of the structure of classical PKCs going from N- to C-terminal where the dark boxes represent modular domains and the white boxes are unstructured variable regions. Each input arrow points at the region in PKC it is known to directly interact with. Phosphorylation is the primary output of PKC, although reports suggest allostery (39) and scaffolding (20) may be additional outputs but remain poorly understood.

In classical PKCs, four conserved protein domains occur separated by peptides with variable sequences. From N- to C- terminus classical PKCs are conventionally broken down into variable region 1 (V1), C1a domain, C1b domain, variable region 2 (V2), C2 domain, variable region 3 (V3), the kinase domain, and variable region 5 (V5 or c-tail). The protein domains and variable regions will be discussed individually below, but it is important to note that many of the structural studies of the various regions have focused on domains in isolation as no complete structure of full-length PKC exists.

1.1.2.2 Kinase domain

The kinase domain is an enzyme that catalyzes phosphorylation. Evolutionarily, kinase domains are one of the most prevalent protein domains and existed in the common biological ancestor for all classes of life (40). The PKC kinase domain is classified into the A kinase, C kinase, G kinase (AGC) evolutionary branch of the kinase domain (41). Most of the 60 proteins containing an AGC kinase domain are multi-domain proteins and participate in diverse and important cellular functions involving the regulated phosphorylation of Ser/Thr residues (41). Structurally, kinase domains have a conserved P-loop fold that is common in most enzymes that catalyze the hydrolysis of the γ-phosphate in ATP (42). The P-loop in kinase domains lies between an N-terminal lobe and a C-terminal lobe and coordinates the positioning of catalytic residues necessary for phosphorylation (43). The structure is conserved in most kinases, but AGC kinases have a few unique features.

Almost each AGC kinase contains a c-terminal amino acid sequence that is atypical for other classes of kinases, but in AGC kinases is critical for catalysis (44). In PKC, this c-terminal amino acid sequence (C-tail for short) is synonymous with the V5 region. The V5 region contains two conserved sites which require phosphorylation for the kinase domain to be catalytically mature. These two sites are termed the hydrophobic motif (HM) and the turn motif (TM). In PKC, both of these sites are considered constitutively phosphorylated, such that the kinase domain is always catalytically mature, except in desensitization in which these sites are targeted by phosphatases as a mechanism for PKC downregulation (45). Of note, protein kinase A (PKA) is one of the best structurally characterized AGC kinase domains. However, PKA is not regulated by phosphorylation at the HM and TM, instead phosphomimetic residues occur at these sites, which is somewhat atypical of the AGC kinase family. Additionally, all AGC kinases must be phosphorylated in a region of the C-terminal lobe termed the activation loop for catalytic maturity (41). Two unique crystal structures of the PKC βII and ι kinase domains with different nucleotides have been reported (46-49) and single structures of the α, θ and η kinase domains (2, 50) with inhibitors have also been reported providing a significant body of structural data. Of note, often the V5 is not fully resolved, or not resolved at all in these crystal structures.

For PKC, and in general most kinases, inhibitors designed for use as research tools or potential therapeutics have targeted the ATP binding site. Several inhibitors have been developed for PKC

and are a commonly used tool to investigate the role of PKC in a given cellular or physiological phenomenon. Unfortunately, currently available PKC inhibitors have limited selectivity between isoforms due to the structural homology of the kinase domain (34). Beyond the limitations of specificity, a study by Cameron et al demonstrated that the use of PKC inhibitors can alter the phosphorylation state of the kinase domain (51). The authors hypothesize that this phenomenon is due to allosteric effects that occur upon inhibitor binding to the kinase domain. How allosteric effects in AGC kinase domains, including PKC, influence biological functions remains a key question. This may have practical consequences as several PKC inhibitors have been developed for therapeutics only to fail in clinical trials for inefficacy (36).

The PKC kinase domain demonstrates a degree of sequence selectivity in substrate phosphorylation. Nishikawa et al examined the optimal phosphorylation motif for each of the PKC kinase domains and identified sequence dependence that correlates with the structure of the kinase domain (10). In general, the motif RXX(S/T)XRX, where X represent any amino acid, is a consensus motif conserved in all PKC isoforms. This sequence dependence of phospho-substrate represents one level of regulation of PKC function. However, discrepancies arise in cellular studies as not all peptides conforming to these motifs are thought to be phosphorylated by PKC, and PKC is anticipated to phosphorylate at residues that do not conform to the consensus (17). Additional factors attributable to the other protein domains are anticipated to further refine the specificity of substrate phosphorylation in PKC.

1.1.2.3 C1 domain

The C1 domain is common in all isoforms of the PKC superfamily. In the classical and novel subfamilies, two tandem C1 domains exist termed C1a and C1b for the C-terminal and N-terminal domains respectively. Each C1 domain is approximately 50 amino acids in length and contains multiple Cystine-Cystine disulfide bonds in its tertiary folded state (52). In both classical and novel subfamilies, C1 domains directly bind to the lipid secondary messenger DAG. In addition, the C1 domains bind to phorbol esters, which are a compound derived from croton oil and have a long history in the study of carcinogenesis (53). While the tandem domains are homologous, they are not identical and appear to participate in different functions. In classical PKCs the C1a domain demonstrates higher affinity for DAG while the C1b domain has higher affinity for phorbol esters (54). Peptides containing the tandem C1 domains can be

expressed in the cytosol of cells, and when the cell is treated with phorbol ester, the peptide will diffusively localize at the plasma membrane where the phorbol ester is known to localize (55). High resolution NMR structures of representative C1b domains from α, θ and γ isoforms have been reported in the protein data base (RSCB ascension numbers 2ENZ, 2E73 and 2EL1) as well as a crystal structure of C1b from the βII and δ isoforms (46, 56). The C1-DAG binding interaction is anticipated to play a critical role in the co-localization of the kinase domain and phospho-substrates as a mechanism for functional regulation.

1.1.2.4 C2 domain

The C2 domain was originally identified in the PKC superfamily, but has subsequently been identified in many signaling molecules and is common to all eukaryotes (57). The functions identified in classical PKC include the sequential binding of two or three Ca^{2+} ions, which bridges an electrostatic interaction with the head group of phosphatidylserine (PS) and subsequently the bindings of the head group of $PI(4,5)P_2$ (58). An important distinction between the classical and novel PKCs is that only the classical C2 domains appear to bind calcium and phospholipids, whereas the novel are reported to bind to phosphotyrosine motifs (59). Within the classical PKCs, the affinity of the C2 domains to calcium are differentially tuned and range from 700 to 5000 nM presumably as a way to selectively bind only a subset of PKC isoforms at low calcium concentrations (60). Similar to the full-length PKC, the C2 domain is expressed and primarily resides in the soluble phase of the cytosol. Upon a cytosolic influx of Ca^{2+} ions both the C2 domain and full-length PKC rapidly (1-10 seconds) accumulate at the plasma membrane in a diffusion limited process conventionally referred to as translocation (61, 62). The C2 domain is typically considered critical in co-localization of PKC with target phospho-substrates following a cytosolic Ca^{2+} signaling event. Crystal structures of several classical PKC C2 domains in complex with Ca^{2+} (63), mimetics of $PI(4,5)P_2$ (58) and the kinase and C1b domain (46) have been reported.

1.1.2.5 Variable regions

Relatively little is known about the variable region structure and functions. The variable regions are generally anticipated to be unstructured and primarily play roles in tethering of the globular domains. A few notable features of the variable regions is the pseudosubstrate in the V1 (64), a

proteolytic cleavage site in V3 (65) and importance of the V5 for kinase domain function (66). The pseudosubsrate corresponds to residues 19 – 36 and is termed such based on its similarity to consensus phosphorylation motifs for PKC kinase domains (64). The cleavage site in the V3 domain was critical for the initial discovery of PKC (6). In general, as the name implies, the characteristics of the variable regions are not conserved between isoforms, with V5 being the major exception (as mentioned above). Several isoform specific functions have been reported for variable regions but will not be addressed in this work (13).

1.2 Emergence in PKC

Here we will define emergence as a functionality of a system of multiple components that could not be inferred when considering the parts in isolation. In the previous section the various protein domains of PKC and their specific functions in isolation were introduced. This work is now concerned with identifying physical interactions between those domains, as occur in the natural, full-length protein, which alter the functionality of PKC **(Figure 1.2)**. What follows are four examples where emergent behaviors/phenomenon of PKC have been reported. In several of these examples it has been previously predicted that intramolecular domain-domain interaction facilitate the emergent phenomenon, but in only one case is direct evidence provided to support the hypothesis. The last paragraph of this section provides a broader context from which this PKC specific hypothesis may be important.

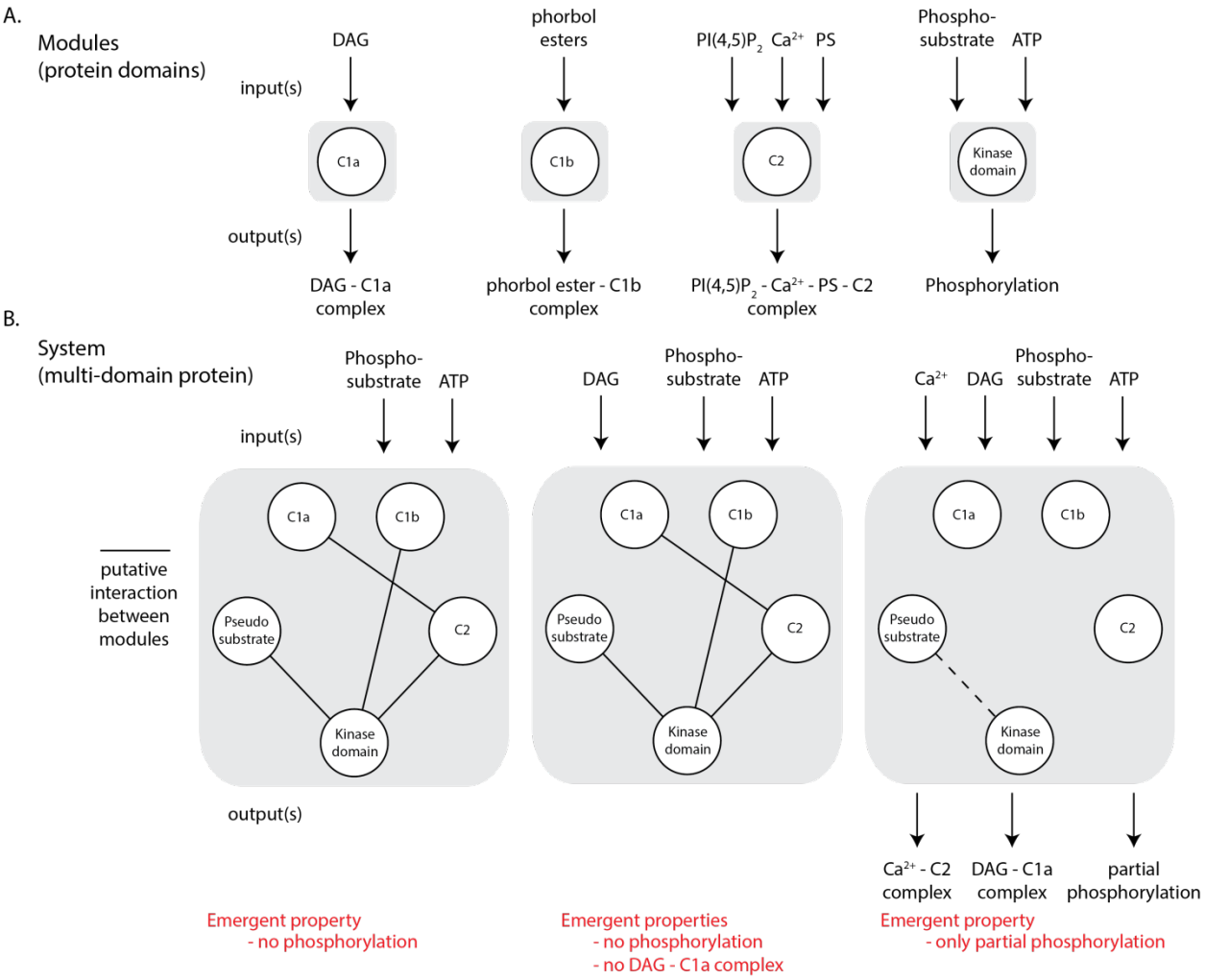

Figure 1.2. Emergent properties arise from domain-domain interactions in PKC. (A.) A schematic highlights the primary chemical information input and output for each of the four protein domains, or modules, found in PKCα. The input/output of the domains were primarily characterized through study of the single domains in isolation. (B.) This schematic considers the chemical information input and output for full length PKCα in which each domain is covalently linked. When the outputs of full length PKC differ from the anticipated outputs of each of the individual domains this is termed an emergent property, or a property that occurs in a system, but is not anticipated from the study of individual modules. Emergent properties are listed in red at the bottom of each scenario. In the gray boxes solid black lines connect the various domains. Each black line represents a putative domain-domain interaction reported in the literature. Domain-domain interactions are predicted to result in the emergent properties of PKCα. In the left example an interaction between the pseudo-substrate and the kinase domain is predicted to inhibit phosphorylation by occluding the phospho-substrate binding site. In the middle example a putative interaction between the C1a and C2 domains is anticipated to occlude the DAG binding site. In the right example concurrent Ca^{2+} and DAG inputs are anticipated to disrupt most domain-domain interactions, however a weakened interaction between the pseudo-substrate and kinase domain may partially occlude the phospho-substrate binding site allowing phosphorylation at a reduced rate.

1.2.1 Emergence in kinase activity

One of the most enduring and well supported hypothesis for emergent structural function of PKC is the auto inhibition of catalytic activity. This hypothesis was initially proposed in 1987 by House and Kemp who identified a region in the V1 of PKCα (residues 19 – 36) which resembled

the consensus phosphorylation sequence of PKC except with an Ala replacing the Ser/Thr residue which would typically be phosphorylated (64). The authors proceeded to synthesize a peptide corresponding to these residues and demonstrate it inhibited kinase activity of PKC in the presence of activators. House and Kemp hypothesized that the pseudosubstrate binds the kinase domain to inhibit catalysis but upon binding of phospholipids to the C1 and C2 domains a conformational change would occur which would disrupt the interaction allowing catalytic activity. This hypothesis has been supported through additional indirect evidence and has remained prevalent in the literature since its first proposal and is incorporated into nearly every molecular model of PKC regulation.

1.2.2 Emergence in DAG sensitivity

A recurring observation noted by several groups is that full length PKC has diminished sensitivity to DAG and DAG analogues compared to the isolated C1 domains to which they directly bind. This fits within our working definition of emergence. As anticipated from our hypothesis, experimental evidence suggests that intramolecular domain-domain interactions are the source of this phenomenon. However, it remains poorly resolved as to what domain interactions are responsible.

Oancea et al were the first to report this observation in a cellular context in 1998 studying the human PKCγ isoform (21). They proposed an eloquent model by which the pseudosubstrate-kinase domain interaction constrains both the C1a and C1b domains such that the DAG binding sites are buried in an interface with the kinase domain and inaccessible. Once PKC is confined at the plasma membrane following a calcium-C2 binding event the pseudosubstrate binds directly to phospholipids and releases the constraint on the C1 domains exposing the DAG binding site. Stensman and Larsson introduced another layer in this mechanism by providing evidence for an interaction between the C2 domain and the kinase domain desensitizing DAG binding to PKC (67). They identified a region of acidic residues on the V5 and basic residues on the C2 domain which unmasked PKC sensitivity to a DAG analogue in cells if charge reversal mutations were introduced in either region, but not both. They further use FRET reporters to provide evidence that these mutations introduce conformational changes in PKC. The authors hypothesize that the conformation of the V5 domain is critical in maintaining the inactive state of PKC mediated through interactions with the C2 and C1 domains.

In 2011 a paper by Leonard et al reported high resolution structural evidence for an intramolecular interaction between the kinase domain and the C1b domain (46). The authors obtained a partial crystal structure of PKC βII in solution in which all but the C1a and some of the variable linkers were resolved. The authors were surprised that an interaction between C1b and the kinase domain was observed as no biochemical or functional data had previously suggested this to be the case. The authors went on to generate point mutations to disrupt the interface between the kinase domain and C1b and investigate the effects on protein localization following phorbol ester treatment of cells expressing the mutant PKC. The authors concluded that the interaction has allosteric effects on the kinase domain that alter the sensitivity of PKC to phorbol esters. In a follow-up report from a separate group, the original interpretation of the X-ray diffraction data was challenged arguing that an interaction between the C2 domain and the kinase domain was additionally observed (68). In this study, point mutations were generated to disrupt the putative binding interface between the C2 domain and kinase domain and demonstrated that these mutants have faster activation kinetics following phorbol ester treatment of cells. An understanding of how these two putative interactions contribute in context with each other remains elusive.

While the work by Oancea, Stensman, Leonard and Antal provided support for masking of the C1 domain through an interaction with the kinase domain or by an interaction between the C2 domain and kinase domain, the work from two separate groups proposed that the C1a and C2 domains directly interact. Studies from the Wonhwa Cho group and from the Christopher Stubbs group provide indirect and direct evidence the C1a DAG binding site is masked through an interaction with the C2 domain (69-71). The best evidence for such an interaction comes from work presented by Slater et al in which surface plasmon resonance (SPR) analysis was used to monitor direct interactions between peptides containing the C1a and C1b domains and peptides containing the C2 , C1a and C1b domains in the presence of phorbol ester (69). From the Cho group, Stahelin et al performed a molecular docking interaction between models of the structure of the C1a and C2 domains to identify putative binding interfaces (70). The authors proceeded to test several of the residues in the putative C1a C2 interaction interface and demonstrated that in cells, mutation in the C2 domain could unmask the C1a domain allowing for the protein to localize at the plasma membrane at lower concentrations of agonist (70). Conversely, from the same group it was demonstrated that a single point mutation in the C2 domain which blocks Ca^{2+}

ion coordination (D246N) renders the C1a unable to bind to DAG (72). From this line of work it is not clear whether the C1a-C2 interaction is exclusive of the C2-kinase domain interaction or C1-kinase domain interaction and what the respective functions of the individual interactions may be. However, Stahelin et al speculate that different isoforms of PKC may have evolved different mechanism by which the domains interact with one another and that each isoform may warrant individual investigation (70). While most of the above work centers on the PKCα isoform, it should be noted that it was the highly homologous βII isoform that was captured in the crystal structure by Leonard et al. It remains unclear which of these domain-domain interactions occurs in which isoform, and how these interactions are functionally dependent or independent of each other.

1.2.3 Emergence in subcellular localization

A key functional hallmark of PKC lies in its sub-cellular spatial-temporal localization. Several studies have suggested that PKC specific scaffolding proteins termed RICKS or RACKS direct the localization of PKC within cells. Additionally, both the C1 and C2 domains can target PKC to specific cellular locations. Within the same cell type PKC can display multiple agonist dependent localizations that are not clearly attributable to scaffolding proteins or direct targeting by PKC domains. We hypothesize that regulation of PKC subcellular localization is an emergent feature primarily dependent on intramolecular domain-domain interactions.

Studies of the subcellular localization of PKC have uncovered several unanticipated behaviors when introducing point mutation or with the use of small molecule kinase inhibitors that are not apparent from structural information of the individual domains (51, 73-75). Different isoforms of PKC localize to various subcellular compartments following stimulation. Further, within the same isoform and cell type, the localization of PKC can change over time or depending on what agonist stimulates the cells. Several reports have demonstrated that point mutations in the kinase domain can alter the localization of PKC (73-75). One particularly insightful study by Maasch et al in 2000 investigated the subcellular localization of a PKC green fluorescent protein (GFP) fusion protein in vascular smooth muscle cells following several different agonists that lead to cytosolic calcium. The agonists including the calcium ionophore ionomycin, depolarization of the cell by KCl, opening internal Ca^{2+} stores with InsP(3) or ryanodine, inhibiting sarcoplasmic reticulum Ca^{2+} re-uptake with thapisgargin, and physiological agonists including thrombin and

PDGF (73). What the authors observed was in each case the fusion protein localized at unique subcellular regions, often times forming speckles, patches or focal domains approximately 0.8 – 1.5 micron in diameter around the anticipated origin of cytosolic calcium. Further, while concomitantly monitoring the focal accumulation of PKC and cytosolic calcium levels, they observed that the focal accumulations formed with the rise in calcium concentration, but persisted even after calcium concentrations returned to basal levels, in some cases for as long as 20 minutes (behavior not observed by the individual domains, only full length PKC). The authors then proceeded to explore the effects on fusion protein localization following a series of truncations and point mutations to PKCα. They found that removal of the kinase domain resulted in the pre-localization of the fusion protein at the plasma membrane but retained the ability to localize at punctae similar to the full-length fusion protein following ionomycin treatment. In contrast, a single point mutation in the kinase domain K368R, commonly used to abolish catalytic activity in kinases, pre-localized at the plasma membrane but did not re-localize into punctae following ionomycin treatment. The authors acknowledge that no regulatory model adequately addresses how a single isoform of PKC in the same cell type differentially localizes following different agonists. They end by speculating that local calcium influxes can initiate binding events between proteins prelocalized at the site of the calcium influx and PKC to explain the observed phenotypes (73). The authors never speculate that interactions between domains contribute to these observations. However, it is striking that a point mutation in the kinase domain influences the functionality of the C2 domain.

In an independent line of research from a different group, Stensman et al explored the effect of the kinase dead K368R mutation as well as kinase inhibitors on PKCα-EGFP subcellular localization in human neuroblastoma cells following charbacol treatment (74). The authors report that wild type PKCα transiently localizes at the plasma membrane and returns to the cytoplasm following charbacol treatment. In contrast, the K368R kinase dead point mutation localizes at the plasma membrane following charbacol treatment and persists there indefinitely. The authors then demonstrate that in cells pretreated with the PKC kinase inhibitor GF109203x, wild type PKCα demonstrates persistent localization at the plasma membrane following charbacol treatment. The authors speculate that these phenomena are both due to an altered conformation of the kinase domain which disrupts domain-domain interactions between the regulatory domains and the kinase domain. They finally state that the large body of literature that has relied on the use of

kinase inhibitors and kinase dead mutations to ascertain the function of PKC specific phosphorylations be reexamined with caution given the additional effects both experimental approaches have on the localization of PKC (74).

A third independent group explored the effect of the kinase inhibitor staurosporine and ATP + Mg^{2+} binding on the subcellular localization of PKCα-EGFP in the HSY human parotid cell line (75). In agreement with the previous finding, Tanimura et al found that pretreatment of the cells with staurosporine stabilized the plasma membrane localization of wild type PKCα. The authors considered the possibility that PKC kinase activity was required for PKC to re-localize back to the cytosol following agonist activation. To test this possibility the authors permeabilized the cells with saponin to leach out nucleotides in a medium containing high free calcium concentrations. Following this treatment of cells, the PKC fusion protein was observed localized at the plasma membrane. The re-localization of PKC fusion protein following the addition of extracellular medium with low free calcium concentration was monitored as a function of time. The authors found that only when ATP + Mg^{2+} was reintroduced at physiological concentrations did PKC re-localize to the cytoplasm. Further, the re-localization to the cytoplasm could be blocked by the addition of the nucleotide competitive kinase inhibitor staurosporine. The authors concluded that kinase activity was critical in the subcellular localization of PKC, although the mechanistic details for why are not known (75). An alternative interpretation could be more akin to that proposed by Stenssman in which nucleotide binding alters the conformation of the kinase domain and subsequently interactions between the kinase domain and the regulatory domains.

This present work hypothesizes that all three of these reports have identified emergent properties of PKCα that arise from domain-domain interactions. When examining all three of these independent studies together it appears likely that conformational changes in the kinase domain can alter domain-domain interactions with the regulatory domains. In fact, it is anticipated that the PKC kinase domain undergoes conformational changes concomitant with nucleotide or inhibitor binding. Providing support for this hypothesis Cameron et al demonstrated a surprising consequence of nucleotide competitive PKC inhibitors on the phosphorylation state of PKC (51). As mentioned earlier, phosphorylation of three key residues on the kinase domain is required for PKC catalytic maturation. The kinase dead mutation, K368R is not phosphorylated at any of the three sites, and this was previously used to support a model by which PKC auto phosphorylates

the three sites. Cameron et al found that a kinase dead PKC molecule could be fully phosphorylated if cells were treated with PKC inhibitors. The study went on to conclude that the K368R mutation blocks ATP binding but not inhibitor binding, and that upon occupation of the binding pocket by an inhibitor a conformational change in the kinase domain facilitated the phosphorylation of the multiple sites by other kinases (51). Together, these reports suggest that feedback exists between conformational states of the kinase domain and interactions with regulatory domains, and those intramolecular domain-domain interactions and the function of the individual domains. We hypothesize a network of physical interactions interconnects the various functions of each of the domains with other domains.

1.2.4 Emergence in scaffolding function

It has been proposed that PKC, specifically the PKCα isoform, may serve as a key scaffold in the origin of membrane localized (but not membrane encompassed) cellular assemblies (20). This hypothesis from Rosse et al is built not on a molecular mechanism (which does not exist), but instead by the repeated observations of PKCα being amongst the first proteins to localize at the site of multiple transient signaling assemblies in multiple different cellular contexts. An interesting parallel phenomenon was observed that calcium dependent PKC could lead to the demixing of certain lipid components within large unilaminar vesicles *in vitro* (76). This work from the Glaser group used fluorescently labeled lipids DAG, and PS as well as fluorescently labeled PKC and phosphorylation substrate myristoylated alanine-rich C-Kinase substrate (MARCKS) peptide to demonstrate that all components colocalized in distinct micron scale domains on the surface of the liposomes specifically in the presence of calcium. The authors then proceeded to use polylysine to displace MARCKS peptide from the DAG, PS, Ca^{2+}, PKC domains but not from binding the liposomes. In concomitant experiments they measured the phosphorylation of MARCKS peptide and found that with increasing concentrations of polylysine, MARCKS phosphorylation was reduced. This result suggests that the proper localization of PKC, its activators and its substrates within domains formed on liposomes is critical for kinase activity. A similar conclusion was arrived at in a separate study in which it was observed that PKC lead to the aggregation of liposomes in a PS, Mg^{2+} and Ca^{2+} dependent manner (77). In experiments monitoring the degree of liposome aggregation as well as autophosphorylation of PKC, a striking linear correlation was observed, where PKC mediated

aggregation of liposomes resulted in increased autophosphorylation levels. In both cases the mechanisms by which these clustered domains on lipid surfaces and/or aggregation of liposomes are formed in these reduced systems are unknown, and it is not entirely clear that corresponding domains are formed in physiological contexts.

Further insight into the phenomenon of lipid demixing caused by PKC and calcium was recently provided by a separate group using fluorescence quenching and nuclear magnetic resonance (NMR) spectroscopy methodologies (78). In this study by the Egea-Jimenez et al it was observed that $PI(4,5)P_2$ demixes *in vitro* on the surface of liposomes in the presence of calcium, but PS only demixes in these conditions if the PKCα C2 domain is additionally present. The PKCα C2 domain directly binds to both $PI(4,5)P_2$ and PS and may serve as a scaffold for the two lipid components. The full-length PKC additionally may directly bind DAG, bringing it into domains that are initiated by $PI(4,5)P_2$ clustering. In line with these *in vitro* observations, it was observed that the C2 domain localizes to punctae on the cellular plasma membrane in a Ca^{2+} and $PI(4,5)P_2$ dependent manner (62). These punctae are formed at caveolae in CHO cells (79). Interestingly, PKC directly binds caveolin-1, a key component of caveolae formation, in a calcium dependent manner (80). Taken together, a mechanism where calcium is sufficient for PKC to become a multivalent scaffold by directly recruiting PS, DAG and caveolin-1 to $PI(4,5)P_2$ clusters on the surface of the plasma membrane can be proposed. The consequence of scaffolding each of these components is not apparent, and the ability for these scaffolding functions to be regulated is not known at all. Like each of the other examples of emergence in PKC discussed above, the degree to which PKC acts as a scaffold, and for what it is scaffolding is likely strongly dependent on interactions between PKC domains which can mask or expose binding interactions.

1.2.5 Domain subunits as modules: multi-domain proteins as systems

Multi-domain proteins correlate with increasing organismal complexity (81). The increased percentage of multi-domain proteins to total proteins encoded in genomes generally tracks with the complexity of organisms (82) notably so in the evolution of multi-cellular organisms (83). It is postulated that multi-domain proteins facilitate the evolution of the complex signal processing behaviors observed in living cells due to physically linking multiple signal inputs and outputs (81). Clearly, understanding the chemical principles by which multi-domain proteins function as compared to single-domain proteins is of broad interest to biologists.

Protein domains, particularly ones that are typically found in multi-domain proteins, are often conveniently termed modules. Modularity is a recurring theme at every level of biology as well as engineered complex systems. A few general features of modules have been noted: modules have (i) identifiable interfaces with other modules (ii) can be evolved somewhat independently (iii) maintain some identity when isolated or rearranged yet (iv) derive additional identity from the rest of the system (84). All of these features are reasonably applied to protein domain modules in a multi-domain protein system. From this perspective a single multi-domain protein may be considered a system composed of multiple protein modules. Knowledge of the protocols by which the modules interface with other modules (for example through auto-inhibition interactions) are necessary to describe this system (84). These protocols may be empirically described by monitoring intra- and inter-molecular domain-domain interactions in a multi-domain protein. Knowledge of protocols can be used to analytically described anticipated functions in a system using coarse-grained modelling approaches (85). We hypothesize that this systems perspective can aid in assessing biological function of multi-domain proteins and may identify previously unanticipated therapeutic opportunities.

We view PKC as a model multi-domain system in which the individual modules are well described, but knowledge (even coarse grained) of interactions between the modules limits predictions of PKC function and consequently therapeutic strategies.

1.3 Hypothesis:

The overarching hypothesis of this work is that emergent biological functions of PKC can be described through interactions between modular domains within the full length protein. The specific ideas tested in this dissertation are:

Hypothesis # 1: Domain-domain interactions between specific modules in the regulatory domains and kinase domain are critical for regulating PKC activation.

Hypothesis # 2: Domain-domain interactions are critical in regulating the spatial organization of PKC and directly interacting molecules in the presence of calcium.

Hypothesis # 3: Nucleotide-induced conformational changes in the kinase domain allosterically modulate the spatial-temporal organization of PKC.

1.4 How to measure intra-molecular domain interactions:

1.4.1 Experimental tools to study biology on the level of protein domains

Adequate experimental methodologies have been a key limitation for studying intramolecular domain-domain interactions. The gold standard approach would entail a high-resolution x-ray crystal structure of the interaction complemented by point-mutagenesis of residues found at the interaction interface that modulate downstream biochemical and cellular functions (86). Unfortunately, in many instances multi-domain complexes must be optimized through labor intensive genetic alterations before they can be crystallized. While many examples exist where this approach has been successfully implemented (and it will likely continue to be streamlined) the process remains too low-throughput to be broadly available for the scope of the questions (consider our model multi-domain protein PKC which has > 10 different functional states and is additionally complicated by localization on a lipid bilayer). Electron microscopy is an exciting area of development which may be better suited for addressing a wide range of functional/conformational states, however currently a protein the size of PKC is at or beyond the lower limits of the methodology. Many biochemical and biophysical approaches are readily available to monitor inter-molecular interactions including conventional genetic assays like yeast 2-hybrids, immunoprecipitation or biochemical assays monitoring the diffusivity of particles, as well as emerging single particle microscopy techniques, spectroscopic approaches and dynamic simulations (87-90). However, in these cases utility is lost when attempting to investigate the contribution of intra-molecular domain-domain interactions as the effects of increased local concentration, and synergistic interactions are difficult to extrapolate from these data. There is a need for the development of new experimental approaches for directly studying intra-molecular domain-domain interactions.

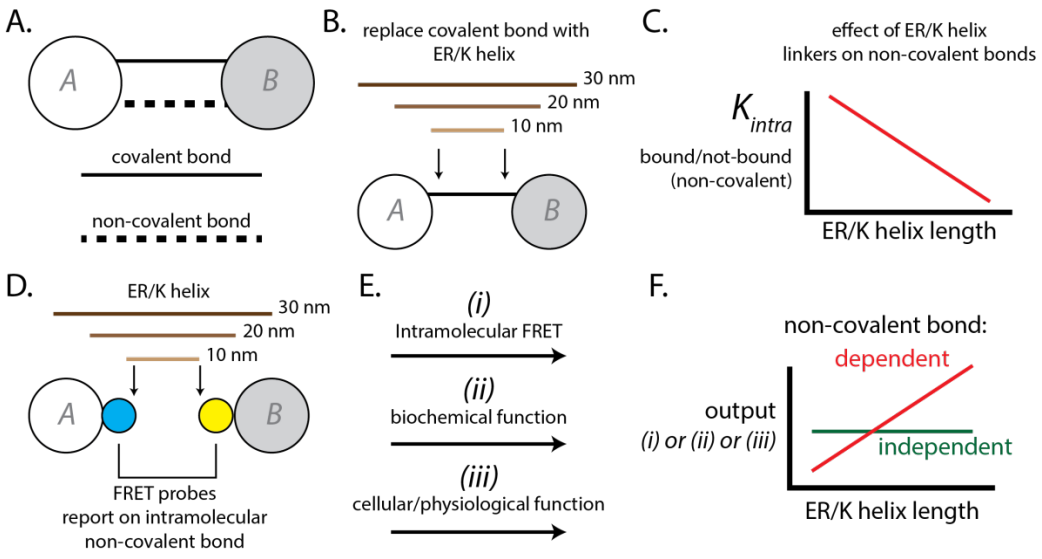

Figure 1.3. SPASM methodology for studying intramolecular domain-domain interactions. (A.) Two protein domains of interest (*A* and *B*) bound covalently and non-covalently. (B.) Genetically engineered proteins can replace the native covalent linker with an ER/K α helix of varying lengths. (C.) The general relationship of the non-covalent intramolecular interaction between domains as a function of the length of ER/K helical linker. (D.) A fluorescent protein FRET pair can be genetically engineered onto either side of the ER/K helical linker. Due to the physical properties of ER/K α helices, FRET will only occur when the protein domains are non-covalently bound. The ER/K linker flanked by fluorescent proteins is termed the SPASM cassette. (E.) The engineered protein can now be studied in parallel with any additional functional assay, ranging from *in vitro* biochemical activity assays, to cellular assays and theoretically phenotypical assays involving model organisms. (F.) By conducting experiments with engineered SPASM proteins of different length ER/K helices, functional dependencies of intramolecular interactions can be assessed. Functions that scale with the length of ER/K helices are anticipated to have direct dependencies on the non-covalent intramolecular interaction being perturbed. Further details and background on the methodology can be found in **Appendix A** and in reference (91).

One of the most successfully utilized approaches to monitor conformational changes in multi-domain proteins is to engineer Förster resonance energy transfer (FRET) biosensors utilizing green fluorescent proteins (GFP). Numerous examples exist where this has been used to explore protein structural changes both *in vitro* and in cellular contexts (92). Two major limitations of this approach are the limited structural resolution obtained, and the challenge of rationally engineering FRET biosensors (93). While the resolution obtained by FRET will never rival structural techniques like x-ray crystallography, it may be sufficient for coarse-graining interactions between domains. To aid in rationally engineering FRET biosensors, particular care must be taken in controlling for linker regions between domains (92). Recently, two strategies have been proposed in which artificial peptide linkers can be inserted between protein domains and fluorescent protein FRET pairs which reliably report on intramolecular interactions in many different engineered peptide contexts (91, 93). One approach utilized unstructured linkers and relies on random walk of unstructured polypeptides to primarily position the FRET probes beyond the Förester radius, while allowing for stochastic sampling of conformations in which

the two domains can directly interact (93). The second approach was similar, but utilized a structured linker which forms an extended single alpha helix (SAH) (sometimes refered to as a Glutamine (E) and Arganine (R) or Lysine (K) (ER/K) linker based on its common sequence) which stochastically collapses at a defined rate allowing for peptides at either end to interact (91). The latter approach was used in part because the number of amino acids in the linker required to extend the fluorescent proteins beyond the Förester radius is reduced.

The structured linker approach was termed systematic protein affinity strength modulation (SPASM) and incorporates a genetic linker whose gene product is a single extended α-helix flanked by mCerleun (mCer – FRET donor) and mCitrene (mCit – FRET acceptor) fluorescent proteins. The SPASM cassette may be sub-cloned into a multi-domain protein of interest such that the FRET output of the gene product will report on intra-molecular interactions between the protein domains on the N- and C- termini of the linker. This approach has previously been implemented in three distinct biological processes in which the FRET output corresponds to an intra-molecular interaction (94, 95). A key advantage of this methodology is the ability to concomitantly monitor the intramolecular interaction as well as other functions dependent on the interactions **(Figure 1.3)**. For example Ritt et al used the SPASM approach to report on the intermolecular interaction between the FERM and kinase domain in focal adhesion kinase (FAK). The authors monitored interactions, autophosphorylation anticipated to require that interaction, as well as downstream physiological responses, in parallel. In this way, a single intramolecular interaction can be modulated and the biochemical and cellular functions can be directly attributed to that single variable. The last key feature of the SPASM methodology is the length of the ER/K linker in the SPASM cassette will dictate the probability that the two peptides are in proximity to interact. By extending the length of the linker, the intramolecular on-rate of the peptide interaction is lowered. In this way, by increasing the length of the ER/K linker, the equilibrium between bound and unbound intramolecular interactions can be shifted towards the unbound. Biochemical assays and cellular assays can be conducted on the engineered protein as a way to investigate functional dependencies of a single intramolecular interaction without the need of detailed knowledge of the binding interface of context specific point mutations. Further details on the mechanism and development of the SPASM approach can be found in **Appendix A**.

1.5 Dissertation objectives

In this work I test the hypothesis that domain-domain interactions in PKCα can contribute to emergent physiological properties. I will use the SPASM methodology in combination with genetic, biochemical and biophysical techniques to identify mechanisms by which domain-domain interactions within PKC can describe emergent functions in *in vitro* reconstituted systems and in cellular systems.

Specifically, I will challenge the models hypothesizing (*i*) a network of domain-domain interactions which inhibit catalytic activity in the absence of calcium, but dissipate in its presence (Chapter 2). (*ii*) That PKC can scaffold or otherwise regulate the spatial organization of molecules in trans through mechanisms regulated by cis domain-domain interactions (Chapter 3 and 4). (*iii*) Conformational states of the kinase domain can regulate the subcellular localization of PKC mediated through cis and trans domain-domain interactions (Chapter 5).

1.6 References:

1. Alberts B (*Essential cell biology* Fourth edition. Ed p 1 volume (various pagings).
2. Whitesides GM & Grzybowski B (2002) Self-assembly at all scales. *Science* 295(5564):2418-2421.
3. Yin P, Choi HM, Calvert CR, & Pierce NA (2008) Programming biomolecular self-assembly pathways. *Nature* 451(7176):318-322.
4. Li P*, et al.* (2012) Phase transitions in the assembly of multivalent signalling proteins. *Nature* 483(7389):336-340.
5. Knox C*, et al.* (2011) DrugBank 3.0: a comprehensive resource for 'omics' research on drugs. *Nucleic Acids Res* 39(Database issue):D1035-1041.
6. Nishizuka Y (2003) Discovery and prospect of protein kinase C research: epilogue. *Journal of biochemistry* 133(2):155-158.
7. Kruse M*, et al.* (1996) Molecular evolution of the metazoan protein kinase C multigene family. *Journal of molecular evolution* 43(4):374-383.
8. Mellor H & Parker PJ (1998) The extended protein kinase C superfamily. *Biochem J* 332 (Pt 2):281-292.
9. Lim W, Mayer B, & Pawson T (*Cell signaling : principles and mechanisms* pp xvi, 400 pages.
10. Nishikawa K, Toker A, Johannes FJ, Songyang Z, & Cantley LC (1997) Determination of the specific substrate sequence motifs of protein kinase C isozymes. *J Biol Chem* 272(2):952-960.
11. Azeloglu EU & Iyengar R (2015) Signaling networks: information flow, computation, and decision making. *Cold Spring Harbor perspectives in biology* 7(4):a005934.
12. Newton AC (1995) Protein kinase C: structure, function, and regulation. *J Biol Chem* 270(48):28495-28498.
13. Steinberg SF (2008) Structural basis of protein kinase C isoform function. *Physiol Rev* 88(4):1341-1378.
14. Kadamur G & Ross EM (2013) Mammalian phospholipase C. *Annual review of physiology* 75:127-154.

15. Hug H & Sarre TF (1993) Protein kinase C isoenzymes: divergence in signal transduction? *Biochem J* 291 (Pt 2):329-343.
16. Gong J*, et al.* (2015) The C2 Domain and Altered ATP-Binding Loop Phosphorylation at Ser(3)(5)(9) Mediate the Redox-Dependent Increase in Protein Kinase C-delta Activity. *Mol Cell Biol* 35(10):1727-1740.
17. Nakashima S (2002) Protein kinase C alpha (PKC alpha): regulation and biological function. *Journal of biochemistry* 132(5):669-675.
18. Dekker LV & Parker PJ (1994) Protein kinase C--a question of specificity. *Trends Biochem Sci* 19(2):73-77.
19. Lipp P & Reither G (2011) Protein kinase C: the "masters" of calcium and lipid. *Cold Spring Harbor perspectives in biology* 3(7).
20. Rosse C*, et al.* (2010) PKC and the control of localized signal dynamics. *Nat Rev Mol Cell Biol* 11(2):103-112.
21. Oancea E & Meyer T (1998) Protein kinase C as a molecular machine for decoding calcium and diacylglycerol signals. *Cell* 95(3):307-318.
22. Castagna M*, et al.* (1982) Direct activation of calcium-activated, phospholipid-dependent protein kinase by tumor-promoting phorbol esters. *J Biol Chem* 257(13):7847-7851.
23. Walker JM & Sando JJ (1988) Activation of protein kinase C by short chain phosphatidylcholines. *J Biol Chem* 263(10):4537-4540.
24. Chauhan VP & Brockerhoff H (1988) Phosphatidylinositol-4,5-bisphosphate may antecede diacylglycerol as activator of protein kinase C. *Biochemical and biophysical research communications* 155(1):18-23.
25. Egea-Jimenez AL, Perez-Lara A, Corbalan-Garcia S, & Gomez-Fernandez JC (2013) Phosphatidylinositol 4,5-bisphosphate decreases the concentration of Ca2+, phosphatidylserine and diacylglycerol required for protein kinase C alpha to reach maximum activity. *PLoS One* 8(7):e69041.
26. Inoue M, Kishimoto A, Takai Y, & Nishizuka Y (1977) Studies on a cyclic nucleotide-independent protein kinase and its proenzyme in mammalian tissues. II. Proenzyme and its activation by calcium-dependent protease from rat brain. *J Biol Chem* 252(21):7610-7616.
27. Flint AJ, Paladini RD, & Koshland DE, Jr. (1990) Autophosphorylation of protein kinase C at three separated regions of its primary sequence. *Science* 249(4967):408-411.
28. Gao T, Brognard J, & Newton AC (2008) The phosphatase PHLPP controls the cellular levels of protein kinase C. *J Biol Chem* 283(10):6300-6311.
29. Mochly-Rosen D & Gordon AS (1998) Anchoring proteins for protein kinase C: a means for isozyme selectivity. *FASEB J* 12(1):35-42.
30. Coussens L*, et al.* (1986) Multiple, distinct forms of bovine and human protein kinase C suggest diversity in cellular signaling pathways. *Science* 233(4766):859-866.
31. Nishizuka Y (1988) The molecular heterogeneity of protein kinase C and its implications for cellular regulation. *Nature* 334(6184):661-665.
32. Way KJ, Chou E, & King GL (2000) Identification of PKC-isoform-specific biological actions using pharmacological approaches. *Trends Pharmacol Sci* 21(5):181-187.
33. Parker PJ & Murray-Rust J (2004) PKC at a glance. *J Cell Sci* 117(Pt 2):131-132.
34. Bain J*, et al.* (2007) The selectivity of protein kinase inhibitors: a further update. *Biochem J* 408(3):297-315.
35. Lee AM*, et al.* (2013) Prkcz null mice show normal learning and memory. *Nature* 493(7432):416-419.
36. Mochly-Rosen D, Das K, & Grimes KV (2012) Protein kinase C, an elusive therapeutic target? *Nature reviews. Drug discovery* 11(12):937-957.

37. Parker PJ*, et al.* (1986) The complete primary structure of protein kinase C--the major phorbol ester receptor. *Science* 233(4766):853-859.
38. Lim WA (2002) The modular logic of signaling proteins: building allosteric switches from simple binding domains. *Curr Opin Struct Biol* 12(1):61-68.
39. Chen JS & Exton JH (2004) Regulation of phospholipase D2 activity by protein kinase C alpha. *J Biol Chem* 279(21):22076-22083.
40. Manning G, Whyte DB, Martinez R, Hunter T, & Sudarsanam S (2002) The protein kinase complement of the human genome. *Science* 298(5600):1912-1934.
41. Pearce LR, Komander D, & Alessi DR (2010) The nuts and bolts of AGC protein kinases. *Nat Rev Mol Cell Biol* 11(1):9-22.
42. Walker JE, Saraste M, Runswick MJ, & Gay NJ (1982) Distantly related sequences in the alpha- and beta-subunits of ATP synthase, myosin, kinases and other ATP-requiring enzymes and a common nucleotide binding fold. *EMBO J* 1(8):945-951.
43. Hanks SK & Hunter T (1995) Protein kinases 6. The eukaryotic protein kinase superfamily: kinase (catalytic) domain structure and classification. *FASEB J* 9(8):576-596.
44. Kannan N, Haste N, Taylor SS, & Neuwald AF (2007) The hallmark of AGC kinase functional divergence is its C-terminal tail, a cis-acting regulatory module. *Proc Natl Acad Sci U S A* 104(4):1272-1277.
45. Newton AC (2003) Regulation of the ABC kinases by phosphorylation: protein kinase C as a paradigm. *Biochem J* 370(Pt 2):361-371.
46. Leonard TA, Rozycki B, Saidi LF, Hummer G, & Hurley JH (2011) Crystal structure and allosteric activation of protein kinase C betaII. *Cell* 144(1):55-66.
47. Grodsky N*, et al.* (2006) Structure of the catalytic domain of human protein kinase C beta II complexed with a bisindolylmaleimide inhibitor. *Biochemistry* 45(47):13970-13981.
48. Messerschmidt A*, et al.* (2005) Crystal structure of the catalytic domain of human atypical protein kinase C-iota reveals interaction mode of phosphorylation site in turn motif. *J Mol Biol* 352(4):918-931.
49. Takimura T*, et al.* (2010) Structures of the PKC-iota kinase domain in its ATP-bound and apo forms reveal defined structures of residues 533-551 in the C-terminal tail and their roles in ATP binding. *Acta Crystallogr D Biol Crystallogr* 66(Pt 5):577-583.
50. George DM*, et al.* (2015) Optimized protein kinase Ctheta (PKCtheta) inhibitors reveal only modest anti-inflammatory efficacy in a rodent model of arthritis. *J Med Chem* 58(1):333-346.
51. Cameron AJ, Escribano C, Saurin AT, Kostelecky B, & Parker PJ (2009) PKC maturation is promoted by nucleotide pocket occupation independently of intrinsic kinase activity. *Nat Struct Mol Biol* 16(6):624-630.
52. Hurley JH, Newton AC, Parker PJ, Blumberg PM, & Nishizuka Y (1997) Taxonomy and function of C1 protein kinase C homology domains. *Protein Sci* 6(2):477-480.
53. Ono Y*, et al.* (1989) Phorbol ester binding to protein kinase C requires a cysteine-rich zinc-finger-like sequence. *Proc Natl Acad Sci U S A* 86(13):4868-4871.
54. Slater SJ*, et al.* (1996) Protein kinase Calpha contains two activator binding sites that bind phorbol esters and diacylglycerols with opposite affinities. *J Biol Chem* 271(9):4627-4631.
55. Raghunath A, Ling M, & Larsson C (2003) The catalytic domain limits the translocation of protein kinase C alpha in response to increases in Ca2+ and diacylglycerol. *Biochem J* 370(Pt 3):901-912.
56. Zhang G, Kazanietz MG, Blumberg PM, & Hurley JH (1995) Crystal structure of the cys2 activator-binding domain of protein kinase C delta in complex with phorbol ester. *Cell* 81(6):917-924.
57. Farah CA & Sossin WS (2012) The role of C2 domains in PKC signaling. *Advances in experimental medicine and biology* 740:663-683.

58. Guerrero-Valero M*, et al.* (2009) Structural and mechanistic insights into the association of PKCalpha-C2 domain to PtdIns(4,5)P2. *Proc Natl Acad Sci U S A* 106(16):6603-6607.
59. Benes CH*, et al.* (2005) The C2 domain of PKCdelta is a phosphotyrosine binding domain. *Cell* 121(2):271-280.
60. Kohout SC, Corbalan-Garcia S, Torrecillas A, Gomez-Fernandez JC, & Falke JJ (2002) C2 domains of protein kinase C isoforms alpha, beta, and gamma: activation parameters and calcium stoichiometries of the membrane-bound state. *Biochemistry* 41(38):11411-11424.
61. Reither G, Schaefer M, & Lipp P (2006) PKCalpha: a versatile key for decoding the cellular calcium toolkit. *J Cell Biol* 174(4):521-533.
62. Evans JH, Murray D, Leslie CC, & Falke JJ (2006) Specific translocation of protein kinase Calpha to the plasma membrane requires both Ca2+ and PIP2 recognition by its C2 domain. *Molecular biology of the cell* 17(1):56-66.
63. Sutton RB & Sprang SR (1998) Structure of the protein kinase Cbeta phospholipid-binding C2 domain complexed with Ca2+. *Structure* 6(11):1395-1405.
64. House C & Kemp BE (1987) Protein kinase C contains a pseudosubstrate prototope in its regulatory domain. *Science* 238(4834):1726-1728.
65. Kishimoto A*, et al.* (1989) Limited proteolysis of protein kinase C subspecies by calcium-dependent neutral protease (calpain). *J Biol Chem* 264(7):4088-4092.
66. Yeong SS*, et al.* (2006) The last 10 amino acid residues beyond the hydrophobic motif are critical for the catalytic competence and function of protein kinase Calpha. *J Biol Chem* 281(41):30768-30781.
67. Stensman H & Larsson C (2007) Identification of acidic amino acid residues in the protein kinase C alpha V5 domain that contribute to its insensitivity to diacylglycerol. *J Biol Chem* 282(39):28627-28638.
68. Antal CE, Callender JA, Kornev AP, Taylor SS, & Newton AC (2015) Intramolecular C2 Domain-Mediated Autoinhibition of Protein Kinase C betaII. *Cell reports* 12(8):1252-1260.
69. Slater SJ*, et al.* (2002) Regulation of PKC alpha activity by C1-C2 domain interactions. *J Biol Chem* 277(18):15277-15285.
70. Stahelin RV*, et al.* (2005) The origin of C1A-C2 interdomain interactions in protein kinase Calpha. *J Biol Chem* 280(43):36452-36463.
71. Bittova L, Stahelin RV, & Cho W (2001) Roles of ionic residues of the C1 domain in protein kinase C-alpha activation and the origin of phosphatidylserine specificity. *J Biol Chem* 276(6):4218-4226.
72. Medkova M & Cho W (1999) Interplay of C1 and C2 domains of protein kinase C-alpha in its membrane binding and activation. *J Biol Chem* 274(28):19852-19861.
73. Maasch C*, et al.* (2000) Protein kinase calpha targeting is regulated by temporal and spatial changes in intracellular free calcium concentration [Ca(2+)](i). *FASEB J* 14(11):1653-1663.
74. Stensman H, Raghunath A, & Larsson C (2004) Autophosphorylation suppresses whereas kinase inhibition augments the translocation of protein kinase Calpha in response to diacylglycerol. *J Biol Chem* 279(39):40576-40583.
75. Tanimura A, Nezu A, Morita T, Hashimoto N, & Tojyo Y (2002) Interplay between calcium, diacylglycerol, and phosphorylation in the spatial and temporal regulation of PKCalpha-GFP. *J Biol Chem* 277(32):29054-29062.
76. Yang L & Glaser M (1996) Formation of membrane domains during the activation of protein kinase C. *Biochemistry* 35(44):13966-13974.
77. Bazzi MD & Nelsestuen GL (1992) Autophosphorylation of protein kinase C may require a high order of protein-phospholipid aggregates. *J Biol Chem* 267(32):22891-22896.

78. Egea-Jimenez AL*, et al.* (2014) Phosphatidylinositol-4,5-bisphosphate enhances anionic lipid demixing by the C2 domain of PKCalpha. *PLoS One* 9(4):e95973.
79. Stubbs CD, Botchway SW, Slater SJ, & Parker AW (2005) The use of time-resolved fluorescence imaging in the study of protein kinase C localisation in cells. *BMC cell biology* 6(1):22.
80. Mineo C, Ying YS, Chapline C, Jaken S, & Anderson RG (1998) Targeting of protein kinase Calpha to caveolae. *J Cell Biol* 141(3):601-610.
81. Bhattacharyya RP, Remenyi A, Yeh BJ, & Lim WA (2006) Domains, motifs, and scaffolds: the role of modular interactions in the evolution and wiring of cell signaling circuits. *Annual review of biochemistry* 75:655-680.
82. Tordai H, Nagy A, Farkas K, Banyai L, & Patthy L (2005) Modules, multidomain proteins and organismic complexity. *The FEBS journal* 272(19):5064-5078.
83. King N*, et al.* (2008) The genome of the choanoflagellate Monosiga brevicollis and the origin of metazoans. *Nature* 451(7180):783-788.
84. Csete ME & Doyle JC (2002) Reverse engineering of biological complexity. *Science* 295(5560):1664-1669.
85. Baaden M & Marrink SJ (2013) Coarse-grain modelling of protein-protein interactions. *Curr Opin Struct Biol* 23(6):878-886.
86. Vogel C, Bashton M, Kerrison ND, Chothia C, & Teichmann SA (2004) Structure, function and evolution of multidomain proteins. *Curr Opin Struct Biol* 14(2):208-216.
87. Phizicky EM & Fields S (1995) Protein-protein interactions: methods for detection and analysis. *Microbiological reviews* 59(1):94-123.
88. Gu L*, et al.* (2014) Multiplex single-molecule interaction profiling of DNA-barcoded proteins. *Nature* 515(7528):554-557.
89. Wollacott AM, Zanghellini A, Murphy P, & Baker D (2007) Prediction of structures of multidomain proteins from structures of the individual domains. *Protein Sci* 16(2):165-175.
90. Chen Y, Wei LN, & Muller JD (2003) Probing protein oligomerization in living cells with fluorescence fluctuation spectroscopy. *Proc Natl Acad Sci U S A* 100(26):15492-15497.
91. Sivaramakrishnan S & Spudich JA (2011) Systematic control of protein interaction using a modular ER/K alpha-helix linker. *Proc Natl Acad Sci U S A* 108(51):20467-20472.
92. Zhang J, Campbell RE, Ting AY, & Tsien RY (2002) Creating new fluorescent probes for cell biology. *Nat Rev Mol Cell Biol* 3(12):906-918.
93. Komatsu N*, et al.* (2011) Development of an optimized backbone of FRET biosensors for kinases and GTPases. *Molecular biology of the cell* 22(23):4647-4656.
94. Ritt M, Guan JL, & Sivaramakrishnan S (2013) Visualizing and manipulating focal adhesion kinase regulation in live cells. *J Biol Chem* 288(13):8875-8886.
95. Malik RU*, et al.* (2013) Detection of G protein-selective G protein-coupled receptor (GPCR) conformations in live cells. *J Biol Chem* 288(24):17167-17178.

Chapter 2: Conserved modular domains team up to latch-open active PKCα

This chapter has been adapted from the following publication:

Swanson, C.J., Ritt, M., Wang, W., Lang, M., Narayan, A., Tesmer, J., Westfall, M., Sivaramakrishnan, S. (2014) Conserved modular domains team up to latch-open active PKCα, *Journal of Biological Chemistry*, **286**, 25460-67.

2.1 Introduction:

The use of modular protein domains has emerged as a prominent feature of increasing phylogenetic complexity (1, 2). Linking modular domains within a single protein allows complex regulation while conserving the sequence and structure of the individual domains, especially for those that have catalytic activity (3). For instance, spatio-temporal control of signaling proteins is often achieved by stringing together a conserved catalytic domain with one or more regulatory modules. These modules can play multiple roles including masking the catalytic site to inhibit basal activity (auto-inhibition), releasing auto-inhibition through conformational changes triggered by second messenger stimuli, and facilitating translocation to subcellular compartments through binding secondary messengers or scaffolding proteins. Each additional module in a signaling protein provides a combinatorial enhancement to its regulation and cellular function (4). The protein-context independent structure and cellular function of individual modules have been extensively researched using biophysical approaches such as x-ray crystallography and NMR (5). However, coordination of interactions between these domains remains unexplored primarily due to the reliance on reductionist structural and biochemical approaches. As a corollary, our current structural understanding of modular signaling proteins does not adequately address the versatility of their cellular function (6-8). In this study, we overcome this limitation with a technique we previously developed to systematically modulate interactions between individual protein domains in the context of the entire molecule (9, 10).

Generally, stark perturbations are required to study intra-molecular interactions in proteins. For instance, to measure the strength of an intra-molecular interaction between two domains it is typical to split them

into two individual peptides (11). An alternative approach is to truncate or mutagenize a proposed interaction interface and look at a functional consequence associated with the loss of the interaction (12-14). In the first approach, the strength of an interaction can be underestimated given that when the two interacting domains are in the same polypeptide, they will likely have a high local concentration which can affect the on-rate of the interaction. In the second approach, it is often difficult to anticipate whether a change in function is directly or tangentially effected by the truncation or mutagenesis.

To address the technical shortcoming in studying intra-molecular domain:domain interactions, we have previously developed and applied a novel genetic method termed Systematic Protein Affinity Strength Modulation (10). This technique utilizes an ER/K motif that has unusual biophysical properties (15). The ER/K motif primarily adopts an extended α-helical secondary structure in solution with end-to-end distance of 10 to 30 nm, depending on the length of the motif (16). However, it is prone to stochastic breaks in helicity that allow the n- and c- termini of the helix to come in close proximity of each other at a low but predictable frequency (10). Capitalizing on this phenomenon, a genetically encoded FRET pair as well as interacting polypeptides can be fused to either end of the ER/K motif to build a single polypeptide (xpolypeptide- FRETdonor- ER/K linker- FRETacceptor- ypolypeptide) (9, 17). At low (nM) concentrations, the interaction between the polypeptides will report a binary high-FRET interacting state or low-FRET non-interacting state that will be averaged out in ensemble measurements (10). It has been empirically determined that the on-rate for interactions in this system are dictated by the frequency that the α-helix stochastically brings its ends in close proximity, while the off-rate is dependent on the interaction between the polypeptides attached to the end of the helix (10). Additionally, the frequency at which the ends of the α-helix come in close proximity is a function of the length of the α-helix; longer helices have a lower frequency of end-to-end proximity (10). By incorporating different length ER/K motifs between interacting polypeptides the on-rate can be modulated such that the apparent concentrations can be varied from 100 nM to 10 μM (10). Finally, the SPASM module is a transposable genetic element that can be incorporated into naturally occurring linkers between modular domains in most proteins. This technology allows intra-molecular interactions to be perturbed in systematic ways such that domain:domain interactions can be directly observed and characterized (9). Here we utilize this technology to explore domain:domain interactions between the multi-domain protein kinase C (PKC).

The PKC family exemplifies the use of modular architecture in cellular function. PKC is composed of a conserved catalytic domain (CD) fused to multiple, modular regulatory domains (RD: pseudo-substrate, C1a, C1b and C2) that are sensitive to different small molecule/second messenger stimuli (α isoform: C1a – diacylglycerol (DAG) and phorbol ester (PMA); C1b- DAG, PMA ; C2 - Ca^{2+}). In the absence of stimuli, the RDs cooperatively mask the catalytic site, whereas conformational changes facilitated by

effector binding to these domains facilitate interactions with cellular membranes and scaffolding proteins (6). While numerous studies have dissected the structure-function relationship of the individual regulatory modules, interactions between modules remain largely unexplored. Hence, the current model of PKC activation presents it as a binary switch that is basally turned off through a RD-CD interaction, and is switched on when effectors bind and release the RD from the CD (18, 19). As a glimpse beyond this binary view, a high affinity inter-molecular interaction between the effector bound C1 and RD (12 nM) has been previously reported (11). Further, PKC activation has been proposed to trigger homo-dimerization (20) with consequent influence on catalytic activity (11, 20). However, these inter-molecular interactions have not been incorporated into current models of PKC activation, presumably due to the lack of mechanistic or structural details.

Here, we demonstrate that PKCα readily homo-dimerizes upon stimulation with activating effectors *in vitro*. We generated and characterized a uni-molecular FRET sensor that is both functional as PKCα and reports on effector-induced dimerization *in vitro* and in CHO cells. We then used multiple FRET sensors, some including the ER/K linker, to dissect domain:domain interactions in the activated state of PKCα to reveal that dimerization stems from several weak interactions involving the C1, C2, and catalytic domains that together contribute to a nano-molar affinity interaction. We then address the functional significance of PKCα dimerization through four separate vignettes. (1) We find that the *in vitro* specific activity of PKCα is more sensitive to dimerization than it is to modulation of the auto-inhibitory interactions. (2) We observe homo-dimerization in the basal state upon mutagenesis of the Turn Motif priming phosphorylation site (Thr→Ala), a finding with implications in PKC maturation. (3) We reveal that PKC function in cells can be modulated in the presence of peptides designed to destabilize the dimer state. (4) We observe that a commonly used PKC inhibitor bisindoylmaleimide I (BimI) can alter PKCα localization by destabilizing basal, auto-inhibitory interactions. We conclude with a simple model in which dimerization allows PKC to overcome a high degree of basal auto-inhibition by latching open the effector stimulated kinase.

2.2 Materials and methods:

Reagents- 1,3-Diolein (DAG) (Sigma Aldrich) and 1,2-Diacyl-sn-glycerol-3-phospho-L-serine (PS) (Sigma Aldrich) were solubilized in chloroform. Aliquots of DAG and PS were dried and re-suspended into a 20 mM HEPES, 5 mM $MgCl_2$, and 0.1 mM EGTA buffer (500 µg/ml and 250 µg/ml respectively) and used as a 10x stock for standard LC conditions (refreshed bi-weekly). Phorbol-12-myristate-13-acetate (PMA) was purchased from CalBiochem and solubilized in DMSO. Bismaleimidohexane (BMH) was purchased from Pierce and solubilized in DMSO immediately prior to cross-linking experiment.

Bisindolylmaleimide I (BimI) was purchased from CalBiochem. MANT- ADP was purchased from Invitrogen. The myristoylated RD peptide corresponding to residues 218-226 (Myr SLNPEWNET) was purchased from Sigma Aldrich (P0102), and the scrambled RD peptide (Myr NPESNLTWE) as well as the CD peptide corresponding to residues 633-642 (Myr GQPVLTPPDQ) and scrambled CD peptides (Myr QPGQPDLPVE) were custom synthesized by GenScript. All peptides were solubilized in slightly basic water (~pH 8.5). Priming phosphorylations were assessed using pS657 (06-822 Millipore) and pT638 (32502 ABCAM) antibodies according to manufacturer's protocol.

Constructs- All PKC constructs were cloned from full-length human cDNA (Open Biosystems) using PCR into unique restriction sites in pBiex1 (Novagen), or pcDNA/FRT (Invitrogen) plasmid vectors. All constructs contain a c-terminal FLAG tag which is used for affinity purification of recombinant protein. $(Gly\text{-}Ser\text{-}Gly)_{2\text{-}4}$ linkers separate each fusion element. In the SPASM constructs, linkers separate fluorophores from the ER/K α-helix and the PKC domains. The Tev protease site was engineered at the n-terminus of the ER/K α-helix. Details on the ER/K α-helices have been previously reported (10). Domain truncation constructs were created by site-directed mutagenesis using Pfu-Turbo (Agilent). In Fig. 2.6a,f the following truncations were made: 32-151 (ΔC1), 158-292 (ΔC2), 606-672 (ΔC-tail), 32-100 (Δ C1a), or 101-151 (Δ C1b). In Fig. 2.6 we define the CD (catalytic domain - 336-672) and RD (Regulatory domains - 1-335). Constructs were analyzed for kinase activity and S657 and T638 phosphorylation (Fig. 2.2), or in the absence of kinase activity MANT- ADP binding (Fig. 2.2 f-h).

Insect cell culture and protein purification- Sf9 cultures in Sf900-II media (Invitrogen) were transiently transfected with pBiex1 vectors using Escort IV transfection reagent (Sigma-Aldrich). 72 hr post transfection, cultures were lysed with 0.5% IGEPAL, 4 mM $MgCl_2$, 200 mM NaCl, 7% Sucrose, 20 mM HEPES, 5 mM DTT, 50 µg/ml PMSF, 5 µg/ml aprotinin, 5 µg/ml leupeptin, pH 7.5. Clarified lysates were incubated with Anti-FLAG M2 Affinity resin (Sigma-Aldrich) for 2 hours. The resin bound protein was washed with 20 mM HEPES, 2 mM $MgCl_2$, 300 mM KCl, 2 mM DTT, 50 µg/ml PMSF, 5 µg/ml aprotinin, 5 µg/ml leupeptin, pH 7.5 three times with 10x resin volume. The protein was eluted with 100 µg/ml FLAG peptide. The buffer was exchanged to 5 mM HEPES, 0.5 mM EGTA, 1 mM DTT, 5 µg/ml aprotinin, 5 µg/ml leupeptin and 2 mM $MgCl_2$ at pH 7.5 using Zeba Spin Desalting Columns (Pierce). Protein concentration was determined from fluorescence emission of mCitrine or mCerulean compared to a matched standard (FluoroMax-4, Horiba Scientific) or A280 using extinction coefficients determined by ExPASy Protparam (SIB).

Mammalian cell culture- CHO Flp-in cells (Invitrogen) were cultured and incubated in DMEM supplemented with 10% FBS, 4.5 g/L D-glucose, 1% glutamax, 20 mM HEPES, pH 7.5, and 1%

antibiotic-antimycotic (Invitrogen) at 37°C and 5% CO_2. Constructs in the pcDNA vector were transiently transfected into CHO cells using Fugene HD (Promega) and harvested after 48 hours. CHO Flp-in cells stably expressing mCer-PKCα-mCit-FLAG constructs were generated according to manufacturer's protocol with cells maintained in 600 µg/ml hygromycin. For live cell imaging, cells were trypsinized and $2x10^5$ cells were re-plated onto a 35 mm glass-bottom dishes (MatTek Corp) coated with 1 µg fibronectin (Sigma Aldrich), and allowed to adhere for 2 hours. The plates were washed with 2 ml of HBS with 0.2% dextrose, and 500 µl of this media was added to the cells prior to imaging. Cells were imaged at 40x or 60x with a Nikon TiE microscope equipped with an Evolve 512x512 EM-CCD camera (Photometrics), a mercury arc lamp, and the appropriate band pass filters. For FRET images, a Dual-View filter (Photometrics) was used for simultaneous acquisition of mCerulean and mCitrine peak fluorescence. Following image acquisition of untreated condition (pre), cells were perfused with HBS containing 10 µM PMA and 900 µM $CaCl_2$ or 50 µM LPA at room temperature. For live cell fluorometer experiments (Fig. 2.2a, 8c), one confluent 10 cm plate was trypsinized, washed with 10 ml DMEM with 10% FBS to inactivate the trypsin, and washed twice with 5 ml HBS with 0.2% dextrose, before being resuspended in 1 mL. This is similar to methods previously reported (17). All conditions involving myristoylated peptides were incubated with 20 µM peptide for 15 min before imaging, or fluorometer experiments. For translocation imaging experiments 1.5 µM BimI was added to cells 2-4 min before image acquisition.

Fluorometer data acquisition- A Fluoromax-4 fluorometer (Horiba Scientific) was used to obtain FRET spectra. Samples were excited at 430 nm (8 nm band pass) and the emission was recorded from 450-650 nm in 1 nm intervals (4 nm bandpass). For uni-molecular sensors, 20-80 nM of protein was used *in vitro*, and, for bi-molecular sensors, 40 nM of mCerulean and 160 nM of mCitrine constructs were used, unless otherwise noted. All *in vitro* assays were performed in a buffer containing 20 mM HEPES, 5 mM $MgCl_2$, 100 µM EGTA, 1 mM DTT, 5 µg/ml aprotinin, 5 µg/ml leupeptin, and were mixed in tubes pre-coated with 0.1 mg/ml BSA. Final concentrations of 1.5 mM $CaCl_2$, 3.2 µM PMA, 10 µM BimI, or 50 µg/ml of DAG and 25 µg/ml of PS were added to the sample where indicated. All conditions were allowed to equilibrate for greater than 30 min at 30°C after the reaction was fully mixed. The figures of FRET depict mean and s.e.m. from three independent spectra obtained using the same batch of recombinant protein and the same reagent preparations on the same day, and are representative of results observed from three independent measurements. For experiments monitoring MANT-ADP binding samples were prepared in the same manner, but obtained spectra with direct excitation of tryptophan at 290 nm (8 nm band pass) and the emission was recorded from 300 – 550 nm at 1 nm intervals (4 nm band pass), or direct excitation of MANT at 340 nm (4 nm band pass) from 400 – 550 nm at 1 nm intervals (2 nm band pass).

Bi-molecular RD:RD, RD:CD, CD:CD FRET assay-The appropriate combination of TEV protease treated RD-mCer-TEV-30nm ER/K-CD-FLAG, RD-mCit-TEV-30nm ER/K-CD-FLAG, RD-TEV-30nm ER/K-mCer-CD-FLAG, and RD-TEV-30nm ER/K-mCit-CD-FLAG constructs were used to probe the individual bi-molecular RD:RD, RD:CD, and CD:CD interactions. Coomassie stained or fluorescent protein scanned SDS-PAGE was used to verify complete TEV cleavage (data not shown).

Kinase assay- Kinase assays were performed using the Kinase-Glo Max Luminescence assay kit (Promega) according to the manufacturer's protocol. Synthetic liposomes were made from Brain Polar Lipid Extract (Porcine) (Avanti; high in PS) mixed with 2% w/w 1,3-Diolein (Sigma Aldrich) using established procedures (21). Briefly, the liposomes were suspended in chloroform for storage, and dried under nitrogen and stored under vacuum for 18 hrs. The mixture was resuspended to a concentration of 12.5 mg/ml in HEPES buffer, and underwent at least three freeze thaw cycles in liquid nitrogen then hot water. The mixture was then extruded (Avanti) using .08 μm Nuclepore Track-Etch Membrane (Whatman), and diluted into a 20x reaction concentration of 1.6 mg/ml. Histone IIIs (Sigma Aldrich), bovine Myelin Binding Protein (MBP; Sigma Aldrich), or MBP residues 4-14 (Santa Cruz Biotechnology, Inc) at final concentrations of 40 μM were used as substrates unless otherwise noted. The reaction was initiated with 40 μM ATP (Sigma Aldrich) and were briefly mixed and incubated with mild shaking at 30^{o}C from 2 to 10 minutes. For all conditions, the ATP consumption is calculated against a matched control without kinase. ATP calibration curves were obtained under identical conditions (without kinase). End-point luminescence was measured in white, 96 well plates (Thermo Scientific) on a Synergy HT (Biotek).

Cross-linking assay- Cross-linking assay was performed as previously reported (20). Briefly, 200-400nM of PKC was pre-incubated in a HEPES buffer containing 2% glycerol, and .02% TritonX-100 and indicated effectors. A 50x stock of BMH (1.25 mM) in DMSO was added to the pre-incubated solution for 2-5 min then quenched with 5x SDS-PAGE loading dye with 20 mM DTT. All blots shown are representative of at least three independent experiments. It should be noted that the level of cross-linking observed is highly dependent on the concentration of BMH resulting in variability between experiments. To circumvent this limitation inherent in cross-linking assays, the extent of cross-linking is always evaluated with respect to a matched control in each experiment.

In vitro *membrane partitioning assay*- This assay was performed as previously described (21). Liposomes were prepared as in the kinase assay except the liposomes were extruded with an equal volume of 340 mM sucrose buffer. Purified protein was clarified at 80,000 rpm, and the clarified protein was incubated in the indicated conditions. The reaction mixture was spun at 80,000 rpm and the supernatant was taken

off (soluble fraction) and the remaining pellet was suspended in an equal volume of 1x SDS-PAGE loading dye (pellet fraction).

Western Blotting- Lysates were prepared from stably expressing CHO cells generated using the Flip-in system (Invitrogen). Cells were plated in six well dishes (NEST) to reach 80-90% confluence within 24 hours and were subsequently serum starved for an additional 24 hours. Cells were treated with the indicated peptides (20 μM) 15 minutes before addition of 1-oleoyl lysophosphatidic acid (LPA, Cayman Chemicals, 10 μM). Cells were incubated with LPA for 15 minutes before lysis on ice with ice-cold buffer (1% Triton X-100, 250 mM NaCl, 50 mM Tris pH 6.8, 4 mM $MgCl_2$, 2 mM EDTA, 1:100 phosphatase inhibitor mixture II (Sigma-Aldrich), and containing 10 μg/ml aprotinin, 10 μg/ml leupeptin, and 1 mM PMSF). Lysates were syringed with a 26-gauge needle and clarified by spinning at 16,000 × *g* (10 min, 4 °C). Total lysate protein was assayed either by Bradford assay or by total ERK1/2 blotting (see below) with no significant difference observed between the two methods. Lysates were separated on 10% polyacrylamide/SDS gels before being transferred to PVDF membranes for 3 h at 300 mA. Blots were blocked with 2% BSA/TBS + 0.1% Tween (TBST) for 1 h at room temperature. Primary phospho ERK1/2 antibody (4376S, Cell Signaling) was used at a concentration of 1:5000 in 2% BSA/TBST and incubated overnight at 4 °C. Blots were washed with TBST (3 x 10 min) before addition of secondary antibody (goat anti-rabbit (Jackson ImmunoResearch Laboratories, Inc.) 1:10,000 in 1% milk/TBST). Blots were washed again with TBST (3 × 10 min) and developed using Immobilon Western chemiluminescent HRP substrate (Millipore). Blots were imaged using a ChemiDoc-it imaging system (UVP). Blots were stripped with Restore PLUS Western stripping buffer (Thermo Scientific) and reblotted with total ERK1/2 antibody (4695S, Cell Signaling; 1:10,000, 2% BSA/TBST). Blots were exposed to secondary as above and developed under the same conditions. All blots shown are representative of at least three independent experiments. Cross-linked PKC was probed (1f) using a PKCα antibody (sc-8393, Santa Cruz Biotechnology, 1:10,000 in 2% BSA/TBST).

Live cell FRET analysis- Images were analyzed using custom software in Matlab (Mathworks Inc.). Briefly, for images of LPA induced cells with constant excitation over the second to minute time scales, images were subjected to a background threshold/subtraction followed by correction for photobleaching using a maximum threshold. FRET ratios were computed as the pixel-by-pixel ratio between mCitrine and mCerulean intensities across the time series. For images of PMA induced cells in which excitation and image acquisition occurred for 200 – 500 ms every 30 seconds for 15 – 20 min, the straight pixel-by-pixel ratio was calculated as little photobleaching effects were observed. Deconvolution was performed using AutoQuant X3 (MediaCybernetics).

Dissociation constant of dimer formation- The equilibrium between mCer-PKCα-mCit (*F* - fluorescent) and PKCα-FLAG (*D* – dark) can be represented by the following five equations, where F_t and D_t are the total concentrations of mCer-PKCα-mCit and PKCα-FLAG respectively.

(1) $F + F \leftrightarrow F \cdot F$

+

(2) $D + D \leftrightarrow D \cdot D$

↕

(3) $D \cdot F$

(4) $F_t = F + F \cdot F + D \cdot F$

(5) $D_t = D + D \cdot D + D \cdot F$

Assuming the three interactions are equivalent and interchangeable, knowledge of the dissociation constant (K_D) is necessary and sufficient to explicitly calculate the partitioning between the species. A custom Matlab substitution solver was used to numerically calculate each of the five species (*F, D, F·F, D·F, D·D*) for a range of K_D values. Knowledge of the individual species allows us to estimate the K_D by evaluating the best fit (least-squares) to the titration curve of measured FRET ratio (R_{obs}) as a function of PKCα-FLAG concentration (D_t). As previously reported[2], R_{obs} can be expressed as a linear combination of the FRET ratio for the dimer ($R_{F\cdot F}$), monomer (R_F), and inter-species dimer ($R_{D\cdot F}$) –

$$(6)\ R_{obs} = \frac{R_{F\cdot F}(F \cdot F)}{F_t} + R_F\left(\frac{F}{F_t}\right) + \frac{R_{D\cdot F}(D \cdot F)}{D_t}$$

$R_{F\cdot F}$ is set to the observed FRET ratio at saturating concentrations (> 100 nM) of mCer-PKCα-mCit, $R_{D\cdot F}$ is set to the observed FRET ratio at high D_t/F_t ratios (> 20), and R_F is set to the basal FRET level in the absence of effectors. With these constraints and K_D as the only free parameter, we find that a K_D < 5 nM provides an indistinguishable fit to the experimental measurements. This competitive-binding measurement with interchangeable, equivalent species can only provide an upper bound to the K_D rather than a precise measurement. Lower concentrations of the mCer-PKCα-mCit can be used to improve this estimate, however they suffer from low signal-to-noise in our fluorometer measurements.

2.3 Results:

To investigate the role of intra-molecular interactions in the regulation of PKCα, several distinct FRET reporters were used throughout the study. These are composed of discrete domains of PKCα fused to ER/K linkers, and the GFP-derived mCitrine (mCit) and mCerulean (mCer) FRET pair **(Fig. 2.1 a)** tethered with $(Gly\text{-}Ser\text{-}Gly)_{2\text{-}4}$ linkers to allow for rotational freedom. Basally within a cell, or in the

presence of EGTA *in vitro*, the regulatory domains (RD; includes n-to-c-terminal pseudosubstrate, C1a, C1b and C2 domains) of PKC are known to engage in *cis* inhibitory intra-molecular interactions with the catalytic domain (CD; includes the kinase domain and the c-terminal extension termed the C-tail)(18, 22). Further, the small molecules Ca^{2+}, DAG/Phorbol ester (PMA), and bisindoylmaleimide I (BimI) have been established to interact primarily with the C2, C1, and catalytic domains respectively (6).

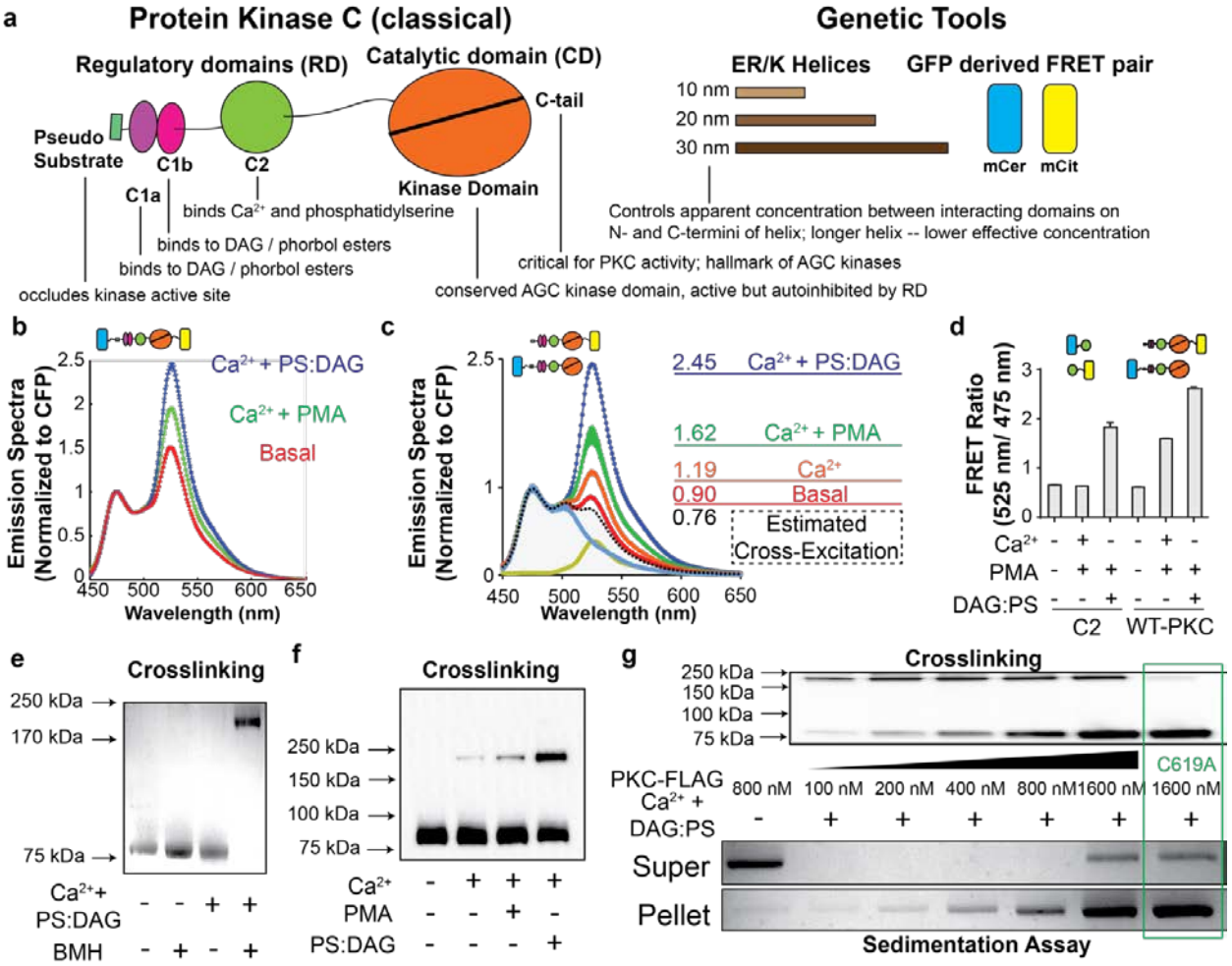

Figure 2.1. Homo-dimerization of activated recombinant PKCα. (**a**) Schematic of PKCα and the genetic tools used in the study. Subsequent figures utilize this scheme to depict FRET reporters (written/depicted left-to-write or top-to-bottom as n-to-c-terminal). (**b,c**) FRET increases following treatment of sensors with different effector combinations. FRET spectra normalized to the FRET donor (mCer) following effector stimulation of recombinant sensor protein. (b) Emission spectra of mCer-PKCα-mCit (50 nM) or (c) mCer-PKCα (30 nM) and PKCα-mCit (100 nM) excited at 430 nm in the presence of EGTA (Basal) or with 1.5mM $CaCl_2$ or the combination of effectors 1.5 mM $CaCl_2$ and 3.2 µM PMA, or 750 µM $CaCl_2$ and 50 µg/ml of DAG and 25 µg/ml of PS. In (c) the emission of 30 nM mCer-PKCα (light blue) and 100 nM PKCα-mCit (yellow) were obtained separately after donor excitation at 430 nm in the presence of EGTA, and the two spectra were added and normalized to the peak donor (mCer) emission value at 475 nm to estimate the FRET independent cross-excitation of the acceptor mCit. (**d**) Bi-molecular FRET sensors composed of the C2 domain (residues 185-292) or full-length PKC, fused to mCit or mCer, at matched concentrations under the specified conditions. The C2 domain shows an increase in FRET following activation with Ca^{2+} + PS:DAG but not Ca^{2+} + PMA. Both activation conditions result in an increase in FRET greater in the full length sensors relative to the C2 domain sensors. Error bars, s.e.m. $n \geq 3$. (**e,f**) Cross-linking of recombinant protein shows homo-dimer formation

following effector stimulation. (e) Representative SDS-PAGE of disulfide cross-linked PKCα-FLAG. Bisimidohexane (BMH; 2 min incubation) increases the apparent molecular weight of PKCα by approximately 2.5 fold in the presence of 750 μM $CaCl_2$ and 50 μg/ml of DAG and 25 μg/ml of PS. Coomassie stain was used for detection. (f) A representative immunoblot using an anti-PKCα antibody resolves single BMH cross-linked bands of equivalent mass but differing intensities after incubation of PKCα-FLAG with indicated effectors as in (c). (**g**) Increasing concentrations of PKCα result in a constant amount of cross-linked protein, despite increased PKC binding to a fixed density of liposomes. (Top) Representative SDS-PAGE of cross-linked PKCα, for a fixed concentration of liposome (~ 80 μg/ml of PS rich Brain Polar Lipid Extract (Porcine) mixed with 2% w/w 1,3-Diolein (DAG)) as a function of increasing concentrations of PKCα-FLAG. All samples were treated with 25 μM of BMH for 3 min. The final well includes C619A mutant PKCα-FLAG under matched conditions. (Bottom) PKCα-FLAG was incubated with or without the sucrose loaded liposomes used in the crosslinking assay (top) and fractionated by ultracentrifugation; the supernatant or pellet was subsequently separated by SDS-PAGE. Saturation of the liposomes with PKCα-FLAG occurred at a concentration between 800 – 1600 nM. PKCα-FLAG (C619A) does not crosslink under the same conditions as WT, but demonstrates a comparable ability to associate with liposomes.

PKCα homo-dimerizes upon stimulation with effectors in vitro

We engineered an initial unimolecular FRET sensor (mCer-PKCα-mCit-FLAG; each element is listed from n- to c- termini and dashes consist of a $(GSG)_{2-4}$ linker) capitalizing on the design scheme of a previously reported PKCδ sensor that elicited changes in FRET upon activation both *in vitro* and in cells (23). This PKCα flanking sensor (50 nM) showed enhanced FRET upon activation with Ca^{2+} and liposomes containing DAG and PS **(Fig. 2.1 b; see section 2.2)**. To address the possibility that the observed increase in FRET is primarily driven by confined localization on the lipid surface, the effect of Ca^{2+} and PMA, which is a soluble effector (24), was measured, with similar results (Fig. 2.1 b). The observed increase in FRET can arise from conformational changes within the PKC molecule or interactions between PKCs. GSG linkers inserted between PKCα and the two fluorophores (mCer and mCit) were designed to make the FRET readout sensitive to changes in distance rather than orientation of the two fluorophores. The current model of PKCα activation anticipates an increase in n-to-c terminal distance (18), and therefore is in contrast with the observed increase in FRET. To address whether inter-molecular interactions contributed significantly to the observed FRET response, we generated a second, bi-molecular FRET reporter system (mCer-PKCα-FLAG and PKCα-mCit-FLAG). Upon addition of Ca^{2+} and liposomes containing DAG:PS, Ca^{2+} and PMA, or Ca^{2+} alone a significant increase in FRET is observed compared to the sensors in their basal state, consistant with an inter-molecular interaction **(Fig. 2.1 c)**. The observed increases in FRET with the bi-molecular FRET reporter are significantly higher than that due to cross-excitation of the acceptor (mCit). The effects of cross-excitation were determined by summing the spectra of samples with only mCer-PKCα (light blue), and only PKCα-mCit (yellow) (**Fig. 2.1 c**; combined spectrum – dashed line). To assess what aspects of these observed increases in mCit/mCer occur from non-intended effects on the fluorophores and/or clustering of the proteins, we generated an additional bi-molecular FRET reporter system containing the C2 domain of PKCα with mCit or mCer (residues 185-292). At equal molarity of each fluorophore, the ratio of mCit/mCer was assessed

for both of the bimolecular FRET reporter systems basally, with Ca^{2+} and DAG:PS, or with Ca^{2+} and PMA **(Fig. 2.1 d)**. Basally, both reporters display equivalent low/negligible levels of FRET, but PKC effectors increase FRET for the sensors containing full length PKCα compared to the controls with only the C2 domain. Of note, the C2 domain sensors displayed a substantial increase in FRET in the condition with liposomes which could be explained by a specific interaction between C2 domains in the presence of both of its cofactors Ca^{2+} and PS, or from the local confinement of the sensors in a PS and DAG rich microdomains that forms in liposomes in the presence of Ca^{2+} (25).

As an orthogonal approach to FRET, a cross-linking assay was used. It has been previously reported that incubation of activated PKCα with a Cys-Cys cross-linker (BMH; 1.3 nm spacer arm) elicits an SDS-PAGE gel shift consistent with dimer formation (20). This result was reproducible with enrichment of cross-linked protein on coomassie stained SDS-PAGE gels between 170-250 kDa accompanied by loss of monomer (75 kDa), following effector stimulation of PKCα-FLAG **(Fig. 2.1 e)**. While a consistent, single, higher molecular weight band between 170-250 kDa was always observed in experiments, the relative partitioning between monomer and cross-linked protein was variable between protein preparations and experimental repeats. Hence, cross-linking results were only compared within each experiment with matched controls. To probe for additional bands on the SDS-PAGE gel after crosslinking with increased sensitivity of detection, gels were transferred to a PVDF membrane and probed with a PKCα antibody **(Fig. 2.1 f)**. Increasing levels of a single cross-linked band were observed with Ca^{2+}, Ca^{2+} and PMA, and Ca^{2+} and DAG:PS **(Fig. 2.1 f)**. The band is consistent with PKCα-FLAG running between the expected molecular weight of dimeric and trimeric PKCα. A recent report used a similar Cys-Cys crosslinking assay (26) for the related PRK kinase and observed a homodimer running above its expected molecular weight. Based on this previous observation and the presence of single higher molecular weight band, PKCα likely homo-dimerizes rather than forming a higher order oligomer.

The extent of cross-linking is independent of the concentration of PKCα-FLAG above concentrations of 100 nM **(Fig. 2.1 g)**. This observation is not consistent with clustering or crowding of PKC on membranes, wherein increasing PKC concentrations with a constant concentration of lipids should increase cross-linked product **(Fig. 2.1 g)**. Importantly, an *in vitro* membrane localization assay shows that PKCα does not saturate the fixed concentration of lipids until greater than 800 nM of PKCα is added **(Fig. 2.1g; bottom panel)**. As an additional control, a C619A mutant of PKCα-FLAG does not cross-link despite its ability to co-sediment with liposomes as well as the WT protein. Homo-dimerization of active PKCα has been previously suggested (11, 20, 27, 28) and together our *in vitro* observations, including the

increase in FRET upon activation of the initial uni-molecular sensor, are consistent with the formation of homo-dimer.

Functional characterization of PKC sensors

The addition of fluorophores and other modifications to PKCα did not compromise the basic enzymatic and processing functions of the WT protein. Several characteristics of PKCα including a single band on SDS-PAGE matching its expected MW, priming phosphorylations at the hydrophobic motif (pS657) and turn motif (pT638) (29), and PKC effector sensitive kinase activity support this observation **(Fig. 2.2 a-d)** (30). Of note we found that three commonly used PKC phosphorylation substrates, Histone IIIs, Mylein Basic Protein (MBP), or a peptide corresponding to residues 4 – 14 of MBP (MBP pep), at equal molarity elicited dramatically (roughly one order of magnitude) different ATPase activities of PKCα **(Fig. 2.2 d)**. We found that PKCα-FLAG and mCer-PKCα-mCit-FLAG behaved interchangeably in the ATPase assays **(Fig. 2.2 e)**. However, the PKCα-ΔC-tail-mCit-FLAG sensor used in Fig. 2.6 a,c lacks the priming phosphorylations, and as previously reported (31) has no detectable ATPase activity. To assess if this sensor retains any of its native tertiary structure in the catalytic domain, and as such can provide useful information on the binding interface, we adopted an assay that has commonly been used to measure nucleotide binding in other ATPases, including in protein kinase A (PKA) (32), but has to our knowledge not been tested with PKCs. MANT labeled ADP is postulated to be a resonance energy acceptor from fluorescing tryptophans in the ATPase domain only if it binds to the catalytic site (32). Enhanced MANT-ADP excitation (450 nm) was detected upon addition of activated PKCα-FLAG, which could be quenched with an excess of unlabeled ADP **(Fig. 2.2 f)**. A titration of MANT-ADP was fit to a One Site – Specific Binding function (Prism) to establish a binding affinity of 20.6 +/- 5.6 μM **(Fig. 2.2 g)**, similar to previous reports of ADP binding affinities of 5.5 μM for S6K (33), and 9.0 μM for PKA (32) . Despite the loss of catalytic activity upon deletion of the C-tail, PKCα-ΔC-tail-mCit-FLAG retained its ability to bind MANT-ADP **(Fig. 2.2 h)**, suggesting retention of its native tertiary structure. This is not surprising when considering homologous kinases such as PDK1 that fold properly without having a C-tail and are capable of kinase activity following *trans* binding of the C-tail of another AGC kinase (34). Taken together, these assays provide a toolbox for assessing the functionality of PKCα derived sensors.

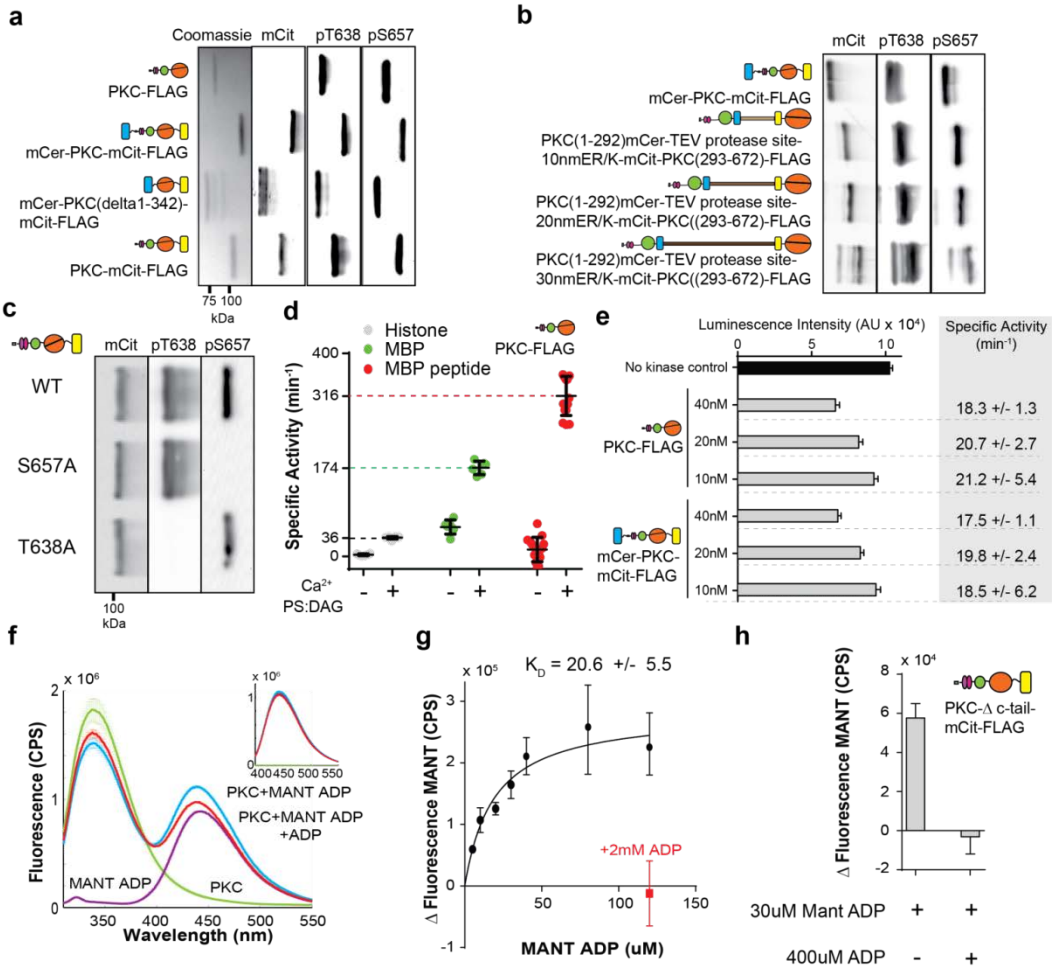

Figure 2.2. Characterization of PKCα sensors. (**a-c**) Sensors were analyzed for expected protein size and priming phosphorylation levels at the turn motif (T638) and hydrophobic motif (S657) sites assessed by immunoblotting with phospho-specific antibodies. Representative blots of (a) PKCα-FLAG, mCer-PKCα-mCit-FLAG, mCer-CD-mCit-FLAG, (b) RD- n nm SPASM- CD (n = 10, 20, or 30), (c) and PKCα-mCit-FLAG WT, T638A and S657A are shown. (**d**) Specific activities of PKCα-FLAG with equimolar concentrations (20 μM) of three different phosphorylation substrates, Histone IIIs, Mylein Basic Protein (MBP) full length, and MBP peptide (residues 4-14). In each case a substantial increase in specific activity was observed following the addition of 750 μM $CaCl_2$ and ~ 80 μg/ml of PS rich Brain Polar Lipid Extract (Porcine) mixed with 2% w/w 1,3-Diolein (DAG). The mean and s.e.m. of n = 6 – 18 reactions are reported. Negligible ATPase activity was observed in the absence of any phosphorylation substrate (data not shown). (**e**) ATPase activity for indicated concentrations of PKCα-FLAG and mCer-PKCα-mCit-FLAG in matched reactions with Histone IIIs (12.5 μM) for 5 min. Raw data of luminescence intensity (proportional to residual ATP concentration at the end of the assay) from Kinase-Glo assay (Promega). Four independent reactions are shown with mean and s.e.m. and the calculated specific activities are shown at right. ATPase activity is comparable between both constructs and neither are sensitive to changes in concentration from 10 – 40 nM. (**f,g**) MANT –ADP can be used to detect nucleotide binding to PKCα. (f) Raw spectra of PKCα-FLAG (1 μM) alone (green), incubated with MANT-ADP (120 μM; blue), or MANT-ADP and ADP (400 μM; red), or MANT-ADP alone (purple) excited at 290 nm (main) or 340 nm (inset) all in the presence of 1.5 mM $CaCl_2$ and 3.2 μM PMA. (g) The difference in MANT-ADP fluorescence at 450 nm with or without PKCα-FLAG (1 μM), in the presence of $CaCl_2$ and PMA, as a function of increasing MANT-ADP concentration. Specificity of MANT-ADP binding assessed by addition of 2 mM ADP in the presence of 120 μM MANT-ADP (red). Data are fit to a One Site – Specific Binding function (Prism) to generate the indicated K_D of MANT-ADP binding to PKCα-FLAG. (**h**) C-tail deleted sensors retain the ability to bind nucleotide. MANT-ADP binding (increase in fluorescence at 450 nm) to PKCα-ΔC-tail-mCit (300 nM) in the presence or absence of ADP (400 μM; MANT-ADP – 30 μM). Measurements are made in the presence of 750 μM $CaCl_2$ and ~ 80 μg/ml of DAG:Brain Extract liposomes. Error bars, s.e.m. $n \geq 3$.

Estimate of PKCα homo-dimer binding affinity and effects on specific activity

The critical concentration at which dimerization of PKCα is observed is beyond the limit of both the bi-molecular FRET and crosslinking assays used in Fig. 2.1. Hence, a bi-molecular FRET competition assay was utilized to estimate the binding affinity of a homo-dimeric PKC complex. The increased FRET for the mCer-PKCα-mCit-FLAG with the addition of Ca^{2+} and PMA, or Ca^{2+} and PS:DAG, can be competed off by the addition of PKCα-FLAG **(Fig. 2.3 a)**. By titrating PKCα-FLAG into a mixture of PS:DAG activated mCer-PKCα-mCit-FLAG, the FRET was systematically quenched to below basal levels **(Fig. 2.3 b)**. The decrease in FRET does not stem from saturation of the liposomes as the total PKCα concentration is well below the saturation limit determined in Fig. 2.1g. The competitive FRET inhibition was fit to an equilibrium partitioning between the three species (see Methods) to yield an upper bound on the bi-molecular dissociation constant (K_D) of 5 nM. Of note, it was previously observed that the specific activity of PKCα increased *in vitro* at concentrations above 4 nM (11). To investigate the sensitivity of specific activity of mCer-PKCα-mCit-FLAG to the dimeric state, a fixed concentration of sensor was mixed with increasing concentration of PS:DAG liposomes. Across a range of 80 – 300 μg/ml of liposomes, a modest decrease in FRET and a correlated decrease in specific activity was observed **(Fig. 2.3 c; R^2 = 0.91)**. These results are consistent with a previous report that systematically demonstrated that the specific activity of PKCα is sensitive to its dilution across lipid vesicles (35). Higher liposomal concentrations did not allow for robust FRET measurements in our assays due to high light scattering from the lipids.

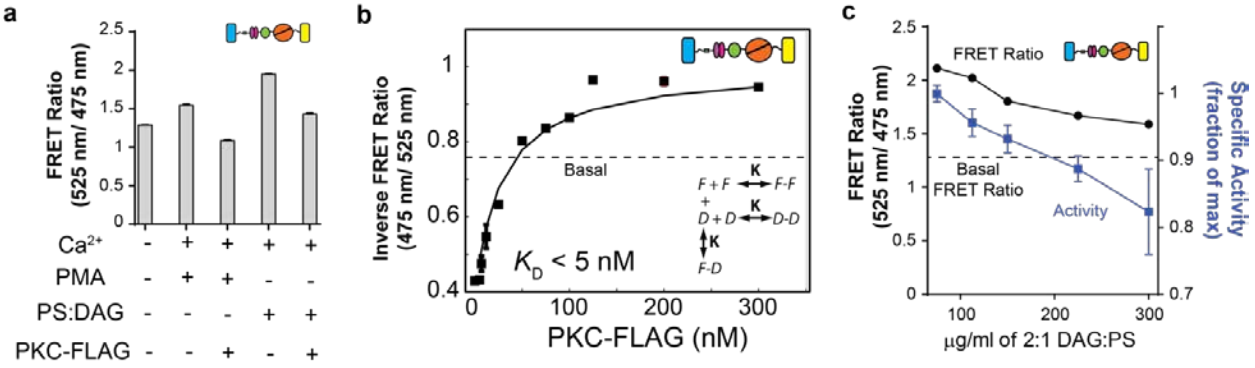

Figure 2.3. Affinity of the homo-dimer interaction and its effect on kinase activity. (**a**) Increased FRET ratio can be quenched by the addition of non-fluorescent PKCα. FRET ratio of mCer-PKCα-mCit-FLAG (50 nM) with the indicated effectors with and without PKCα-FLAG (200 nM). (**b**) Competitive inhibition of PKCα dimerization can be used to estimate equilibrium dissociation constant (K_D). Increasing concentrations of PKCα-FLAG quench FRET levels of activated mCer-PKCα-mCit (Ca^{2+}+PS:DAG). Data are represented as inverse FRET ratio (475 nm/525 nm). ↑ Inverse FRET ratio = ↓ FRET. Equilibrium equations (inset) were fit to data to calculate a K_D < 5 nM. (**c**) Specific activity correlates with extent of dimer formation. FRET levels (black; left Y-axis) and specific activity (blue; right Y-axis) of mCer-PKCα-mCit with increasing lipid concentration (R^2 = 0.91). Error bars, s.e.m. n ≥ 3.

FRET increase from mCer-PKCα-mCit-FLAG is observed upon PMA and LPA activation in live cells

The flanking FRET sensor (mCer-PKCα-mCit-FLAG) was stably expressed in CHO cells to ~ 8-fold above endogenous PKCα levels (data not shown). The sensor basally resided in the cytosol and, consistent with previous studies using (n-terminal) eGFP-tagged PKCα, translocated to the plasma membrane after stimulation with PMA **(Fig. 2.4 a,c)**, effectively mimicking the canonical response for PKCα (36). The basolateral membrane of the cell was imaged to provide a larger surface area for integration of FRET levels. The mean pixel-by-pixel FRET ratio increased steadily for the first 3 min post PMA stimulation and remained elevated through 15 min of imaging **(Fig. 2.4 b; black)**. As a control, DMSO treatment did not induce translocation or significant changes in FRET **(Fig. 2.4 b)**. As an orthogonal approach to measure FRET (17), the FRET response to addition of PMA was determined using a live cell suspension in a spectrofluorometer **(Fig. 2.4 b; green)**. A substantial increase in FRET was observed following PMA addition, with a peak at 4 min, following a gradual decrease to basal levels within 8 min **(Fig. 2.4 b; green)**. Together, our measurements suggest that cellular activation of mCer-PKCα-mCit-FLAG by PMA causes an increase in FRET, but cell physiology plays a role in the persistence of the FRET response past the initial activation. A typical timelapse of the accumulation of fluorescence at the basolateral membrane post PMA stimulation is shown **(Fig. 2.4 c)**, as well as a deconvolved Z-stack of the same cells at the 16 min timepoint **(Fig. 2.4 d)**. Most of the fluorescence accumulates at the plasma membrane, although a small fraction accumulates in the cytosol and nucleus consistent with results reported in NIH 3T3 cells (37). CHO cells stably expressing the sensor protein elicit a characteristic downstream PMA response by phosphorylating ERK1/2 **(Fig. 2.4 e)**. The PMA dependent ERK1/2 phosphorylation persists over 30 min following stimulation **(Fig. 2.4 e)**. The PMA stimulated ERK1/2 phosphorylation is dependent on PKC activity, as it is abolished by the PKC-specific inhibitor BimI (1.5 μM) **(Fig. 2.4 f)**.

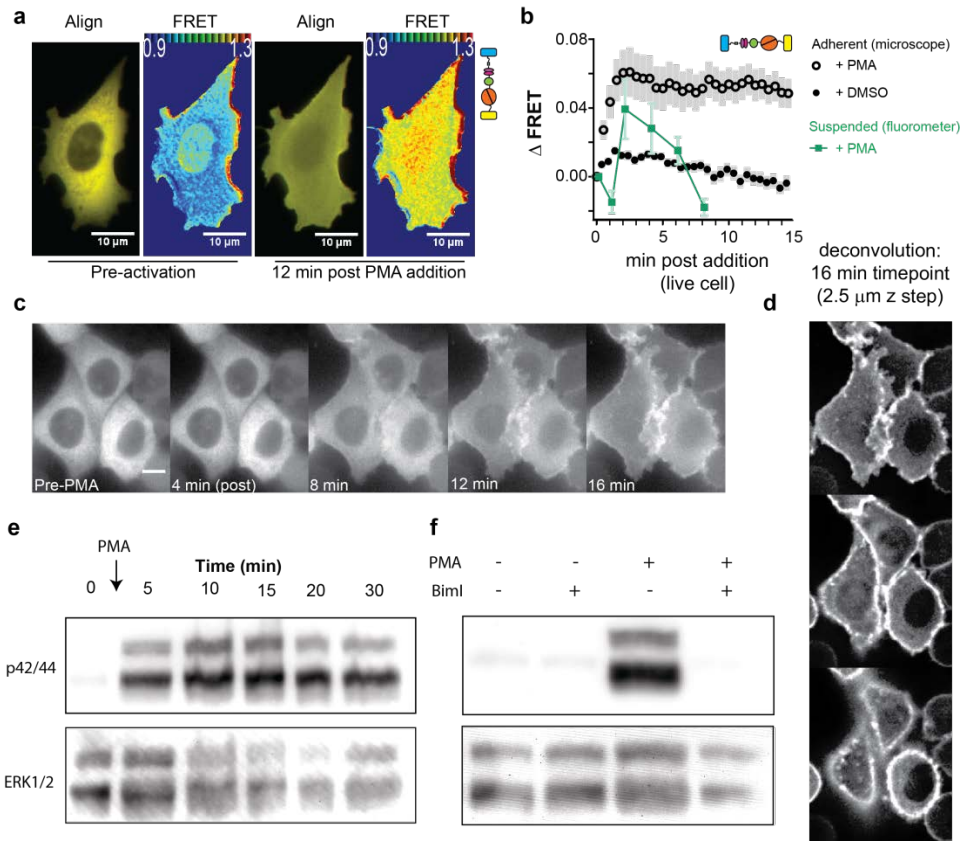

Figure 2.4. FRET increase and ERK1/2 phosphorylation are observed in CHO cells following PMA stimulation. (**a-c**) PMA stimulation induces membrane translocation and increased FRET. (a) Representative image of a CHO cell stably expressing mCer-PKCα-mCit-FLAG before and 12 min after PMA stimulation (10 µM). 'Align' is the alignment of the FRET donor (green), and FRET acceptor (red) channels. 'FRET' is the pseudocolored pixel-by-pixel ratio of FRET acceptor to donor channel intensities using the indicated heat map. The microscope was focused on the basolateral cell membrane, where the fluorescent protein accumulates upon PMA stimulation. This method was chosen as a means to provide a larger surface area to integrate FRET ratios compared to the peripheral accumulation of fluorescence observed in a cross-sectional view of the cell (d). (**b**) The change in FRET in individual adherent cells by microscopy (open black circles) or suspended cells by spectroscopy (green squares) as a function of time post addition of PMA or DMSO control (closed black circles). For microscopy, results are mean ± s.e.m. from 6–8 independent experiments (n > 51 cells). For spectroscopy, results are mean ± s.e.m of n ≥ 3 independent experiments. (**c**) Representative time course of PMA stimulation images of CHO cells stably expressing mCer-PKCα-mCit-FLAG (mCit fluorescence). Scale bar – 10 µm. (**d**) PKC translocates primarily to the plasma membrane with residual localization in the cytosol, nucleus, and cellular punctae. Deconvolved images of the 16 min timepoint (c) at three different z-sections (2.5 µm apart). (**e,f**) PMA stimulates PKC specific phosphorylation of ERK1/2. (e) Representative blot of the phosphorylation status of ERK1/2 in the same cell line (a) following addition of PMA (1.92 µM) at the indicated time points. (f) Representative blot of ERK1/2 phosphorylation before or 15 min after PMA stimulation in the presence or absence of the PKC specific inhibitor BimI (1.5 µM).

PMA activates PKC directly by binding its C1 domains (38). As a physiological stimulus, lysophosphatidic acid (LPA) was used to stimulate PKC as previously demonstrated (39). Unlike PMA, LPA elicits the characteristic membrane translocation response in only ~ 50% of the cells, consistent with previous reports (40). A transient PKC translocation to the plasma membrane was observed following LPA stimulation **(Fig. 2.5 a)**. Membrane translocation was accompanied by a transient increase in FRET

for mCer-PKCα-mCit-FLAG **(Fig. 2.5 a,b)**. The sensor protein also induced a bi-phasic ERK1/2 phosphorylation response with a dramatic increase at 2 min post stimulation, return to basal levels at 4 min, followed by sustained increase at 6 and 8 min **(Fig. 2.5 c)**. The persistent ERK1/2 phosphorylation 15 min post LPA treatment was inhibited by pretreatment with the PKC inhibitor BimI **(Fig. 2.5 d)**. We speculate that the bi-phasic ERK1/2 response to LPA is caused by bifurcation in LPA-induced PKC signaling with re-convergence of the signals at the downstream ERK1/2 at different time scales. Together, the LPA and PMA responses are consistent with mCer-PKCα-mCit-FLAG reporting an activated dimeric state for PKCα, consistent with our *in vitro* observations. However, other factors including clustering of the sensor at the plasma membrane, or conformational changes independent of homo-dimerization may also contribute to the observed cellular FRET response following PKC activation.

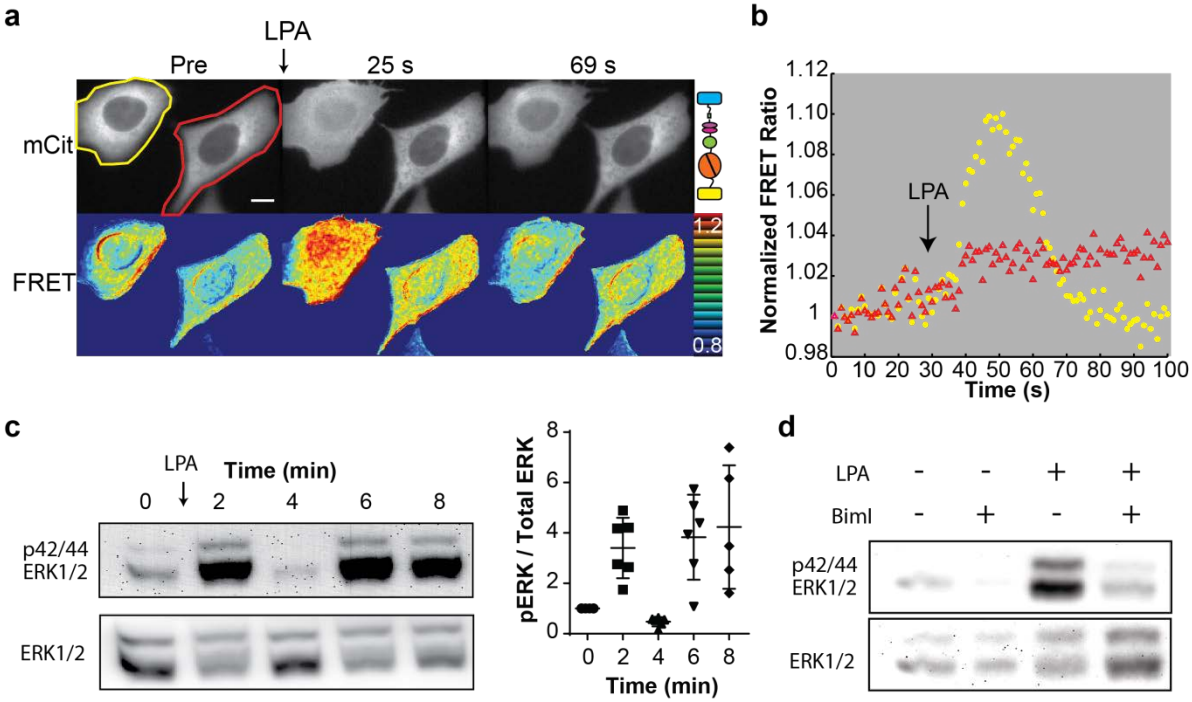

Figure 2.5. FRET increase and ERK1/2 phosphorylation are observed in CHO cells following LPA stimulation. (**a,b**) Concurrent transient membrane translocation and FRET increase following LPA (50 μM) stimulation. (a) (Top) Representative images of CHO cells with stable expression of mCer-PKCα-mCit. Translocation of the sensor from a diffuse cytosolic distribution (pre) to an accumulation on the basolateral membrane (25 s post LPA), which dissipates over time (69 s), depicts the canonical PKC response to activation. As would be expected based on previous observations (40), ~ 50% of cells show the characteristic membrane translocation response following LPA stimulation. (Bottom) FRET measurements are depicted as a heat map in corresponding images. Scale bar = 10 μm. Data are representative of n > 25 cells. (b) FRET ratio for cells in (a). FRET ratios are normalized to the value at t = 1 s and adjusted for photo bleaching. (**c**) Bi-phasic ERK1/2 response to LPA stimulation. Representative blot and quantification of n ≥ 5 independent replicates of ERK1/2 phosphorylation following LPA treatment (10 μM). (**d**) Representative blot of ERK1/2 phosphorylation before or 15 min after LPA stimulation, in the presence or absence of the PKC specific inhibitor BimI (1.5 μM).

Elements in both the regulatory domain (RD) and catalytic domain (CD) are critical for homo-dimerization

To identify the domains contributing to homo-dimerization *in vitro*, several domain truncations were made into the bi-molecular FRET reporter system (mCer-PKCα-FLAG + PKCα-mCit-FLAG). It was observed that deletion of either both of the C1 domains or the conserved C-terminal extension of the AGC kinase domain (C-tail (V5) domain) completely abolished the effector induced increase in FRET, whereas the deletion of the C2 domain retained a partial response **(Fig. 2.6 a)**. The involvement of the C1 and C2 domains in homo-dimerization is consistent with a previous report of a high affinity interaction between C1 and RD following activation (11). To probe for individual interactions between RD and CD (RD:RD, RD:CD, CD:CD), bi-molecular FRET pairs containing only the RD or CD were engineered. While these confirm an enhanced RD:RD interaction **(Fig. 2.6 b)**, no appreciable interaction involving the CD (RD:CD, CD:CD) is detected upon activation even at concentrations much higher than the K_D (150 nM). These latter observations are in contrast with the effects of C-tail truncations in the context of full-length PKCα **(Fig. 2.6 a)**. The C-tail truncated catalytic domains retain their ability to bind nucleotide, attesting to the retention of a folded catalytic site (Fig. 2.2 h). The C-tail is a conserved region of the kinase domain that is required to stabilize the active state of the kinase and is critical for hetero-dimerization of almost all AGC kinases (41). An alternative interpretation for the lack of FRET response for the C-tail deletion sensor is the displacement of the C-terminal mCit fluorphore such that no FRET is detected despite the occurrence of homo-dimerization. To test this possibility, a second bi-molecular FRET pair (mCer-PKCα-FLAG + mCit-PKCα-FLAG) was tested. The increase in FRET upon activation was found to be independent of which termini the fluorophores are positioned on PKC **(Fig. 2.6 c)**. The C-tail's involvement in homo-dimerization was confirmed by an almost complete loss of FRET after deletion of only one C-tail in either of the bi-molecular FRET pairs (mCer-PKCα + PKCα-ΔC-tail-mCit; mCer-PKCα-ΔC-tail + mCit-PKCα) **(Fig. 2.6 c)**. Together, these observations suggest that inter-molecular interactions involving both the RD and CD contribute to homo-dimerization.

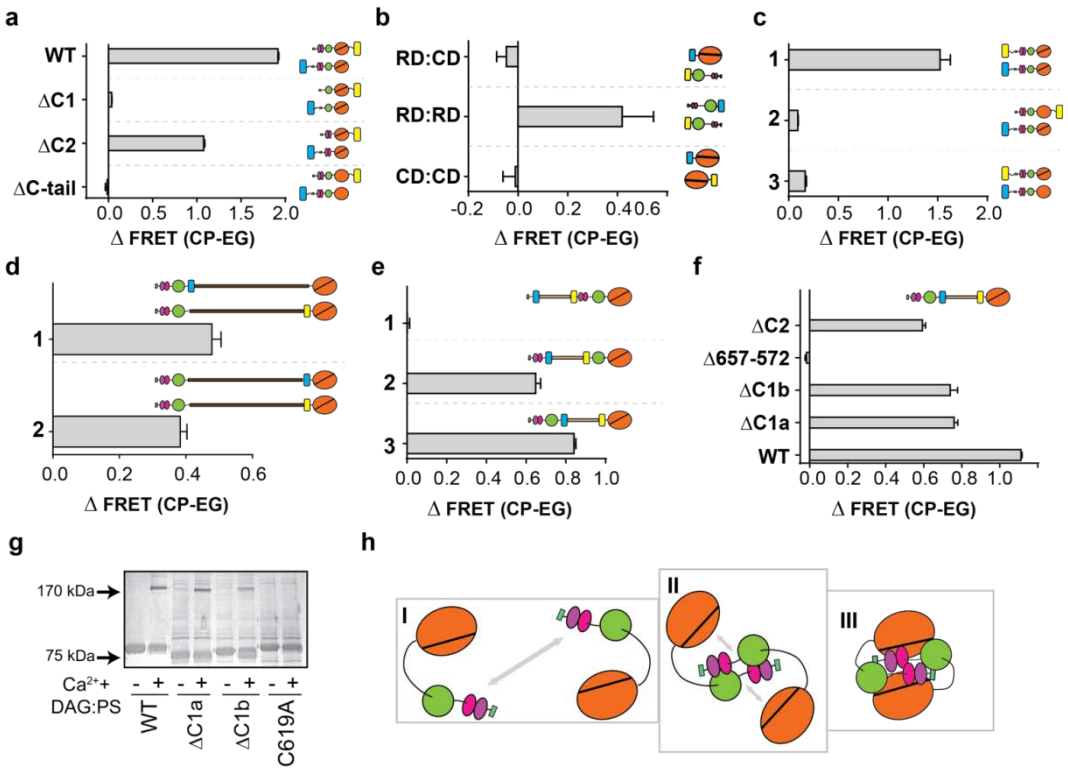

Figure 2.6. Conformation of the PKC homodimer. (**a-d**) Change in FRET ratio (Δ FRET) from basal (EG - EGTA) to activating (CP - Ca^{2+} + PMA) conditions for the indicated sensors. (a-d) FRET donor and acceptor are on different sensors. Increase in FRET indicates an inter-molecular interaction. (e,f) FRET donor and acceptor are on the same sensor, but separated by an ER/K linker. In the absence of an interaction, the 10 nm ER/K linker separates domains beyond FRET distance. Increase in FRET indicates enhanced interaction between domains at either end of the ER/K linker. (a) C1 and C-tail domains are essential for PKCα homo-dimerization. mCer-PKCα + PKCα-mCit with no truncation (WT) or ΔC1, ΔC2, ΔC-tail in both proteins. (b) A bi-molecular RD:RD interaction, but not a RD:CD, or CD:CD interaction is detected following activation. RD:CD - mCer-CD + mCit-RD. RD:RD – mCit-RD + mCer-RD. CD:CD – mCer-CD + mCit-CD (50 nM donor sensor, 100 nM acceptor sensor). (c) The C-tail in the catalytic domain is essential for homo-dimerization. 1 – mCer-PKCα + mCit-PKCα. 2 – mCer-PKCα + PKCα-ΔC-tail-mCit. 3 – mCer-PKCα-ΔC-tail + mCit-PKCα. (d) Both the regulatory (RD) and catalytic domains (CD) reside at the dimerization interface. 1 – RD-mCer-30nmERK-CD + RD-30nmERK-mCit-CD. 2 – RD-30nmERK-mCer-CD + RD-30nmERK-mCit-CD. (**e**) Enhanced RD-CD interaction in the PKC homo-dimer. 1 – PS-mCer-10nmERK-mCit-C1-C2-CD. 2 – PS-C1-mCer-10nmERK-mCit-C2-CD. 3 – RD-mCer-10nmERK-mCit-CD. (**f**) C1a, C1b, and C2 domains partially contribute to dimerization, whereas the c-terminal 15 residues of the C-tail are essential. Change in FRET upon activation of type 3 configuration (as in 6e), with truncation of the C1a, C1b, C2 domains or the c-terminal 15 residues of the C-tail. (**g**) Proximity of the C-tail to the homo-dimer interface. Representative coomassie stained gel of PKCα-FLAG protein under basal or activated (Ca^{2+}+DAG:PS) conditions. Data for full length PKCα (WT), domain deletions (ΔC1a, ΔC1b), and mutant (C619A) proteins are shown. Note the complete loss of detectable dimerization upon mutagenesis of a Cys619 in the C-tail region of the CD. The BMH cross-linker has a maximal reach of 1.4 nm. For reference the C1b domain is about 3 x 2 x 2 nm (18). (**h**) Model for dimer formation based on data presented in a-g. I – RDs interact with each other upon effector stimulation to nucleate homo-dimerization. II – RD-CD interaction in trans facilitated by the C-tail. III – proposed conformation for the PKC homo-dimer. (a-f) Error bars, s.e.m. $n \geq 3$.

SPASM technique demonstrates that the RD and CD interact in the dimeric state

In the context of the intact PKC protein, all domains are tethered in close spatial proximity, which increases their local effective concentration. Hence, weak interactions between domains (RD:CD,

CD:CD) that are nonetheless essential for homo-dimerization may not be detected in bi-molecular assays. To address this limitation, SPASM modules were spliced into different locations of full-length PKCα. The SPASM module consists of a FRET pair (mCit/mCer) flanking an ER/K linker, which controls the effective concentration of the interaction between proteins fused to its ends (10). These modules are designed to (a) artificially increase the local concentration of domains as compared to untethered domains, while (b) using the FRET readout to resolve effector-stimulated changes in interactions between domains. Given that the bi-molecular RD:RD interaction is enhanced following PKC activation (11), it can serve to nucleate additional RD:CD and CD:CD interactions. Thus, a SPASM module was spliced in between the RD and CD to test for an inter-molecular RD:CD or CD:CD interaction that can stabilize a high affinity dimer. To avoid potential complications from intra-molecular interactions, a 30 nm ER/K linker was used (low effective concentration of the intra-molecular interaction (10)), and the system was engineered to report only on bi-molecular interactions (FRET donor placed adjacent to either the RD or CD; FRET acceptor adjacent to the CD of a different sensor). Both sensor pairs showed a comparable increase in FRET upon activation providing direct evidence for a RD:CD interaction, with the potential for a CD:CD interaction in the homo-dimeric state **(Fig. 2.6 d)**. Next a 10 nm SPASM module was inserted in three separate locations in the PKC gene (1 - between the pseudosubstrate (PS) and C1a domain; 2 - between the C1b and C2 domains; 3 - between the C2 and CD). While the PS is known to interact with the CD basally (42), this interaction is not changed following activation (type 1; **Fig. 2.6 e**). In contrast, the C1 domains display a marked enhancement in interaction with either the C2 or CD following activation (type 2), while collectively the RDs interact very prominently with the CD following activation (type 3; **Fig. 2.6 e**). Using the type 3 configuration to directly report on the interaction between the RD and CD, deletions of C1a, C1b, C2, or the C-terminal 15 residues of the C-tail were made. Surprisingly, the activated RD:CD interaction remained partially intact after the deletion of any of the three regulatory domains, but shortening of the C-terminus of the C-tail completely disrupted this interaction **(Fig. 2.6 f)**. Together, these data suggest that all three regulatory domains (C1a, C1b, and C2) contribute to the dimer interface, but the C-tail is absolutely critical for the interaction. Given that the C-tail is essential for the active conformation of the kinase domain (43), these data cannot distinguish between a direct role for the C-tail as part of the dimerization interface, and its indirect contribution through the global conformation of the kinase domain.

To probe for precise interfaces involved in homo-dimerization we sought to identify Cys residues that were being crosslinked by BMH, which requires two Cys residues to be within 1.3 nm. The only Cys residues within PKCα are found in the Cys rich C1a and C1b domains, and within the CD. Activation specific crosslinking was still detected after deletion of either the C1a or C1b, yet a single point mutation

in the C-tail (C619A) completely abolished the crosslinking response **(Fig. 2.6 g)**. Interestingly, the corresponding residue in PKCβII (Cys 622), which is found in the AST region, is buried within an interaction interface with the C1b domain in a recent crystal structure (18). This raises the possibility that the interaction between the C1b and c-tail captured in the crystal structure could be an interaction utilized in dimerization. Regardless, our data propose a new conformation for activated PKC, wherein the CD, C1a, C1b, and the C2 domains all contribute to stabilizing a homo-dimer **(Fig. 2.6 h)**. It was reported from two separate groups that truncation of the C-terminal 10 residues in the C-tail (31) or alanine mutagenesis of regions from the C1a and C2 domains (44) completely abolished catalytic activity of PKCα. A potential explanation for these observations is the disruption of homo-dimerization and its consequent effects on PKC catalytic activity. To probe the function of a homo-dimeric conformational state, we report on four independent vignettes concerning different aspects of PKCα function. Each provide some insight and highlight how our mechanistic understanding of PKCα function is enhanced when considering this additional state.

Equilibrium between closed, open, and dimerized conformations of PKCα

In the absence of effectors PKCα predominantly populates a 'closed' conformation with the CD auto-inhibited by the RD (18). Splicing a SPASM module between the RD and CD should decrease the effective concentration of the RD for the CD in proportion to the length of the linker. 'Prying' open the RD:CD interaction with SPASM modules containing increasing length ER/K linkers systematically reduces the basal level of FRET **(Fig. 2.7 a)** and increases the basal level of activity (**Fig. 2.7 b**; 10 nm ~ 22 / 12 %, 30 nm ~ 37 / 22 % maximum activity, compared to ~ 3 / 3 % for WT PKCα (Histone IIIs / MBP pep)). Of note, prying open the RD:CD interaction alone is not sufficient to induce dimerization in the absence of effectors. Yet the presence of effectors increases FRET regardless of ER/K linker length **(Fig. 2.7 a)**. Given the importance of RD:CD interactions for dimer formation (Fig. 2.6), it is not surprising that increasing ER/K linker length also disrupts dimer formation **(Fig. 2.7 a)**. Despite the different levels of FRET with 10 and 30 nm ER/K linkers following activation, they both have specific activity similar to that of the CD in the absence of the RD (TEV cleaved) (**Fig. 2.7 b**; 10 nm ~ 88 / 86 %, 30 nm ~ 94 / 95 % maximum activity, (Histone IIIs/ MBP pep)). Following TEV treatment the RD should partition to the lipid vesicles leaving the CD completely uninhibited. It is observed that in the presence of effectors both the 10 and 30 nm ER/K linkers demonstrate similar activities, despite different levels of FRET. Taken together these results are consistent with a dynamic equilibrium for PKCα between a closed (basal auto-inhibited: medium/low FRET), an open (no auto-inhibition: low FRET), and a dimeric conformation (no auto-inhibition: high FRET), with equivalent specific activities in the open and dimer forms **(Fig. 2.7 c)**. In the proposed model for mature PKCα, the activity of the catalytic domain is

regulated by only one parameter namely, the ratio of non- auto-inhibited catalytic domains to the total number of catalytic domains in a given reaction.

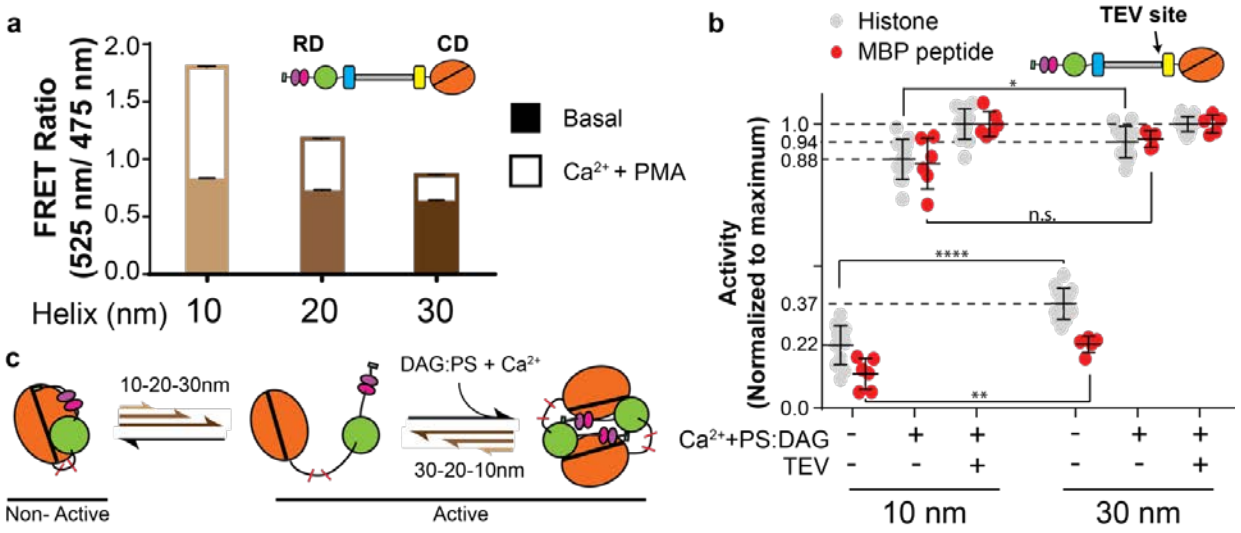

Figure 2.7. Dimerization facilitates high kinase activity through disruption of auto inhibition. (**a**) Effector binding and not disruption of the RD:CD interaction is necessary for homo-dimer formation. Perturbation of the basal RD:CD interaction with an ER/K linker does not induce dimerization. The basal (solid) and activated (hollow) FRET ratio of three PKC reporters with 10- 20- and 30 nm SPASM modules inserted between the RD and CD (between E292 and G293). All three sensors have increased FRET after addition of Ca^{2+} + PMA. (**b**) Disruption of the basal RD:CD interaction only modestly increases specific activity. Activity of the 10 and 30 nm sensors (80 nM) under the indicated conditions with Histone IIIs (grey) or MBP peptide (red) as substrate. TEV treatment cleaves a specific site engineered at the n-terminus of the ER/K linker separating the RD from the CD. TEV treatment followed by the addition of Ca^{2+} and DAG:PS yields maximal activity of the catalytic domain due to membrane partitioning of the RD and soluble partitioning of the CD. The basal activity but not the activity in the presence of effectors was significantly enhanced when increasing the SPASM module length from 10 nm to 30 nm (student's t-test 99 % CI: P-values for n.s. = 0.073, * = 0.0212, ** = 0.0042, **** < 0.0001). (a-b) Error bars, s.e.m. $n \geq 3$. **(c)** Schematic of the effect of the different length ER/K linkers on the three-state equilibrium for PKCα.

Loss of the Turn Motif priming phosphorylation causes basal dimerization

We next aimed to bridge our global structural model of PKC to high-resolution x-ray crystallographic data. A recent partial crystal structure of PKCβII suggests a direct binding interaction between its C1b and C-tail domains (18). To investigate the possibility that this interaction is similar to the one utilized in homo-dimerization of PKCα, individual point mutations in PKCα (K621A, D357A, H633G, T638A) were engineered in an attempt to disrupt the C1b-C-tail interaction. The residues are mapped onto the crystal structure of PKCβII (orange surface rendering), as well as C619 (yellow surface rendering) for visual reference **(Fig. 2.8 a)**. Each mutation engineering into the bi-molecular FRET reporters elicited modest effects, except for T638A, which counter intuitively increased the FRET response under basal and effector stimulated conditions **(Fig. 2.8 b,c)**. Crosslinking analysis of the T638A mutant confirmed the basal formation of a dimeric species **(Fig. 2.8 d)**. Residue T638 is an essential priming phosphorylation

site (turn motif/TM) in PKCα that is essential for full catalytic activity following activation (45). The T638A mutant has ~ 36 / 22 % (histone / MBP pep) of WT PKCα activity following activation with Ca^{2+} + PS:DAG (data not shown), similar to previous reports (45). The T → A mutant is commonly incorporated in the TM site to mimic the loss of TM site phosphorylation (45-47). Using such an approach for multiple AGC kinases including PKCζ, it has been broadly suggested that TM phosphorylation functions to anchor the C-terminal portion of the C-tail, containing the hydrophobic motif (HM), to the catalytic domain (47). Based on this model, it might be anticipated that basal homo-dimerization of PKCα-T638A is the result of an indirect destabilization of the interaction of the catalytic domain with the phosphorylated HM site on the C-tail. To assess this possibility, phospho-null mutation of the HM site (S657A) was incorporated into the FRET sensors. In contrast with the proposed model, basal homo-dimerization induced by T638A is independent of the S657A mutation **(Fig. 2.8 e)**. The mechanism by which T638A induces basal dimerization is informed by an alignment of two crystal structures of the catalytic domain of PKCβII (**Fig. 2.8 f**; (48)). The region just n-terminal of the TM site (AST region (43)) undergoes a dramatic conformational change when bound to C1b (cyan), yet in both structures the C-tail converges at the phosphorylated TM residue that appears tightly anchored to the catalytic domain by electrostatic interactions with four basic residues (red) **(Fig. 2.8 f)**. We postulate that disruption of the anchoring pTM site allows the AST region of the C-tail to adopt a conformation that can induce homo-dimerization in the absence of effectors. Independent of this interpretation, the finding that an unphosphorylated TM can basally homodimerize may provide a mechanism by which PKCα, unlike most AGC kinases, is auto phosphorylated at its three priming sites (6, 49) and deserves further investigation.

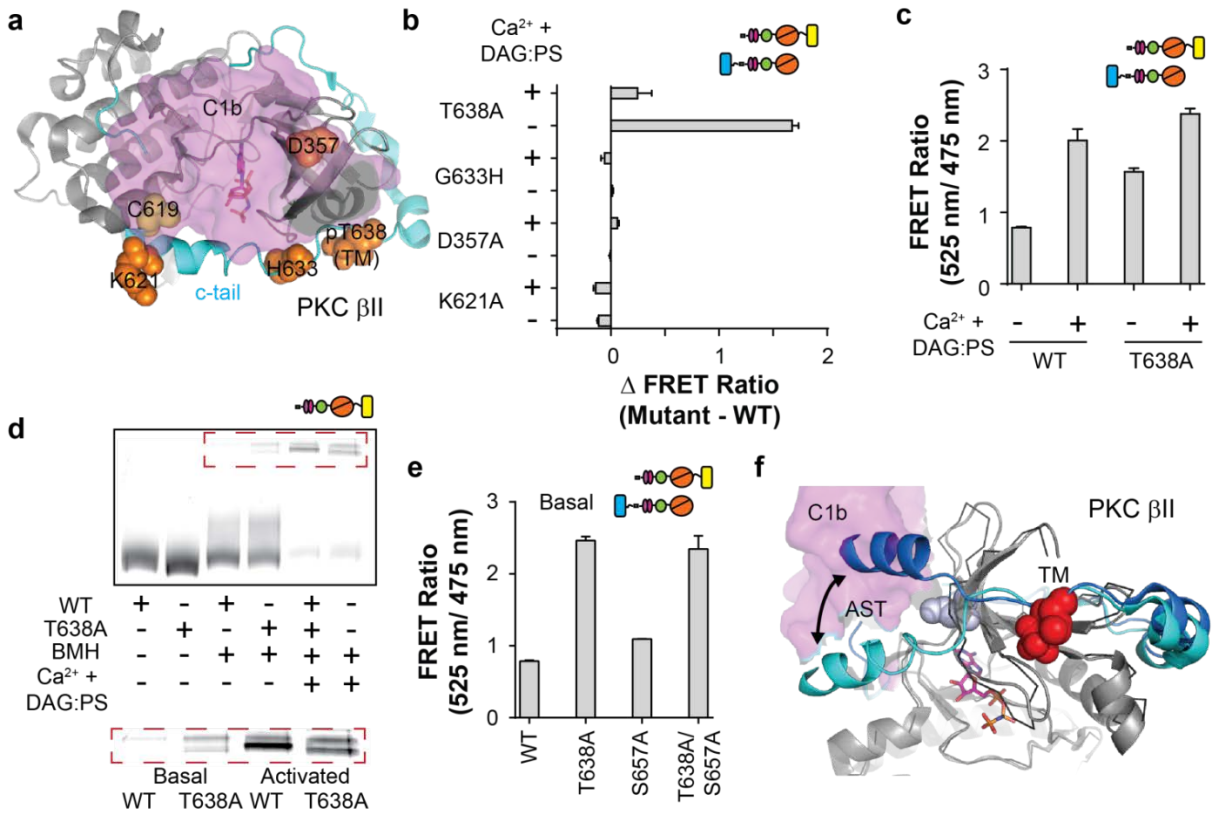

Figure 2.8. Point mutation in the Turn Motif (TM) phosphorylation site causes PKCα to dimerize basally *in vitro*. (**a**) Schematic of the interface between C1b (magenta surface contour) and the catalytic domain of PKCβII (PDB: 3PFQ) highlighting the c-tail (cyan cartoon), the BMH crosslinked C619 (yellow spheres), and residues mutagenized (orange spheres). (**b,c**) Only T638A (turn motif) shows a substantial change in FRET compared to WT in both basal and effector stimulated conditions when inserted into both mCer-PKCα-FLAG + PKCα-mCit-FLAG sensors. (**d**) BMH cross-linking supports enhanced basal dimerization of T638A mutant. Wild type or T638A PKCα-mCit-FLAG crosslinking was assessed under the indicated conditions. Inset shows the contrast-adjusted intensity from the same gels. mCit fluorescenc was detected. (**e**) Loss of turn-motif phosphorylation does not induce dimerization solely through allosteric changes in hydrophobic motif site. Basal FRET levels for WT, turn motif mutant (T638A), hydrophobic motif mutant (S657A), and double mutant (T638A/S657A) bi-molecular FRET sensors (mCer-PKCα-FLAG + PKCα-mCit-FLAG). (**f**) Pymol aligned crystal structures (2I0E – blue and black ribbon; 3PFQ – cyan and grey) of the PKCβII catalytic domain highlighting the relative positions of the c-tail (615 - 669). The phosphorylated turn motif residue (T638; red spheres) interacts tightly with the catalytic domain through four conserved electrostatic interactions (in PKCβII K350, K355, K374, R415) that appear to serve as a fulcrum point around which conformational changes in the c-tail are centered.

Disruption of PMA/LPA induced high FRET state in cells modulates PKC specific phosphorylation of ERK1/2

To test the functional significance of dimerization in cells, one peptide each from the RD and CD were selected to specifically disrupt (relative to a matched scrambled peptide; all myristoylated) prospective PKCα dimerization interfaces. While the effects of the peptides on FRET were modest *in vitro*, they were specific and concentration dependent across two different sensor systems **(Fig. 2.9 a-b)**. Additionally, the RD peptide did not disrupt liposome binding in sedimentation assays **(Fig. 2.9 c)**. When treating cells

with the myristoylated RD peptide, the PMA induced high FRET state of mCer-PKCα-mCit-FLAG was disrupted in live cell suspensions (**Fig. 2.9 d**; fluorometer measurements). Both the RD and CD peptides had a significant and sustained dampening effect on the PMA induced increase in FRET of the sensor compared to their respective scrambled peptide controls (**Fig. 2.9 e**; microscope measurements). Additionally, neither peptide had a noticeable effect on the rate nor relative degree of basolateral membrane translocation of the sensor in CHO cells following PMA treatment (**Fig. 2.9 f**; data not shown). Next, the effect the peptides had on the PMA and LPA induced phosphorylation of ERK1/2 was assessed by pre-treatment of cells for 15 min prior to stimulation with PMA or LPA. The native RD peptide specifically lowered the level of ERK1/2 phosphorylation following PMA **(Fig. 2.9 g)** or LPA treatment **(Fig. 2.9 h)**, relative to the scrambled control. When the cells were stimulated with serum, which is expected to activate ERK1/2 through both PKC-dependent and independent pathways (50), both the RD peptide and the known PKC inhibitor BimI had comparable partial effects **(Fig. 2.9 i)**. Last, the CD peptide was able to specifically disrupt LPA induced ERK1/2 phosphorylation compared to its scrambled control **(Fig. 2.9 j)**. Together, these results are consistent with a model in which disruption of PKCα homo-dimerization is capable of inhibiting PKC mediated downstream ERK1/2 phosphorylation.

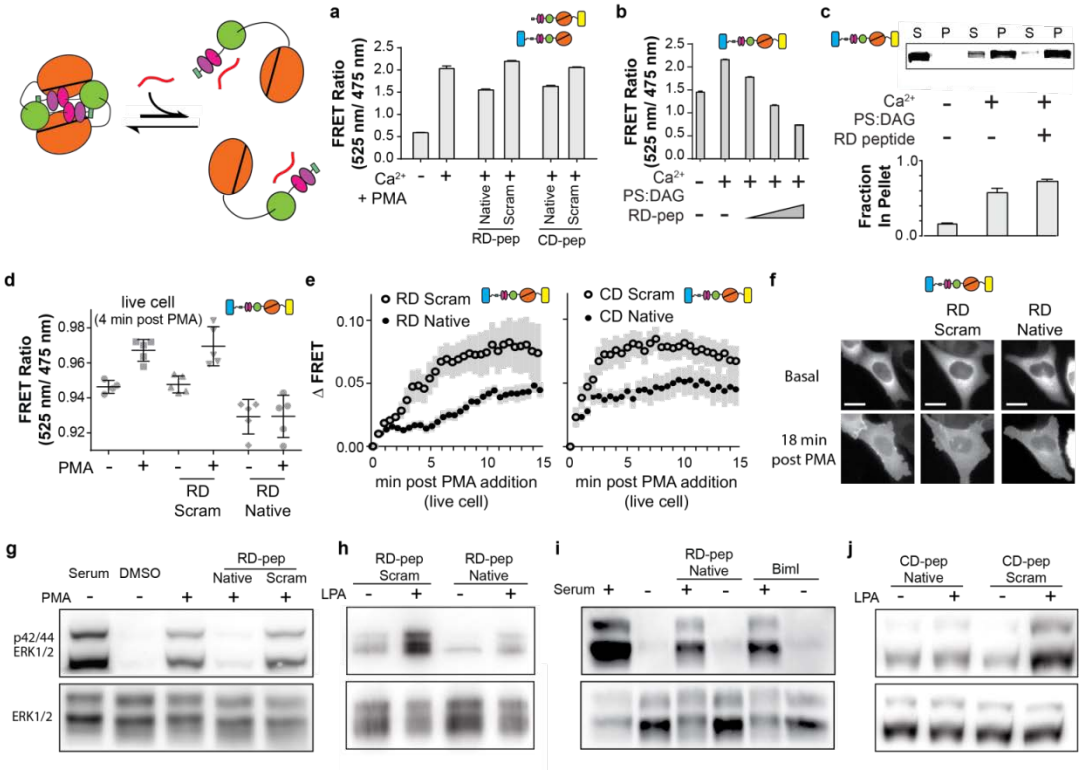

Figure 2.9. Disruption of activation induced PKC sensor high FRET state in CHO cells modulates PKC function. (**a**) Peptides from the regulatory (RD) and catalytic (CD) domains can disrupt dimerization in recombinant protein. FRET ratio for mCer-PKCα (40 nM) combined with PKCα-mCit (160 nM) under the indicated conditions. Ca^{2+}+PMA – 1.5 mM $CaCl_2$ + 3.2 μM PMA. RD-pep and CD-pep are myristoylated peptides analogous to residues 218-226 in the regulatory domain, and 633-642

in the catalytic domain. Native – native PKC sequence; Scram – matched scrambled sequence control. Peptides concentrations are 10 μM. (**b**) Peptides decrease FRET in a concentration-dependent manner. The in-vitro FRET ratio of mCer-PKCα-mCit-FLAG with increasing concentrations of RD-pep (0, 10, 20, 50 μM). (**c**) Peptide does not alter membrane translocation of PKC. mCer-PKCα-mCit-FLAG was incubated with Ca^{2+} and sucrose loaded PS:DAG vesicles, with and without the native RD-pep, before ultra-centrifugation. After ultracentrifugation, the pelleted and supernatant fractions were run on an SDS-PAGE gel and scanned for mCit fluorescence. Top: a representative gel image and Bottom: quantification from three separate experiments. (**d,e**) Peptides suppress the characteristic increase in mCer-PKCα-mCit FRET following PMA stimulation in live cells. (d) FRET ratio of suspended CHO cells (fluorometer detection) stably expressing mCer-PKCα-mCit-FLAG, pre and 4 min post 10 μM PMA addition, in the presence or absence of 20 μM of the indicated peptide. Maximum FRET was observed 4 min post PMA stimulation (see Fig. 2.2a). Error bars, s.e.m. n > 5 (e) Microscope based detection of changes in FRET ratio (Δ FRET) in adherent cells, pre-incubated for 15 minutes with the indicated peptides (10 μM), followed by stimulation with 10 μM PMA. Error bars, s.e.m. n = 13-24 cells. (**f**) Peptides do not influence membrane translocation of PKCα. Representative images of cells pre- and 18 min post PMA addition. Scale bars = 10 μm. (**g-j**) RD and CD peptides, but not matched scrambled controls disrupt PMA or LPA stimulated of ERK1/2 phosphorylation. Peptides do not influence PKC-independent (serum) driven phosphorylation of ERK1/2. Serum starved CHO cells stably expressing mCer-PKCα-mCit-FLAG were pre-incubated with 20 μM of the indicated peptide (or 1.5 μM BimI) for 15 minutes prior to stimulation (10% serum, 10 μM LPA, or 1.92 μM PMA) and lysed 15 minutes post stimulation. Representative western blots of phospho and total ERK1/2.

Destabilizing the closed conformation provides stable PKCα translocation to the membrane

The PKC inhibitor GF109203x is known to stabilize the translocation of PKCα following effector stimulation (46). Stensman et al. (46) hypothesized that the mechanism of GF109203x-influenced translocation sensitivity is due to a destabilization of the basal RD:CD interaction. Additionally, several analogues of this inhibitor, including BimI, are known to induce conformational changes in the CD (51). Using a PKCα sensor with a SPASM module inserted between the RD and CD, we directly detect a reduction in the strength of the interaction between RD and CD when incubated with BimI under basal conditions **(Fig. 2.10 a)**. Based on the three-state model (Fig. 2.7c), destabilization of the closed conformation should drive the equilibrium towards dimer formation following effector stimulation. Accordingly, we find increased dimerization of PKCα in the presence of BimI **(Fig. 2.10 b,c)**. We hypothesize that both the open and dimeric conformations of PKCα can engage with the plasma membrane. Consistent with this concept, LPA stimulation of cells stably expressing the flanking sensor (mCer-PKCα-mCit), substantially increased the fraction of cells with stable localization of the sensor at the membrane in the presence of BimI **(Fig. 2.10 d,e)**. Our findings provide direct evidence that a small molecule that can destabilize the closed conformation can facilitate both dimerization and stabilize membrane localization of PKCα in the presence of effectors. This opens the possibility of other small molecules or interacting proteins influencing localization of PKC by influencing the stability of either the closed or dimer states. As a corollary, PKC translocation is not necessarily an appropriate proxy for PKC activation in live cells, as demonstrated by the decoupling of activity and translocation with the peptide inhibitors (Fig. 2.9) and BimI (Fig. 2.10 d,e).

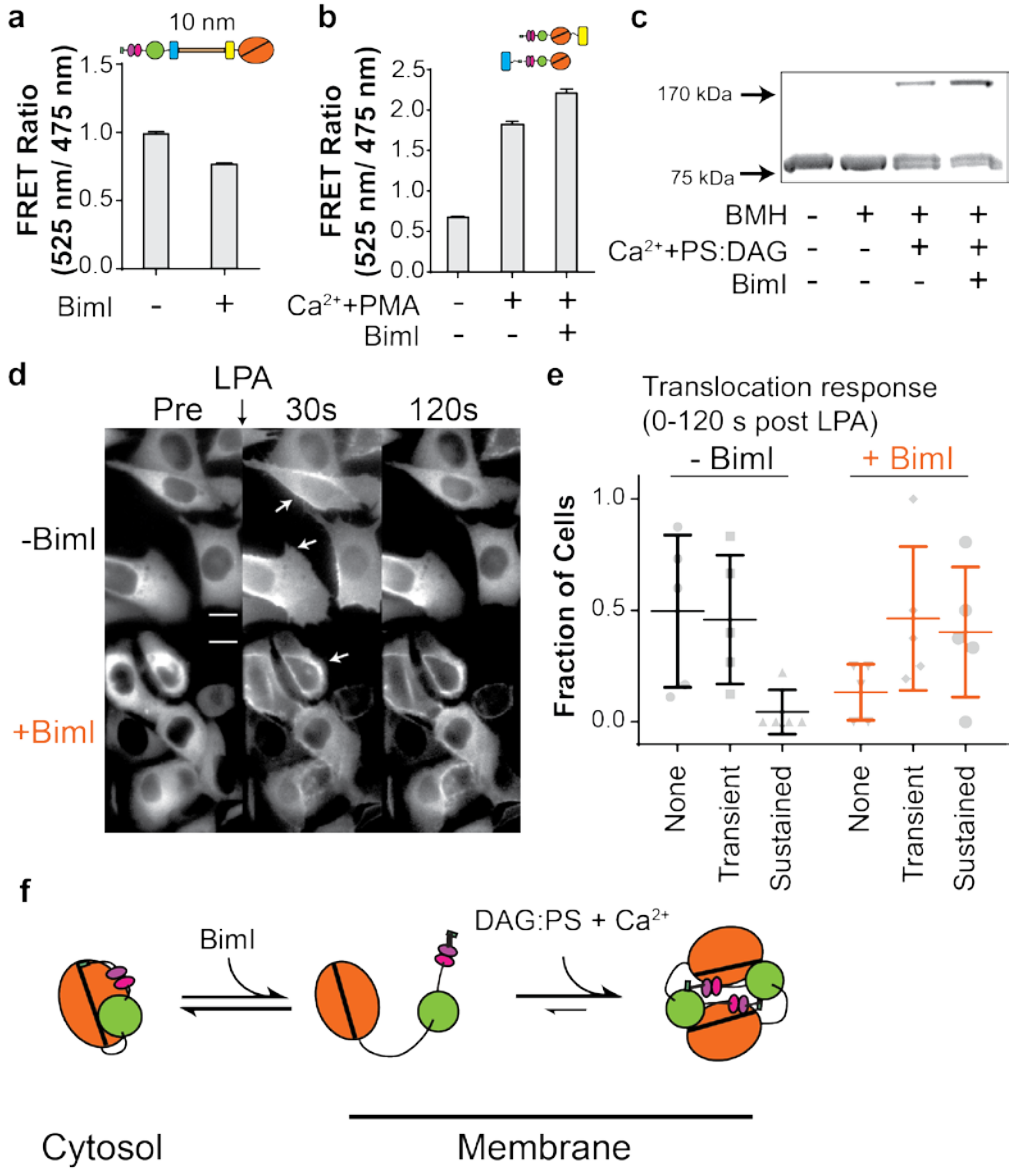

Figure 2.10. Disruption of the auto-inhibited state prolongs translocation. (**a**) BimI (10 μM) destabilizes the auto-inhibited state. FRET ratio in the absence of effectors of sensor with a SPASM module inserted between RD and CD (between E292 and G293). (**b,c**) BimI increases dimer formation following effector stimulation. (b) FRET ratio for mCer-PKCα with PKCα-mCit. (c) Cross-linking analysis of PKCα-FLAG incubated with Ca^{2+} and PMA. (**d,e**) BimI induces sustained translocation of PKCα (d) (Top) Representative images of CHO cells stably expressing mCer-PKCα-mCit pre, 30-, and 120 seconds post LPA (50 μM) stimulation. Two cells with transient translocation are highlighted (white arrows). Translocation is observed as either a ring of high intensity fluorescence, or the appearance of fluorescence along the basolateral membrane of the cell. (Bottom) Representative images with the addition of 1.5 μM BimI two min prior to LPA stimulation. The white arrow highlights a cell with a sustained translocation response. Scale bars = 10 μm. (e) Translocation response in CHO cells stably expressing the mCer-PKCα-mCit sensor in response to LPA stimulation (50 μM) without or with 1.5 μM BimI pretreatment. Cells were binned as no apparent response (None), a transient translocation response (Transient - translocation occurs and recedes within 120s), or a sustained translocation response (Sustained - translocation is still present after 120s). Data points represent five independent experiments ~ 20 cells per experiment. The fraction of the cells binned in each category, for each experiment, is plotted with spread in the data indicated as mean±sem. (**f**) Schematic illustrating the effect of BimI on the three-state equilibrium of PKCα.

2.4 Discussion:

PKC: a conservative and dynamic kinase

The negative consequences of unregulated PKC activity have been apparent since its discovery as the receptor for tumor-producing phorbol esters (38). In the subsequent decades it has been observed that the dysregulation of PKC function is tied with several different pathologies (52-55). Concurrently, multiple distinct mechanisms of auto-inhibition of PKC have been described (18, 42, 56, 57). Collectively these findings portray PKC as a conservative signaling protein that is only capable of functioning under a limited ensemble of conditions. In contrast, an increasing body of evidence positions PKC as a lynchpin in intra-cellular communication in diverse signaling environments (58). The mechanisms allowing PKC to transition from the tightly regulated auto-inhibited state to a catalytically active state, in a dynamic manner, and in the context of multiple signaling inputs have been largely unexplored. In this study, we find that homo-dimerization is an additional regulatory mechanism exploited by PKCα to overcome intramolecular auto-inhibition.

Three state model

Our data confirm previous reports that find a positive correlation between PKC concentration or dimerization and specific activity (11, 20, 35)(Fig. 2.3 c; data not shown). A possible explanation is that inter-molecular interactions in the homo-dimer enhance the catalytic activity of the kinase domain. However, the fully activated homo-dimeric PKC is less active (86%) than just the catalytic domain (Fig. 2.7). Further, varying the fraction of activated PKC in the monomer and dimer states with different length ER/K helices between the RD and CD did not affect specific activity in the presence of effectors (Fig. 2.7). Orthogonally, it was observed that prying open the basal auto-inhibitory interactions using ER/K helices only modestly increased specific activity (Fig. 2.7). These observations lead us to propose a model wherein dimerization acts as a 'mass action sink' by sequestering the regulatory domains away from their autoinhibitory interactions. In our proposed three state model, PKC is in dynamic equilibrium between the autoinhibited state that has no catalytic activity (0 %), the monomeric and non-autoinhibited (open) state that has full catalytic activity (100 %), and the homo-dimeric state that also has full catalytic activity (100 %). In **Fig. 2.11** we use this model to demonstrate how dimerization can influence the specific activity of PKC. Of particular note, in this three state model there are now two largely independent ways in which PKC could be activated; through disruption of the auto-inhibitory interactions (K_{open}) or through stabilization of the homo-dimer (K_{dimer}). Likely, canonical PKC effectors, such as those used in this study, will modulate both equilibrium constants. We postulate that for the nuanced regulation observed in cells,

interactions between PKC and small molecules or proteins may differentially influence these two parameters.

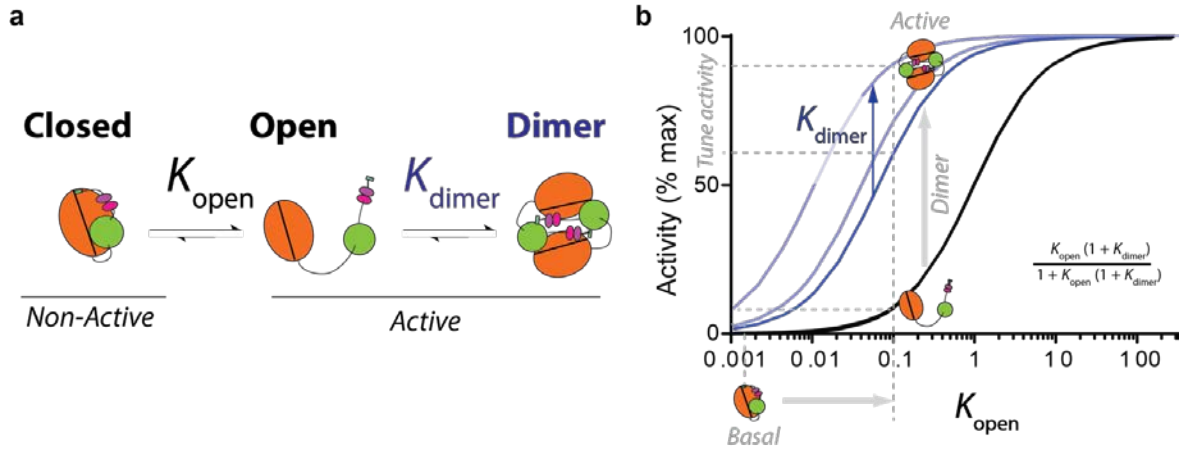

Figure 2.11. Dimerization latches open the stimulated kinase. Dimer formation allows for more specific activity from lower levels of effectors. (**a**) PKC activation is modeled as a three-state (closed, open, or dimer) equilibrium with equilibrium constants K_{open} and K_{dimer}. (**b**) The specific activity of PKC when the closed state is inactive, and both the open and dimer state are fully active, is plotted as a function of opening PKC (↑ K_{open}). For a given potency of effectors in releasing PKC auto-inhibition (defined K_{open}), dimer formation can substantially enhance specific activity. Factors that control dimer formation (K_{dimer}), including local concentration of protein, co-factors, and small molecules can tune local PKC activity over a wide range. The black line represents PKC with no ability to form a dimer, while the blue lines have increasingly higher values of K_{dimer}.

Peptides and small molecules can modulate PKC function through two distinct mechanisms

In this study, we demonstrate the feasibility and physiological significance of peptide and small molecule modulation of intra-molecular interactions in PKC. Two peptides were identified and characterized that selectively disrupt the homo-dimeric state (K_{dimer}) of PKC (Fig. 2.9 a-f). When introduced into a cellular system, both peptides specifically and dramatically reduced the PKC driven downstream phosphorylation of ERK1/2 (Fig. 2.9 g-j). Conversely, we observed that the small molecule PKC inhibitor BimI disrupted the interaction between the auto inhibited and open states (K_{open}; Fig. 2.10 a), which in turn leads to an increase in the homo-dimeric state (Fig. 2.10 b,c). When introduced into a cellular system, BimI was able to alter the translocation response of PKC post LPA stimulation (Fig. 2.10 d,e). These results demonstrate potential approaches for PKC intervention, as well as provide precedence and detailed mechanism for non-canonical PKC regulation that could be utilized in physiological contexts.

Dimeric state versus higher order oligomerization

While the results presented here are consistent with homo-dimerization of PKCα, they do not rule out the formation of higher order oligomers. The FRET measurements do not differentiate between homo-dimers and higher order oligomers. However, the cross-linking studies show a single dominant higher molecular

weight band that is consistent with a dimer. Given that BMH cross-linking is limited to the close proximity (1.3 nm) of two Cysteines, it is possible that higher order oligomers are not efficiently cross-linked, resulting in dimerization as the predominant species detected using this method. With the absence of evidence for higher order oligomerization, we have presented concepts along the lines of the simplest oligomeric state (dimer). Notably, the concept of dimerization sequestering the regulatory domains away from the auto-inhibited state is compatible with higher order oligomerization. In regards to higher order oligomerization, it has been previously reported that PKC as well as certain PKC phosphorylation substrates can drive phase separation on lipid membranes (25). Additionally, the potent PKC activator protamine sulfate has been shown to aggregate PKC in an active state in the absence of additional effectors *in vitro* (59). Further studies are necessary to probe the possibility of higher order PKC oligomerization and its physiological relevance.

Domain:domain interactions in other AGC kinases

Interactions between modular domains are known to broadly regulate AGC kinases. However, none of them have been proposed to utilize the specific mechanism described here. The AGC kinase phosphoinositide-dependent kinase 1 (PDK1) is known to heterodimerize with several AGC kinases including PKCs, AKT, PKN, and S6K through interactions involving the PIF-binding pocket on the PDK1 catalytic domain, and the HM found on the other kinases' C-tail (34). This interaction has been shown to dramatically enhance PDK1 catalytic activity and cellular function (34). In contrast, homo-dimerization facilitated by interactions between the catalytic and PH domains has been speculated to down regulate PDK1 activity in cells (60). In the protein kinase c related protein 2 (PRK2), an inhibitory homo-dimerization occurs between the N-terminal regulatory domains (including a C2 domain) and the catalytic domains (26). The AGC Rho-associated kinase I and II (ROCK I, II) are also observed forming a homodimer between regulatory domains and the C-tail (61). While dimerization of ROCKI does not appear to grossly stimulate or inhibit kinase activity, it does alter enzyme kinetics by lowering the Km of ATP by 60-80 fold (61). Homo-dimeric truncations of ROCKI and II, and subsequently MRCKβ, have been crystalized demonstrating the involvement of the C-tail at the inter-molecular interface (62-64). In PKCζ an inhibitory intra-molecular interaction between the C1 domain and PIF-pocket on the catalytic domain has been previously reported (14). Together these studies suggest that domain:domain interactions in either an inter-molecular or intra-molecular context are common regulatory mechanisms in AGC kinases. Further, they hint at the recurrence of particular domain:domain interactions, such as between the C1 and AGC kinase C-tail domains. Detailed studies in related kinases are necessary to further our understanding of AGC kinase regulation. However, as we report here, the domains involved in auto-inhibitory interactions in PKCα also engage under activated conditions. The conformational

flexibility apparent in multi-domain interactions belies traditional structural approaches including x-ray crystallography and NMR and also complicates insight gained from truncation and site-directed mutagenesis. As such, we propose that the SPASM technique can bridge the gap between our knowledge of modular domain structure and multiplexed cellular function.

2.5 Conclusions:

In this Chapter we have explored the relationship between intramolecular domain interactions and kinase activity in PKCα. We conclude that in the absence of free calcium and liposomes, a relationship between intramolecular interactions between the regulatory domains (PS, C1a, C1b and C2) and the kinase domain and the inhibition of kinase activity exists. This finding is consistent with contemporary models of autoinhibition found in the literature. Surprisingly, in the presence of free calcium and liposomes containing DAG (or soluble DAG analogue PMA) we continue to observe domain-domain interactions between the regulatory domains and the kinase domain. We conclude that under these conditions the domain-domain interactions occur in trans between two or more PKC molecules. In contrast to the basal intra-interaction between the regulatory domains and kinase domain, we conclude that the active inter-interaction has little or no effect on the kinase activity of PKC. We conclude the inter-molecular interaction is still critical for function; the use of pharmacological compounds that disrupt PKC oligomerization and downstream function support this conclusion.

2.6 References:

1. Copley RR, Schultz J, Ponting CP, & Bork P (1999) Protein families in multicellular organisms. *Curr Opin Struct Biol* 9(3):408-415.
2. Lander ES*, et al.* (2001) Initial sequencing and analysis of the human genome. *Nature* 409(6822):860-921.
3. Pawson T & Nash P (2003) Assembly of cell regulatory systems through protein interaction domains. *Science* 300(5618):445-452.
4. Bhattacharyya RP, Remenyi A, Yeh BJ, & Lim WA (2006) Domains, motifs, and scaffolds: the role of modular interactions in the evolution and wiring of cell signaling circuits. *Annual review of biochemistry* 75:655-680.
5. Letunic I, Doerks T, & Bork P (2012) SMART 7: recent updates to the protein domain annotation resource. *Nucleic Acids Res* 40(Database issue):D302-305.
6. Steinberg SF (2008) Structural basis of protein kinase C isoform function. *Physiol Rev* 88(4):1341-1378.
7. Yang Q & Guan KL (2007) Expanding mTOR signaling. *Cell Res* 17(8):666-681.
8. Tesmer JJ (2009) Structure and function of regulator of G protein signaling homology domains. *Prog Mol Biol Transl Sci* 86:75-113.
9. Ritt M, Guan JL, & Sivaramakrishnan S (2013) Visualizing and manipulating focal adhesion kinase regulation in live cells. *J Biol Chem* 288(13):8875-8886.
10. Sivaramakrishnan S & Spudich JA (2011) Systematic control of protein interaction using a modular ER/K alpha-helix linker. *Proc Natl Acad Sci U S A* 108(51):20467-20472.

11. Slater SJ*, et al.* (2002) Regulation of PKC alpha activity by C1-C2 domain interactions. *J Biol Chem* 277(18):15277-15285.
12. Stensman H & Larsson C (2007) Identification of acidic amino acid residues in the protein kinase C alpha V5 domain that contribute to its insensitivity to diacylglycerol. *J Biol Chem* 282(39):28627-28638.
13. Ziemba BP*, et al.* (2014) Single-Molecule Studies Reveal a Hidden Key Step in the Activation Mechanism of Membrane-Bound Protein Kinase C-alpha. *Biochemistry* 53(10):1697-1713.
14. Lopez-Garcia LA*, et al.* (2011) Allosteric regulation of protein kinase PKCzeta by the N-terminal C1 domain and small compounds to the PIF-pocket. *Chem Biol* 18(11):1463-1473.
15. Sivaramakrishnan S, Spink BJ, Sim AY, Doniach S, & Spudich JA (2008) Dynamic charge interactions create surprising rigidity in the ER/K alpha-helical protein motif. *Proc Natl Acad Sci U S A* 105(36):13356-13361.
16. Sivaramakrishnan S*, et al.* (2009) Combining single-molecule optical trapping and small-angle x-ray scattering measurements to compute the persistence length of a protein ER/K alpha-helix. *Biophys J* 97(11):2993-2999.
17. Malik RU*, et al.* (2013) Detection of G protein-selective G protein-coupled receptor (GPCR) conformations in live cells. *J Biol Chem* 288(24):17167-17178.
18. Leonard TA, Rozycki B, Saidi LF, Hummer G, & Hurley JH (2011) Crystal structure and allosteric activation of protein kinase C betaII. *Cell* 144(1):55-66.
19. Violin JD, Zhang J, Tsien RY, & Newton AC (2003) A genetically encoded fluorescent reporter reveals oscillatory phosphorylation by protein kinase C. *J Cell Biol* 161(5):899-909.
20. Huang SM, Leventhal PS, Wiepz GJ, & Bertics PJ (1999) Calcium and phosphatidylserine stimulate the self-association of conventional protein kinase C isoforms. *Biochemistry* 38(37):12020-12027.
21. Giorgione J & Newton AC (2003) Measuring the binding of protein kinase C to sucrose-loaded vesicles. *Methods Mol Biol* 233:105-113.
22. Kirwan AF*, et al.* (2003) Inhibition of protein kinase C catalytic activity by additional regions within the human protein kinase Calpha-regulatory domain lying outside of the pseudosubstrate sequence. *Biochem J* 373(Pt 2):571-581.
23. Braun DC, Garfield SH, & Blumberg PM (2005) Analysis by fluorescence resonance energy transfer of the interaction between ligands and protein kinase Cdelta in the intact cell. *J Biol Chem* 280(9):8164-8171.
24. van Duuren BL, Banerjee S, & Witz G (1976) Fluorescence studies on the interaction of the tumor promoter phorbol myristate acetate and related compounds with rat liver plasma membranes. *Chem Biol Interact* 15(3):233-246.
25. Yang L & Glaser M (1996) Formation of membrane domains during the activation of protein kinase C. *Biochemistry* 35(44):13966-13974.
26. Bauer AF*, et al.* (2012) Regulation of protein kinase C-related protein kinase 2 (PRK2) by an intermolecular PRK2-PRK2 interaction mediated by Its N-terminal domain. *J Biol Chem* 287(24):20590-20602.
27. Mochly-Rosen D & Koshland DE, Jr. (1987) Domain structure and phosphorylation of protein kinase C. *J Biol Chem* 262(5):2291-2297.
28. Walker JM & Sando JJ (1988) Activation of protein kinase C by short chain phosphatidylcholines. *J Biol Chem* 263(10):4537-4540.
29. Flint AJ, Paladini RD, & Koshland DE, Jr. (1990) Autophosphorylation of protein kinase C at three separated regions of its primary sequence. *Science* 249(4967):408-411.
30. Nishizuka Y (1988) The molecular heterogeneity of protein kinase C and its implications for cellular regulation. *Nature* 334(6184):661-665.

31. Yeong SS*, et al.* (2006) The last 10 amino acid residues beyond the hydrophobic motif are critical for the catalytic competence and function of protein kinase Calpha. *J Biol Chem* 281(41):30768-30781.
32. Ni Q, Shaffer J, & Adams JA (2000) Insights into nucleotide binding in protein kinase A using fluorescent adenosine derivatives. *Protein Sci* 9(9):1818-1827.
33. Keshwani MM & Harris TK (2008) Kinetic mechanism of fully activated S6K1 protein kinase. *J Biol Chem* 283(18):11972-11980.
34. Biondi RM*, et al.* (2000) Identification of a pocket in the PDK1 kinase domain that interacts with PIF and the C-terminal residues of PKA. *EMBO J* 19(5):979-988.
35. Sando JJ, Chertihin OI, Owens JM, & Kretsinger RH (1998) Contributions to maxima in protein kinase C activation. *J Biol Chem* 273(51):34022-34027.
36. Raghunath A, Ling M, & Larsson C (2003) The catalytic domain limits the translocation of protein kinase C alpha in response to increases in Ca2+ and diacylglycerol. *Biochem J* 370(Pt 3):901-912.
37. Schmalz D, Hucho F, & Buchner K (1998) Nuclear import of protein kinase C occurs by a mechanism distinct from the mechanism used by proteins with a classical nuclear localization signal. *J Cell Sci* 111 (Pt 13):1823-1830.
38. Castagna M*, et al.* (1982) Direct activation of calcium-activated, phospholipid-dependent protein kinase by tumor-promoting phorbol esters. *J Biol Chem* 257(13):7847-7851.
39. van Corven EJ, Groenink A, Jalink K, Eichholtz T, & Moolenaar WH (1989) Lysophosphatidate-induced cell proliferation: identification and dissection of signaling pathways mediated by G proteins. *Cell* 59(1):45-54.
40. Dubin AE, Herr DR, & Chun J (2010) Diversity of lysophosphatidic acid receptor-mediated intracellular calcium signaling in early cortical neurogenesis. *J Neurosci* 30(21):7300-7309.
41. Pearce LR, Komander D, & Alessi DR (2010) The nuts and bolts of AGC protein kinases. *Nat Rev Mol Cell Biol* 11(1):9-22.
42. House C & Kemp BE (1987) Protein kinase C contains a pseudosubstrate prototope in its regulatory domain. *Science* 238(4834):1726-1728.
43. Kannan N, Haste N, Taylor SS, & Neuwald AF (2007) The hallmark of AGC kinase functional divergence is its C-terminal tail, a cis-acting regulatory module. *Proc Natl Acad Sci U S A* 104(4):1272-1277.
44. Guo B, Reed K, & Parissenti AM (2006) Scanning mutagenesis studies reveal multiple distinct regions within the human protein kinase C alpha regulatory domain important for phorbol ester-dependent activation of the enzyme. *J Mol Biol* 357(3):820-832.
45. Bornancin F & Parker PJ (1997) Phosphorylation of protein kinase C-alpha on serine 657 controls the accumulation of active enzyme and contributes to its phosphatase-resistant state. *J Biol Chem* 272(6):3544-3549.
46. Stensman H, Raghunath A, & Larsson C (2004) Autophosphorylation suppresses whereas kinase inhibition augments the translocation of protein kinase Calpha in response to diacylglycerol. *J Biol Chem* 279(39):40576-40583.
47. Hauge C*, et al.* (2007) Mechanism for activation of the growth factor-activated AGC kinases by turn motif phosphorylation. *EMBO J* 26(9):2251-2261.
48. Grodsky N*, et al.* (2006) Structure of the catalytic domain of human protein kinase C beta II complexed with a bisindolylmaleimide inhibitor. *Biochemistry* 45(47):13970-13981.
49. Dutil EM & Newton AC (2000) Dual role of pseudosubstrate in the coordinated regulation of protein kinase C by phosphorylation and diacylglycerol. *J Biol Chem* 275(14):10697-10701.
50. Roberts PJ & Der CJ (2007) Targeting the Raf-MEK-ERK mitogen-activated protein kinase cascade for the treatment of cancer. *Oncogene* 26(22):3291-3310.

51. Cameron AJ, Escribano C, Saurin AT, Kostelecky B, & Parker PJ (2009) PKC maturation is promoted by nucleotide pocket occupation independently of intrinsic kinase activity. *Nat Struct Mol Biol* 16(6):624-630.
52. Liu Q & Molkentin JD (2011) Protein kinase Calpha as a heart failure therapeutic target. *J Mol Cell Cardiol* 51(4):474-478.
53. Alkon DL, Sun MK, & Nelson TJ (2007) PKC signaling deficits: a mechanistic hypothesis for the origins of Alzheimer's disease. *Trends Pharmacol Sci* 28(2):51-60.
54. Geraldes P & King GL (2010) Activation of protein kinase C isoforms and its impact on diabetic complications. *Circ Res* 106(8):1319-1331.
55. Tam WL*, et al.* (2013) Protein Kinase C alpha Is a Central Signaling Node and Therapeutic Target for Breast Cancer Stem Cells. *Cancer Cell* 24(3):347-364.
56. Kheifets V & Mochly-Rosen D (2007) Insight into intra- and inter-molecular interactions of PKC: design of specific modulators of kinase function. *Pharmacol Res* 55(6):467-476.
57. Oancea E & Meyer T (1998) Protein kinase C as a molecular machine for decoding calcium and diacylglycerol signals. *Cell* 95(3):307-318.
58. Rosse C*, et al.* (2010) PKC and the control of localized signal dynamics. *Nat Rev Mol Cell Biol* 11(2):103-112.
59. Huang KP (1989) The mechanism of protein kinase C activation. *Trends Neurosci* 12(11):425-432.
60. Masters TA*, et al.* (2010) Regulation of 3-phosphoinositide-dependent protein kinase 1 activity by homodimerization in live cells. in *Sci Signal*, p ra78.
61. Doran JD, Liu X, Taslimi P, Saadat A, & Fox T (2004) New insights into the structure-function relationships of Rho-associated kinase: a thermodynamic and hydrodynamic study of the dimer-to-monomer transition and its kinetic implications. *Biochem J* 384(Pt 2):255-262.
62. Jacobs M*, et al.* (2006) The structure of dimeric ROCK I reveals the mechanism for ligand selectivity. *J Biol Chem* 281(1):260-268.
63. Heikkila T*, et al.* (2011) Co-crystal structures of inhibitors with MRCKbeta, a key regulator of tumor cell invasion. *PLoS One* 6(9):e24825.
64. Yamaguchi H, Kasa M, Amano M, Kaibuchi K, & Hakoshima T (2006) Molecular mechanism for the regulation of rho-kinase by dimerization and its inhibition by fasudil. *Structure* 14(3):589-600.

Chapter 3: Protein Kinase C α self-assembles in parallel with activation

This chapter has been adapted from the following publication currently in revision:

Swanson, C.J., Sommese, R., Petersen, K.J., Ritt, M., Karslake, J., Thomas, D.D., Sivaramakrishnan, S. (2016) Protein kinase C α self-assembles in parallel with activation, PLoS One (*in revision*).

3.1 Introduction:

Signal transduction in cells emerges from transient protein interactions that occur in a highly crowded cytoplasmic environment (1, 2). Pairing of signaling input and output is often achieved by compartmentalization of molecules on a membrane or protein scaffold (3). An orthogonal mechanism for segregating molecular components involves the self-assembly of macro-scale complexes nucleated by one or more proteins (4). While such self-assembled macro-molecular complexes are fairly common in cellular processes such as vesicle trafficking (5), cytoskeletal organization (6), and cell division (7) they are much less appreciated in the context of cell signaling and form the focus of this study.

The PKC family of protein kinases functions as a nodal regulator in signaling networks (8). PKCs function at multiple locations within the cell and tune their function to couple diverse stimuli to distinct outputs (9). The diversity of PKC function is achieved, in part, by a series of modular domains linked to the conserved catalytic domain. These modular domains render the PKC sensitive to different factors. For instance the C2 domain in PKC binds Ca^{2+} ions, phosphatidylserine (PS) and $PI(4,5)P_2$, whereas the C1 domains bind diacylglycerol (DAG), and the catalytic domain binds nucleotides and phosphosubstrates (8). Several researchers have documented the focal accumulation of fluorescently labeled PKCs in response to distinct stimuli and have suggested this as a mechanism to localize and multiplex PKC function in response to

different inputs (10-13). The molecular mechanisms driving these events and the underlying biomolecules that lead to PKC 'clustering' remain unknown. Here, we test the hypothesis that interactions between the modular domains of PKC are necessary and sufficient to drive self-assembly of PKC into clusters without the need for membrane scaffolds or other regulatory co-factors.

In this study, we report that PKCα readily self-assembles into large clusters *in vitro* in the presence of calcium. Self-assembly of PKCα is reversible, it occurs at calcium concentrations consistent with reported Ca^{2+}- C2 domain binding and is abolished by a single point-mutation in the C2 domain. Endogenous PKCα in HEK lysates differentially fractionates in the presence of calcium consistent with self-assembly. While C2 domain proteins are known to oligomerize, we find that PKCα clustering requires at least the C1 and C2 domains. Cluster size and number can be modulated by the strength of the C1a-C2 interaction suggesting a mechanism to regulate this phenomenon. Sensors encoding only the C1a and C2 domains are capable of self-association in live cells in response to the calcium influx following ionomycin treatment. In contrast, both ionomycin and PMA are required to observe self-association in full length PKCα in live cells. The degree of self-association correlates positively with specific activity of PKCα suggesting that clustering occurs in parallel with the sequence of events leading to kinase activation.

3.2 Materials and methods:

Fluorescence coverslip assay: All experiments contained 200 nM of PKCα-mCit incubated at 25 ⁰ C unless otherwise stated. For calcium cycling experiments, an aliquot of stock sample was incubated at a final free calcium concentration to 300 μM for 10 min. A small amount was removed for imaging, and the rest was incubated with saturating EGTA for 10 min. Again a small amount was removed for imaging. For imaging, each sample was then gently sandwiched between an ethanol cleaned slide and coverslip and sealed by valap (vasoline/lanolin/paraffin). Slides were imaged on a Nikon TiE equipped with a mercury arc lamp, a yellow GFP filter cube (Nikon; 500/20 nm excitation, 515 nm LP, 535/30 nm emission), perfect focus system (Nikon), a 100X 1.4 NA Plan-Apo oil-immersion objective (Nikon), Evolve EMCCD camera (Photometrics), and the Nikon NIS-elements software. Image planes were focused on the coverslip surface and ND filters and exposure time were adjusted to avoid saturation before

being fixed for all slides in the matched experiment. Stage translation was performed with the shutter in to avoid field of view bias and images were taken at 5 – 15 locations per slide. The free calcium concentration was assessed using MAXCHELATOR (http://maxchelator.stanford.edu/CaEGTA-TS.html).

Differential fractionation: The indicated protein (300 nM) was fractionated with a 30 min spin at 2.8 x 10^5 rcf at 22° C. The supernatant was separated, and the ′pellet′ fraction was resuspended by pipetting in an equal volume of matched buffer. An equal volume aliquot was retained from each fraction for subsequent analysis, and the supernatant fraction was brought to a free calcium concentration of 300 µM and incubated at 22° C for 10 min before a second fractionation (30 min, 2.8 x 10^5 rcf at 22° C). Following fractionation, the supernatant was separated, and the pellet fraction was resuspended in an equal volume of matched buffer without free calcium. Aliquots were retained, and the pellet was adjusted for a final EGTA concentration of 700 µM and incubated for 10 min at 22° C. A third fractionation was performed with matched conditions (30 min, 2.8 x 10^5 rcf at 22° C). All aliquots were separated on an SDS-PAGE, and for the PKC α-mCit-FLAG experiment visualized by mCit fluorescence (Typhoon imager, GE Life Sciences), and the PKCα-FLAG transferred and probed with a PKCα specific antibody (see next section for Western analysis). Fractionation was quantified in ImageJ by manually selecting regions, subtracting backgrounds and comparing the band intensities in the pellet and supernatant fractions.

HEK lysate experiment: HEK cells were trypsinized and resuspended in DMEM containing 10% FBS (Invitrogen) and Glutamax (GIBCO) and pelleted by low speed centrifugation (250 rcf) at 22° C. The cells were resuspended in (~ 5 fold dilution) in working buffer containing 5 µg/ml Aprotinin, 5 µg/ml Leupeptin, 50 µg/ml phenylmethylsulfonyl fluoride, 2 mM dithiothreitol pH 7.5, and rotated (all subsequent steps at 4° C) for 20 min before mechanical lysis with a 26 gauge 1 ml syringe. The lysate was spun at 2.8 x 10^5 rcf for 30 min and the soluble fraction (clarified lysate) was immediately separated from the pellet fraction. The clarified lysate was treated with 800 µM of EGTA or $CaCl_2$ incubated for 3 min and fractionated (2.8 x 10^5 rcf for 30 min). The supernatant was removed and the pelleted fraction was resuspended in matching buffer and

volume as the supernatant. Samples were separated on 10% SDS-PAGE before being transferred to PVDF membrane for 3 h at 300 mA. Blots were blocked with 2% BSA/TBS + 0.1% Tween (TBST) for 1 h at room temperature. Primary PKCα antibody (sc-8393, Santa Cruz Biotechnology, 1:10,000) was added and incubated overnight at 4° C. Blots were washed with TBST and incubated for 1 h with secondary (goat anti-Rabbit - Jackson ImmunoResearch Labratories, Inc., 1:10,000 in 2% BSA/TBST). Blots were washed with TBST, developed with Immobilin Western chemiluminescent HRP substrate (Millipore), and imaged with ChemiDoc-it imaging system (UVP). Silver-stain analysis performed according to manufacturer's protocol (Pierce).

Dynamic Light scattering: DLS data was collected on a DynaPro NanoStar (Wyatt Technology) at 25° C. Protein (1 µM) was in standard HEPES buffer with no BSA added. Sequentially the buffer was brought to a final concentration of 800 µM $CaCl_2$ and 1 mM EGTA using concentrated stocks at 2.5% of the final volume. Each autocorrelation is the mean of 10 repetitive readings of 10s each, and error bars represent the mean and standard deviation of 3 independent readings. Autocorrelation data were least squares fit to a single exponential decay function (GraphPad) to obtain τ values. Additionally, the regularization and cumulant fits where performed using the Wyatt Technology software platform (Dynamics V7.1.7) utilizing the isotropic spheres model. The mean of the monomer peak was obtained by averaging the MW from each acquisition from 3 batches of protein. The particle mass was determined by a single cumulant fit, and each reading was normalized by the mean of the initial EGTA buffered condition.

Time-resolved fluorescence anisotropy: We performed and analyzed time-resolved fluorescence anisotropy of mCitrene data using time-correlated single photon counting (TCSPC) and direct waveform recording (DWR) methods as described previously (14, 15). A 480 nm laser line with 515 nm LP was used in TCSPC experiments and a 532 nm laser line with 570 nm LP was used for DWR experiments. All time-resolved experiments started with 500 nM of protein, and sequential polarized measurements of 0^o, 54.7^o and 90^o were recorded for each condition. Using analysis software described previously (16) the single exponential fluorescence lifetime (τ) was first assessed using fluorescent recordings obtained at 54.7^o. Subsequently the fluorescence data at 0^o and 90^o were fit to a 2 exponential decay function using a fixed τ value. Steady-state

anisotropies were calculated as the weighted average of the fluorescence anisotropy (r) decay given by the best-fit model parameters:

$$(1)\ r = \frac{\int_0^\infty r(t)F(t)dt}{\int_0^\infty F(t)\,dt} = r_0\left(\chi_1\frac{\phi_1}{\phi_1+\tau} + (1-\chi_1)\frac{\phi_2}{\phi_2+\tau}\right)$$

where r_0 is the initial anisotropy, ϕ_1, ϕ_2 are the correlation times, χ_1 is the fractional contribution to the anisotropy decay, τ is the fluorescence lifetime, and the final anisotropy is assumed to be zero.

Mammalian cell imaging: CHO Flp-in cells were cultured as previously described (17). Cells were transiently transfected with indicated constructs using X-tremeGENE Hifi (Roche). Cells were transferred to fibronectin (Sigma-Aldrich) coated (1:100 dilution incubated for 1 hr) glass bottom 35 mm tissue culture plates (MatTek Corp.) 24 – 48 h post transfection as previously described. Cells were allowed to adhere for 1 - 4 h in culturing media before cells were imaged. Cells were washed and resuspended (500 µl) in freshly prepared HBS (20 mM HEPES, 5mM KCl, 45mM NaCl, 2mM $CaCl_2$, 1mM $MgCl_2$, 0.2% dextrose, brought to pH 7.4 by NaOH) media. The plates were transferred to the scope and a field of view was manually selected guided by fluorescence expression and morphology of cells. Cells were exposed every 500 ms over a 5 min time course. Either a 2x stock of ionomycin or a concentrated stock of EGTA in matched buffer was manually pipetted onto the culture plate during imaging at predetermined time points. Experiments were performed at 22° C. Anisotropy image data was analyzed with custom MatLab code. Both polarized images per frame were registered using the imregister MatLab function. A background region is manually selected, and the mean of the background in each polarization channel is subtracted from the corresponding image. The anisotropy value r is calculated using the parallel and perpendicular pixel intensities corrected for the G factor:

$$(2)\ r = \frac{I_\parallel - G\cdot I_\perp}{I_\parallel + 2G\cdot I_\perp}$$

Anisotropy values above and below theoretical limits are excluded and a mean of all anisotropy values are calculated for each image in the series. For representative images the images were cropped, median filtered and the 'Fire' look up table was applied (ImageJ). The correlation coefficient was calculated in the same custom MatLab code as the anisotropy analysis. Following

registration and background subtraction, an image of the total intensity ($I_{\parallel} + 2G \cdot I_{\perp}$) was generated. The corrcoef function was applied between each frame and the first frame. Translocation in this metric is defined by a redistribution of fluorescence intensity within the cell.

3.3 Results:

3.3.1 Calcium induced self-assembly in vitro

Self-assembly is specific and reversible

Previous work from Huang et al suggested that both calcium and phosphatidylserine were necessary for PKCα self-assembly (18). In contrast, our previous study observed that calcium alone was sufficient for PKCα self-assembly, albeit at an attenuated level (17). Both of these studies used chemical cross-linking to assess self-assembly, which may be dependent on conformational states of the protein and bias the conclusions. We chose to re-address whether PKCα self-assembles in the presence of calcium using techniques based on the size of particles including differential sedimentation (**Fig. 3.1 a**), dynamic light scattering (DLS) (**Fig. 3.1 b**), single-particle fluorescence microscopy (**Fig. 3.1 c**) and size-exclusion chromatography (SEC) (**Appendix B.1**). Where possible, PKCα self-assembly was assessed without a fluorophore (Fig 3.1 b,c), and in all cases constructs with fluorophores utilized the monomeric versions of Cerulean and Citrine (mCer and mCit respectively). Overall, each methodology supports our conclusion that PKCα specifically and reversibly oligomerizes in the presence of free calcium. When Ca^{2+} ion coordination is blocked by introducing the D246N point mutation in the C2 domain (19), this self-assembly is inhibited (Fig 3.1 b, Fig. B.1). Additionally, cycling PKCα between low (< 1 nM) and high (>100 μM) free calcium conditions demonstrates that the phenomenon is partially reversible. Interestingly, the oligomers have several unexpected characteristics. Notably, they are much larger than the previously reported homo-dimers (17, 18). Following a 30 min incubation in high free calcium conditions, SEC analysis indicates that oligomers are at least 10-fold larger than monomers (**Appendix B**), and DLS analysis supports a mean increase in particle size of ~13-fold (**Appendix B, Fig. B.2**). Second, the number of oligomers, their size, and the fraction of PKCα molecules oligomerized are time- and concentration- dependent. This result is most evident in quantitative analysis of single-particle

fluorescence microscopy (**Appendix B, Fig. B.3**). We tested if oligomerization is observable when using physiologically relevant free calcium concentrations (<10 μM)(20). PKCα oligomerization was monitored as a function of free calcium concentration by differential sedimentation and single-particle fluorescence microscopy. In both cases, oligomerization fit well to single-phase binding curves with K_D values falling within physiologically relevant ranges (K_D = 1.6 ± 0.3 μM by microscopy, K_D = 0.32 ± 0.26 μM by sedimentation) (**Fig. 3.1 d**).

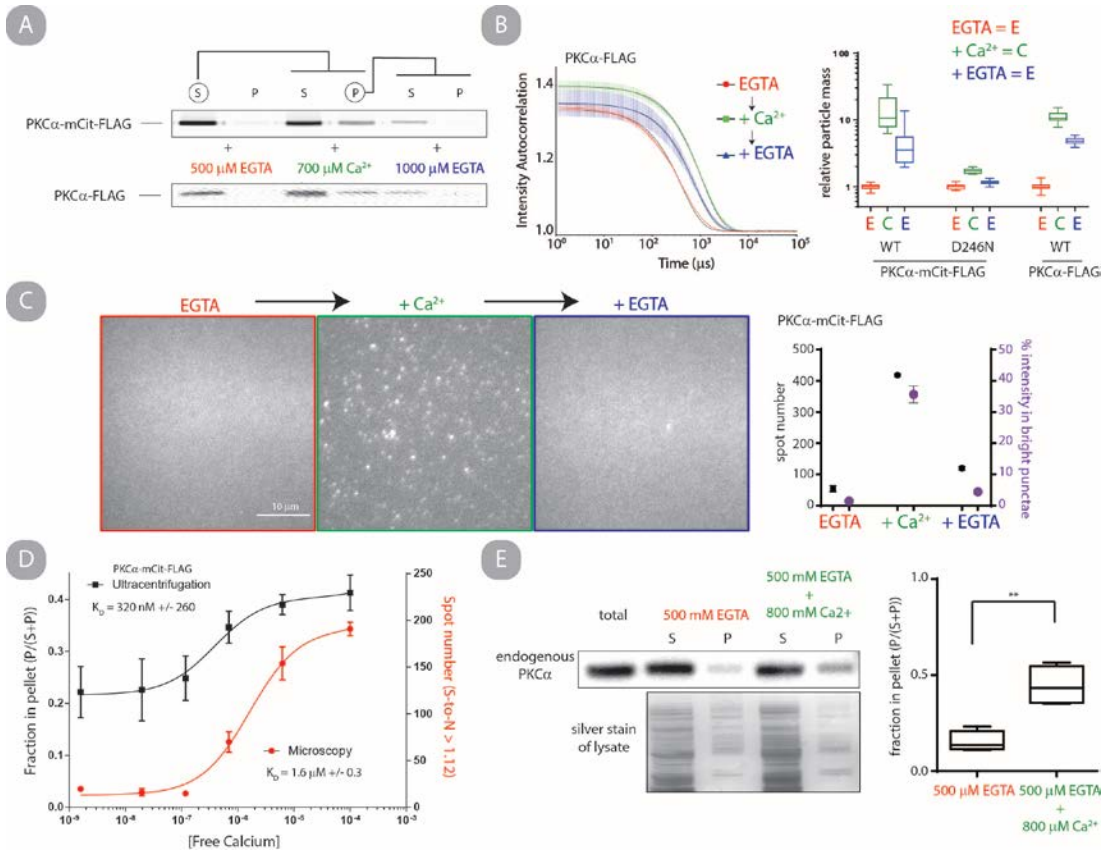

Figure 3.1. Calcium induces reversible self-assembly of PKCα *in vitro*. (**a**) Recombinant PKCα-mCit-FLAG or PKCα-FLAG (300 nM) was differentially fractionated into soluble (S) and pellet (P) fractions following high speed centrifugation in two independently performed experiments. Fractionation occurred sequentially in indicated buffers, where the fractions circled were retained. Fractions were separated on SDS-PAGE and probed with mCit fluorescence (top) or an anti-PKCα antibody (bottom). (**b**) Intensity autocorrelation of dynamic light scattering (DLS) of recombinant PKCα-FLAG (1 μM) sequentially diluted into buffers containing excess EGTA, free calcium, and EGTA with 15 min incubation between readings. Black line is a single exponential fit, and error bars are s.e.m. of 3 independent readings (left). Quantification of the ensemble particle mass normalized to the initial condition of indicated protein from DLS (Right; n ≥ 8, box-and-whisker represents min, max, 25 and 75 percentile and median). (**c**) Representative fluorescent images of recombinant PKCα-mCit-FLAG (200 nM) sequentially in indicated buffer non-specifically adhered to a glass coverslip. Samples were incubated in buffers for 10 minutes at 22° C before being adhered to slides. (left) Bright spots were identified when the ratio of mCit intensity deviates by >1.12 from the neighboring pixels. Data was quantified from 6 fields of view for each condition (right). (**d**) Differential sedimentation and spot number on coverslips were assessed as a function of free calcium concentration. The data are least squares fit to a single binding function (solid lines). Error bars represent standard deviation (n = 3 differential sedimentation and n = 5 microscopy). (**e**) Representative blot and quantification of differential fractionation of endogenous PKCα in 5x diluted HEK cell lysate (detergent free) probed with anti-PKCα antibody and corresponding silver stain (left) and quantified (Right; n = 4; min, max, 25 and 75 percentile and median; ** indicates a student's t-test with a p-value of 0.0023).

Endogenous mammalian PKCα self-assembles

All of the above experiments used recombinant human PKCα minimally fused with a C-terminal FLAG peptide tag. To assess whether the observed self-assembly was an artifact of either Sf9 expression or the FLAG tag, endogenous mammalian expressed PKCα was assessed for differential sedimentation. Clarified HEK293 cell lysate was fractionated with either high free calcium or EGTA and PKCα was probed with a PKCα specific monoclonal antibody **(Fig. 3.1 e)**. A significantly larger fraction of endogenous PKCα pelleted in the presence of free calcium.

3.3.2 C1a and C2 domains are minimally sufficient for calcium induced self-assembly

The C2 domain is not sufficient for self-assembly

There have been several suggestions in the literature that suggested the C2 domain is responsible for oligomerization (21-26). To determine the minimal domains required for oligomerization, we created a series of PKCα sensors containing an N-terminal mCerulean and a C-terminal mCitrine. In each sensor, we inserted a tobacco etch virus protease (TEV protease) site between either the V1 and C1a domains, the C1b and C2 domains, or the C2 and the kinase domains. Following TEV proteolysis, we could then identify whether PKCα sensors tagged with the N-terminal, C-terminal, both, or neither fluorescent protein oligomerize in the presence of high free calcium. The purpose of this experiment is to identify polypeptide regions that are sufficient to oligomerize. By fluorescent microscopy, neither the V1 nor the kinase domain was necessary for punctae formation. However, separation of the C1 and C2 domains significantly reduced oligomerization **(Fig. B.4 a-b)**. We next assessed the fusion protein with the TEV protease site between the C2 and kinase domains by DLS along with a C2-mCit fusion protein. We pre-treated the construct with TEV protease or bovine serum albumin (BSA), and then measured the relative increase in particle size following a 2 min incubation with free calcium. The three conditions correspond to the panels represented as full-length, regulatory domains or C2 domain **(Fig. 3.2 a)**. The intact PKCα sensor has a mean particle size increase of 5.61 ± 0.31 compared to 2.61 ± 0.25 for the regulatory domains alone and 1.40 ± 0.06 for the C2 domain alone. Collectively, these data indicate that both the C1 and C2 domains are required to be in the same peptide for self-assembly.

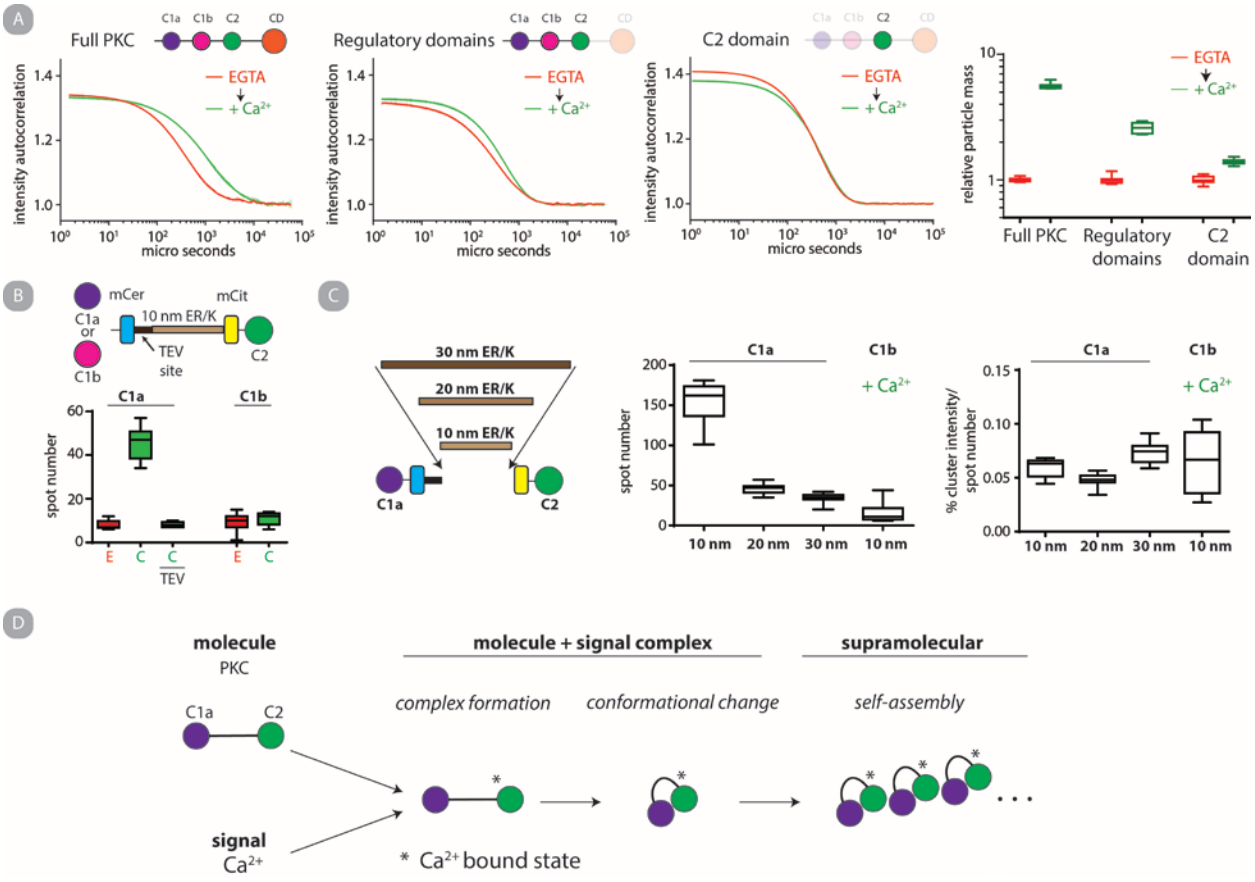

Figure 3.2. The C1a and C2 domains are minimally sufficient for self-assembly. (**a**) Mean DLS autocorrelation data before (red) or after addition of free calcium (green) of full length PKCα (left), the regulatory domains (middle), and C2 domain (right) at matched time points (2 min incubation) and concentration. Normalized particle mass is quantified at the far right. (**b**) A biosensor schematically depicted on top containing the C1a and C2 but not C1b and C2 forms punctae on glass coverslips in the presence of free calcium. The response is abrogated with pretreatment of the biosensor with TEV protease. Data from 6 fields of view per condition. (**c**) C1a-C2 biosensors with 3 lengths of ER/K linkers are assessed for punctae formation on glass coverslips all in the presence of free calcium, data from ≥ 10 fields of view per condition. The longer length linkers systematically reduced punctae formation (middle) with no systematic effect on the relative intensity of punctae (right). (**d**) A model of calcium induced self-assembly of PKCα domains wherein calcium binds the C2 domain, a conformational change results in a C1a·C2 interaction which is the minimal unit for self-assembly. As self-assembly i) progresses over time up to at least 3hrs (**Appendix 2 Fig. 3**) and ii) is reversible in the absence of free calcium (Fig. 3.1 a,b,c) this process is likely far from equilibrium in all experiments. This model is depicted to draw parallels with early schematics of supra-molecular chemistry (27). All box and whisker plots represent min, max, 25 and 75 percentile and median.

C1a and C2 domains self-assemble

There have been several suggestions in the literature that the C2 domain interacts with one or both of the C1 domains (28, 29). We built two sensors containing the C2 domain and either the C1a or C1b domains separated by a 10 nm SPASM cassette (30). By fluorescence microscopy, we found that only the sensor containing the C1a and C2 domains formed punctae in the presence of free calcium. Further, when the C1a-SPASM-C2 protein was cleaved by TEV protease, neither the C1a domain nor the C2 domain peptide formed punctae **(Fig. 3.2 b)**. From

these results, we hypothesize that an *inter*molecular interaction between C1a and C2 domain is required for self-assembly. To test this hypothesis, we built two additional sensors in which 20 nm and 30 nm SPASM cassettes were fused between the C1a and C2 domains. The SPASM cassettes have fully extended α-helices with lengths of 10, 20 and 30 nm and are designed, through spontaneous helix breaking, to have *intra*-molecular effective concentrations of 4 μM, 0.4 μM and 0.1 μM respectively(30). As expected if a C1a·C2 complex is necessary for self-assembly, increasing the helix length decreased the number of fluorescent punctae without affecting the average intensity of punctae **(Fig. 3.2 c)**. As our SPASM cassettes also contained a mCitrine and a mCerulean, we were able to monitor an interaction between the C1a and C2 domains by hetero-FRET. We found that hetero-FRET in our C1a-C2 sensors increased with the presence of calcium, and that this increase is also dependent on linker length and concentration **(Fig. B.5, Appendix B.2)**. Finally, the concentration-dependent change in hetero-FRET is fit well by a Hill binding model, providing a half-maximal value of 61.1 ± 1.2 nM (best fit and standard error), which serves as an estimate of the free in solution equilibrium dissociation constant **(Fig. B.5 c)**. From these data we propose a model in which (*i*) the C1a and C2 domains are the minimal unit required for self-assembly and *(ii*) an intra-molecular C1a·C2 interaction is required for self-assembly **(Fig. 3.2 d)**.

3.3.3 Monitoring PKCα self-assembly by homo-FRET

In vitro *characterization*

As hetero-FRET is sensitive to both *intra*- and *inter*-molecular interactions in our sensors, we used homo-FRET of mCit to specifically report inter-molecular contributions. Homo-FRET in fluorescent proteins is assessed by the fast ($\tau < 1$ ns) depolarization of fluorescence, whereas in the absence of FRET only depolarization on the time scale of rotational diffusion will be observed ($\tau \sim 15$ ns)(31, 32). Using time-correlated single photon counting (TCSPC) and direct waveform recording (DWR) (14) we can monitor anisotropy up to 15 ns after an excitation pulse is applied to a sample. This time-resolved anisotropy can be used to differentiate between the two modes of depolarization and detect contributions from homo-FRET.

We assessed PKCα-mCit, PKCα-mCit + liposomes, mCit-PKCα, and C1a -10 nm SPASM- C2 with and without free calcium. In the PKCα-mCit + liposomes as well as the C1a-10 nm

SPASM-C2 conditions, the addition of free calcium clearly results in a fast depolarization consistent with homo-FRET **(Fig. 3.3 a; Table 3.1**). However, we do not observe homo-FRET for PKCα-mCit or mCit-PKCα in the absence of liposome (**Fig. B.6; Table 3.1**). The time-resolved anisotropy results were converted to steady-state anisotropy values by fluorescence lifetime-weighted averaging of the best-fit correlation times. Orthogonally, the actual steady-state anisotropy was measured for the corresponding conditions. We find good agreement between the two values and note that depolarization due to homo-FRET results in a lower steady-state anisotropy value as expected **(Fig. 3.3 a)**. We use this finding to justify the use of steady-state anisotropy measurements to assess homo-FRET in subsequent *in vitro* and cellular experiments.

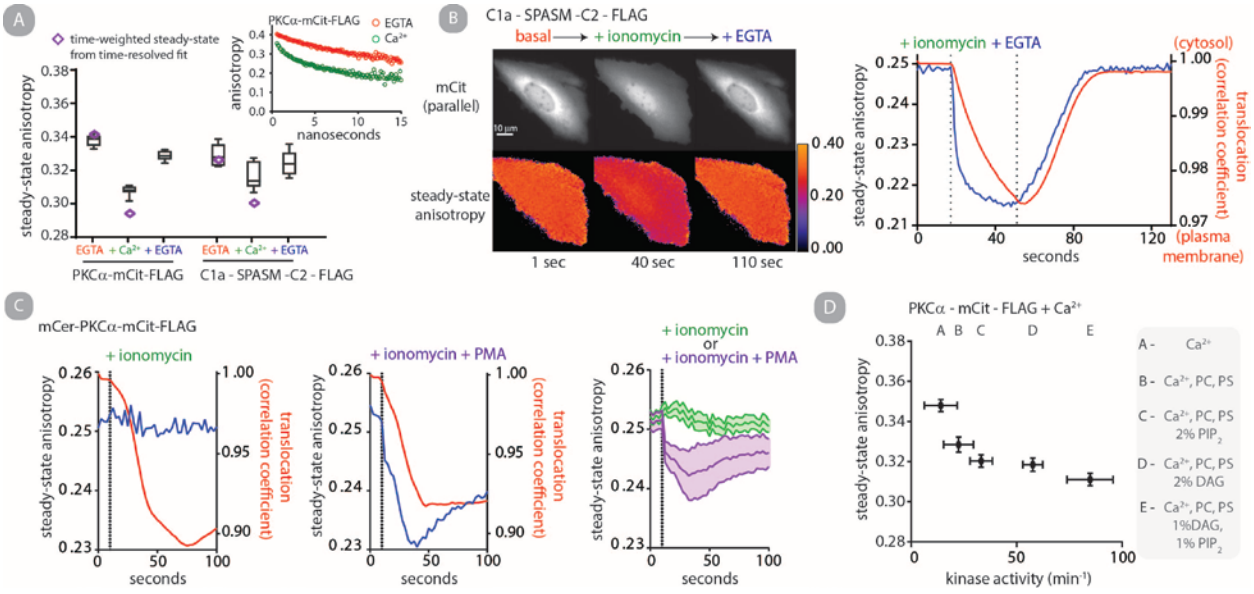

Figure 3.3. Homo-FRET distinguishes functional states of PKCα in cells. Fluorescence anisotropy can be used to monitor homo-FRET (EM-FRET). A characteristic feature of homo-FRET in fluorescent proteins is a depolarization of fluorescence on the time scale of energy migration (10^{-10} – 10^{-9} seconds) in addition to depolarization occurring from rotational diffusion (tau > 10^{-8} seconds). (**a**) Steady-state fluorescence anisotropy of mCit in C1a-SPASM-C2 and PKCα-mCit + liposomes as the protein is sequentially treated with excess EGTA, free calcium and EGTA (N = 16 for steady state measurements). The purple diamonds are simulated steady-state anisotropy values derived from a two-exponential fit of direct waveform recording (DWR) time-resolved anisotropy measurements. The inset shows observed anisotropy obtained by TCSPC of PKCα-mCit-FLAG plus liposomes with and without free calcium. The unilaminar liposome contained 88%PC:10%PS:2%DAG (molar %; PS to PKC molar ratio 32:1). (**b**) Representative polarized fluorescence intensity and anisotropy heat-map of a CHO cell transiently expressing C1a-SPASM-C2 in a buffer containing 2mM $CaCl_2$ basally, after perfusion with 1 µM ionomycin, and after perfusion with excess extracellular EGTA (scale bar is 10 µm). At right is the corresponding quantitation of the mean anisotropy (blue) and translocation (red). (**c**) Representative anisotropy and translocation coefficients of individual CHO cells transiently expressing mCer-PKCα-mCit following perfusion of 1 µM ionomycin (left) or 1 µM ionomycin + 1 µM PMA (middle) and mean and s.e.m. (right) of corresponding steady-state anisotropy measurements (n = 7 cells ionomycin and n = 4 cells ionomycin + PMA). (**d**) PKCα-mCit-FLAG + liposomes with various molar percentages of known PKC activators were assessed for catalytic activity and steady-state anisotropy in the presence of 300 µM free Ca^{2+} (mean and standard deviation of N = 12 anisotropy measurements, and N = 7 kinase activity reactions).

Self-assembly in cells

To examine self-assembly in cells, we first examined the steady-state fluorescence anisotropy of the C1a – 10 nm SPASM –C2 construct transiently expressed in CHO cells. We monitored single cells in an extracellular media containing 2 mM $CaCl_2$ and sequentially perfused the open chamber with a buffer containing the Ca^{2+} ionophore ionomycin, followed by a concentrated solution of EGTA. As anticipated with a construct containing the C2 domain, fluorescence accumulated at the plasma membrane following ionomycin treatment and returned to its basal state following EGTA treatment (**Fig. 3.3 b, Fig. B.7 b**). We concomitantly monitored fluorescence anisotropy and observed a dramatic decrease following ionomycin treatment which resolves to basal levels following EGTA perfusion. These cellular data are consistent with reversible oligomerization of C1a – 10 nm SPASM –C2 in the presence of cytosolic free calcium.

We performed similar cellular experiments monitoring steady-state mCit anisotropy of mCer-PKCα-mCit. We observed that despite translocation occurring, ionomycin treatment alone did not result in a change in steady-state anisotropy **(Fig. 3.3 c, Fig. B.7)**. However, if the cells were perfused with ionomycin and phorbol myristate acetate (PMA), anisotropy decreased concomitant with translocation. This finding is in agreement with our *in vitro* results that homo-FRET is only observed for full length PKCα if both free calcium and a liposome containing PS and DAG is present, where PMA is used to mimic the effect of DAG on PKC in cells.

Catalytic activity is correlated with PKCα clustering

Finally, we assessed both catalytic activity and homo-FRET under different activation conditions. The effects of lipid composition on PKCα steady-state catalytic activity are well documented (33). Recent reports have demonstrated that $PI(4,5)P_2$ i.) is a potent activator of PKCα *in vitro* (34), ii.) forms clusters in liposomes in the presence of free calcium (35) and, iii.) induces clustering of PS if calcium and PKCα C2 domain are present (which binds both PS and $PI(4,5)P_2$) (21). The latter two observations suggest that $PI(4,5)P_2$ induce clustering of PKCα independently of a C1a-C2 interaction. We confirm this by monitoring steady-state anisotropy of the C2 domain alone as well as full-length PKCα with point mutations disrupting the $PI(4,5)P_2$ binding pocket (**Fig. B.8**). We observe homo-FRET from the C2 domain alone only when

$PI(4,5)P_2$ is present, whereas homo-FRET is observed with full length PKCα even when $PI(4,5)P_2$ is absent. We then compared the steady-state anisotropy and specific catalytic activities for five activating conditions all in the presence of free calcium. We observed a negative nonlinear correlation between the two outputs (**Fig. 3.3 d**). This result suggests that, independent of how PKC is clustered, clustering promotes higher ensemble catalytic activity.

3.4 Discussion:

Unlike many AGC kinases, PKCα is constitutively 'primed' through phosphorylation of regulatory sites in its C-tail. Hence, rather than its phosphorylation state, membrane localization of PKC has been used to evaluate cellular activation. Spatial temporal localization alone does not address how a diversity of regulatory inputs (calcium, diacylglycerol, phospholipids) influences the functional state of PKCα. Here, we identify PKC self-assembly as a new dimension along which to view PKC function. We find that different second messenger combinations that activate PKC also modulate the extent of PKC self-assembly as measured by changes in steady-state fluorescence anisotropy. Further, anisotropy of PKC is correlated with kinase specific activity, suggesting that self-assembly can serve as a measure for the PKC activity state in cells. Interestingly, the steps identified in PKCα self-assembly parallel the sequence of events leading to PKC activation in cells. Specifically, (*i*) intra-cellular calcium binds to the C2 domain of cPKC leading to its translocation to the plasma membrane, where (*ii*) the C1 and C2 domains interact with phospholipids such as $PI(4,5)P_2$ and diacylglycerol to (*iii*) release an auto-inhibitory interaction and activate the kinase. By comparison, we find that (*i*) calcium stimulates PKC self-assembly through the C2 domain; (*ii*) the C1a-C2 interaction is necessary and sufficient for the growth of PKC clusters; and (*iii*) greater self-assembly correlates with enhanced PKC activity. If the PKC catalytic activity were only dependent on the conformation of PKC, we would not expect it to change with time. Instead, we observe that PKC clusters grow with time *in vitro* (Fig. B.3), suggesting that through self-assembly PKC satisfies the properties of a 'supra-molecule' that can integrate different signals by altering its assembly state (27).

Several lines of evidence in the literature suggest that the C2 domain is sufficient for self-assembly. First, the C2 domain of PKCβII was observed forming a homo-dimer in the asymmetric unit of a crystal structure (22). Most studies suggest that one or two Ca^{2+} ions bind

the C2 domain under physiological conditions, but a third Ca^{2+} ion may bind at very high free calcium concentrations. In this crystal structure it was the third Ca^{2+} ion that directly bridged the two C2 domains. However, mutagenesis of residues coordinating only the third Ca^{2+} ion (T250A and T251A) had no effect on self-assembly in our experiments. Second, we found reports of C2 domains in 4 classes of proteins that appear to mediate oligomerization through different mechanisms (23-26). However, no clustering of the PKCα C2 domain alone was observed in any of our assays. Third, a previous study found clustering of phosphatidylserine (PS) on liposomes containing $PI(4,5)P_2$ in the presence of both calcium and the PKCα C2 domain. Accordingly, we did observe clustering of the C2 domain by homo-FRET in the presence of liposomes containing $PI(4,5)P_2$. However, given that C2 by itself does not form clusters in solution in the presence of calcium, this phenomenon is restricted to lipid membranes with $PI(4,5)P_2$. Nonetheless, our measurements show that both the C1a and C2 domains together are minimally sufficient to form clusters in the presence of calcium alone. Given that these domains respond to distinct stimuli (C1a - PMA/diacylglycerol and C2 - calcium/PS/$PI(4,5)P_2$) our findings suggest a mechanism for regulation of PKC self-assembly by controlling the strength of this interaction (Fig. 3.2). Accordingly, the PKC self-assembly state as measured by homo-FRET varies with different combinations of C1 and C2 domain effectors, which in turn correlates with the specific activity of the kinase. Hence, the involvement of multiple domains in self-assembly allows for a nuanced regulation of the self-assembly state that is consistent with the multiplicity of PKC function.

The results of this study are consistent with the self-assembly of PKCα in live cells. We have previously reported that an intra-molecular sensor (mCer-PKCα-mCit) showed increased hetero-FRET upon activation with PMA or LPA in CHO cells (17). While our observations were consistent with self-assembly of PKCα observed in activated recombinant protein, they did not distinguish between the contributions of intra- and inter-molecular interactions. In a separate study hetero-FRET was observed between CFP-PKCβII-CFP and YFP-PKCβII-YFP following phorbol ester treatment of MDCK cells (36). These measurements are subject to the relative stoichiometry of expression of the donor and acceptor fusions. Here, homo-FRET of a single fluorophore (mCit of mCer-PKCα-mCit) provides an orthogonal measure of selective PKCα self-assembly in live cells. Treatment of cells with a combination of ionomycin and PMA, but not ionomycin alone, resulted in a significant decrease in steady-state anisotropy in live cells

(Fig. 3.3 and Fig. B.7). These results suggest interactions between PKCα and phospholipids introduce additional regulatory mechanisms in cells.

Self-assembly of PKCα, both *in vitro* and in live cells provides a novel context in which to interpret the crowding of PKCα-GFP fusions following activation (11). At least three separate studies reported clustering of PKCα in response to different stimuli. First, physiological and synthetic agonists of cytosolic calcium lead to the non-homogeneous subcellular distribution of PKCα in vascular smooth muscle cells (VSMC) (12). The size, morphology, distribution and other characteristics of PKCα localization were dependent on the mechanism by which cytosolic calcium was induced. Second, it was observed that Madin-Darby canine kidney (MDCK) cells expressing PKCα C2 domain treated with ionomycin formed both apical and basolateral punctae that was dependent on the ability to bind $PI(4,5)P_2$ (13). Third, Reither et al. found that PKCα-GFP accumulated at distinct focal points, which were termed local translocation events, in COS1 cells stimulated with ATP (11). These focal accumulations were surprisingly spatially restricted and were attributed to the binding of PKC to an unidentified biomolecule that limited lateral diffusion. The diversity of spatio-temporal localizations observed in these studies are consistent with our findings that PKCα self-assembly is a dynamic process that is sensitive to the combination of effectors (calcium, DAG, and $PI(4,5)P_2$) present in cells. Lastly, the correlation between the extent of self-assembly and kinase activity suggests that these focal accumulations parallel the activation of kinase functions in cells. Future studies must address how both of these emergent properties of PKC dictate function in different multi-protein signaling networks.

3.5 Conclusions:

The present chapter is aimed to address if PKCα oligomerization, as observed in **Chapter 2**, is regulated by domain-domain interactions. First, we conclude PKCα is sufficient to reversibly self-assemble in vivo in the presence of calcium. Rather than a precisely defined homo-oligomerization, we observe a nonhomogeneous clustering which drives towards larger assemblies over time. Next we conclude that the C1a and C2 domains are minimally sufficient to self-assemble. Using SPASM, we provide evidence that the intramolecular interaction between these two domains is critical in nucleating self-assemblies in the presence of calcium. Finally, we conclude that self-assembly of full length PKCα in cells and on lipid bilayers may have

additional regulatory mechanisms not fully elucidated in this study as homo-FRET could only observe self-assembly when both calcium and a DAG mimetic were exposed to cells. However, we observe a positive correlation between self-assembly on bilayers and kinase activity.

3.6 References:

1. Ellis RJ & Minton AP (2003) Cell biology: join the crowd. *Nature* 425(6953):27-28.
2. Csete ME & Doyle JC (2002) Reverse engineering of biological complexity. *Science* 295(5560):1664-1669.
3. Bhattacharyya RP, Remenyi A, Yeh BJ, & Lim WA (2006) Domains, motifs, and scaffolds: the role of modular interactions in the evolution and wiring of cell signaling circuits. *Annual review of biochemistry* 75:655-680.
4. Whitesides GM & Grzybowski B (2002) Self-assembly at all scales. *Science* 295(5564):2418-2421.
5. Brodsky FM, Chen CY, Knuehl C, Towler MC, & Wakeham DE (2001) Biological basket weaving: formation and function of clathrin-coated vesicles. *Annual review of cell and developmental biology* 17:517-568.
6. Pollard TD (2007) Regulation of actin filament assembly by Arp2/3 complex and formins. *Annu Rev Biophys Biomol Struct* 36:451-477.
7. Karsenti E & Vernos I (2001) The mitotic spindle: a self-made machine. *Science* 294(5542):543-547.
8. Steinberg SF (2008) Structural basis of protein kinase C isoform function. *Physiol Rev* 88(4):1341-1378.
9. Newton AC (2001) Protein kinase C: structural and spatial regulation by phosphorylation, cofactors, and macromolecular interactions. *Chem Rev* 101(8):2353-2364.
10. Rosse C*, et al.* (2010) PKC and the control of localized signal dynamics. *Nat Rev Mol Cell Biol* 11(2):103-112.
11. Reither G, Schaefer M, & Lipp P (2006) PKCalpha: a versatile key for decoding the cellular calcium toolkit. *J Cell Biol* 174(4):521-533.
12. Maasch C*, et al.* (2000) Protein kinase calpha targeting is regulated by temporal and spatial changes in intracellular free calcium concentration [Ca(2+)](i). *FASEB J* 14(11):1653-1663.
13. Evans JH, Murray D, Leslie CC, & Falke JJ (2006) Specific translocation of protein kinase Calpha to the plasma membrane requires both Ca2+ and PIP2 recognition by its C2 domain. *Molecular biology of the cell* 17(1):56-66.
14. Muretta JM*, et al.* (2010) High-performance time-resolved fluorescence by direct waveform recording. *The Review of scientific instruments* 81(10):103101.
15. Muretta JM, Petersen KJ, & Thomas DD (2013) Direct real-time detection of the actin-activated power stroke within the myosin catalytic domain. *Proc Natl Acad Sci U S A* 110(18):7211-7216.
16. Petersen KJ*, et al.* (2014) Fluorescence lifetime plate reader: resolution and precision meet high-throughput. *The Review of scientific instruments* 85(11):113101.
17. Swanson CJ*, et al.* (2014) Conserved modular domains team up to latch-open active protein kinase Calpha. *J Biol Chem* 289(25):17812-17829.
18. Huang SM, Leventhal PS, Wiepz GJ, & Bertics PJ (1999) Calcium and phosphatidylserine stimulate the self-association of conventional protein kinase C isoforms. *Biochemistry* 38(37):12020-12027.

19. Medkova M & Cho W (1998) Mutagenesis of the C2 domain of protein kinase C-alpha. Differential roles of Ca2+ ligands and membrane binding residues. *J Biol Chem* 273(28):17544-17552.
20. Clapham DE (2007) Calcium signaling. *Cell* 131(6):1047-1058.
21. Egea-Jimenez AL*, et al.* (2014) Phosphatidylinositol-4,5-bisphosphate enhances anionic lipid demixing by the C2 domain of PKCalpha. *PLoS One* 9(4):e95973.
22. Sutton RB & Sprang SR (1998) Structure of the protein kinase Cbeta phospholipid-binding C2 domain complexed with Ca2+. *Structure* 6(11):1395-1405.
23. Chapman ER, An S, Edwardson JM, & Jahn R (1996) A novel function for the second C2 domain of synaptotagmin. Ca2+-triggered dimerization. *J Biol Chem* 271(10):5844-5849.
24. Xu L*, et al.* (2011) Dysferlin forms a dimer mediated by the C2 domains and the transmembrane domain in vitro and in living cells. *PLoS One* 6(11):e27884.
25. Ramakrishnan NA, Drescher MJ, Morley BJ, Kelley PM, & Drescher DG (2014) Calcium regulates molecular interactions of otoferlin with soluble NSF attachment protein receptor (SNARE) proteins required for hair cell exocytosis. *J Biol Chem* 289(13):8750-8766.
26. Kang CH*, et al.* (2013) Rice small C2-domain proteins are phosphorylated by calcium-dependent protein kinase. *Molecules and cells* 35(5):381-387.
27. Lehn JM (1985) Supramolecular chemistry: receptors, catalysts, and carriers. *Science* 227(4689):849-856.
28. Stahelin RV*, et al.* (2005) The origin of C1A-C2 interdomain interactions in protein kinase Calpha. *J Biol Chem* 280(43):36452-36463.
29. Slater SJ*, et al.* (2002) Regulation of PKC alpha activity by C1-C2 domain interactions. *J Biol Chem* 277(18):15277-15285.
30. Sivaramakrishnan S & Spudich JA (2011) Systematic control of protein interaction using a modular ER/K alpha-helix linker. *Proc Natl Acad Sci U S A* 108(51):20467-20472.
31. Gautier I*, et al.* (2001) Homo-FRET microscopy in living cells to measure monomer-dimer transition of GFP-tagged proteins. *Biophys J* 80(6):3000-3008.
32. Sharma P*, et al.* (2004) Nanoscale organization of multiple GPI-anchored proteins in living cell membranes. *Cell* 116(4):577-589.
33. Nishizuka Y (1995) Protein kinase C and lipid signaling for sustained cellular responses. *FASEB J* 9(7):484-496.
34. Egea-Jimenez AL, Perez-Lara A, Corbalan-Garcia S, & Gomez-Fernandez JC (2013) Phosphatidylinositol 4,5-bisphosphate decreases the concentration of Ca2+, phosphatidylserine and diacylglycerol required for protein kinase C alpha to reach maximum activity. *PLoS One* 8(7):e69041.
35. Wang YH*, et al.* (2012) Divalent cation-induced cluster formation by polyphosphoinositides in model membranes. *J Am Chem Soc* 134(7):3387-3395.
36. Antal CE, Violin JD, Kunkel MT, Skovso S, & Newton AC (2014) Intramolecular conformational changes optimize protein kinase C signaling. *Chem Biol* 21(4):459-469.

Chapter 4: Autoinhibition interaction in PKCα increases size of calcium stimulated self-assemblies through ring opening polymerization

4.1 Introduction:

The fields of materials sciences and supramolecular chemistry often cite natural and biological systems as sources of inspiration for new polymer designs (1-3). The ability of proteins and other biomolecules to assemble and organize is a hallmark of biological systems, and facilitates emergent properties and structures (4). In the past decade, many new examples of self-assembling proteins have been reported by biologists but in many cases the biological relevance is not well understood (5-9). In such cases, an understanding of the design principles of molecular self-assembly, as is often considered by engineers and chemists attempting to develop novel supramolecular schemes for specific functions, may inform on potential biological functions (10, 11).

The human protein kinase C (PKC) is one example of a biologically important protein that has recently been reported to self-assemble during certain biological situations yet the biological significance of self-assembly is not clearly resolved (12-14). The biological role of PKC has been described as a 'molecular processor' of cellular information. PKC functions through a combination of phosphorylating, allosterically activating and scaffolding specific proteins (15-18). PKC regulates cellular functions ranging from maintaining homeostasis, to proliferation and cytoskeletal rearrangement, and its dysregulation is implicated in several chronic diseases including diabetes, Alzheimer's Disease, various cancers and heart failure (19-22). PKC is a family of multi-domain signal transduction proteins that phosphorylate Ser/Thr residues following binding to the secondary messengers cytosolic Ca^{2+} and diacylglycerol (DAG). The structure of classically studied PKC isoforms can be broken down into four independently functioning domains linked by unstructured peptide linkers; the C1a domain which binds to

DAG, the C1b domain which binds to phorbal esters (PMA), the C2 domain which sequentially binds to Ca^{2+}, phosphatidyl serine (PS) and phosphoinositile bis(4,5)phosphate (PI(,4,5)P_2), and the enzymatic kinase domain responsible for catalyzing phosphorylation reactions (23). Together these domains self-interact to tightly regulate phosphorylation activity both temporally and spatially within cellular systems (24).

In **Chapter 2 and 3** we provide evidence that activating conditions, including calcium, stimulate the far from equilibrium self-assembly of PKC *in vitro* (12-14). While PKC is primarily anticipated to function through its kinase activity, only the regulatory domains and in particular the C1a and C2 domains are required for self-assembly (12). Despite the kinase domain not being necessary for self-assembly and self-assembly not being necessary for enzymatic activity, the two properties are correlated across a range of biological conditions (12, 13). Critically, it has been recently reported that commonly employed approaches to study PKC function in cellular and physiological contexts including kinase inhibitors and kinase dead mutations influence both kinase activity, kinase phosphorylation and self-assembly of PKC (14, 25). Independent of the self-assembly literature, it has recently been postulated that PKC functions as a scaffold in the assembly of multiple cellular signaling complexes including focal adhesions and cell-cell junctions (16), and examples have emerged where only elements of the PKC regulatory domains (and not the kinase domain) have been demonstrated to be sufficient to rescue various cellular phenotypes (26-29). Collectively, these reports suggest fundamental molecular properties of PKC need to be re-examined and re-evaluated in order to understand its physiological and pathophysiological functions.

We anticipate that knowledge of domain-domain interactions within PKC is the critical missing component in understanding its molecular and biological functions. While several intramolecular domain-domain interactions are anticipated to regulate PKC function, it has remained challenging to obtain direct evidence. Recently, the first crystal structure of a PKC isoform containing both regulatory domains and kinase domain was reported (30). Interestingly, the only intramolecular interaction observed in the structure between C1b and kinase domains was never anticipated from previous biochemical studies yet the authors subsequently demonstrated a functional relevance of the interaction (30).

In this study we consider how the combination of intramolecular interaction between regulatory domains and the kinase domain (**Chapter 2**) combined with the intermolecular assembly of C1a and C2 domains (**Chapter 3**) may lead to non-linear properties in PKC self-assembly. Non-covalent macrocyclization, or ring opening polymerization (R.O.P.), describes the process of oligomerization arising from a single molecule that contains two components which can cyclize and interact with each other, in the case of PKC this is the interaction between regulatory domains and kinase domains. At equilibrium the partitioning between different oligomeric states through R.O.P. assuming no steric constraints can be described by the following model from Ercolani et al (31):

(1) $K_{inter} = \frac{[A \cdot B]}{[A][B]}$

(2) $K_{intra} = \frac{[cyclic]}{[acyclic]}$

(3) $[M_1]_0 = \frac{K_{intra}}{K_{inter}} \sum_{i=1}^{\infty} i^{-3/2} x^i + \frac{1}{K_{inter}} \sum_{i=1}^{\infty} i x^i$

Where $[M_1]_0$ is the starting molar concentration of monomer, i is the polymeric state, x is the fraction of reacted end groups defined as $x^i = [M_i]K_{inter}$ and this model does not account for any steric strain differentiating intra or inter interactions.

Bastings et al quantitatively assessed this equilibrium model of macrocylization using a protein based system (32). In this study they used flexible ethylene glycol linkers of different lengths to separate two peptides, S-peptide and S-protein which interact non-covalently, and assessed the degree of polymerization while varying initial sample concentration. They observed that the thermodynamic model well described oligomerization arising from changes in concentration as well as changes in the K_{intra}term with altered linker lengths. They noted that oligomers larger than 4-mers were not observed and speculated that constraints in protein solubility limits the ability of linear polymers to form from such a design scheme.

For PKC we will consider the interaction between the regulatory domains and the kinase domain as a R.O.P. In combination with R.O.P. a secondary intermolecular interaction occurs interdependently, the clustering of C1a – C2 domains in the presence of calcium (12)(**Chapter 3**). We hypothesize that the combination of these two intermolecular interaction mechanisms constitute an unexamined supramolecular design scheme that will lead to unanticipated

properties of PKC. In this work we will test the contribution of R.O.P. to calcium stimulated self-assembly of PKC.

4.2 Materials and methods:

Materials: The protein constructs and expression and purification methods are all as previously reported (14). All PKC constructs were cloned from full length human cDNA (Open Biosystems) into pBiex1 (Novagen). SPASM genetic cassettes (ER/K linkers plus mCitrine and mCerulean fluorescent proteins) (33) were spliced in between residues 335 and 336. The wild type PKC used in these experiments contains an N-terminal mCerulean and a C-terminal mCitrine. All PKC constructs contain a C-terminal Flag tag. The pBiex1 containing appropriate construct was transiently transfected (Escort IV; Sigma) into Sf9 cultures (Sf900-II media; Invitrogen). Sf9 cells were hypotonically lysed 72 hours post transfection, and batch purified using anti-FLAG M2 affinity resin (Sigma), and eluted with Flag peptide (Sigma). Protein was buffer exchanged into 20 mM HEPES, 0.5 mM EGTA, 5mM $MgCl_2$, 2mM DTT, pH 7.5 (Zeba Spin Desalting columns; Pierce). Prior to experiments protein was centrifuged at ~220,000 xg for 10 min to remove insoluble protein, and mCitrine fluorescence was measured (FluoroMax-4; Horiba) against a standard curve to obtain protein concentration. Experiments were performed within 4 days of protein expression. Unless otherwise stated all reagents were obtained from Sigma.

Kinase activity: Kinase activity was assessed as previously described (14). The indicated protein was split into two stocks and treated with .01 mg/ml BSA or 0.01 mg/ml TEV protease on ice overnight. The PKC protein was diluted to 20 nM in a HEPES buffer with BSA (20 mM HEPES, 0.5 mM EGTA, 5mM $MgCl_2$, 2mM DTT, 0.1 mg/ml BSA, pH 7.5) and myelin-binding protein peptide residues 4 - 14 (MBP pep, Santa Cruz Biotechnology, Inc) and ATP at a final concentration of 40 μM. The TEV treated sample (used to obtain maximal kinase activity) additionally contained 300 μM free calcium and 4 μM PMA. All reactions were performed for 2 min at room temperature before being quenched, and total ATP concentration quantified using the Kinase-Glo Max Luminescence assay kit (Promega) in 96 well plates (Thermo Scientific) on a Synergy HT (Biotek).

R.O.P. model: A custom MATLAB solver was built to solve for the molar concentration for the first 5 polymeric states ($M_i \; for \; i = 1 - 5$) as a function of K_{intra} values according to Eq. 1. A

K_{inter} value of 200 nM was used in all cases. The reported value 'fraction of $A - B$ interactions intermolecular' was calculated as $\frac{\sum_{i=2}^{5} M_i}{\sum_{i=1}^{5} M_i}$.

Fluorescence microscopy: These experiments were performed as previously described (Chapter 3). All experiments contained 200 nM of PKCα protein incubated at 25° C in HEPES buffer with BSA (20 mM HEPES, 0.5 mM EGTA, 5 mM $MgCl_2$, 2 mM DTT, 0.1 mg/ml BSA, pH 7.5) with or with a final free calcium concentration to 300 μM. Samples were incubated for 10 min before imaging. Each sample was gently sandwiched between an ethanol cleaned slide and coverslip and sealed by VALAP (vasoline/lanolin/paraffin). Slides were imaged on a Nikon TiE equipped with a mercury arc lamp, a yellow GFP filter cube (Nikon; 500/20 nm excitation, 515 nm LP, 535/30 nm emission), perfect focus system (Nikon), a 100X 1.4 NA Plan-Apo oil-immersion objective (Nikon), Evolve EMCCD camera (Photometrics), and the Nikon NIS-elements software. Image planes were focused on the coverslip surface and ND filters and exposure time were adjusted to avoid saturation before being fixed for all slides in the matched experiment. Stage translation was performed with the shutter in to avoid field of view bias and images were taken at 5 – 15 locations per slide. For the TEV experiment mCerulean and mCit were monitored using a dual view module (Photometrics; 505 nm beam splitter, D480/30 nm and 535/40nm) and two images were sequentially taken with mCerulean excitation (custom filter cube 436/20 nm excitation, 455 nm LP) followed by mCitrine excitation (GFP cube). Only the mCerulean excitation – mCerulean emission and mCitrine excitation – mCitrine emission channels were analyzed. The protein sample was incubated with TEV protease 10 min prior to the protein being aliquoted into the final imaging conditions. Spot identification was performed using custom MATLAB code as previously described (Chapter 3).

Dynamic Light Scattering: DLS data was collected on a DynaPro NanoStar (Wyatt Technology) at 25° C. Protein (1 μM) was in HEPES buffer (20 mM HEPES, 0.5 mM EGTA, 5 mM $MgCl_2$, 2 mM DTT, pH 7.5). Sequentially the buffer was brought to a final concentration of 800 μM $CaCl_2$ and 1 mM EGTA using concentrated stocks at 2.5% of the final volume with 5 min incubations between measurments. Each autocorrelation is the mean of 10 repetitive readings of 10s each. A regularization fit was performed using the Wyatt Technology software platform (Dynamics V7.1.7) utilizing the isotropic spheres model. The particle mass was normalized by the mean of

the initial EGTA buffered condition (assumed as a monomer). Autocorrelation data were least squares fit to a single exponential decay function (GraphPad) to obtain τ values. For the TEV treatment experiment, a final concentration of 100 nM TEV protease, or 100 nM BSA (control) was added to the sample 5 minutes prior to the EGTA measurement.

4.3 Results:

The aim of this paper is to assess if R.O.P. between the PKC regulatory domains and kinase domain contributes to self-assembly of PKC in the presence of calcium **(Fig. 4.1 a)**. To address this question we chose a strategy whereby the structure of PKC would be modified to perturb the K_{intra} parameter, and the self-assembly of the modified PKC protein would be monitored **(Fig. 4.1 b)**. We can then compare the experimental results with an established theoretical model of R.O.P. (Eq. 4.1).

Modified PKC protein containing ER/K α helical linkers genetically inserted between the regulatory domains and kinase domain were used to specifically perturb K_{intra}. For convenience and to adhere to the generality of Eq. 4.1-3, the regulatory domains will be referred to as *A* and the kinase domain will be referred to as *B* in the study **(Fig. 4.1 c)**. These constructs have been previously reported to perturb the intramolecular interaction using intramolecular FRET (14). Here we used kinase catalytic activity to obtain approximate values of K_{intra} by monitoring the functional autoinhibition of kinase activity by the intramolecular interaction between the kinase and regulatory domains if [PKC] << K_{inter}:

(4) $$K_{intra} = \frac{[cyclic]}{[acyclic]} = \frac{[bound]}{[unbound]} \approx \frac{[kinase\ inactive]}{[kinase\ active]}$$

Under basal (EGTA buffered) or free calcium conditions in the absence of liposomes and the presence of phosphorylation substrate and ATP, the ATP consumption by the three linker constructs was monitored at a fixed time point as a readout of kinase activity. In parallel, the ATP consumption was monitored in a matched condition in which the protein was site-specifically proteolyzed by TEV protease and liposomes were included to sequester the regulatory domains. The TEV proteolyzed condition served as a normalization factor, or 100% kinase activity, and the non-proteolyzed protein was used to assess the equilibrium between active and inactive states **(Fig. 4.1 d)**. We previously reported similar findings for the 10 nm and

30 nm proteins (14). We calculated K_{intra} values of 9.47 ± 2.39 (10 nm), 4.08 ± 0.49 (20 nm) and 3.24 ± 0.08 (30 nm) (mean and standard error) **(Fig. 4.1 e)**. We measured kinase activity at low (20 nM) concentrations of PKC where [PKC] << K_{inter} so we could make the approximation of two states (cyclic and acyclic). We did not observe an effect on the kinase activity if calcium was present or absent indicative that the K_{intra} term is independent of calcium (not shown).

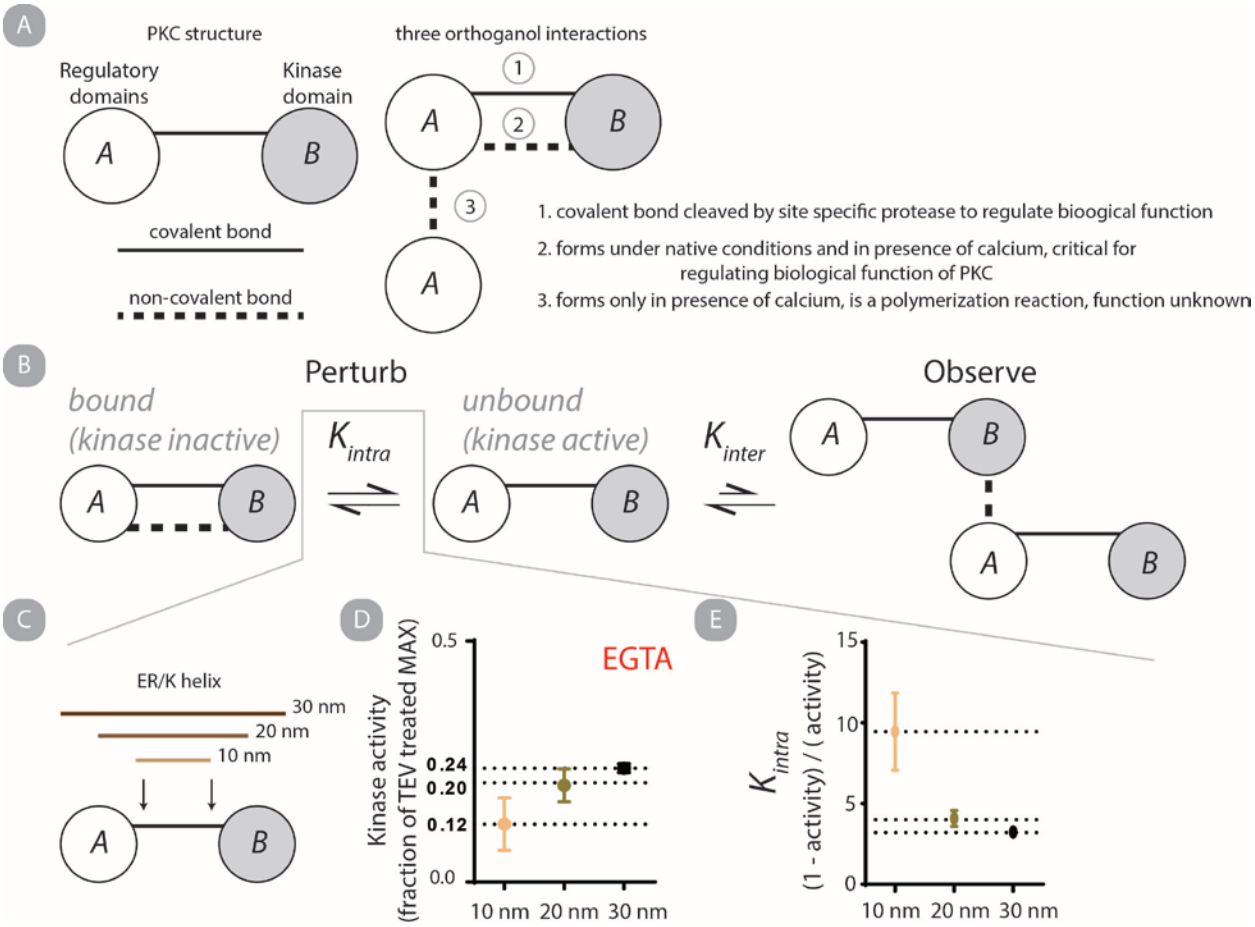

Figure 4.1. ER/K linkers can perturb intramolecular interaction between PKCα regulatory and kinase domains. (**a**) A generalized schematic of PKC structure and three interactions that are considered in this study. Regulatory domains comprised of the pseudosubstrate, C1a, C1b, C2 domains and the unstructured linkers between the domains are referred to as A, and the kinase domain is referred to as B. (**b**) A schematic of the equilibrium between a monomeric and dimeric molecule mediated through ring opening polymerization (R.O.P.). The experimental scheme in this report is to perturb the K_{intra} term and observe the changes in oligomerization/self-assembly of PKC. In gray, two previously identified functional attributes of PKC in the two states are highlighted. (**c**) To perturb the K_{intra} equilibrium term, ER/K α helical linkers of three lengths (10 nm, 20 nm and 30nm – end to end distance in when fully α helical) were genetically inserted between A and B in PKC. (**d**) The *in vitro* kinase activity of the three ER/K linked proteins when buffered with EGTA, normalized to the maximum kinase activity when the kinase domain is isolated and measured in matched conditions. Shown is the mean and SEM of 4 independent measurements. (**e**) The same kinase data in d is plotted as K_{intra} values.

We next simulated the fraction of PKC molecules with an intermolecular $A - B$ interaction according to the R.O.P. model as a function of K_{intra} at several different PKC concentrations and a fixed K_{inter} value (200 nM). We find that at all concentrations, lower K_{intra} values result in an increased fraction of intermolecular interactions **(Fig. 4.2 a)**. We plotted the three empirically derived K_{intra} values from Fig. 1b onto the results as well as an approximation of K_{intra} for wild-type PKC (based on ~1% kinase activity of basal PKC compared to the maximal recorded activity). At a fixed concentration of PKC (1 μM) the predicted fold change in intermolecular $A - B$ interactions from wild-type to the 10 nm, 20 nm and 30 nm constructs is 15, 24 and 27 respectively. Finally, we assessed self-assembly of wild-type and the 3 mutant PKC constructs. We previously developed several methodologies to characterize PKCα self-assembly in the presence of calcium including by single particle punctae formation on glass coverslips and by dynamic light scattering (DLS). Neither of these methodologies is particularly well-suited to study monomer-dimer transitions, instead they are best utilized to report on large changes in particle size. No large-scale self-assembled PKC was observed in the absence of calcium for any of the PKC protein by the fluorescent punctae assay **(Fig. 4.2 b)**. However, following a 5 min incubation with free calcium, large PKC punctae can be observed. Qualitatively, the PKC punctae increase in size as the linker lengths increase. Analysis of particle size by DLS is consistent with this finding **(Fig. 4.2 c)**. In otherwise matched conditions, linker lengths of 10 nm, 20 nm and 30 nm increase the mean ensemble particle mass in solution with calcium 9-fold, 14-fold and 19-fold compared to wild-type PKC **(Fig. 4.2 d)**. WT PKC ensemble mass increases 13.1 ± 2.2 fold following calcium incubation compared with 113.5 ± 2.4 (10 nm), 179.4 ± 6.5 (20 nm) and 248.4 ± 9.4 (30 nm) (mean and SEM of N = 10). In each case, the particle mass is partially reduced following a 5 min incubation with excess EGTA, suggestive of the reversibility of the self-assembly. The relative increase in the particle size appears to scale consistent with the prediction of the degree in which R.O.P. accounts for intermolecular interactions. Discrepancies between the measured and predicted change in mass contributed by R.O.P. likely arise through error in estimates of K_{intra} and K_{inter} values, as well as steric effects which are not accounted for in our model. Further it is noted that DLS is an ensemble measurement of all light scattering particles in solution, such that any contaminating protein or peptide will decrease the apparent change in mass, and any aggregated protein (through independent mechanisms) will have the

opposite effect. Together, these results suggest that R.O.P. directly regulates the size or degree of PKC self-assembly in the presence of calcium.

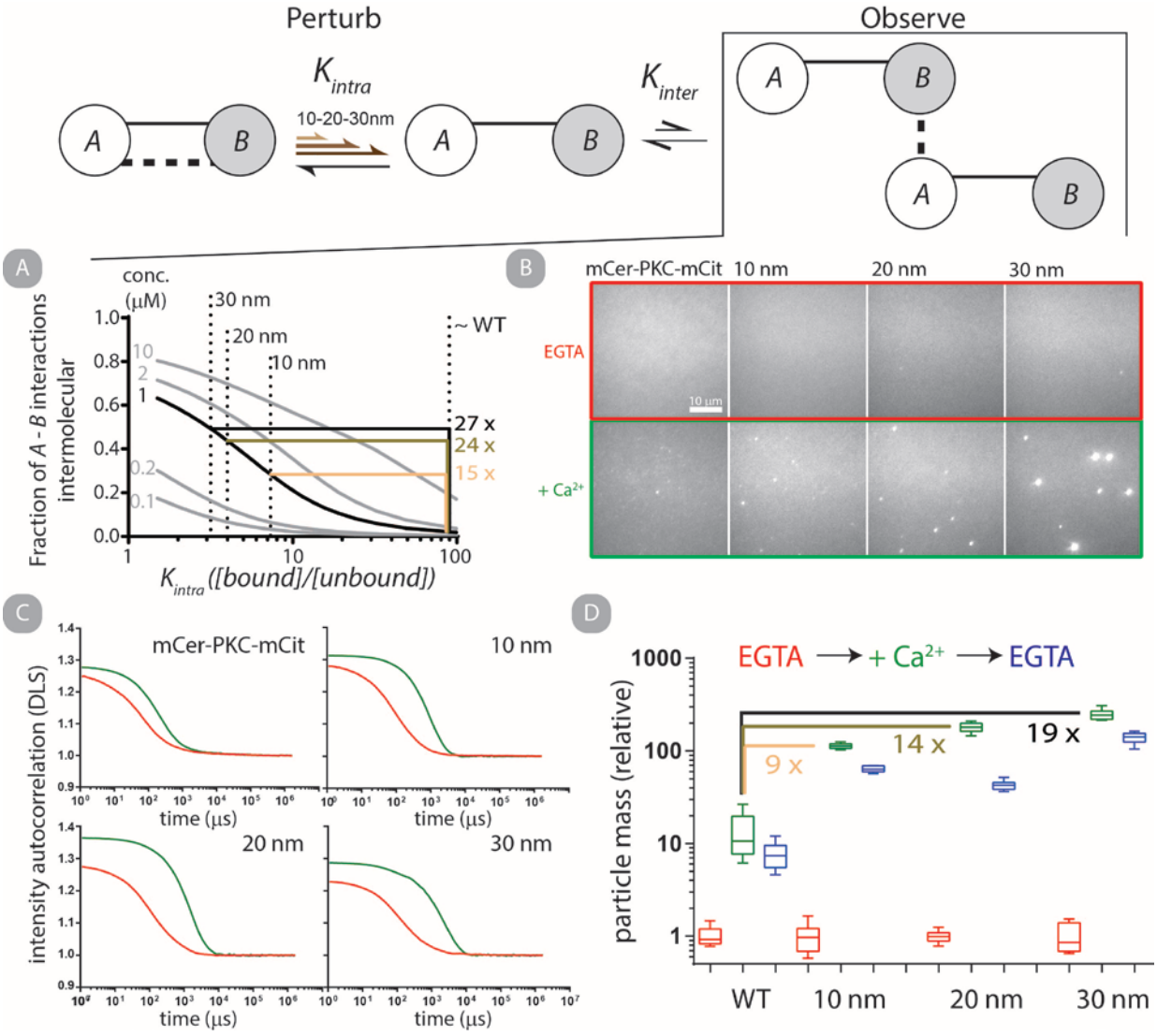

Figure 4.2. Decreased intramolecular interactions between PKC regulatory and kinase domains facilitate enlargement of calcium stimulated self-assemblies consistent with ring opening polymerization. (**a**) Predicted fraction of intermolecular interactions between PKC mediated by R.O.P. as a function of K_{intra} for various concentrations. The vertical dashed lines represent the empirically defined K_{intra} values for the three ER/K linked PKC protein, as well as an estimate for the wild-type K_{intra} in which basal kinase activity is ~1% of the maximally achievable kinase activity. At 1 μM of PKC, R.O.P. predicts that 1.8% of PKC molecules will be engaged in intermolecular interactions through R.O.P. compared to 28%, 44% and 49% for the 10 nm, 20 nm and 30 nm PKC protein respectively. R.O.P. predicts most of the intermolecular species are dimeric. (**b**) Fluorescence distribution of the indicated PKC protein deposited on a glass coverslip (200 nM), before or after a 5 min incubation with free calcium (300 μM). Shown are representative images with matched imaging conditions. (**c**) Intensity autocorrelation of dynamic light scattering (DLS) of 1 μM of the indicated PKC protein before or after a 5 min incubation with free calcium (300 μM). Shown is the mean of 10, 10 s acquisitions. (**d**) Quantification of DLS data shown in c, in which the degree of particle size changes sequentially as free calcium is introduced and finally 5 min after excess EGTA is added to the sample. The three lines are comparing the fold increase in particle mass size between WT PKC and the three ER/K PKC molecules in the presence of calcium.

A physiological mechanism of PKC regulation entails the proteolysis of the linker between the regulatory domains and the kinase domain by calpain I and II (34). Such a proteolysis event would be expected to completely remove the R.O.P. contribution towards self-assembly. We wanted to experimentally address this possibility. The three PKC constructs containing ER/K helices contain a tobacco etch virus (TEV) site specific proteolysis sequence within the linker region with a mCerulean fluorescent protein on the N-terminal side and a mCitrine fluorescent protein on the C-terminal side. The protein was briefly incubated with either BSA or TEV protease followed by an incubation with free calcium before being deposited on a glass coverslip and sandwiched on a glass slide. Representative images of both treatments of the protein are shown in the corresponding mCitrine (*B* - kinase domain) and mCerulean (*A* - regulatory domains) fluorescent channels **(Fig. 4.3 b)**. Without TEV treatment large punctae colocalized in both fluorescent channels, whereas the sample incubated with TEV only formed punctae in the regulatory domain channel. This experiment indicates that the kinase domain itself does not self-assemble in a calcium induced manner like the regulatory domains. Consistent with our prediction, proteolysis of the covalent linkage between *A* and *B* (and disruption of R.O.P.) results in strikingly stunted PKC assemblies. When quantified, the intensity of TEV treated punctae where approximately 1/3 of the intact sample, but the total number of punctae was approximately 3-fold greater **(Fig. 4.3 b right)**. This finding is consistent with results obtained from DLS. The PKC protein with 20 nm linker was assessed with and without TEV protease treatment. The TEV treated sample had a shift in intensity autocorrelation specifically resulting from calcium, although the shift was substantially attenuated compared to the non-TEV treated control **(Fig. 4.3 c)**. When quantified in terms of particle mass, the ensemble mass increases 2-fold versus 48-fold upon calcium addition for the TEV treated and control sample respectively **(Fig. 4.3d)**. TEV treatment of all three ER/K linked constructs resulted in a significant, but modest ~2-fold increase in particle mass following calcium treatment. In contrast, the wild-type PKC which lacks a TEV protease site increased 7 fold under matched conditions. This result supports our conclusion that R.O.P. facilitates an enhanced degree of self-assembly in the presence of calcium than the oligomerization of the regulatory domains alone. If we compare the TEV treated ER / K constructs versus the WT condition we anticipate that R.O.P. contributes to ~2 fold increase in particle size after a 5 min calcium incubation at 1 μM PKC concentration.

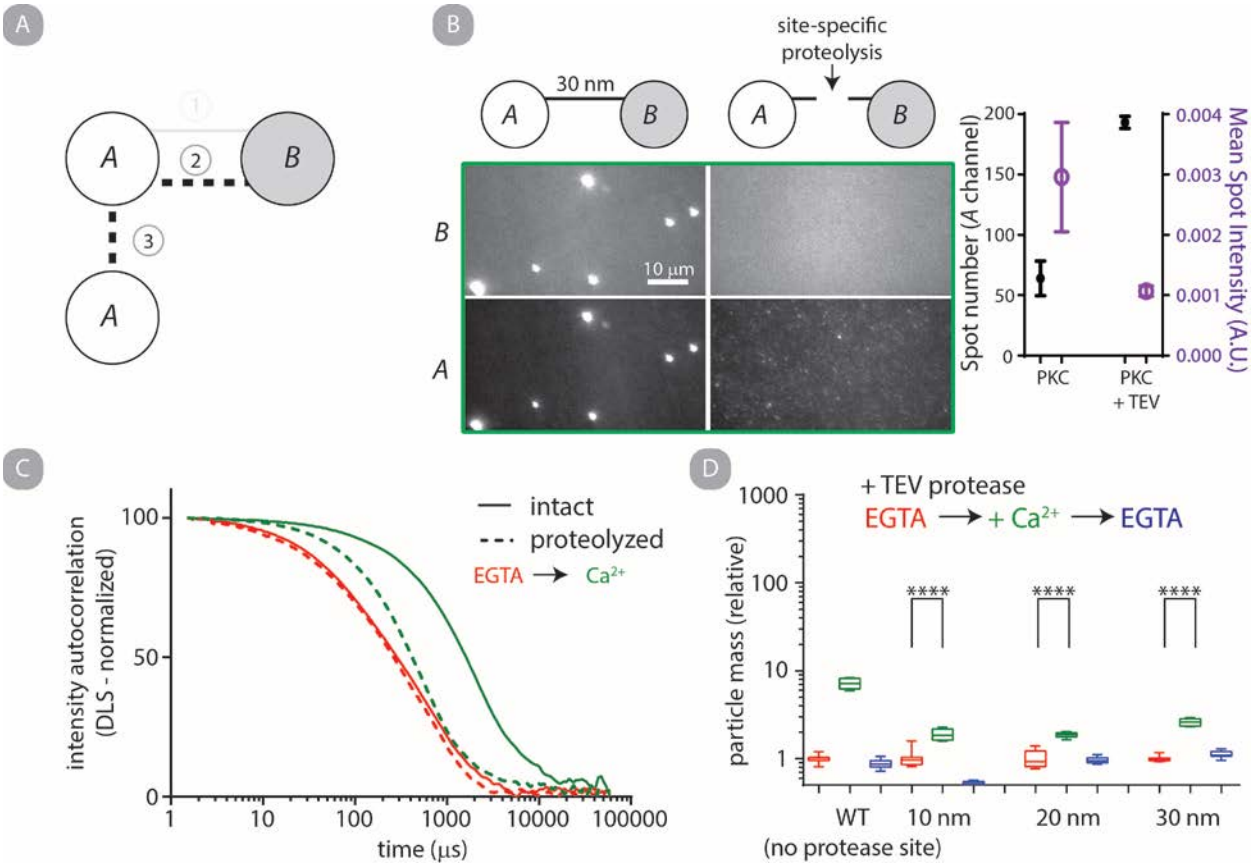

Figure 4.3. Disruption of ring opening polymerization through proteolysis of the covalent linkage between the regulatory and kinase domains substantially attenuates calcium induced self-assembly of PKC. (**a**) Proteolysis of the covalent linkage between A and B inhibits R.O.P. (**b**) Representative fluorescence distribution of 30 nm PKC treated or not treated with a site-specific TEV protease deposited on a glass coverslip (mCerulean linked to A; mCitrine linked to B) following a 5 min incubation with free calcium. Quantification of 4 fields of view in the A channel on the right, shown is mean and SEM. (**c**) Normalized intensity autocorrelation of 20 nm PKC treated (dashed) or not treated (solid) with TEV protease before and after a 5 min incubation with free calcium. Shown is the mean of 10 acquisitions. (**d**) Quantification of relative particle mass from DLS experiments of TEV treated PKC samples sequentially treated with free calcium and excess EGTA. The WT PKC does not contain a TEV protease site and is still capable of R.O.P. Box and whisker represent the min, max, 25, 75 and median of 10 measurements and **** indicates a P value < 0.001 by a students unpaired t-test.

4.4 Discussion:

Here we propose a model and provide evidence that PKC can self-assemble in part through R.O.P. mediated by the non-covalent interaction between PKC regulatory domains and kinase domain. We introduced genetic ER/K linkers between the regulatory domains and kinase domain and observed that longer linkers perturbed the K_{intra} parameter between the regulatory and kinase domains **(Fig. 4.1)**. We next observed that PKC with lowered K_{inter} values systematically increased the size of PKC self-assembly in the presence of calcium in a manner consistent with R.O.P. **(Fig. 4.2)**. Last, we observed that when the covalent interaction between the regulatory

and kinase domains are proteolyzed, the size of calcium stimulated PKC self-assemblies is dramatically attenuated **(Fig. 4.3)**. Together this data supports a model in which two interdependent process result in PKC self-assembly; *i*) calcium stimulated oligomerization of the PKC regulatory domains and *ii*) R.O.P. between the regulatory and kinase domain **(Fig. 4.4)**.

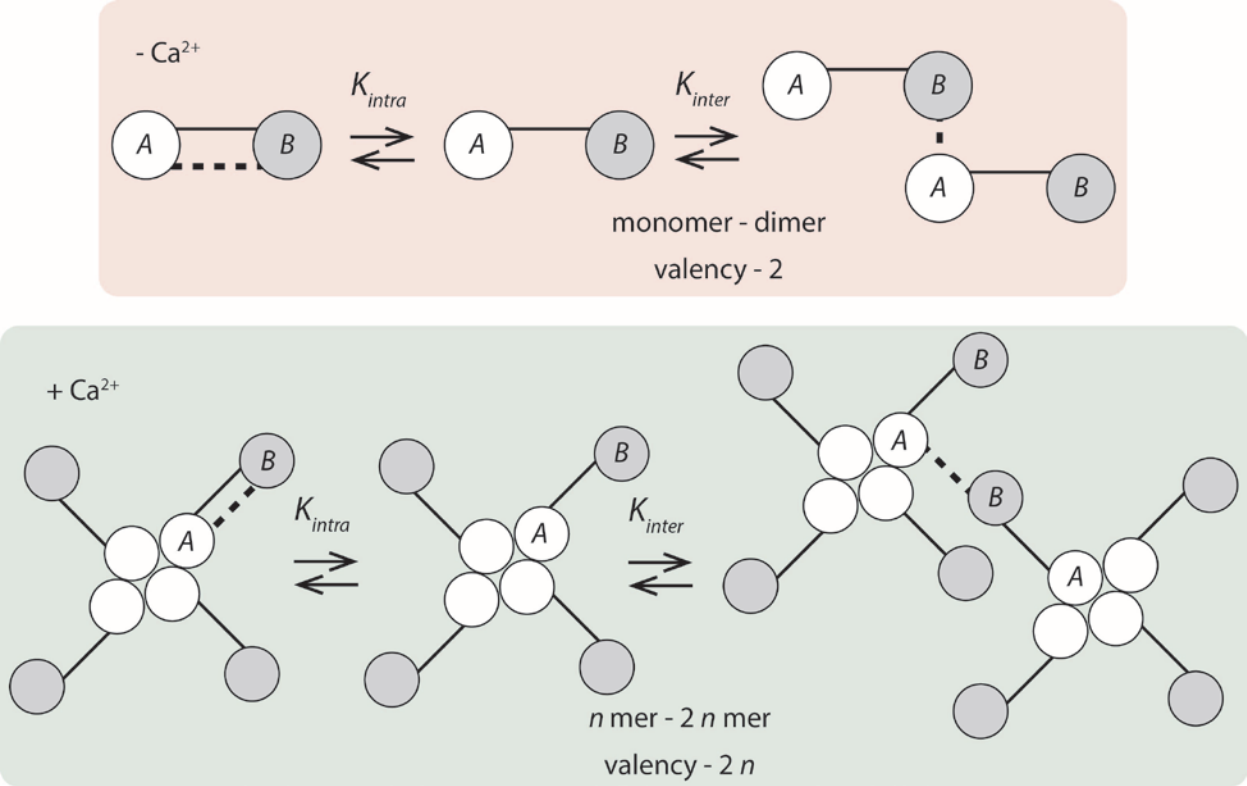

Figure 4.4. Combination of two interdependent self-assembly mechanisms impart new properties on self-assembling PKC. (top) A schematic of R.O.P. between a monomer and dimer. (Bottom) A schematic of R.O.P. in which A is an n mer (in this illustration a 4 mer). Two key parameters change between the two schematics, the total mass linked by an R.O.P. interaction increases by n-fold, and the valency increases by a factor of n, both of which are anticipated to contribute to the growth in size of PKC self-assemblies.

The biological significance of this work remains unclear at this point, however, the mechanism reported here may be useful in evaluating a large number of biomolecules. Many examples of auto-inhibition in signaling proteins have been reported, for example Cam Kinase II (35, 36), however to our knowledge the phenomenon of R.O.P. has never been evaluated in signal transduction proteins. An intriguing aspect of R.O.P. is the sharp dependence on concentration. The anticipated cellular concentration of PKCα (across an entire cell volume) ranges from 1 - 300 nM (37, 38), a concentration range where R.O.P. may be coarsly regulated. During signaling events PKC can be sharply enriched by several orders of magnitude in certain subcellular locations through binding of specific phospholipids and or scaffolding proteins. This can be

observed by patchy or clustered distributions of PKC at locations like cell-cell junctions, signaling complexes, stress granules or cavaeoli (16, 29, 39-41). PKC localization may selectively result in high local concentrations which may drive R.O.P. Many other signaling proteins with autoinhibition interactions are likewise enriched in specific subcellular locations which may facilitate R.O.P. (42, 43).

PKC may provide clues to how biology has evolved molecular processing capacities like memory formation. Key aspects of this PKC self-assembly design may be in understanding the rate of association versus dissociation. It appears likely that dissociation of PKC self-assemblies may be slowed by R.O.P. (44) which may facilitate a point of asymmetry in which PKC self-assemblies persist longer than calcium spikes – such a property could facilitate the gradual accumulation, or integration, of PKC into self-assembled clusters. It is intriguing to speculate that in chronic diseases like Alzheimer's (AD) where calcium dysregulation and the chronic re-localization of PKC within cells are observed in early stages, self-assembly of PKC may play a direct role (20, 45). An interesting consideration is the role of calpain proteases, which are dysregulated in neurodegenerative processes like AD (46). The proteolysis of PKC by calpains generates PKM (the free proteolyzed PKC kinase domain), but it may have other consequences in the disruption of self-assembled PKC linked through R.O.P. In studies of long term potentiation (LTP) it has been demonstrated that a peptide inhibitor termed ZIP can erase memories (47). The ZIP peptide is derived from an autoinhibitory peptide in PKCzeta, and was anticipated to block PKMzeta kinase activity by directly binding the kinase domain. However, the ZIP peptide effect on LTP was found to be independent of PKMzeta and it is thought that at concentrations used to elicit the LTP effect other kinases including Cam Kinase or other isoforms of PKC may be the target (48-50). In light of the present findings of R.O.P. in self-assembly of PKCα we can hypothesize the ZIP peptide acts as the *A* peptide and an excess of *A* can compete with the cyclization of *A – B*. It is of great interest to further understand the physical and information properties of self-assembling molecules as well as to understand information processing in biology. Better communication between engineering and chemistry fields and biologists may be the key factor in the design of life changing materials and identification of sophisticated therapeutic strategies.

4.5 Conclusions:

In this chapter we explored the contributions of R.O.P. mediated by the interaction between PKCα kinase and regulatory domains. We conclude that the size of calcium stimulated self-assemblies are regulated in part by R.O.P. By incorporating the SPASM methodology we were able to increase the size of PKC self-assembled particles by -9 -14 and -19 fold compared to wild-type PKC in modest agreement with the anticipated fraction of PKC dimerized through R.O.P. If the R.O.P. mechanism is disrupted, PKC self-assembled particle sizes were -3.5 fold smaller than wild-type.

4.6 References:

1. Whitesides GM & Grzybowski B (2002) Self-assembly at all scales. *Science* 295(5564):2418-2421.
2. Lehn JM (2002) Toward complex matter: supramolecular chemistry and self-organization. *Proc Natl Acad Sci U S A* 99(8):4763-4768.
3. Mattia E & Otto S (2015) Supramolecular systems chemistry. *Nature nanotechnology* 10(2):111-119.
4. Misteli T (2001) The concept of self-organization in cellular architecture. *J Cell Biol* 155(2):181-185.
5. Narayanaswamy R*, et al.* (2009) Widespread reorganization of metabolic enzymes into reversible assemblies upon nutrient starvation. *Proc Natl Acad Sci U S A* 106(25):10147-10152.
6. Kato M*, et al.* (2012) Cell-free formation of RNA granules: low complexity sequence domains form dynamic fibers within hydrogels. *Cell* 149(4):753-767.
7. Sieber JJ*, et al.* (2007) Anatomy and dynamics of a supramolecular membrane protein cluster. *Science* 317(5841):1072-1076.
8. Ebersbach G, Briegel A, Jensen GJ, & Jacobs-Wagner C (2008) A self-associating protein critical for chromosome attachment, division, and polar organization in caulobacter. *Cell* 134(6):956-968.
9. Garcia-Parajo MF, Cambi A, Torreno-Pina JA, Thompson N, & Jacobson K (2014) Nanoclustering as a dominant feature of plasma membrane organization. *J Cell Sci* 127(Pt 23):4995-5005.
10. Li P*, et al.* (2012) Phase transitions in the assembly of multivalent signalling proteins. *Nature* 483(7389):336-340.
11. Wodak SJ, Malevanets A, & MacKinnon SS (2015) The Landscape of Intertwined Associations in Homooligomeric Proteins. *Biophys J* 109(6):1087-1100.
12. Slater SJ*, et al.* (2002) Regulation of PKC alpha activity by C1-C2 domain interactions. *J Biol Chem* 277(18):15277-15285.
13. Huang SM, Leventhal PS, Wiepz GJ, & Bertics PJ (1999) Calcium and phosphatidylserine stimulate the self-association of conventional protein kinase C isoforms. *Biochemistry* 38(37):12020-12027.
14. Swanson CJ*, et al.* (2014) Conserved modular domains team up to latch-open active protein kinase Calpha. *J Biol Chem* 289(25):17812-17829.

15. Steinberg SF (2008) Structural basis of protein kinase C isoform function. *Physiol Rev* 88(4):1341-1378.
16. Rosse C*, et al.* (2010) PKC and the control of localized signal dynamics. *Nat Rev Mol Cell Biol* 11(2):103-112.
17. Oancea E & Meyer T (1998) Protein kinase C as a molecular machine for decoding calcium and diacylglycerol signals. *Cell* 95(3):307-318.
18. Hu T & Exton JH (2003) Mechanisms of regulation of phospholipase D1 by protein kinase Calpha. *J Biol Chem* 278(4):2348-2355.
19. Geraldes P & King GL (2010) Activation of protein kinase C isoforms and its impact on diabetic complications. *Circ Res* 106(8):1319-1331.
20. Alkon DL, Sun MK, & Nelson TJ (2007) PKC signaling deficits: a mechanistic hypothesis for the origins of Alzheimer's disease. *Trends Pharmacol Sci* 28(2):51-60.
21. Griner EM & Kazanietz MG (2007) Protein kinase C and other diacylglycerol effectors in cancer. *Nat Rev Cancer* 7(4):281-294.
22. Churchill E, Budas G, Vallentin A, Koyanagi T, & Mochly-Rosen D (2008) PKC isozymes in chronic cardiac disease: possible therapeutic targets? *Annu Rev Pharmacol Toxicol* 48:569-599.
23. Igumenova TI (2015) Dynamics and Membrane Interactions of Protein Kinase C. *Biochemistry* 54(32):4953-4968.
24. Kheifets V & Mochly-Rosen D (2007) Insight into intra- and inter-molecular interactions of PKC: design of specific modulators of kinase function. *Pharmacol Res* 55(6):467-476.
25. Cameron AJ, Escribano C, Saurin AT, Kostelecky B, & Parker PJ (2009) PKC maturation is promoted by nucleotide pocket occupation independently of intrinsic kinase activity. *Nat Struct Mol Biol* 16(6):624-630.
26. Zeidman R, Lofgren B, Pahlman S, & Larsson C (1999) PKCepsilon, via its regulatory domain and independently of its catalytic domain, induces neurite-like processes in neuroblastoma cells. *J Cell Biol* 145(4):713-726.
27. Stensman H & Larsson C (2007) Identification of acidic amino acid residues in the protein kinase C alpha V5 domain that contribute to its insensitivity to diacylglycerol. *J Biol Chem* 282(39):28627-28638.
28. Cameron AJ, Procyk KJ, Leitges M, & Parker PJ (2008) PKC alpha protein but not kinase activity is critical for glioma cell proliferation and survival. *International journal of cancer* 123(4):769-779.
29. Kobayashi T, Winslow S, Sunesson L, Hellman U, & Larsson C (2012) PKCalpha binds G3BP2 and regulates stress granule formation following cellular stress. *PLoS One* 7(4):e35820.
30. Leonard TA, Rozycki B, Saidi LF, Hummer G, & Hurley JH (2011) Crystal structure and allosteric activation of protein kinase C betaII. *Cell* 144(1):55-66.
31. Ercolani G, Mandolini L, Mencarelli P, & Roelens S (1993) Macrocyclization under thermodynamic control. A theoretical study and its application to the equilibrium cyclooligomerization of .beta.-propiolactone. *J Am Chem Soc* 115(10):3901-3908.
32. Bastings MMC, de Greef TFA, van Dongen JLJ, Merkx M, & Meijer EW (2010) Macrocyclization of enzyme-based supramolecular polymers. *Chemical Science* 1(1):79-88.
33. Sivaramakrishnan S & Spudich JA (2011) Systematic control of protein interaction using a modular ER/K alpha-helix linker. *Proc Natl Acad Sci U S A* 108(51):20467-20472.
34. Kishimoto A*, et al.* (1989) Limited proteolysis of protein kinase C subspecies by calcium-dependent neutral protease (calpain). *J Biol Chem* 264(7):4088-4092.
35. Goldberg J, Nairn AC, & Kuriyan J (1996) Structural basis for the autoinhibition of calcium/calmodulin-dependent protein kinase I. *Cell* 84(6):875-887.
36. Lim WA (2002) The modular logic of signaling proteins: building allosteric switches from simple binding domains. *Curr Opin Struct Biol* 12(1):61-68.

37. Beck M*, et al.* (2011) The quantitative proteome of a human cell line. *Molecular systems biology* 7:549.
38. Ziemba BP, Burke JE, Masson G, Williams RL, & Falke JJ (2016) Regulation of PI3K by PKC and MARCKS: Single-Molecule Analysis of a Reconstituted Signaling Pathway. *Biophys J* 110(8):1811-1825.
39. Maasch C*, et al.* (2000) Protein kinase calpha targeting is regulated by temporal and spatial changes in intracellular free calcium concentration [Ca(2+)](i). *FASEB J* 14(11):1653-1663.
40. Evans JH, Murray D, Leslie CC, & Falke JJ (2006) Specific translocation of protein kinase Calpha to the plasma membrane requires both Ca2+ and PIP2 recognition by its C2 domain. *Molecular biology of the cell* 17(1):56-66.
41. Stubbs CD, Botchway SW, Slater SJ, & Parker AW (2005) The use of time-resolved fluorescence imaging in the study of protein kinase C localisation in cells. *BMC cell biology* 6(1):22.
42. Hudmon A*, et al.* (2005) A mechanism for Ca2+/calmodulin-dependent protein kinase II clustering at synaptic and nonsynaptic sites based on self-association. *J Neurosci* 25(30):6971-6983.
43. Hudmon A, Kim SA, Kolb SJ, Stoops JK, & Waxham MN (2001) Light scattering and transmission electron microscopy studies reveal a mechanism for calcium/calmodulin-dependent protein kinase II self-association. *Journal of neurochemistry* 76(5):1364-1375.
44. Tanimura A, Nezu A, Morita T, Hashimoto N, & Tojyo Y (2002) Interplay between calcium, diacylglycerol, and phosphorylation in the spatial and temporal regulation of PKCalpha-GFP. *J Biol Chem* 277(32):29054-29062.
45. Wang HY, Pisano MR, & Friedman E (1994) Attenuated protein kinase C activity and translocation in Alzheimer's disease brain. *Neurobiology of aging* 15(3):293-298.
46. Ferreira A (2012) Calpain dysregulation in Alzheimer's disease. *ISRN biochemistry* 2012:728571.
47. Ling DS*, et al.* (2002) Protein kinase Mzeta is necessary and sufficient for LTP maintenance. *Nature neuroscience* 5(4):295-296.
48. Volk LJ, Bachman JL, Johnson R, Yu Y, & Huganir RL (2013) PKM-zeta is not required for hippocampal synaptic plasticity, learning and memory. *Nature* 493(7432):420-423.
49. Lee AM*, et al.* (2013) Prkcz null mice show normal learning and memory. *Nature* 493(7432):416-419.
50. Bogard AS & Tavalin SJ (2015) Protein Kinase C (PKC)zeta Pseudosubstrate Inhibitor Peptide Promiscuously Binds PKC Family Isoforms and Disrupts Conventional PKC Targeting and Translocation. *Mol Pharmacol* 88(4):728-735.

Chapter 5: Protein kinase C α nucleotide-bound state regulates quaternary structure

This chapter has been adapted from the following publication:

Swanson, C.J., Udayasuryan, B., Sivaramakrishnan, S. (2016) Protein kinase C α nucleotide bound state regulates quaternary structure, *in preparation*.

5.1 Introduction:

Nearly all classes of NTPases found in biology functionally utilize the distinct nucleotide dependent conformational states inherently adopted in the NTPase catalytic cycle to modulate non-substrate molecular interactions (1). For example, molecular motors including myosin convert ATPase activity into processive unidirectional motility by exploiting the differential affinity of nucleotide states for the protein actin (2). Actin itself has differential propensity to self-assemble or assemble with other cytoskeletal proteins dependent on nucleotide state (3). Studies of naturally occurring, catalytically dead pseudo-kinases have clearly resolved nucleotide dependent allosteric functions (4) suggesting that kinase domains are likely capable of functioning with similar mechanisms (5). How nucleotide dependent conformational states contribute to protein kinase function is still poorly understood. It remains challenging to differentiate allosteric and enzymatic functions of kinases and a need exists for novel experimental techniques, like those available to other ATPases including molecular motors.

Protein kinase C is an important subfamily of AGC kinases involved in many cellular processes including growth factor pathways (6). PKCα is the most studied isoform and is hypothesized to function in regulating the assembly of signaling complexes that arise at cell-cell and cell-ECM junctions (7). We and others have reported the homo-oligomerization of PKCα in

response to effectors (8-10). It is reported that a key oligomerization interface involves the kinase domain and that a nucleotide-competitive inhibitor stabilizes oligomerization and modulates PKCα spatial-temporal function following agonist activation of cells (8). Additionally, a single point mutation in the kinase domain (T638A) that confers constitutive oligomerization of PKCα under *in vitro* basal conditions was reported (8). Together these findings lead us to hypothesize that nucleotide induced conformational changes in the PKCα kinase domain allosterically modulate homo-oligomerization.

This report is focused on a subset of the nucleotide states adopted in the catalytic cycle of a protein kinase; adenosine triphosphate bound (ATP), adenosine diphosphate bound (ADP), and nucleotide free. In each case, we used a saturating concentration of nucleotide (100 μM), and the buffer contains physiological concentrations of $MgCl_2$. We also tested an inhibited state in which the nucleotide competitive PKC inhibitor bisindolylmaleimide 1 (BimI) is incubated at saturating concentrations (10 μM) (11) **(Fig 5.1 a)**. The scope of our experimental methodologies is to examine the molecular effects of nucleotide binding on the quaternary structure of PKC. Several studies have previously explored the structural effects of nucleotide binding on the conformation of the catalytic domain of PKC and other kinases and we refer readers to the following (12-14).

5.2 Materials and methods:

Materials: Unless otherwise stated, all materials were purchased from Sigma-Aldrich. Bisindolylmaleimide I (BimI) was purchased from CalBiochem. MANT- ADP was purchased from Invitrogen. Phorbol-12-myristate-13-acetate (PMA) was purchased from CalBiochem and solubilized in DMSO. Bismaleimidohexane (BMH) was purchased from Pierce and solubilized in DMSO immediately prior to cross-linking experiment. Liposomes were prepared from brain polar lipid extract (Avanti) mixed with 2% w/w DAG (1,2-dihexadecanoyl-*sn*-glycerol; Avanti). The lipid components were stored in chloroform and within 48 hours of experiments the components were mixed and dried under nitrogen, stored under vacuum for 18 hours before being hydrated in assay buffer (see below) for 1 hour at 37 ^{o}C. The suspension was freeze thawed 3 times in liquid nitrogen then hot water, and extruded (Avanti) using 0.2 μm Nuclepore Track-Etch Membrane (Whatman).

Constructs: All PKC constructs were cloned from full-length human cDNA of PKCα (Open Biosystems) using PCR into unique restriction sites in pBiex1 (Novagen), or pcDNA/FRT (Invitrogen) plasmid vectors. All constructs contain a c-terminal FLAG tag. $(Gly\text{-}Ser\text{-}Gly)_{2\text{-}4}$ linkers separate fluorophores from PKC domains and were previously reported (8).

Expression and purification: Sf9 expression and purification was performed as previously described (8). Briefly, Sf9 cells in suspension were transiently transfected with desired DNA constructs using Escort IV transfection reagent (Sigma-Aldrich) and harvested 72 h later. Protein was batch purified with anti-FLAG M2 Affinity gel (Sigma-Aldrich), and buffer-exchanged using Zeba Spin Desalting columns (Pierce) into the working buffer (20 mM HEPES, 0.5 mM EGTA, 5 mM $MgCl_2$, 2 mM DTT brought to pH 7.5 with KOH). Protein was further diluted into this working buffer plus 0.1 mg/ml BSA for all experiments unless otherwise described. Protien concentration was quantified using A280 (NanoDrop 2000, Thermo Scientific) and calculated extinction coefficient (ExPasy), or mCitrine fluorescence fit to a standard curve (FluoroMax-4, Horiba Scientific) prior to each experiment. Protein batches were made fresh and experiments performed within 72 hours of Sf9 cell harvesting.

Spectroscopy measurements: Spectroscopy measurements taken on a Horiba Fluoromax 4 are as previously reported (8). Protein sensors were incubated at room temperature for 30 min with saturating concentrations of nucleotides (100 μM ATP or ADP or 10 μM BimI). Protein concentration for the bimolecular FRET experiment is 40 nM FRET donor mixed with 120 nM FRET acceptor. MANT-ADP binding experiments were performed as previously described (8). All statistics were performed using Prism (GraphPad).

Cross-linking: Cys-Cys cross linking was performed as previously reported using bismaleimidohexane (BMH; Pierce) (8). The working buffer containing 200 nM PKCα-FLAG, 500 μM free Ca^{2+}, 80 μg of PS rich brain polar lipid extract + 2% w/w DAG (Avanti), and 100 μM ATP or ADP or 10 μM BimI was incubated for 5 min at 22^0C before 5 μM of BMH in DMSO was added and vigorously mixed by pipetting. The BMH crosslinking occurred for 2 min before quenching with a gel loading dye to a final concentration of 4 mM DTT and the sample was placed on ice until run on a 10% SDS-PAGE for 1.5 hours at 200v. The gel was stained with coomassie brilliant blue and imaged ChemiDoc-it imaging system (UVP).

Differential sedimentation: Performed as previously described (8). Experimental conditions are matched with those used in spectroscopy measurements, with one difference, 160 nM of PKC – mCit is used (instead of 40 nM mCer – PKC + 120 nM PKC – mCit).

FRET kinetic measurements: Kinetic measurements were obtained on the FlexStation 3Microplate Reader (Molecular Devices). Using flex kinetic mode and monitoring two fluorescent channels (430 nm excitation 475 nm emission; 430 nm excitation 525 nm emission) and using the inline automated injection function. All experiments used 40 nM of mCer- PKC + 120 nM PKC – mCit, and liposomes were prepared as described for other experiments. In all cases after injection of $CaCl_2$ the free calcium concentration in solution is 333 μM, nucleotides were injected to a final concentration of 100 μM, PS48 and PS47 to a final concentration of 200 μM, BimI to a final concentration of 10 μM, and EGTA to a final concentration of 833 μM. Buffer blanks were used to match any dilution effects (10 μl / injection; starting volume of 50 μl). Reported values are the raw ratio of mCit / mCer fluorescence at matched time points. Normalization as in Fig. 5.3b and 5d entailed subtraction of the raw ratio of the –calcium control and normalized to a time point 2 seconds before the second injection. In every case, the presented values are the mean of 3 independent experiments. All data fitting, either single or double exponential functions, were performed in Prism (Graphpad) using non-weighted least squares and constraints to injection times, plateaus and y_0 where appropriate (ie normalized data).

Immunoblotting: Immunoblotting was performed as previously described (8). Recombinant protein samples were separated on 10% polyacrylamide/SDS gels before being transferred to PVDF membrane for 3 h at 300 mA. Blots were blocked with 2% BSA/TBS + 0.1% Tween (TBST) for 1 h at room temperature. Primary PKCα antibody (sc-8393, Santa Cruz Biotechnology, 1:10,000) was added and incubated overnight at 4^0 C. Blots were washed with TBST and incubated for 1 h with secondary (goat anti-Rabbit; Jackson ImmunoResearch Laboratories, Inc., 1:10,000 in 2% BSA/TBST). Blots were washed with TBST, developed with Immunobilin Western chemiluminescent HRP substrate (Millipore), and imaged with ChemiDoc-it imaging system (UVP).

Immunoprecipitation: Anti-PKCα monoclonal antibody (H-7) sc-8393 (Santa Cruz Biotechnology) was diluted to 2 µg / ml in a PBS solution with 50 mM sodium bicarbonate pH 9.1. The solution was added to a clear bottom black walled 96 well polystyrene plate (Greiner Bio One; 50 µl / well) and incubated overnight at 4^0 C. As a control for nonspecific binding 2% BSA in working buffer was pairwise added to matching wells and incubated overnight at 4^0 C. The solutions were aspirated and washed with 2% BSA solution for 2 hrs at room temperature. The test solution containing PKCα-mCit (80 nM) and indicated nucleotides and effectors was added to each well and incubated at room temperature for 1 hr. Each well was washed 3 times with matched buffer and resuspended in matching buffer. mCit fluorescence was quantified by a typhoon phosphoimager (488 nm excitation, 526 sp, 1000 volt gain, focal plane +3 mm). The fluorescent image was analyzed using ImageJ by measuring intensity well by well and pairwise subtracting the nonspecific binding. The specific fluorescent values were normalized by the mean values of the condition on the plate with maximal specific binding.

CHO cell translocation: CHO Flp-in cells (Invitrogen) stably expressing mCer-PKCα-mCit-FLAG were cultured as previously described (8). Cells were transferred to fibronectin coated glass bottom 35 mm tissue culture plates (MatTek Corp.). Cells were allowed to adhere for 1 - 4 h in culturing media before cells were imaged. Cells were washed and resuspended (500 µl) in freshly prepared HBS media (20 mM HEPES, 5mM KCl, 45mM NaCl, 2mM $CaCl_2$, 1mM $MgCl_2$, 0.2% dextrose, brought to pH 7.4 by NaOH). The plates were transferred to the scope and a field of view was manually selected guided by fluorescence expression, and morphology of cells. Cells were exposed for 500 ms once every 30 s for 1,000 s. A 2x perfusion stock in matched buffer was manually pipetted onto the culture plate during imaging after the 5^{th} time point (pipetting took ~3 s). Experiments were performed at 22^0 C. Images were obtained with a Nikon TiE equipped with a mercury arc lamp, a yellow GFP filter cube (Nikon; 500/20 nm excitation, 515 nm LP, 535/30 nm emission), perfect focus system (Nikon), a 40 x 1.4 NA Plan-Apo oil-immersion objective (Nikon), Evolve EMCCD camera (Photometrics), and the Nikon NIS-elements software. Subcellular localization data was analyzed with custom Matlab code where a background region is manually selected, and the mean of the background is subtracted from the corresponding image. The corr2 function is applied to compare each image in a stack with the first image and the output correlation coefficient is used as the metric for translocation. In Fig. 5.6 B the change in correlation coefficient of the DMSO DMSO control (1 – correlation

coefficient for each time point) was calculated and added to the corresponding time point in the other experimental conditions. The 'baseline adjusted' correlation coefficients were least squares fit to the 'one phase decay' function in Prism (Graphpad) to obtain the half-life value.

CHO cell FRET: FRET experiments were conducted the same as translocation experiments with only alterations in the optical path and analysis. A CFP filter cube (Nikon; 436/20 nm excitation, 455 nm LP, and the emission filter removed) and dual-view beam splitter (Photometrics; 505 nm dichroic, and 480/30 nm and 535/40 nm clean up filters) were used for imaging data. The two split channel images per frame were registered using the imregister Matlab function. A background region is manually selected, and the mean of the background in each channel is subtracted from the corresponding image. The FRET value is calculated pixel by pixel by determining the FRET channel/ Donor channel emission. FRET ratio values above and below limits of 4 and 0.5 are excluded as values beyond these limits were empirically found to represent spurious background fluctuations or misalignment between images (and only represent 2.05 ± 0.26% of total measurements). The mean of all FRET ratio values are calculated for each image in the series.

5.3 Results:

Intermolecular FRET biosensors can report nucleotide specific active PKC structural states

An *in vitro* bimolecular FRET assay previously demonstrated to report on direct PKC-PKC interactions (8) was used to assess the effects of nucleotides. The assay involves mCer – PKC + PKC – mCit and requires both free calcium and liposomes in order to observe intermolecular FRET. It was observed that ATP, ADP and AMP-PNP reduced FRET in this assay (**Fig. 5.1 b, C**). ATP and ADP quenched the FRET readout to 0.51 ± 0.17 and 0.73 ± 0.20 of the nucleotide free condition while BimI increased FRET by 1.06 ± 0.18 (mean ± STD.). One consideration is ATP results in autophosphorylation of PKC which alters the intermolecular FRET. However, ATP and its non-hydrolyzable analogue AMP-PNP have statistically indistinguishable effects in this assay suggesting that autophosphorylation is not the primary contributor to changes in FRET in this assay. Other considerations to account for the change in FRET may arise from non-specific effects the nucleotides have on the fluorescence of mCit and mCer or to some idiosyncratic conformational effect due to the fluorescent protein localization next to PKC

domains. To experimentally address the non-specific fluorescence consideration we modified the assay by using mCer - C2 + C2 – mCit (C2 domain from PKC which localizes to plasma membrane and clusters on liposomes in presence of calcium, PS and PI(4,5)P_2 (15)). To address the second consideration we performed the experiment using mCer – PKC + mCit – PKC (where the fluorescent proteins were both fused on the N – terminus of PKC where its orientation is anticipated to be less influenced by conformational changes of the kinase domain). With otherwise matched experimental conditions it was observed that the C2 domain FRET pair had elevated intermolecular FRET levels in the presence of calcium and liposomes, but only 52 % of the FRET response of mCer – PKC + PKC – mCit, and 22 % of mCer – PKC + mCit – PKC. Further, FRET between the C2 domains was independent of nucleotides (**Fig. 5.1 c**). Conversely, the mCer – PKC + mCit – PKC retained sensitivity to nucleotides, and had a greater dynamic range than mCer – PKC + PKC – mCit. We speculate that the dynamic range is higher when fluorescent proteins are both fused on the N-terminal as they are closer in proximity to the C1 and C2 domains which directly interact between PKC molecules (10). For both full length PKC FRET pairs the ATP condition drops FRET to levels similar to the C2 FRET pair. This suggests that ATP disrupts any contribution of intermolecular FRET that arises independent of the C2 domain clustered on liposomes alone. These experimental results provide support that intermolecular FRET in this assay is reporting on structural effects of PKC upon binding to different nucleotides which alter the proximity between PKC molecules.

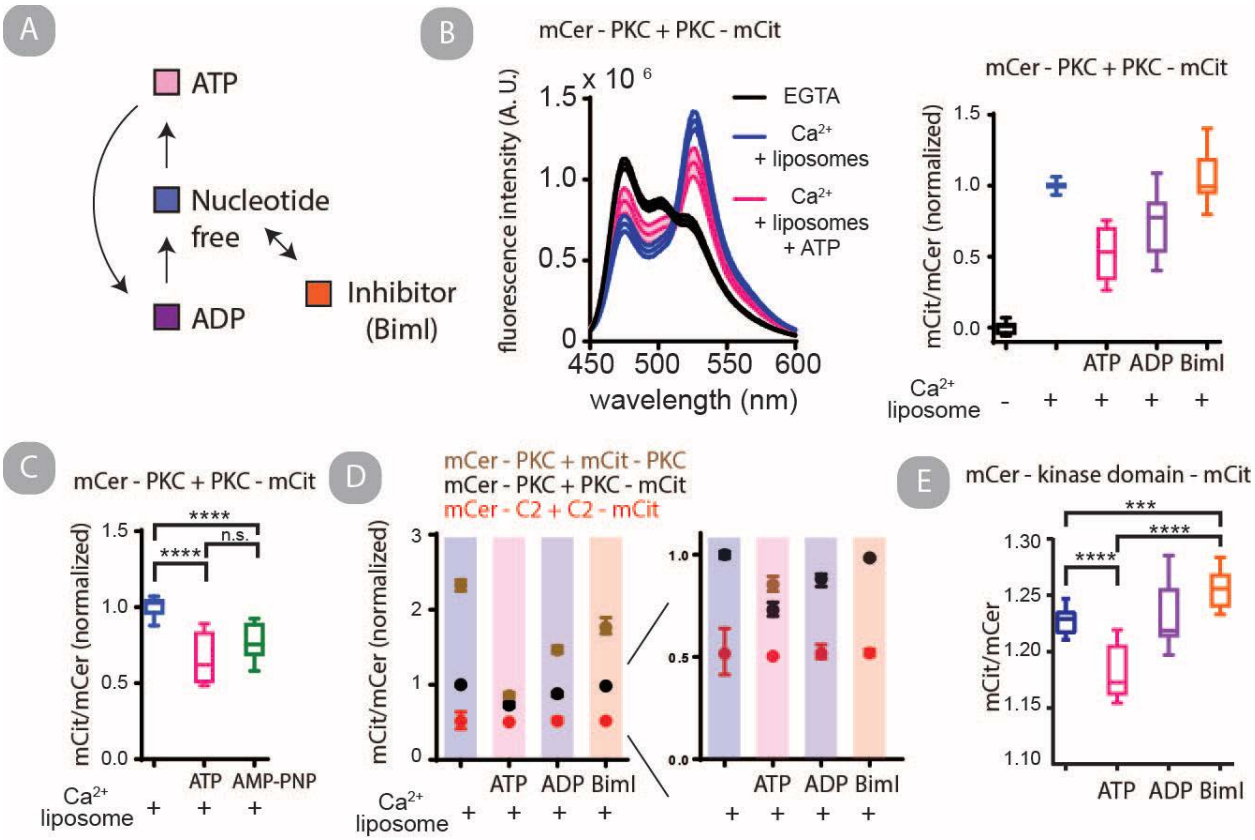

Figure 5.1. Nucleotides induce distinct PKC structural states following activation observable by intermolecular FRET reporters. (**a**) Schematic of implicit nucleotide states in the kinase catalytic cycle and off-pathway ATP-competitive kinase inhibitor bound state. (**b**) (left) Raw fluorescent spectra of mCer – PKC + PKC – mCit (40 and 120 nM respectively) in an EGTA buffered solution (black), in the presence of free calcium and liposomes containing PS, DAG and PI(4,5)P_2 (purple), and in presence of free calcium, liposomes and 100 μM ATP (pink). Shown is mean and STD. of 3 independent measurements. (right) The ratio of mCit/mCer (peaks at 525 nm and 475 nm) with indicated cofactors where the mean ratio of the EGTA condition is subtracted and set as the baseline (0.0) and ratios are normalized to the Ca^{2+} + liposome conditions. Each condition is significantly distinct from all other conditions except for the nucleotide free compared to BimI (P value < 0.005 from student's unpaired t test; N = 15). (**c**) Experiment as in B. comparing the effects of ATP and AMP-PNP which were not statistically (n.s.) distinct from each other (P value > 0.05 from student's unpaired t test; N = 11). (**d**) Fluorescence obtained and normalized as in (b) comparing the relative mCit/mCer ratios of three different bimolecular FRET pairs in matched conditions; mCer – C2 + C2 – mCit (red), mCer – PKC + PKC – mCit (black), and mCer –PKC + mCit – PKC (gold). Shown is mean and STD. of 3 independent experiments, right is a zoomed view of the data on the left. E. A unimolecular FRET biosensor containing the PKC kinase domain equilibrated with indicated nucleotides (*** = P value < 0.001, **** = P value < 0.0001 from student's unpaired t test; N = 9). All box and whisker plots represent min, max, median, 25 and 75 percentiles.

We developed a kinase domain conformational FRET biosensor (mCer – PKC kinase domain – mCit; Fig. 5.1B). We found that both the ATP and BimI but not ADP conditions elicit significantly distinct ensemble FRET measurements from the nucleotide free condition. Additionally, the ATP and BimI states are significantly different from each other **(Fig. 5.1 d)**. These experiments provide support in agreement with previous structural studies investigating nucleotide dependent conformational states in which nucleotide inhibitors are anticipated to stabilize conformations distinct from those formed when bound to nucleotides (16, 17).

Nucleotides disrupt PKC – PKC interactions

We next aimed to assess if nucleotide induced changes in intermolecular FRET resulted from changes in PKC oligomerization. Chemical cross-linking has previously been used as a fluorescent protein independent method to report on PKC clustering (8, 9). Further, chemical crosslinking of PKC is largely independent of the relative concentration of PKC to liposome in solution (8). We observe PKC crosslinking to be sensitive to nucleotides (**Fig. 5.2 a**). Cys-Cys cross linking of PKCα-FLAG under activating conditions resolves a partial depletion of oligomer species with the addition of ATP and ADP while BimI increases the cross-linked species (**Fig. 5.1 d**; ATP – 0.31 ± 0.07, ADP – 0.57 ± 0.15, BimI – 1.56 ± 0.41 normal to nucleotide free cross-linking, mean ± STD.; N = 3). One possibility is all of the observed changes in FRET and crosslinking result purely from confinement on liposomes. If this is the case, the changes in FRET and crosslinking arise from differences in the amount of PKC localized to liposomes. It is known that the off-rate of PKC from liposomes in the presence of calcium is very slow (on the order of days)(18), making differential sedimentation of liposomes a reasonable approach to monitoring the degree of PKC bound to liposomes. To assess differential sedimentation, PKC was pre-incubated with nucleotides prior to the sequential addition of liposomes and calcium. After equilibration, the samples were ultracentrifugated and the pellet and supernatant fractions were run on SDS-PAGE gel (**Fig. 5.2 b**). The fraction of PKC pelleted showed a modest dependence on nucleotide, although substantially less dependence than both intermolecular FRET changes and chemical cross-linking (fraction of PKC pelleted = 0.96 (nucleotide free), 0.81 (ATP), 0.95 (ADP) and 0.98 (BimI)). This result suggests that confinement on liposomes alone is not sufficient to explain the changes in intermolecular FRET although it may contribute. We next completely removed liposomes from the experimental conditions and instead used the soluble PMA molecule which acts as a potent diacylglycerol (DAG) mimetic and directly binds to the C1 domains. Nanomolar-affinity oligomeric interactions between PKC in the presence of calcium and PMA were originally discovered through SPR analysis (10) and we previously confirmed intermolecular PKC interactions through FRET (8). In this experimental condition both ATP and ADP almost entirely quenched intermolecular FRET from both mCer – PKC + PKC – mCit as well as mCer – PKC + mCit – PKC (**Fig. 5.2 c**). This experiment provides strong evidence that nucleotides disrupt direct PKC - PKC interactions, and that changes in intermolecular FRET are primarily reporting on this property.

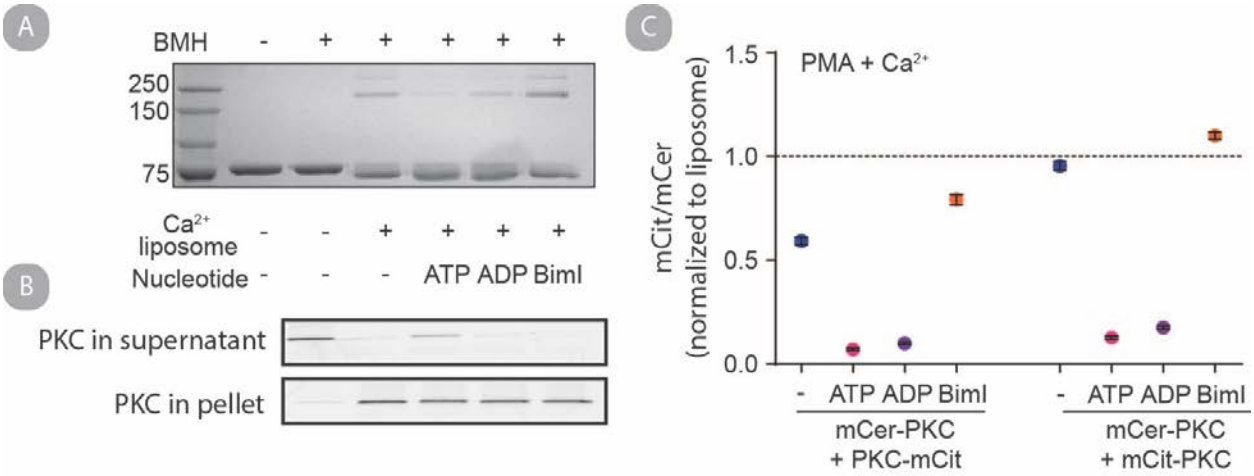

Figure 5.2. Nucleotide induced intermolecular FRET change is dependent on direct PKC interactions. (**a**) Representative coomasie stained SDS-PAGE gel distinguishes between monomeric and oligomeric recombinant PKCα treated with the Cys-Cys crosslinking agent BMH. (**b**) A representative SDS-PAGE of PKCα fractionated by ultracentrifugation in the presence of the indicated cofactors. mCit fluorescence is detected. (**c**) Bimolecular FRET experiments as in figure 1 b – d, however no liposomes are present and instead the soluble PMA (potent DAG mimetic) is used. Data normalized to mean mCit/mCer ratio of mCer-PKC + PKC-mCit in the presence of liposomes. Shown is mean and STD. of 3 repeats.

Dynamic regulation of active PKC structural states

To gain further insight into the dynamic properties associated with nucleotide induced structural states, we performed a coarse (0.33 Hz) kinetic analysis monitoring the change in intermolecular FRET between PKC following injection of nucleotides. Qualitatively, injection of ATP or BimI had dramatic time-dependent effects on intermolecular FRET between activated PKC (**Fig. 5.3 a**). Unfortunately, the sampling frequency is not sufficient to fit the fast decay following injection of ATP. An increased sampling frequency and rapid-mixing techniques will be required for kinetic analysis on the time-scale of phosphorylation reactions in PKC (~5 – 10 Hz) (19). One unanticipated kinetic event is observed as BimI results in a rapid decrease followed by a gradual increase in intermolecular FRET over the course of 1000s of seconds.

We next considered if nucleotide states could influence the dissociation of intermolecular FRET between PKC. To assess this, PKC, liposomes and the indicated nucleotide were preincubated and intermolecular FRET was monitored as free calcium was introduced and subsequently removed from the reaction with the injection of EGTA. We observed that ATP substantially accelerated and BimI substantially retarded the dissociation of intermolecular FRET between PKC following the chelation of free calcium in relation to the nucleotide free condition on the order of 100 – 1000s of seconds (**Fig. 5.3 b**). The normalized dissociation of intermolecular

FRET was reasonably least squares fit to a 2 phase exponential decay constrained to the max and min (r^2 1-phase fit = 0.71 (nucleotide free), 0.62 (ATP), and -0.05 (BimI); r^2 2-phase fit = 0.89 (nucleotide free), 0.84 (ATP), and 0.20 (BimI)) and three terms were evaluated; half-life$_{fast}$, half-life$_{slow}$ and fraction-of-decay$_{fast}$. In all cases the half-life$_{fast}$ were very similar and likely limited by the temporal resolution of the data and as such set as a shared value between all three conditions with no effects on r^2 (95% CI of half-life$_{fast}$ = 5.5 – 10.9 s). In contrast, the half-life$_{slow}$ and fraction-of-decay$_{fast}$ were unique for each condition (95% CI of half-life$_{slow}$ = 517 – 568 s (nucleotide free), 291 – 331 s (ATP), 1689 – 1976 s (BimI); 95% CI of fraction-of-decay$_{fast}$ = 0.25 – 0.29 (nucleotide free), 0.37 – 0.42 (ATP), 0.26 – 0.29 (BimI)). Monitoring intermolecular FRET between PKC resolves kinetic differences that are dependent on nucleotide state but independent of kinase activity.

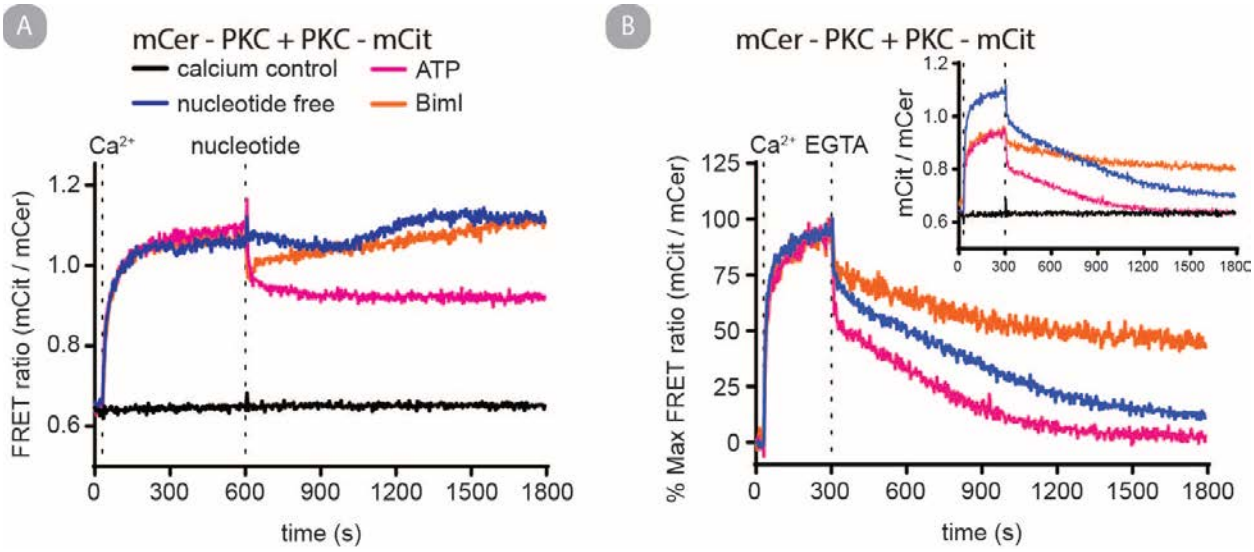

Figure 5.3. ATP accelerates and kinase inhibitor slows off-rate of intermolecular FRET between PKC following calcium chelation. (**a**) Dynamics of the raw FRET ratio following injection of free calcium, and subsequent injection of ATP or BimI. All conditions have matched starting compositions including liposomes, mCer – PKC and PKC – mCit. Data are the mean of 3 independent experiments. (**b**) Four conditions in which matched liposome and protein compositions are premixed with ATP (pink), BimI (orange) or buffer blank (blue and black). The conditions were injected with free calcium and subsequently with excess EGTA. The inset shows the raw mCer/mCit ratio, while the main figure shows the data with the calcium control subtracted and normalized to the FRET ratio three seconds before injection of EGTA. Data are the mean of 3 independent experiments.

PKC hydrophobic motif accessibility is modulated by nucleotides

We identified a monoclonal antibody that demonstrates significantly enhanced binding to activated PKCα. A commercially available monoclonal antibody was raised against a peptide corresponding to residues 647 – 672 of PKCα. Initially through immunoblotting we found

enhanced binding to a constitutively oligomerized mutant of PKCα (T638A) over wild-type **(Fig. 5.4 a)**. Subsequently, we probed immunoprecipitation of PKC wild-type under basal or oligomeric conditions as well as the constitutively oligomerized mutant under basal conditions and activating conditions **(Fig. 5.4 b)**. We report that oligomeric PKC, either wild-type (WT) under activating conditions, or constitutively oligomerized under basal conditions has significantly elevated levels of immunoprecipitation over the monomeric protein (P value from student's unpaired t test ≥ 0.0021). Next, we assessed immunoprecipitation of PKCα (WT) under activating conditions with various nucleotides. The addition of ATP and ADP reduced immunoprecipitation of PKCα to 0.10 ± 0.13% and 0.15 ± 0.21% of the nucleotide free oligomeric condition respectively **(Fig. 5.4 c);** mean ± STD.). This line of experimental probing identifies a correlation in intermolecular FRET and immunoprecipitation; however, the BimI condition does not conform as it demonstrates elevated FRET levels, and cross-linking but minimal immunoprecipitation. Importantly, this experiment illuminates an epitope on the kinase domain with nucleotide dependent accessibility, namely the region of the kinase domain referred to as the hydrophobic motif (HM) based on an AGC kinase family conserved Phe-X-X-Phe motif found at residues 653 – 656 (20).

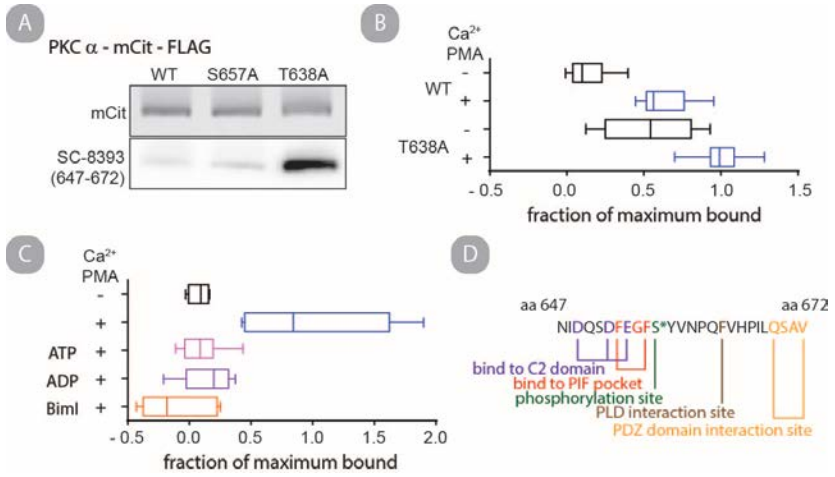

Figure 5.4. Accessibility of PKCα residues 647 – 672 is dependent on nucleotide state. (**a**) PKC probed with a monoclonal antibody raised against a peptide corresponding to residues 647 – 672 (bottom) and total protein loaded (top). SDS-PAGE conditions once buffer exchanged into water following electrophoresis or transferred to PVDF allow for strongly folding domains to retain secondary/tertiary structural features; in the case of mCitrine, fluorescence is maintained, and in the case of the kinase domain, conformational states are distinguishable by antibody binding. The phosphorylation site at T638 is critical in stabilizing the conformation of the C-terminal residues which are probed by the antibody (21). (**b**) Immunoprecipitation of purified PKC WT or T638A in EGTA buffered or in the presence of calcium + PMA (N = 16). (**c**) Immunoprecipitation of PKC with the indicated nucleotides and effectors (N = 6). All box and whisker plots represent min, max, median, 25 and 75 percentiles. (**d**) Amino acid sequence of PKCα residues 647 – 672 with select conformational-dependent functions attributed to specific residues highlighted.

PKC nucleotide states are sensitive to a conserved kinase domain allosteric pathway

Previous structural and dynamic studies of PKC and other AGC kinases have uncovered a conserved allosteric regulatory mechanism in which the hydrophobic motif is a critical component (22). The allosteric pathway links the nucleotide binding pocket with the 'PIF' pocket, a conserved structural element in which the hydrophobic motif binds; this pathway has been most prominently studied in the AGC kinase PDK1 (23). In a comparative crystallographic study of PDK1 (24) (**Fig. 5.5 a**), as well as a MD simulation study of PKCθ (13), it was observed that a single residue corresponding to F353 (PKCα numbering) on the Glycine-rich loop in the nucleotide binding pocket adopts unique conformations dependent on whether the PIF pocket is occupied by the HM or a small-molecule compound (PS48) that mimics the HM. Further, a phosphorylation site (S657) immediately c-terminal of the HM in PKCα is proposed to stabilize the HM-PIF pocket interaction and phosphorylation state allosterically regulates nucleotide binding (13). Comparing crystal structures of PKCβII kinase domain bound to AMP-PNP (25) or a kinase inhibitor (26), the residue corresponding to F353 dramatically alters conformation, although the HM is bound to the PIF pocket in both structures (**Fig. 5.5 a right**). We made two point mutations, F353A and S657A, chosen to disrupt the nucleotide binding pocket-PIF pocket allosteric pathway. We found that both point mutations disrupted nucleotide effects on oligomerization **(Fig. 5.5 b)**. This finding provides a link between the structurally described allosteric pathway and intermolecular FRET between active PKC.

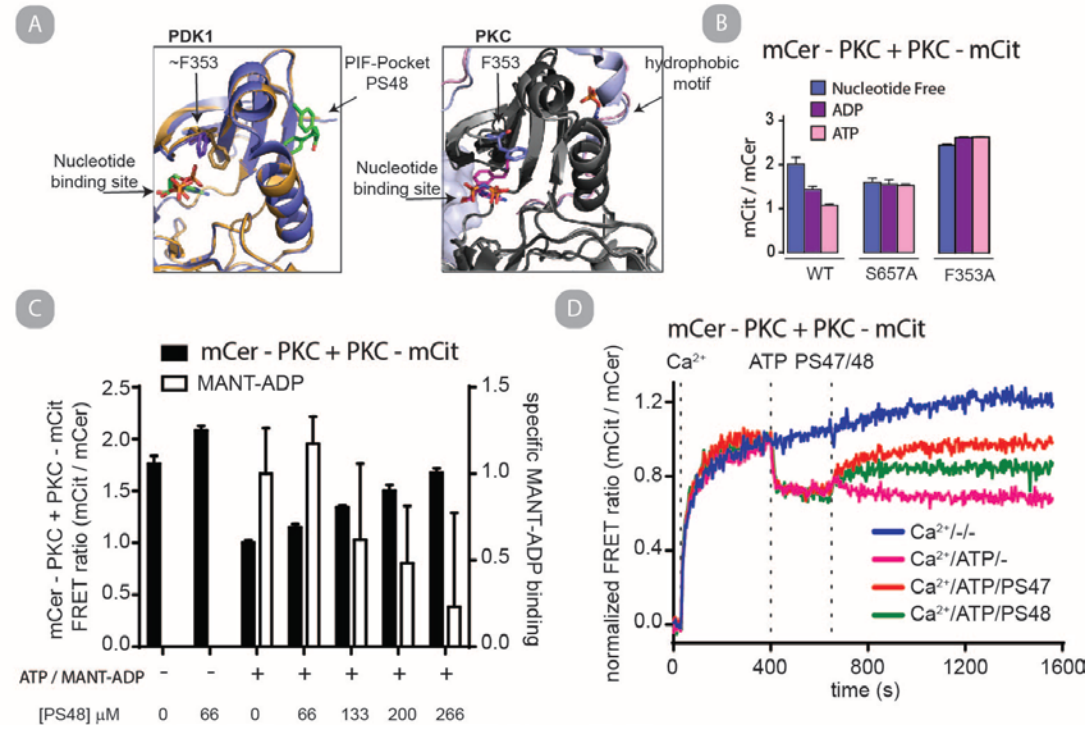

Figure 5.5. PIF pocket occupation is antagonistic with nucleotide pocket occupation. (**a**) Structural alignment of PDK1 with and without PS48 bound to the PIF pocket (left) and structural alignment of PKCβII bound to kinase inhibitor or AMP-PNP (right). Residues corresponding to F353 and S657 are shown as sticks. (**b**) Intermolecular FRET ratio PKC constructs with or without indicated point mutations in matched conditions in the presence of calcium and liposomes, mean and STD. of 3 independent experiments are shown. (**c**) FRET ratio of mCer – PKC + PKC – mCit all in the presence of calcium and liposomes with the presence of 100 μM ATP and indicated concentration of PS48 (black bars). Specific MANT-ADP (100 μM) bound to PKC in matched conditions (white bars); bars represent mean and STD. of 3 independent experiments. (**d**) The normalized FRET ratio following three sequential injections of free calcium (all conditions shown), ATP (pink, red and green) or buffer blank (blue) and PS47 (red) or PS48 (green) or buffer blank (pink and blue). Shown is the mean of 3 independent experiments with baseline subtracted (buffer blank injected all three times) and normalized to the value 3 seconds prior to the second injection.

We next considered if the allosteric PIF pocket could be targeted to modulate PKC function. Given the functional conservation of the PIF pocket/HM interaction in several AGC kinases, including PKC and PDK1, we reasoned that a small molecule targeting the PDK1 PIF pocket should have limited selectivity over the PKC PIF pocket. We measured the effect of PS48 on activated PKCα nucleotide binding (Mant-ADP) and intermolecular FRET. We observed that PS48 had an antagonistic effect on nucleotide binding, in both assay types **(Fig. 5.5 c)**. We next assessed the kinetics of intermolecular FRET between PKC as PS48 and PS47 (stereoisomer of PS48) were injected into solution containing ATP. Both compounds competed the effects of ATP by increasing the intermolecular FRET (**Fig. 5.5 d**). When adjusted for the baseline FRET (blue condition) the change upon injection of PS48 and PS47 could be fit well with a single exponential function (r^2 = 0.64 (PS48), 0.84 (PS47)) and half-life of the function could be

obtained (95% CI half-life = 58 – 80 s (PS48), 80 – 95 s (PS47)). The direct competition between ATP and PS47/48 is at least an order of magnitude slower than the transition between nucleotide free to ATP bound states and ~ two orders of magnitude slower than PKC phosphorylation reactions. These slow kinetics likely limit these particular compounds use as kinase inhibitors. Instead, we considered if these compounds might have an effect on a longer time scale function of PKC.

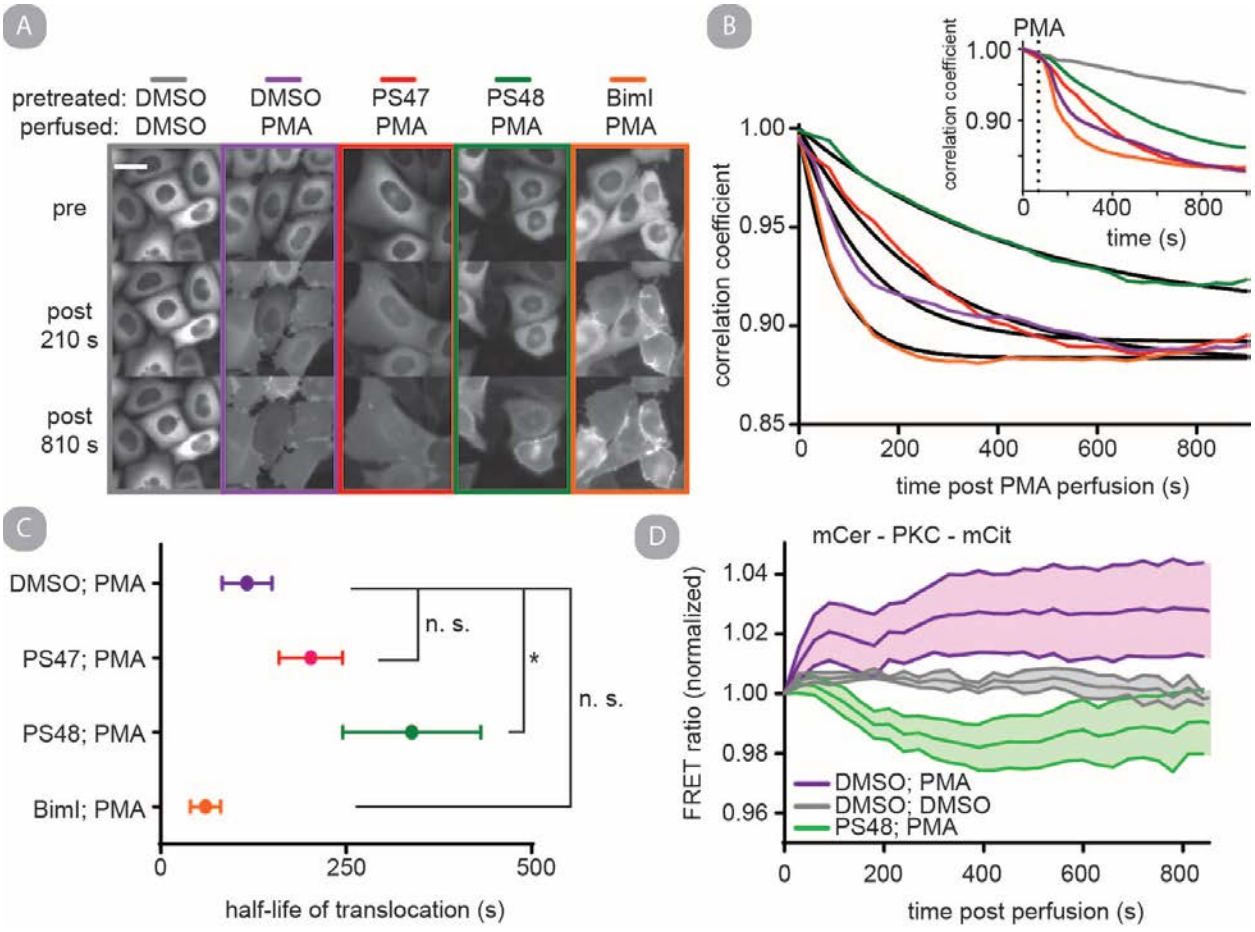

Figure 5.6. PS48 retards PKCα localization in response to PMA in cells (a) Cho cells stably expressing mCer – PKCα – mCit were monitored for mCit fluorescence every 30 s following perfusion with 6 μM of PMA. The cells were pretreated with the indicated compound for 5 min prior to imaging (200 μM PS47 or PS48; 12 μM BimI). Shown are representative images for each condition. The scale bar is 10 μm. **(b)** The correlation coefficient was calculated between the original image in a time series and each subsequent image to quantify the degree of change in fluorescence intensity over time. The correlation coefficient was adjusted for non-specific changes (DMSO condition) and the data were least square fit to a single exponential decay function (corr. coef. = exp(-k*time)). Shown are the mean correlation coefficients with color scheme corresponding to panel A. and the best fit (black lines). Inset shows unadjusted correlation coefficients. N ≥ 4 perfusion chambers and n ≥ 73 cells per condition. **(c)** The mean and S.E.M. of the fitted half-life (half-life = ln(2)/k) of translocation for each individual experiment. The difference between DMSO; PMA and PS48;PMA conditions are statistically significant by a student's unpaired t test (P value = 0.0442) while the other compounds did not alter the half-time significantly (P value > 0.05). **(d)** The mean and S.E.M. FRET ratio of mCer – PKCα – mCit for the indicated conditions following perfusion with DMSO control (gray) or 6 μM PMA (green and purple) and 5 minute pretreatment with DMSO control (gray and purple) or 200 μM PS48 (green); N = 4 perfusion chambers, 70, 57 and 54 individual cells respectively.

We explored if PS47 or PS48 would influence the gradual accumulation of PKC to the plasma membrane of CHO cells following PMA stimulation. In CHO cells stably expressing mCer – PKC – mCit, PMA treatment resulted in a permanent change in the fusion protein subcellular localization that occurred with a mean half-time of 116 s post perfusion (**Fig. 5.6 a-c**). Pretreatment of the cells with PS47, PS48 or BimI qualitatively did not influence where the fusion protein localized following PMA treatment, but did alter the half-time by which the process occurred, however only the PS48 effect was statistically significant (Mean and S.E.M. of half-life = 116 ± 33 s (DMSO, PMA; N = 7), 339 ± 93 s (PS48, PMA; N = 7)). To assess if PS48 had direct effects on the conformation of mCer- PKC – mCit we monitored the ratio of mCit/mCer under matched experimental conditions. Following PMA perfusion onto the CHO cells, the FRET ratio had dramatically different effects in the PS48 treated cells (**Fig. 5.6 d**). This result strongly suggests that PS48 has effects that directly alter the structural state of the PKC FRET sensor, and those effects lead to the retardation of the sensor's subcellular localization.

5.4 Discussion:

While non-substrate interactions prominently influence the catalytic cycle of NTPases such as myosins and ABC transporters, they are yet to be widely appreciated in kinase biology. In this study, we demonstrate that the nucleotide/inhibitor state of activated PKCα influences a previously characterized inter-molecular interaction (8). The measured dissociation kinetics of this intermolecular interaction suggest a structural mechanism by which PKC can increase its residence time at a spatial location close to a local pool of phosphorylatable substrate (**Fig. 5.7**). The phosphorylation state of PKCα (Fig. 5.5), PKC inhibitors (Fig. 5.1 - 4), and small molecule allosteric modulators that disrupt nucleotide binding (Fig. 5.6) influence PKC function by modulating this phenomenon. Together, our findings highlight the coordination between nucleotide binding and inter-molecular interactions in this nodal kinase.

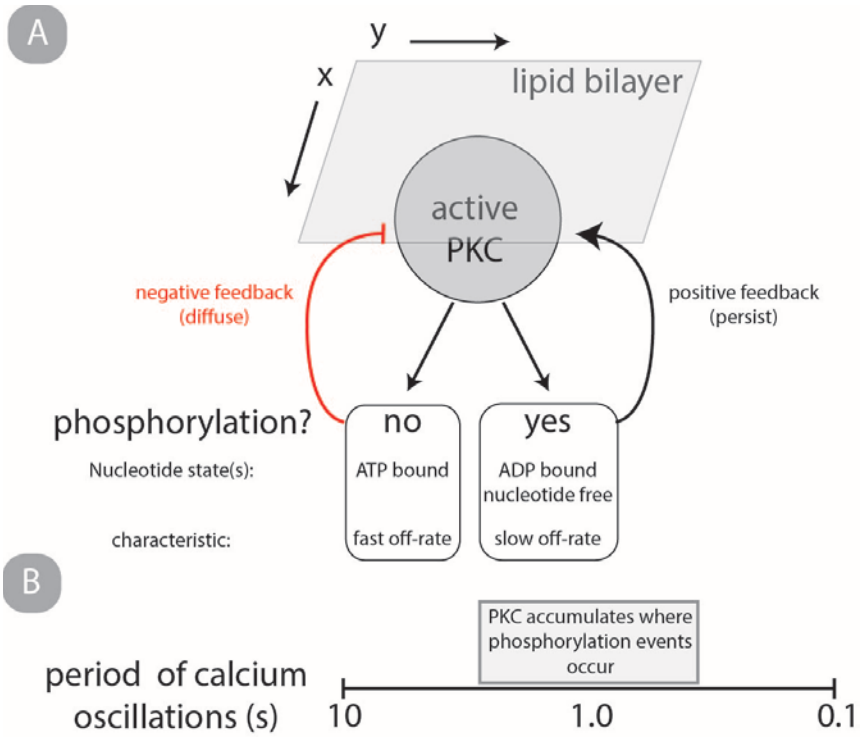

Figure 5.7. Information retention in PKC after phosphorylation. (**a**) Model in which a spatially constrained and fully active PKC molecule either phosphorylates, or does not phosphorylate an arbitrary protein substrate. Based on measured intermolecular FRET dissociation rates between PKC molecules, the persistence of PKC within Forster's radius of other PKC molecules either through direct PKC oligomerization or indirect co-accumulation on liposomes is shortest in conditions when bound to ATP. We hypothesize that nucleotide exchange (ADP bound and nucleotide free states) following a phosphorylation event will result in spatially persistent PKC molecules such as those previously characterized in cells which persist temporally for either ~0.5 s or > 4 s (27). (**b**) We extend our hypothesis to make a prediction on how this may have functional implications in specific biological circumstances. PKC has been observed to integrate calcium oscillations by shifting its distribution between subcellular localizations in specific biological conditions, for example following fertilization in mammalian oocytes (28), but the phenomenon has not been thoroughly explored. Our model anticipates that in a specific band of calcium oscillation periods, PKC may persist specifically at membrane bound localizations where phosphorylation events have recently occurred.

Intracellular signal transduction must balance rapid signal amplification while maintaining high-fidelity information transfer. To facilitate these dual specifications, signaling proteins generally fall into two classes. Signal amplification occurs through activation of high substrate turnover enzymes, for example ion channels or secondary messenger producing enzymes. Specificity emerges from spatially and temporally regulated protein-protein interactions with limited or no catalytic capacities, for example G-proteins and scaffold proteins. Protein kinases involved in signal transduction (as opposed to metabolic processes) have low substrate turnover and are likely more critical for signal specificity as opposed to signal amplification (5). As such, it is not surprising that PKC has evolved the capacity (like many other NTPases) to use distinct nucleotide states to transfer information in the form of molecular interactions to enhance specificity; in this case a combination of homo-oligomerization and protein – lipid interactions

influencing the spatial-temporal localization of the molecule. We identified one region in particular, residues 647 – 672 which is only accessible to immunoprecipitation by a monoclonal antibody in the activated nucleotide free state (Fig. 5.4). Interestingly, several conformation dependent binding interactions have been attributed to specific residues within this region including binding to the PKC C2 domain (29), the allosteric activation of phospholipase D (PLD) (30, 31), and recruitment of PICK1 to the plasma membrane (32, 33) (**Fig. 5.4 d**). It will be interesting to consider if those functions are dependent on nucleotide state. Further, this region is absolutely required for kinase activity and in molecular dynamic simulations is anticipated to be the most dynamic within the kinase domain (34).

In this study we kinetically resolve two components of intermolecular FRET dissociation following rapid calcium chelation, very rapid (< 10 s) and long (~100 – 1000 s) persisting populations (Fig. 5.3 b). This data is consistent with an interpretation that intermolecular FRET arises from PKC oligomerization as well as confinement on liposomes. In such a case it is reasonable that the intermolecular FRET arising from oligomerized PKC will have a slower dissociation than the contribution resulting purely from liposome binding. Alternatively, all intermolecular FRET may occur through non-specific interactions brought about by confinement on liposomes. In such a case the fast and slow dissociations observed in Fig. 5.3 B may be caused by the so called ‘weakly bound state’ and ‘tightly bound state’ that differ in how the C1 domains interact with DAG and other phospholipids (27, 35). The observations that nucleotide induced changes in intermolecular FRET are independent of liposomes (Fig. 5.2 c) and that nucleotides have only modest effects on PKC - liposome binding (Fig. 5.2 b) support the first interpretation. Independent of either interpretation, the dissociation of the C2 domain from liposome upon calcium chelation has been reported to occur within ~2 ms (36) suggesting that other PKC structural effects sensitive to nucleotides have profound effects on PKC interactions with liposomes or other PKC molecules persisting up to 5 orders of magnitude longer than the C2 domain alone (Fig. 5.3b). These *in vitro* results are consistent with experiments performed in permeabilized cells where it is reported that ATP depletion and PKC kinase inhibitors in the same class as BimI dramatically slow the off-rate of plasma membrane bound PKC in cells following a reduction in free calcium (37). It is intriguing to speculate that nucleotide dependent dissociation of PKC – lipid complexes may relate to the observation that spatially constrained PKCα residence time on the plasma membrane is bifurcated into short (< 0.5 s; approximate time

of phosphorylation event) and long-lived (> 4 s) events (27) (Fig. 5.7). Similarly, it was observed that at the level of net cellular translocation of PKCα on and off the plasma membrane following histamine or carbachol stimulation of HEK293 a bifurcation of fast and slow off-rates differing by nearly an order of magnitude occurs (~2 – 20 s) (38). In such an instance, if we assume PKC is primarily bound to ATP, nucleotide exchange following a phosphorylation event may lead to longer temporal persistence at a given spatial location than if no phosphorylation event occurs. This is directly supported by our finding that ATP promotes accelerated dissociation of PKC compared to nucleotide free (Fig. 5.3 b). In order to assess such a model, detailed studies investigating the kinetic cycle of PKC must be conducted in cellular environments. A major long-term goal is to develop methodologies in which this type of information can be obtained.

Kinase domain conformational effects on the quaternary structure of PKC provides new insight into many previous findings. Several reports characterize altered spatial temporal localization or posttranslational processing of PKC as unanticipated effects of point-mutations in the kinase domain or nucleotide competitive inhibitors (16, 29, 39). The effects that point mutations have on quaternary structure may be pertinent to PKC function. For example, PKC activation by phorbol ester has an unambiguous role in tumorigenesis, yet a recent report studying point mutations in PKC occurring in human cancers found that most reduced catalytic output (40). We anticipate that allosteric effects caused by these point mutations may contribute to tumorigenesis and homo-oligomerization may explain the reported haploinsufficiency of PKC (40). The PKC family has been a long-standing druggable candidate for several indications, yet despite significant effort and resources, no PKC inhibitor has been clinically effective (41). An understanding of any allosteric functions of PKC may uncover unique therapeutic strategies. Last, based on the structural homology (20), we anticipate that many AGC kinases incorporate nucleotide-induced plasticity to regulate function.

5.5 Conclusions:

In this chapter we explore how conformational changes localized in a single domain alter molecular functions of the entire protein. In **Chapter 2 and 4** we characterized functional relationships between the kinase domain and regulatory domains. In **Chapter 3** we identified the intramolecular interaction between the regulatory domains C1a and C2 as the key determinants

of self-assembly. In this chapter we provide initial evidence that all of these domain interactions are interconnected and responsive to each other. We conclude that nucleotides induce conformational changes in the kinase domain. We further conclude that the nucleotide induced conformational states of the kinase domain elicit unique structural properties reflected in how full PKC are oriented with one another on lipid bilayers. We postulate that the distinct nucleotide states of PKC arise through changes in internal domain-domain interactions and a fully active kinase domain will constantly be cycling between these states.

5.6 References:

1. Vetter IR & Wittinghofer A (1999) Nucleoside triphosphate-binding proteins: different scaffolds to achieve phosphoryl transfer. *Quarterly reviews of biophysics* 32(1):1-56.
2. Lymn RW & Taylor EW (1971) Mechanism of adenosine triphosphate hydrolysis by actomyosin. *Biochemistry* 10(25):4617-4624.
3. Straub FB & Feuer G (1950) [Adenosine triphosphate, the functional group of actin]. *Kiserletes orvostudomany* 2(2):141-151.
4. Zeqiraj E & van Aalten DM (2010) Pseudokinases-remnants of evolution or key allosteric regulators? *Curr Opin Struct Biol* 20(6):772-781.
5. Shaw AS, Kornev AP, Hu J, Ahuja LG, & Taylor SS (2014) Kinases and pseudokinases: lessons from RAF. *Mol Cell Biol* 34(9):1538-1546.
6. Steinberg SF (2008) Structural basis of protein kinase C isoform function. *Physiol Rev* 88(4):1341-1378.
7. Rosse C*, et al.* (2010) PKC and the control of localized signal dynamics. *Nat Rev Mol Cell Biol* 11(2):103-112.
8. Swanson CJ*, et al.* (2014) Conserved modular domains team up to latch-open active protein kinase Calpha. *J Biol Chem* 289(25):17812-17829.
9. Huang SM, Leventhal PS, Wiepz GJ, & Bertics PJ (1999) Calcium and phosphatidylserine stimulate the self-association of conventional protein kinase C isoforms. *Biochemistry* 38(37):12020-12027.
10. Slater SJ*, et al.* (2002) Regulation of PKC alpha activity by C1-C2 domain interactions. *J Biol Chem* 277(18):15277-15285.
11. Toullec D*, et al.* (1991) The bisindolylmaleimide GF 109203X is a potent and selective inhibitor of protein kinase C. *J Biol Chem* 266(24):15771-15781.
12. Huse M & Kuriyan J (2002) The conformational plasticity of protein kinases. *Cell* 109(3):275-282.
13. Seco J, Ferrer-Costa C, Campanera JM, Soliva R, & Barril X (2012) Allosteric regulation of PKCtheta: understanding multistep phosphorylation and priming by ligands in AGC kinases. *Proteins* 80(1):269-280.
14. Kannan N, Haste N, Taylor SS, & Neuwald AF (2007) The hallmark of AGC kinase functional divergence is its C-terminal tail, a cis-acting regulatory module. *Proc Natl Acad Sci U S A* 104(4):1272-1277.
15. Egea-Jimenez AL*, et al.* (2014) Phosphatidylinositol-4,5-bisphosphate enhances anionic lipid demixing by the C2 domain of PKCalpha. *PLoS One* 9(4):e95973.

16. Cameron AJ, Escribano C, Saurin AT, Kostelecky B, & Parker PJ (2009) PKC maturation is promoted by nucleotide pocket occupation independently of intrinsic kinase activity. *Nat Struct Mol Biol* 16(6):624-630.
17. Messerschmidt A*, et al.* (2005) Crystal structure of the catalytic domain of human atypical protein kinase C-iota reveals interaction mode of phosphorylation site in turn motif. *J Mol Biol* 352(4):918-931.
18. Bazzi MD & Nelsestuen GL (1991) Highly sequential binding of protein kinase C and related proteins to membranes. *Biochemistry* 30(32):7970-7977.
19. Sando JJ, Chertihin OI, Owens JM, & Kretsinger RH (1998) Contributions to maxima in protein kinase C activation. *J Biol Chem* 273(51):34022-34027.
20. Pearce LR, Komander D, & Alessi DR (2010) The nuts and bolts of AGC protein kinases. *Nat Rev Mol Cell Biol* 11(1):9-22.
21. Hauge C*, et al.* (2007) Mechanism for activation of the growth factor-activated AGC kinases by turn motif phosphorylation. *EMBO J* 26(9):2251-2261.
22. Frodin M*, et al.* (2002) A phosphoserine/threonine-binding pocket in AGC kinases and PDK1 mediates activation by hydrophobic motif phosphorylation. *EMBO J* 21(20):5396-5407.
23. Gold MG, Barford D, & Komander D (2006) Lining the pockets of kinases and phosphatases. *Curr Opin Struct Biol* 16(6):693-701.
24. Hindie V*, et al.* (2009) Structure and allosteric effects of low-molecular-weight activators on the protein kinase PDK1. *Nat Chem Biol* 5(10):758-764.
25. Leonard TA, Rozycki B, Saidi LF, Hummer G, & Hurley JH (2011) Crystal structure and allosteric activation of protein kinase C betaII. *Cell* 144(1):55-66.
26. Grodsky N*, et al.* (2006) Structure of the catalytic domain of human protein kinase C beta II complexed with a bisindolylmaleimide inhibitor. *Biochemistry* 45(47):13970-13981.
27. Reither G, Schaefer M, & Lipp P (2006) PKCalpha: a versatile key for decoding the cellular calcium toolkit. *J Cell Biol* 174(4):521-533.
28. Halet G, Tunwell R, Parkinson SJ, & Carroll J (2004) Conventional PKCs regulate the temporal pattern of Ca2+ oscillations at fertilization in mouse eggs. *J Cell Biol* 164(7):1033-1044.
29. Stensman H, Raghunath A, & Larsson C (2004) Autophosphorylation suppresses whereas kinase inhibition augments the translocation of protein kinase Calpha in response to diacylglycerol. *J Biol Chem* 279(39):40576-40583.
30. Hu T & Exton JH (2003) Mechanisms of regulation of phospholipase D1 by protein kinase Calpha. *J Biol Chem* 278(4):2348-2355.
31. Chen JS & Exton JH (2004) Regulation of phospholipase D2 activity by protein kinase C alpha. *J Biol Chem* 279(21):22076-22083.
32. Masukawa K, Sakai N, Ohmori S, Shirai Y, & Saito N (2006) Spatiotemporal analysis of the molecular interaction between PICK1 and PKC. *Acta histochemica et cytochemica* 39(6):173-181.
33. Staudinger J, Zhou J, Burgess R, Elledge SJ, & Olson EN (1995) PICK1: a perinuclear binding protein and substrate for protein kinase C isolated by the yeast two-hybrid system. *J Cell Biol* 128(3):263-271.
34. Yeong SS*, et al.* (2006) The last 10 amino acid residues beyond the hydrophobic motif are critical for the catalytic competence and function of protein kinase Calpha. *J Biol Chem* 281(41):30768-30781.
35. Ziemba BP*, et al.* (2014) Single-Molecule Studies Reveal a Hidden Key Step in the Activation Mechanism of Membrane-Bound Protein Kinase C-alpha. *Biochemistry* 53(10):1697-1713.
36. Nalefski EA & Newton AC (2001) Membrane binding kinetics of protein kinase C betaII mediated by the C2 domain. *Biochemistry* 40(44):13216-13229.

37. Tanimura A, Nezu A, Morita T, Hashimoto N, & Tojyo Y (2002) Interplay between calcium, diacylglycerol, and phosphorylation in the spatial and temporal regulation of PKCalpha-GFP. *J Biol Chem* 277(32):29054-29062.
38. Sinnecker D & Schaefer M (2004) Real-time analysis of phospholipase C activity during different patterns of receptor-induced Ca2+ responses in HEK293 cells. *Cell calcium* 35(1):29-38.
39. Maasch C*, et al.* (2000) Protein kinase calpha targeting is regulated by temporal and spatial changes in intracellular free calcium concentration [Ca(2+)](i). *FASEB J* 14(11):1653-1663.
40. Antal CE*, et al.* (2015) Cancer-associated protein kinase C mutations reveal kinase's role as tumor suppressor. *Cell* 160(3):489-502.
41. Mochly-Rosen D, Das K, & Grimes KV (2012) Protein kinase C, an elusive therapeutic target? *Nature reviews. Drug discovery* 11(12):937-957.

Chapter 6: Conclusions and future directions

6.1 General Conclusions:

In this dissertation we have employed the SPASM methodology to assess relationships between domain-domain interactions and functions of protein kinase C α (PKCα). Through the pursuit of this aim a new function of PKCα was identified: spontaneous and reversible self-assembly. Three functions of domain-domain interactions have been identified: 1.) the autoinhibition of kinase catalytic activity through an intramolecular interaction with the regulatory domains, 2.) the calcium stimulated self-assembly of PKC through an intramolecular interaction between the C1a and C2 domain, and 3.) the heterologous conjoining of self-assembled PKC clusters through ring opening polymerization (R.O.P.) mediated through kinase domain and regulatory domain interactions. Next, it was discovered that nucleotide induced conformations of the kinase domain alter the functionality of disparate domains. Together, this work provides the foundation for new research directions directed at understanding the regulation and dysregulation of PKC in physiological phenomena. Finally, this work establishes PKC as a molecular system defined and regulated through interactions between its constituent protein domains.

This dissertation work began by exploring the mechanism of autoinhibition of kinase activity in PKCα. In particular, we aimed to establish that (i) autoinhibition arises through intramolecular interactions between the kinase domain and regulatory domains and (ii) these interactions are disrupted upon PKC binding of calcium and diacylglycerol. Through utilization of SPASM methodology we observed a negative correlation between intramolecular interactions and the specific kinase activity of PKC *in vitro* in the absence of calcium or diacylglycerol **(Chapter 2)**. This provides direct evidence for autoinhibition mediated through intramolecular interactions in PKCα and is fully consistent with contemporary models of PKC regulation (1, 2). Future work may extend on this question by using the constructed SPASM containing PKC proteins or

derivatives of it to identify specific interfaces between protein domains that facilitate autoinhibition.

In contrast to contemporary models, we observed that domain-domain interactions persist even in the presence of calcium and diacylglycerol. Through the use of bi-molecular FRET reporters and Cys-Cys crosslinking we demonstrated that domain-domain interactions occur *in trans* resulting in oligomerization of PKC in the presence of calcium and other effectors. We observed a modest correlation between kinase activity and oligomerization, wherein the disruption of oligomerization resulted in reduced kinase activity indicating that the domain-domain interactions are distinct between the autoinhibited and oligomerized states of PKC. We further provided evidence that oligomerization occurs in mammalian cells following agonist activation of PKC. Finally, we developed pharmacological agents to disrupt PKC oligomerization *in vitro* and in mammalian cells. We found that use of these pharmacological PKC oligomerization inhibitors completely disrupted a cellular downstream function of PKC. Together, these results provide evidence for a new functional state of oligomerized PKCα. We propose a model in which oligomerization may reduce the free energy of PKC to balance the anticipated increase in free energy resulting from the disruption of autoinhibitory interactions.

We next aimed to address several shortcomings and unaddressed questions remaining after our initial characterization of oligomerization of PKCα. We focused on three questions in **Chapter 3**: (*i*) is oligomerization driven by PKC-PKC interactions, or instead by organization of lipid components within lipid bilayers? (*ii*) What are the minimal PKC components and their organization required for oligomerization? (*iii*) Can we obtain more direct evidence for PKC oligomerization in cells? We found that self-assembly of PKCα can occur independent of lipid components altogether in a calcium dependent manner. We identified two covalently linked domains, the C1a and C2 domains, are minimally required for self-assembly. We incorporated SPASM methodology to demonstrate the dependence of self-assembly on the intramolecular interactions between the C1a and C2 domains. Finally, we incorporated homo-FRET methodology to provide direct evidence of intermolecular FRET between activated PKC in mammalian cells.

We next followed up on the observations from Chapter 3 that the kinase domain, while not necessary, contributes to self-assembly of PKCα. In **Chapter 4** we explore if ring opening

polymerization (R.O.P.) may contribute to the size of PKCα self-assemblies. Using SPASM methodology, we find an inverse correlation between intramolecular interactions and the size of self-assemblies. When comparing with an analytical model for R.O.P., we find modest agreement in the fold increase in the size of self-assemblies and the fraction of monomeric PKC molecules anticipated to dimerize through R.O.P. This result presents an unanticipated function of PKC resulting from a known intramolecular interaction.

Finally, we explore how the functionality of a single domain impacts the functionality of other domains. In **Chapter 5** we explore conformational changes within the kinase domain and how these changes impact domain-domain interactions as well as functionality of PKC as a whole. We observed that nucleotide or nucleotide competitive inhibitor binding elicits conformational changes that regulate self-assembly. These nucleotide dependent structural states can be tied to differences in the dynamic localization of PKC in cells providing insight to a number of previously observed cellular phenomena. Together these observations suggest a mechanism by which domain-domain interactions within PKC and are constantly changing in line with the catalytic cycle of the kinase domain. We have proposed a mechanism by which the turnover of a catalytic cycle initiated by the phosphorylation of a substrate will result in the spatial accumulation of PKC in a subcellular region.

6.2 Future directions: PKC biology

The work presented in this dissertation provides a new framework to understand PKC conformation that will require substantial future efforts in order to define the physiological functionality of domain-domain interactions and self-assembly of PKC. Some immediate questions entail exploring the relationship between chronic dysregulation of PKC and the emergence of pathophysiologies. For example, Alzheimer's disease entails chronic dysregulation of calcium and PKC, and leads to dysregulation of PKC localization (3, 4). It will be critical to evaluate the role of self-assembly of PKC in mediating chronic effects. A common theme in biology is the persistence of molecular assemblies beyond the lifetime of any of the constituent molecules. One could envision the physiological role of proteolysis of PKC between the regulatory domains and kinase domain as a mechanism to regulate assemblies of PKC as demonstrated in **Chapter 4**.

Ongoing efforts have been exploring the role of PKC in the formation of dynamically regulated assemblies of signaling molecules on the plasma membrane (5). One postulation of PKC function can be as a dynamic hub that nucleates the assembly of signaling complexes. The ability for PKC to rapidly localize and self-assemble at distinct plasma membrane focal points presents at least two orthogonal mechanisms by which distinct signaling assemblies may form. First and most simple, PKC may directly scaffold proteins at this indicated focal point. Second, PKC kinase activity may be a mechanism to generate a localized environment recruiting specific signaling molecules. For example, the bona fide PKC substrate MARCKS is a disordered protein in ~100 fold molar excess of PKC which binds and sequesters the majority of the cellular pool of $PI(4,5)P_2$ in plasmalemmal rafts (6-9). Local calcium release at the plasma membrane leads to a local increase in free [$PI(4,5)P_2$] as calcium/calmodulin binds to MARCKS and disrupts its interaction with $PI(4,5)P_2$ (9). PKC rapidly accumulates to areas of local calcium release and is activated by directly binding $PI(4,5)P_2$ (even in the absence of DAG) (10-13). Upon phosphorylation by PKC, the electrostatic interactions between the highly basic MARCKS protein and $PI(4,5)P_2$ are disrupted further increasing the free [$PI(4,5)P_2$] within a corralled pool of MARCKS sequestered $PI(4,5)P_2$ (9). Exposed $PI(4,5)P_2$ recruits other signaling molecules and alters actin cytoskeletal regulation in order for many cell signaling complexes to form including focal adhesions, adheren junctions and synapses with the nervous system (9, 14). The potential role PKC self-assembly plays in the formation and regulation of such signaling complexes appears an important and promising direction of future research.

6.3 Future directions: multi-domain proteins as molecular systems

The point that protein domains facilitate modular signaling systems in biology has been established over a decade ago (15). Functional modules comprising two or more multi-domain proteins that strongly interact with each other to perform a common function (protein complexes) are ubiquitous in cellular signaling, and these modules participate within networks by directly interacting with other modules (16). A good example of this is the MAPK module, in which proteins interact to form a complex and perform a common function which directly interfaces with other modules forming a signaling network (17). If the signaling network changes, the MAPK module can still assemble and perform its function however interfacing with a different subset of modules. This dissertation is concerned with a similar concept where the system is

composed of a single multi-domain protein in which each domain is a module. Through a network of direct interactions between the domains, the multi-domain protein system has a distinct function. In such a case the function of the system is dependent on the network of interactions between domains. In this present work we explored how the function of PKCα, either evaluated as kinase activity or self-assembly, is dependent on the network of domain-domain interactions.

Each multi-domain system is likely a module, or part of a module within broader cellular signaling systems. What are the implications of a single multi-domain protein having multiple functions within different signaling networks? For example, does PKCα have a conserved molecular function within the same cellular system following PLC activity as an action potential? It appears doubtful given the vastly different timescales of these cellular inputs (ms compared to hours). As introduced in **Chapter 1**, the currency of PKCα regulation lies in domain-domain interactions. The biological significance of PKCα is well established, but without a comprehensive understanding of domain-domain interactions and their functional consequences, studies will continue to be relegated to cumbersome empirical approaches in cell lines and model organisms where the ability to predict function may not be further refined. For a protein that is universally expressed in all human cell types, and often has multiple functions within the same cell type, it is not feasible to empirically describe each of these functions. Rather, an understanding of the general principles by which the molecule may be differentially regulated, and how those changes result in different molecular functions may facilitate a deeper understanding of how biological phenomena emerge.

Finally, it remains to be established if other multi-domain proteins have similar characteristics, or if PKCα is exceptional. Future efforts are needed to establish improved methodologies for investigating intramolecular domain-domain interactions such that appropriate conceptual frameworks, terminology and predictive models may be developed. In conjunction, appropriate venues must be identified for presenting advancements in this direction.

6.4 References:

1. Violin JD, Zhang J, Tsien RY, & Newton AC (2003) A genetically encoded fluorescent reporter reveals oscillatory phosphorylation by protein kinase C. *J Cell Biol* 161(5):899-909.
2. Oancea E & Meyer T (1998) Protein kinase C as a molecular machine for decoding calcium and diacylglycerol signals. *Cell* 95(3):307-318.
3. Wang HY, Pisano MR, & Friedman E (1994) Attenuated protein kinase C activity and translocation in Alzheimer's disease brain. *Neurobiology of aging* 15(3):293-298.
4. Alkon DL, Sun MK, & Nelson TJ (2007) PKC signaling deficits: a mechanistic hypothesis for the origins of Alzheimer's disease. *Trends Pharmacol Sci* 28(2):51-60.
5. Rosse C*, et al.* (2010) PKC and the control of localized signal dynamics. *Nat Rev Mol Cell Biol* 11(2):103-112.
6. Yang L & Glaser M (1996) Formation of membrane domains during the activation of protein kinase C. *Biochemistry* 35(44):13966-13974.
7. Ziemba BP, Burke JE, Masson G, Williams RL, & Falke JJ (2016) Regulation of PI3K by PKC and MARCKS: Single-Molecule Analysis of a Reconstituted Signaling Pathway. *Biophys J* 110(8):1811-1825.
8. Hartwig JH*, et al.* (1992) MARCKS is an actin filament crosslinking protein regulated by protein kinase C and calcium-calmodulin. *Nature* 356(6370):618-622.
9. McLaughlin S, Wang J, Gambhir A, & Murray D (2002) PIP(2) and proteins: interactions, organization, and information flow. *Annu Rev Biophys Biomol Struct* 31:151-175.
10. Maasch C*, et al.* (2000) Protein kinase cα targeting is regulated by temporal and spatial changes in intracellular free calcium concentration [Ca(2+)](i). *FASEB J* 14(11):1653-1663.
11. Egea-Jimenez AL, Perez-Lara A, Corbalan-Garcia S, & Gomez-Fernandez JC (2013) Phosphatidylinositol 4,5-bisphosphate decreases the concentration of Ca2+, phosphatidylserine and diacylglycerol required for protein kinase C α to reach maximum activity. *PLoS One* 8(7):e69041.
12. Reither G, Schaefer M, & Lipp P (2006) PKCα: a versatile key for decoding the cellular calcium toolkit. *J Cell Biol* 174(4):521-533.
13. Evans JH, Murray D, Leslie CC, & Falke JJ (2006) Specific translocation of protein kinase Cα to the plasma membrane requires both Ca2+ and PIP2 recognition by its C2 domain. *Molecular biology of the cell* 17(1):56-66.
14. Laux T*, et al.* (2000) GAP43, MARCKS, and CAP23 modulate PI(4,5)P(2) at plasmalemmal rafts, and regulate cell cortex actin dynamics through a common mechanism. *J Cell Biol* 149(7):1455-1472.
15. Pawson T & Nash P (2003) Assembly of cell regulatory systems through protein interaction domains. *Science* 300(5618):445-452.
16. Alon U (2003) Biological networks: the tinkerer as an engineer. *Science* 301(5641):1866-1867.
17. Schaeffer HJ & Weber MJ (1999) Mitogen-activated protein kinases: specific messages from ubiquitous messengers. *Mol Cell Biol* 19(4):2435-2444.

Appendices

Appendix A: Structural properties of ER/K α-helices

This chapter has been adapted from the following publication:

Swanson, C.J., Sivaramakrishnan, S. (2014) Harnessing the unique structural properties of isolated α-helices, *Journal of Biological Chemistry*, **289**, 25460-67.

A.1 Coiled-coil or single α-helical (SAH) domain ?

The α-helix is a ubiquitous secondary structural element that is almost exclusively observed in proteins when stabilized by tertiary or quaternary interactions. However, beginning with the unexpected observations of α-helix formation in the isolated C-peptide in ribonuclease A, there is growing evidence that a significant percentage (0.2 %) of all proteins contain isolated stable single α-helical domains (SAH). These SAH domains provide unique structural features essential for normal protein function. A subset of SAH domains contain a characteristic ER/K motif, comprised of a repeating sequence of ~ four consecutive glutamic acids (E) followed by ~ four consecutive basic arginine or lysine (R/K) residues. The ER/K α-helix, also termed the ER/K linker, has been extensively characterized in the context of the myosin family of molecular motors, and is emerging as a versatile structural element for protein and cellular engineering applications. Here, we review the structure and function of SAH domains, and the tools to identify them in natural proteins. We conclude with a discussion of recent studies that have successfully used the modular ER/K linker for engineering chimeric myosin proteins with altered mechanical properties, as well as synthetic polypeptides that can be used to monitor and systematically modulate protein interactions within cells.

Until recently, SAH domains in natural proteins were predicted by secondary structure prediction algorithms to form a coiled-coil, in part due to the high concentration of charged and polar

residues that are also the hallmark of the coiled-coil motif (1). Among the multiple folds in globular proteins that stabilize α-helices, the coiled-coil motif has been extensively characterized and in general is the most predictable form of tertiary protein structure (2). In the coiled-coil motif, two or more α-helices are individually stabilized by sequence-specific packing at consensus hydrophobic patches. Extensive studies have elicited general sequence and structure rules that govern coiled-coil interactions. Briefly, the amino acid sequence of each α-helix in a coiled-coil is divided into heptads (7 residues) that form nearly two complete α-helical turns and span 1.05 nm along the helical axis. Each amino acid in the heptad is described by its relative position, moving from the N- to C-terminus, using the nomenclature *abcdefg*. In canonical dimeric coiled-coils, the *a* and *d* positions radiate away from the core of the α-helix, 60 degrees apart and offset by 0.45 nm along the helix length, and are typically occupied by aliphatic hydrophobic residues, while polar residues comprise the rest of the positions. As the heptad is repeated, it forms a continuous hydrophobic patch located along a single face of the α-helix compatible with a tight intermolecular interaction between polypeptides with the same or similar heptad pattern (2). However, often times polar or charged residues occupy the *a* and *d* positions, leading to local destabilization of the coiled-coil motif (2-4). By extension, when most or all of the *a* and *d* sites in consecutive heptads are occupied by polar residues, individual α-helices cannot be mutually stabilized through hydrophobic packing. In this event, the polypeptide will either exist as a monomeric random coil or in some cases will form a SAH domain. The SAH domain is a **s**table, monomeric, extended **α-h**elix that is encoded by its primary amino acid sequence, and exists in polar solvent independent of tertiary interactions with other protein motifs.

A.1.1 Stable synthetic alanine-based α-helices

The rules governing the helicity of isolated peptides have been extensively studied. We highlight select studies of particular interest, and refer to (5) for a more comprehensive review. Prior to work on synthetic peptides from the Baldwin laboratory, including one derived from ribonuclease A (6-8), peptides shorter than 20 amino acids were not expected to show measurable helix formation in aqueous solution based on the statistical Zimm-Bragg model, which focuses on the propagation of spontaneous helicity and does not account for long distance electrostatic interactions between side chains (9). Marqusee et al. (6) found that a synthetic

peptide, 16 residues long, containing primarily alanine residues sparsely interspersed with a single E or K for solubilization, had high helical content (up to 80%) in aqueous solution as measured by circular dichroism (CD). This study highlighted the inherent helix forming potential of alanine in the absence of electrostatic interactions between side chains. In a separate study, Marqusee and Baldwin synthesized peptides containing 16 residues with three pairs of an E and a K separated by either three (*i*, *i + 3*) or four (*i*, *i + 4*) alanines (7). These peptides were synthesized, in part, to characterize the influence of electrostatic interactions between E and K on α-helix formation. Both peptides were soluble and monomeric in aqueous solution, and had detectable helical content as determined by CD. However, the (*i*, *i + 4*) (i.e. $(EAAAK)_3$) spacing yielded significantly higher helicity compared to (*i*, *i + 3*) presumably due to the preferred rotamer configurations of the E and K side chains. Interestingly, the measured helicity was preserved at extremes of pH (2-12) and at high concentrations of NaCl, suggesting that the electrostatic interactions were primarily derived from salt bridges (H-bonded ionic interactions) rather than direct ionic interactions. The helix stabilizing effects of E-K interactions on an alanine backbone were subsequently extended to D-K, E-R, D-R pairs (10). A subsequent study with alanine-based peptides also defined the role of capping residues at the N- and C-termini in stabilizing isolated α-helices. In general, α-helix formation is aided by negatively charged residues at the N-terminus and positively charged residues at the C-terminus (11). This observation is consistent with an interaction of appropriately charged capping residues with the dipole moment of the protein α-helix, which is directed from its C- to N-terminus. Further, in the context of peptides, the charged residues at the ends can also undergo stabilizing electrostatic interactions with the free NH_2 and COOH groups (11). These studies of synthetic alanine-based peptides provided precedence and laid the groundwork for identifying and predicting the stability of isolated α-helices.

The $(EAAAK)_n$ motif was subsequently incorporated into various synthetically engineered polypeptides. Arai et al. (12) evaluated the utility of $(EAAAK)_n$ (n = 2 - 5) motifs as rigid spacing linkers between a pair of green fluorescent protein variants (EBFP and EGFP). The linkers did not interfere with EBFP and EGFP folding as evaluated from their fluorescence spectra. Fluorescence resonance energy transfer (FRET) between EBFP and EGFP decreased, whereas helicity increased with linker length suggesting that stabilization of the α-helix

increased the spacing between the fluorescent proteins fused to the ends of the linker. In a subsequent study, the conformation of the $(EAAAK)_n$ linkers were evaluated by Small Angle X-ray Scattering (SAXS). Short linkers ($n \leq 3$) showed multimerization, whereas longer linkers ($n \geq 4$) remain monomeric even at high concentrations (> 25 μM). The radius of gyration increased with linker length and is higher than flexible unstructured linkers $(GGGGS)_n$ of the same length (13). Together, these studies support the use of the EAAAK linkers as extended spacers between polypeptides. Utilizing this structural property, the EAAAK linker has been employed to increase expression (14) and bioactivity (15) of fusion proteins. However, of concern for the use of tethering generic peptides with this particular linker, the EAAAK motif has been reported to have auto-cleavage properties at pH 6-7 (16). Regardless, this SAH domain demonstrates both the feasibility and highlights potential utility of a modular genetic element to control intramolecular spacing between protein domains.

A.1.2 Stability of ER/K α-helices

In a parallel vein, helix formation through E-K interactions, independent of alanine, was examined by Lyu et al. (17) with 18 amino acid peptides with either $(E_2K_2)_4$ or $(E_4K_4)_4$ repeats. While the composition was exactly the same for both peptides, CD and H^1 NMR data showed that the E_4K_4 peptide has 65% helical content, while the E_2K_2 peptide is essentially a random coil. This is consistent with studies in alanine peptides discussed earlier, wherein (*i, i + 4*) interactions, as in E_4K_4, stabilize the helical conformation whereas the (*i, i + 2*) spacing in E_2K_2 cannot facilitate these ionic interactions (Fig.1b,c). These results were independent of peptide concentration in a range of 20-250 μM indicating that oligomerization was not a factor in augmenting helicity. Additionally, pH and salt titrations showed that both direct ionic (E-K) and salt bridge interactions (H-bonded) likely contribute to the stability of E_4K_4 helices. This is in contrast to $(EAAAK)_n$ that appear to be primarily stabilized by salt bridge interactions (7). Free energy calculations yielded 0.5 kcal/mol stabilization for each (*i, i + 4*) interaction in E_4K_4, the contribution from each interaction is proposed to stabilize the isolated α-helical conformation.

The mechanisms that underlie the stability of E_4K_4 helices are also evident in molecular dynamics (MD) simulations. Sivaramakrishnan et al. performed a replica exchange MD simulation on a $(E_4K_4)_2$ peptide (18) **(Fig. A.1 c)**. Starting from either a random coil or a fully

formed α-helix, both simulations converged on an α-helix. Thermal melting curves derived from the MD simulations matched previous experimentally measured helicities of this peptide (17). The simulations revealed dynamic and continuous interactions between side chains, with preferential *i - 4* and *i + 3* interactions centered on E(*i*) residues, and *i – 3* and *i + 4* interactions centered on K(*i*) residues **(Fig. A.1 c)**. These computations parallel experimental measurements by Olson et al., who measured the influence of E-R side chain spacing on helicity (19). Monitoring the distances between the side chains in MD simulations, it was estimated that 45% of the time direct ionic interactions occur between E and K, whereas solvent separated salt bridges occur 37% of the time. This observation is consistent with the presence of both ionic and salt-bridge interactions in E_4K_4 inferred from the pH dependence of helicity (17). Additionally, it was observed that the bulky side chains were able to partially shield backbone hydrogen bonds from the polar solvent. Thus, stability of the α-helical core appears to arise from both shielded backbone hydrogen bonds, and ER/K side chain interactions. In this regard, the ER/K motif has been likened to a tensegrity structure that is stabilized by the juxtaposition of 'contractile' (backbone hydrogen bonds) and 'tensile' (side chain) interactions (20). Overall, the observations in synthetic E-R/K peptides have important structural implications in natural proteins as discussed in the next section.

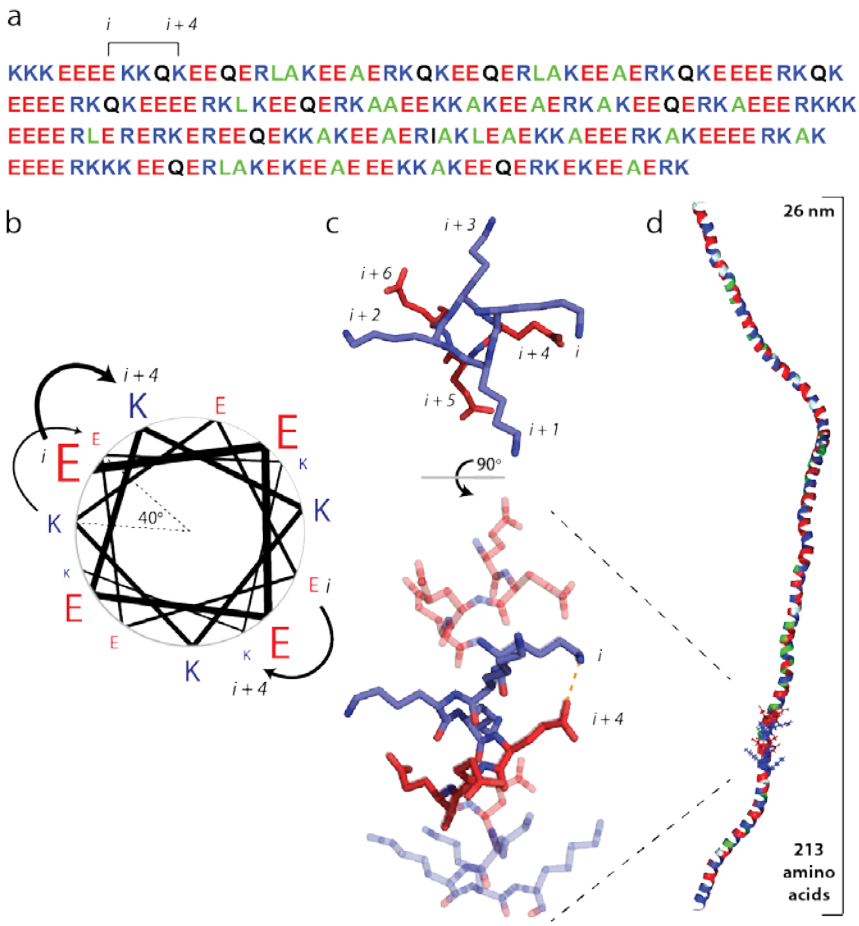

Figure A.1. Glu (E) and Arg (R)/ Lys (K) side chain interactions stabilize a monomeric α-helix in solution. (**a**) The primary amino acid sequence of the ER/K motif in Kelch-motif family protein from *Trichomonas vaginalis*. Positively charged residues (R and K) are shown in blue, negatively charged E is depicted in red, polar residues in black, and hydrophobic residues in green. Note the recurrence of E and R/K spaced at (*i*, *i* + *4*) intervals. (**b**) A pinwheel diagram representing the spacing of residues along an α-helix. The (*i*, *i* + *4*) spacing in the ER/K motif positions amino acids 40° apart, with a distance of 0.6 nm along the helical backbone. (Pinwheel adapted from (21)) (**c**) Ionic interactions and H-bonded salt bridges occur between E and R/K sidechains with (*i*, *i* + *4*) spacing. (*Top panel*) Top view down the backbone from the N-terminus of one heptad of $(E_4K_4)_2$ peptide from an MD simulation (18). (*Bottom panel*) A 90° rotation visualizing the entire 16 amino acid peptide with a E-K interaction highlighted. (**d**) A representative snap shot from a Monte-Carlo simulation of the Kelch-motif family protein ER/K α-helix (as in (a); (22)) highlighting the extended α-helical conformation in a large polypeptide (~ 30 kDa).

A.1.3 Identification and characterization of SAH domains in natural proteins

While the $(EAAAK)_n$ motif was the first identified to form SAH domains, SAH domains identified in natural proteins to date more closely resemble the ER/K motif (i.e. $(E_4(R/K)_4)_n$). Smooth muscle caldesmon contains an ~ 150 residue stretch in its central region that is essentially repeating segments of KAEEEKKAAEEK (23). Wang et al. (21) extensively characterized a 285 residue fragment of caldesmon that encompasses this ER/K stretch. CD revealed ~ 55% helicity, which is consistent with a near continuous 150 amino acid α-helical region. The sedimentation profile of this polypeptide in ultracentrifugation experiments suggests

a monomeric species over a wide range of protein concentrations (0.1 – 3.5 mg/ml). Rotary shadowed electron micrographs (EM) revealed rods with an average length of 35 nm that is near the predicted length of an extended 150 residue α-helix. The rod thickness in EM was significantly less than coiled-coils from tropomyosin or the myosin rod segment, again suggesting a single extended α-helix. In addition to stabilizing the α-helix, Wang et al. proposed that the regularly spaced salt bridges may protect this α-helix from proteolytic cleavage. Caldesmon interacts with both actin and myosin through distinct domains located at the ends of its SAH domain. While muscle caldesmon serves to inhibit the actin activated ATPase activity of myosins, it does not inhibit the actin-myosin interaction (24). Therefore, the extended single α-helix in caldesmon likely serves as a spacer to allosterically modify this interaction. However, not all SAH domains identified are expected to function solely as spacers, for example the human programmed cell death 5 (PDCD5) protein.

The N-terminal 26 amino acid fragment (GSADEELEALRRQRLAELQAKHGDPG) of PDCD5 was demonstrated by Liu et al. (25) to form a single α-helix by both CD and NMR spectroscopic measurements **(Fig. A.2 c)**. Deletion of the N-terminal α-helix of PDCD5 significantly attenuated the apoptosis-promoting effects triggered by serum withdrawal. Based on the differential nuclear translocation of full length and truncated PDCD5, Liu et al. propose a role for this SAH domain in the nuclear targeting of PDCD5.

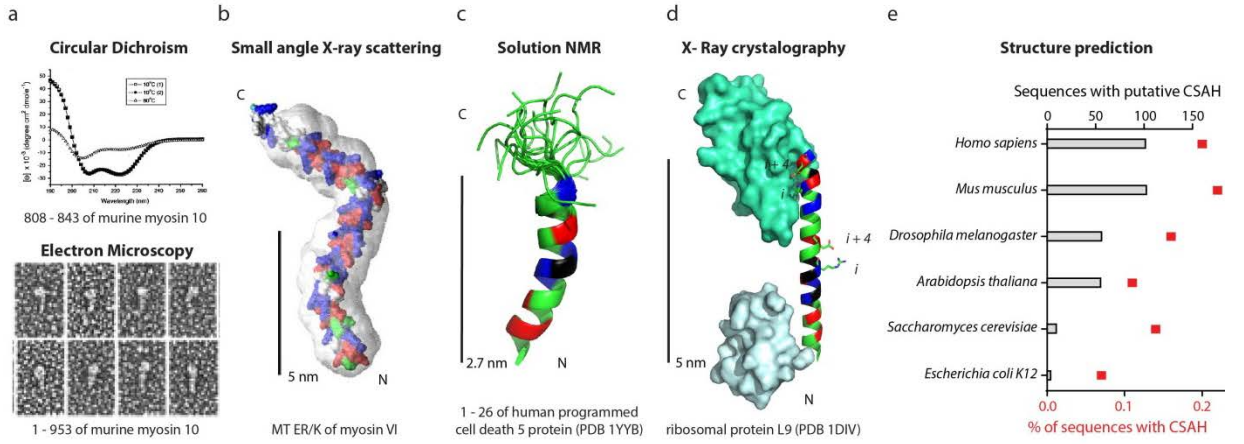

Figure A.2. SAH domains have been observed in natural peptides or full length proteins with multiple structural techniques. (**a**) From reference (1) the putative coiled-coil region of myosin 10 forms a SAH domain. (*Top*) circular dichroism (CD) of a peptide from murine myosin 10 has a canonical alpha helical spectrum at 10°C with a negative ellipticity at 222 nm (before and after heating to 80°C) and a random coil spectra (with loss of ellipticity at 222 nm) at 80°C. (*Bottom*) rotary shadowed transmission electron microscopy (rs –TEM) of recombinant murine myosin 10 fragments. (**b**) From reference (18), the predicted structure of the MT ER/K region (residues 916 – 981) of myosin VI docked into its small angle X–ray scattering

(SAXS) envelope. (**c**) From reference (25), an alignment of 20 solution states, determined by NMR, for the programed cell death 5 protein residues 1 – 26 following ^{1}H –^{15}N HSQC. (**d**) From reference (26), the x-ray crystal structure of ribosomal protein L9. (**e**) From reference (27), the number and percentage of total sequences of putative charged SAH domains (CSAH) identified from the primary amino acid sequences of the indicated organisms listed in SwissProt and TrEMBL databanks utilizing the CSAH server. (b-d) Residues in SAH domains are colored as in Figure a. 1.

The first high resolution structure of a SAH domain was revealed in a crystal structure of the *B. sterthermophilis* ribosomal protein L9 (26). This protein contained a rigid and fully extended 34 amino acid linker region between two compact globular domains **(Fig. A.2 d)**. A subsequent study synthesized the corresponding peptide, and found the peptide was primarily monomeric at concentration up to 1 mM in analytical ultracentrifugation studies and primarily (~ 70%) α-helical as determined by CD spectroscopy, a much higher degree of helicity than was expected based on its primary sequence (PANLKALEAQKQKEQRQAAEELANAKKLKEQLEK) (28). Further, they found that the helicity of the peptide could be disrupted by moderate salt concentrations (< 500 mM NaCl), indicative of ionic side-chain interactions contributing to the net stability of the α-helix. While this peptide is far from the ideal E_4K_4 motif, it does have several predicted (*i, i + 4*) electrostatic interactions. The single α-helix was postulated to act as a rigid spacer between two globular domains of the L9 ribosomal protein such that they are properly positioned to bind RNA. In addition to its structural role in the intact proteins, the authors also suggest that the folding of the α-helix may initiate and stabilize the folding of the two domains at its ends. Specifically, if the α-helix does initiate the folding process, then the folding of the two domains at the ends will be interdependent.

The most extensively characterized SAH domains to date are the ER/K α-helices found in myosin X and VI. A study by Knight et al. investigated a putative coiled-coil motif in murine myosin X that was highly enriched in charged residues in the *a* and *d* positions of the heptad repeats (1). The authors identified this as a peptide that did not conform with typical coiled-coil motifs, and coined the term SAH to describe an isolated stable single α-helix **(Fig. A.2 a)**. The 36 residue peptide studied (RQLLAEKRELEEKKRREEEKKREEEERERERAQR) resembles an ideal ER/K motif. Using H^1 NMR they found that the n-terminal 6 residues form a random coil, while all other residues in the peptide are α-helical. Using analytical ultracentrifugation they determined the peptide to be monomeric at concentrations up to 700 μM. Surprisingly, they found that the α-helical content, as determined by CD, is less sensitive to higher salt concentrations than a synthetic 19 amino acid E_4K_4 peptide, presumably due to more stable

electrostatic interactions. The study also investigated the SAH domain in the context of a nearly intact myosin X, which included a directly N-terminal putative coiled-coil region (120 amino acid total), by rotary shadowing and negative stain EM **(Fig. A.2 a)**. They found that 90% of the peptide was monomeric, whereas 10% appeared dimerized. Further, in the dimeric population only a small portion of the α-helical region appeared to be interacting. The 'head' region of the entire myosin was 15 nm longer than expected (34.7 nm versus an expected 18.4 nm), corresponding to the expected length of 18 nm if the entire 120 amino acid region were in an extended α-helix. Finally, this study made predictions for two additional SAH domains in regions putatively described as coiled-coil regions in myosin VI and MyoM (Dictyostelium myosin) based on the ER/K motif in their primary amino acid sequence, both of which were subsequently confirmed.

Spink et al. (29) demonstrated that an ER/K motif was necessary for the large (36 nm) step size of dimeric myosin VI. The myosin VI medial tail was previously proposed to form a coiled-coil (30) based on a prediction of the PAIRCOILS algorithm. Spink et al. showed that a polypeptide derived from the medial tail failed to demonstrate a co-operative melting profile characteristic of coiled-coil domains. Using a combination of spectroscopic approaches, the medial tail was found to be monomeric even at high concentrations (> 200 μM). Small angle X-ray scattering (SAXS) reconstructions revealed an extended conformation (~ 10 nm) consistent with the medial tail as an ER/K motif **(Fig. A.2 b)**. Forced dimerization of the medial tail, by insertion of a canonical coiled-coil at its N-terminus, substantially diminished the step size and processivity of myosin VI. The rigidity of this ER/K α-helix is evident in its ability to extend the mechanical stroke of myosin VI as it resists an external force applied by optical tweezers (22). By pairing SAXS and optical trapping measurements of this and another naturally occurring ER/K motif (10 and 30 nm) the persistence length of the ER/K motif based on an ideal worm-like-chain was estimated to be 15 nm (22) **(Fig. A.1 d)**.

A.1.4 Predicting SAH domains from primary sequence

Until recently, the identification of the SAH domain was limited to the handful of natural proteins where it had been biochemically characterized. Searching specifically for the minimal ER/K motif $(E_4(R/K)_4)_2$ Sivaramakrishnan et al. identified 123 distinct proteins in 137 organisms

ranging from archea to humans, that had an average of 80% conformity to this motif (18). Peckham et al. sought to identify SAH domains by examining sequences predicted to be coiled-coils based on their high charge density, but failed to have hydrophobic residues in the *a* and *d* sites. After a manual screen of putative coiled-coil domains that were homologous to the *bona fide* SAH domain in murine myosin X, they found that up to 4% of proteins classified as coiled-coils might indeed be SAH domains instead. This study provides an upper bound of 0.5% of all proteins in the human database contain a SAH domain (31).

Suveges et al. took a more systematic and analytical approach to identify charged SAH domains (32). They generated two conceptually different computational models, one a scoring function that identifies characteristic (*i, i + 4*) or (*i, i + 3*) salt bridges (SCAN4CSAH), and a second fast Fourier transform approach to find like-charged residues approximately 1 heptad apart (FT_CHARGE). These methods detected several putative SAH domains by cross examining the Swiss-Prot database for regions larger than 40 amino acids (32). Both search databases are available at the charged SAH (termed CSAH) server (http://csahserver.chem.elte.hu). Applied to the UniProt database, they provide a conservative estimate of 0.2% of all proteins in an organism as containing CSAH structural motifs **(Fig. A.2 e)**. Interestingly, *Homo sapiens* were identified to have the highest number of CSAH containing sequences in their genome. Of almost 300,000 proteins identified in this search, only one had a published high resolution structure suggestive of the difficulty of obtaining x-ray crystal structures of CSAH domains. The identified sequences had high overlap with servers identifying unstructured regions and coiled-coil motifs. The authors postulate that this motif may be rapidly evolving and that single charge mutations may lead to fine tuning of sequences between SAH, coiled-coil and disordered segments (27). As an alternative to differentiating between SAH and coiled-coil domains, Sunitha et al. (3) have developed a new computational tool termed COILCHECK+ (http://caps.ncbs.res.in/coilcheckplus). This web interface informs the user of the strength of a potential coiled-coil interaction at the interface region based on the relative density of both the charged residues and the characteristic repeat pattern of hydrophobic residues. While these bioinformatics screens require additional experimental verification, it appears that SAH are a ubiquitous protein domain.

A.2 Applications for modular ER/K motifs in protein engineering

The ER/K motif has readily found applications in protein engineering. Three separate studies have used chimeric approaches to investigate the interplay of ER/K α-helix mechanical properties on myosin function **(Fig. A.3)**. Baboolal et al. (33) demonstrated that an ER/K α-helix can function as a lever arms in myosin V by extending a single myosin stroke nearly as efficiently as its native rigid calmodulin-stabilized lever arm **(Fig. A.3 a)**. However, in contrast to the native lever, the ER/K α-helix was not able to coordinate the chemomechanical cycles of the two myosin heads within a single dimer, possibly due to its lower bending rigidity. Nagy and Rock (34) demonstrated that the ER/K α-helix from myosin X was necessary and sufficient to engineer preferential processive movement of both myosin X and V on fascin-linked actin bundles. Engineering additional flexibility into the native myosin X abolishes selectivity for actin bundles, suggesting that the ER/K α-helix selectively biases the orientation of the myosin heads within a dimer **(Fig. A.3 b)**. Hariadi et al. (35) found that ensembles of myosin VI but not myosin V undergo linear-directed movement on a dense cellular actin meshwork. Stochastic simulations revealed that myosin lever arm rigidity alone was sufficient to dictate the skewness of movement patterns on cellular actin networks. Swapping a portion of the myosin V lever with the ER/K α-helix from myosin VI was sufficient to linearize myosin V trajectories and vice versa **(Fig. A.3 c)**. Together, these reports bridge mechanical properties of ER/K α-helices with specific functions in myosin.

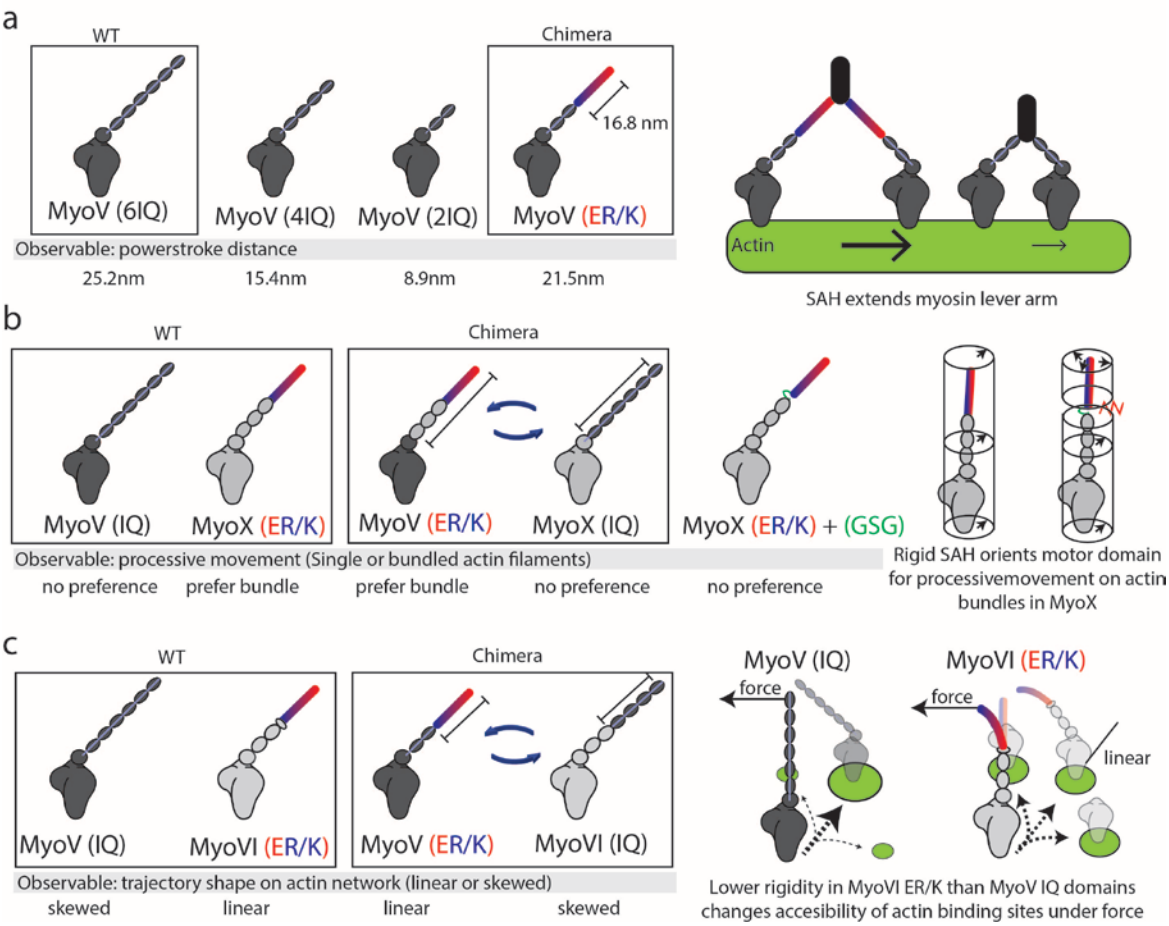

Figure A.3. The ER/K α-helix is a modular genetic motif that can be used to create myosin chimeras with altered mechanical properties. (**a**) Baboolal et al. (33) created a myosin V (MyoV) chimera containing the putative ER/K α-helix from Dictylostelium myosin M. (*Left*) The powerstoke distances of WT myosin V, myosin V with truncation of 2 or 4 calmodulin stabilized IQ domains, and a chimera of myosin V with 2 native IQ domains and a 16.8 nm ER/K α-helix. (*Right*) An extended and rigid ER/K α-helix can propagate force generated in the myosin catalytic domain to facilitate long processive steps on actin filaments. (**b**) Nagy and Rock (34) generated multiple chimeras between myosin V and myosin X (MyoX) to assess structural elements that allows myosin X to preferably move on fascin-actin bundles. (*Left*) Representative chimeras that were used to identify that in myosin X, the ER/K α-helix and not the motor domain or step size dictates processive movement on fascin-actin bundles. (*Right*) Insertion of unstructured Gly-Ser-Gly residues between the SAH and IQ domains of myosin X disrupts preferential processivity on fascin-actin bundles. The ER/K α-helix alters the orientation of the motor domain, allowing it to favorably bind actin sites uniquely presented in fascin-actin bundles. (**c**) Hariadi et al. (35) generated chimeras swapping the ER/K α-helix from myosin VI (MyoVI) with the IQ domains from myosin V while investigating the collective movement of multiple myosins tethered together. (*Left*) Multiple myosin V, but not myosin VI, display meandering trajectories while traversing actin meshworks. Swapping regions of the lever arm containing the ER/K α-helix is able to reverse this phenomenon. (*Right*) The IQ-domains are likely more rigid than the ER/K α-helix, such that the inter-myosin force can selectively alter the accessibility of actin binding sites for the less rigid myosin VI.

In a radically different approach to protein engineering the ER/K linker has also been used to tether and dictate the effective concentration of intramolecular protein-protein interactions **(Fig. A.4 a)**. Sivaramakrishnan and Spudich (36) engineered a single polypeptide sensor containing an ER/K linker with an N-terminal calmodulin (CaM) and cyan fluorescent protein (CFP) variant attached by a flexible $(GSG)_2$ linker, and a C-terminal yellow fluorescent protein (YFP) variant

attached with a $(GSG)_2$ linker to a peptide known to dimerize with the Ca^{2+} bound CaM. The calcium induced intramolecular interaction between CaM and its binding partner was detected by changes in fluorescence resonance energy transfer (FRET) between CFP and YFP variants. In the absence of calcium, no significant FRET was detected with ER/K linkers of 73 amino acids or more (corresponding to > 10 nm length along the α-helical backbone). A dramatic increase in FRET was observed upon addition of calcium. Unexpectedly, calcium stimulated FRET was independent of the concentration of sensor at levels below the bimolecular dissociation constant, indicating that an intramolecular interaction was bringing the FRET pair on either end of the ER/K linker into close proximity. Competitive inhibition of FRET with increasing concentrations of unlabeled CaM was used to quantify the effective concentration of the intramolecular interaction. Regardless of the bimolecular dissociation constant, the effective concentration decreased by about an order of magnitude for each additional 10 nm of ER/K linker. Essentially, changing ER/K linker length from 10-30 nm altered the effective concentration of the intramolecular interaction from 10 μM to 100 nM **(Fig. A.4 c)** (for reference, the effective concentration of a 60 residue unstructured linker is ~ 100 μM (37)). Further, similar results are observed when CaM and the CaM binding peptide are replaced by different interacting peptides **(Fig. A.4 b)**. This trend is in contrast to the expected behavior of an ideal worm-like-chain. One possible explanation is that a sensor in the closed state may introduce unfavorable conformations of the ER/K linker, which could increase the off-rate of the CaM-peptide interaction. However, the measured off-rate was found to be independent of ER/K linker length. The authors proposed a structural interpretation of these observations by suggesting the ER/K linker undergoes rare stochastic breaks in helicity that create pivot points to facilitate interactions between the ends. The frequency of stochastic breaks scales linearly with α-helix length (α L). However, the breaks are unlikely to be spatially coordinated resulting in far fewer conformations (α $1/L^2$) that bring the ends in close enough proximity to precipitate CaM-peptide interactions. While this interpretation needs further testing, it is consistent with a previous SAXS study suggesting that certain α-helical peptides exhibit breaks along their length (38). The use of the ER/K linker to modulate protein-protein interactions was termed Systematic Protein Affinity Strength Modulation (SPASM). A key feature of the SPASM approach is its modularity, and the individual protein/peptide/fluorophore domains can be easily exchanged with basic molecular biology tools in most research labs.

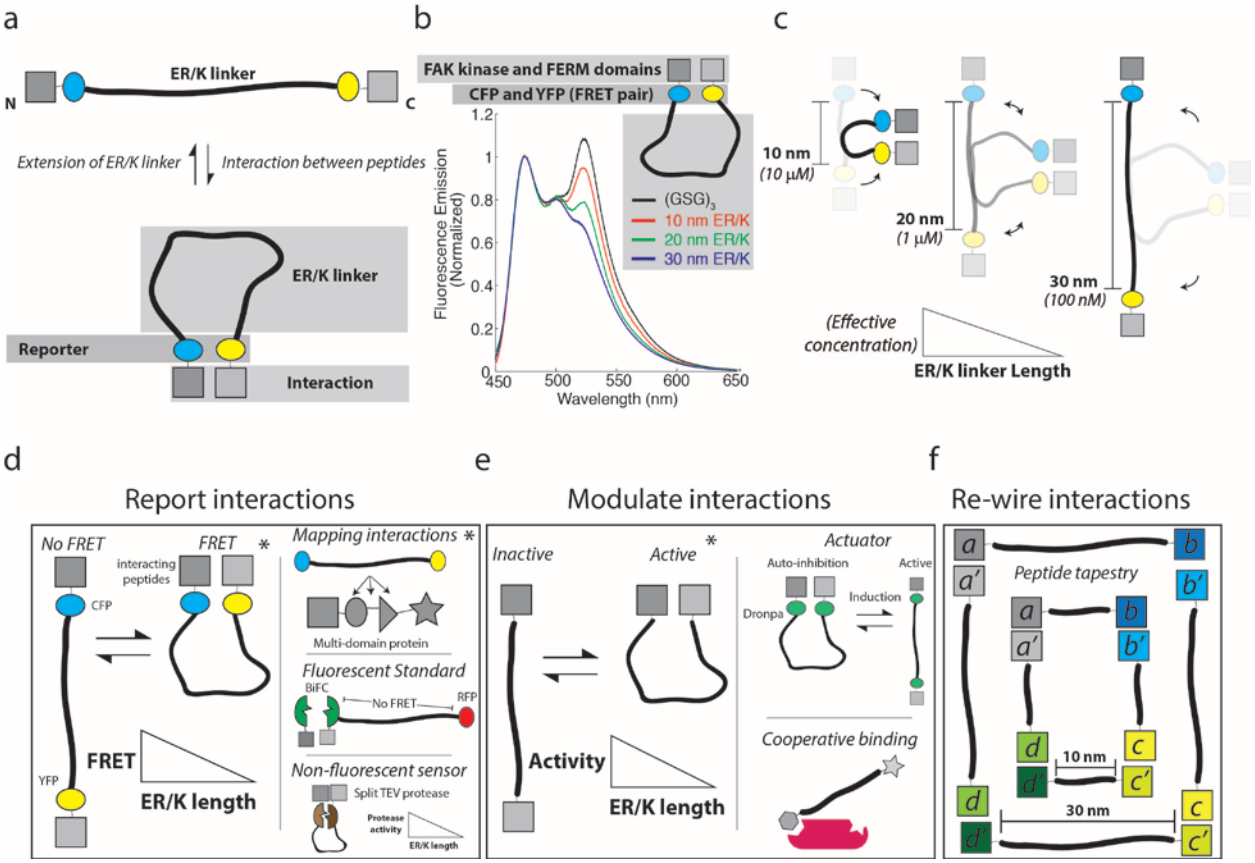

Figure A.4. The ER/K α-helix dictates the effective concentration of peptides attached to its distal ends and can be used for protein/cellular engineering applications. (**a**) (*Top*) The ER/K α-helix adopts an extended conformation in the absence of an interaction between polypeptides fused to its ends; *(Bottom*) Interaction between peptides stabilizes the closed conformation of the ER/K α-helix, which is detected by a reporter system (eg: FRET between CFP and YFP). (**b**) From reference (39), an example of the schematic depicted in (a), in which the interacting focal adhesion kinase (FAK) FERM domain and kinase domains, as well as the fluorescent protein FRET pair CFP and YFP are separated by a disordered GSG linker, or ER/K linkers with extended lengths of 10- 20- and 30 nm. Fluorescence emission of these polypeptides was monitored at concentrations significantly lower than the bimolecular dissociation constant for the kinase-FERM domain interaction; FRET is assessed by the characteristic increase in fluorescence at 525 nm. (**c**) Sivaramakrishnan and Spudich (36) found that the effective concentration of the intramolecular interaction was dependent on the ER/K α-helix length. Longer ER/K α-helix length leads to a lower effective concentration. (**d-f**) Sample applications, some experimentally demonstrated (*) and others conceptual, of a modular ER/K linker in protein engineering (d; *Left*) Reporting protein-protein interactions using fluorescent protein FRET reporters between conditionally interacting protein/peptide pairs, as reported by Malik et al. investigating GPCR-G protein interactions (40). (d; *Top right*) ER/K linker with flanking FRET reporters inserted between domains of a multi-domain protein as reported by Swanson et al. investigating protein kinase C (41). (d; *Middle right*) Tethering a BiFC (42) pair to fluorescent protein with an ER/K α-helix, places the fluorescent protein beyond FRET distance, to allow for quantification of expression levels of the sensor. (d; *Bottom right*) A non-fluorescent readout of a conditional protein-protein interaction, for example, enzymatic activity of a split TEV protease, or deriving antibiotic resistance from a split beta-lactamase (43). These approaches allow for increased stringency of detection by increasing the ER/K α-helix length, while controlling for stoichiometry of interacting proteins. (e; *Left*) ER/K α-helix length modulates protein-protein interactions to control the activity resulting from the interaction. For instance, an activity that is dependent on two proteins interacting can occur more or less frequently depending on the length of the ER/K α-helix as demonstrated by Ritt et al. investigating the intramolecular interaction between FERM and kinase domains of focal adhesion kinase (39). (e; *Top right*) The ER/K α-helix can be used to generate single polypeptide actuators, using inducible protein interaction pairs. For instance, the optogenetically controlled dimeric dronpa fluorescent proteins (44) can be used to modulate auto-inhibition of a catalytic domain. (e; *Bottom right*) The ER/K α-helix can be used to control co-recruitment of peptides to an intermolecular complex. While the initial interaction will be dependent on polypeptide concentration, recruitment of the second peptide tethered by the ER/K linker will be dependent on the linker length. (f) ER/K α-helices can be used to engineer structural scaffolds from polypeptides. A schematic of one such design is depicted in which the size of the structure can be adjusted by the length of the ER/K α-helix.

The SPASM approach has since been used to engineer protein-protein interactions in live cells. Single polypeptide FRET sensors based on SPASM have been used to detect G protein-selective conformations of G protein-coupled receptors (GPCRs) (40) **(Fig. A.4 d)**. Modulating effective concentration with varying ER/K linker length has been used to modify the enzymatic activity of focal adhesion kinase (FAK) and dissect the differential effects of kinase activity and domain-domain interactions in controlling cellular migration (39) **(Fig. A.4 e)**. The ER/K linker provides control over the stoichiometry of expression, with minimal FRET in the absence of an intramolecular interaction. This feature has been used to understand the pH dependence of FAK regulation, while correcting for the effects of pH on the fluorescence levels of GFP variants. Additionally, the ER/K linker has found utility in modulating domain-domain interactions in multi-domain proteins, which has yielded a coarse configuration of both intra- and intermolecular interactions in protein kinase C (41) **(Fig. A.4 d)**. Beyond these studies, we propose that the ER/K linker may be readily used in conjunction with other synthetic protein tools, including split proteins and inducible protein interactions, as a means to study individual interactions or to engineer cellular systems **(Fig. A.4 d-f)**.

A.3 Conclusions:

The SAH domain is a structural element found in numerous proteins, where it appears to operate as a semi-rigid structural element that tethers globular domains. Although it has only been extensively characterized in a few natural proteins, its sequence specifications and structural properties allow for its identification distinct from coiled-coils. The ER/K motif is a subset of SAH domains that has been extensively characterized through studies of the myosin family of molecular motors. ER/K α-helices, encoded by this motif, have already found applications for monitoring or systematically modulating protein interactions. The modularity of the ER/K motif makes it a versatile protein structural element in an expanding toolbox of technologies that are being deployed to dissect an integrated cellular signaling network. In addition to informing cellular function, sensors developed on an ER/K platform have direct applications for identifying new small molecule therapeutics.

A.4 References:

1. Knight PJ*, et al.* (2005) The predicted coiled-coil domain of myosin 10 forms a novel elongated domain that lengthens the head. *J Biol Chem* 280(41):34702-34708.
2. Woolfson DN (2005) The design of coiled-coil structures and assemblies. *Adv Protein Chem* 70:79-112.
3. Sunitha MS*, et al.* (2012) Structural attributes for the recognition of weak and anomalous regions in coiled-coils of myosins and other motor proteins. *BMC Res Notes* 5:530.
4. Kreuzer SM & Elber R (2013) Coiled-coil response to mechanical force: global stability and local cracking. *Biophys J* 105(4):951-961.
5. Scholtz JM & Baldwin RL (1992) The mechanism of alpha-helix formation by peptides. *Annu Rev Biophys Biomol Struct* 21:95-118.
6. Marqusee S, Robbins VH, & Baldwin RL (1989) Unusually stable helix formation in short alanine-based peptides. *Proc Natl Acad Sci U S A* 86(14):5286-5290.
7. Marqusee S & Baldwin RL (1987) Helix stabilization by Glu-...Lys+ salt bridges in short peptides of de novo design. *Proc Natl Acad Sci U S A* 84(24):8898-8902.
8. Bierzynski A, Kim PS, & Baldwin RL (1982) A salt bridge stabilizes the helix formed by isolated C-peptide of RNase A. *Proc Natl Acad Sci U S A* 79(8):2470-2474.
9. Zimm BH & Bragg JK (1959) Theory of the Phase Transition between Helix and Random Coil in Polypeptide Chains. *The Journal of Chemical Physics* 31(2):526-535.
10. Huyghues-Despointes BM, Scholtz JM, & Baldwin RL (1993) Helical peptides with three pairs of Asp-Arg and Glu-Arg residues in different orientations and spacings. *Protein Sci* 2(1):80-85.
11. Doig AJ & Baldwin RL (1995) N- and C-capping preferences for all 20 amino acids in alpha-helical peptides. *Protein Sci* 4(7):1325-1336.
12. Arai R, Ueda H, Kitayama A, Kamiya N, & Nagamune T (2001) Design of the linkers which effectively separate domains of a bifunctional fusion protein. *Protein Eng* 14(8):529-532.
13. Arai R, Wriggers W, Nishikawa Y, Nagamune T, & Fujisawa T (2004) Conformations of variably linked chimeric proteins evaluated by synchrotron X-ray small-angle scattering. *Proteins* 57(4):829-838.
14. Amet N, Lee HF, & Shen WC (2009) Insertion of the designed helical linker led to increased expression of tf-based fusion proteins. *Pharm Res* 26(3):523-528.
15. Bai Y & Shen WC (2006) Improving the oral efficacy of recombinant granulocyte colony-stimulating factor and transferrin fusion protein by spacer optimization. *Pharm Res* 23(9):2116-2121.
16. Wu YJ, Fan CY, & Li YK (2009) Protein purification involving a unique auto-cleavage feature of a repeated EAAAK peptide. *J Chromatogr B Analyt Technol Biomed Life Sci* 877(31):4015-4021.
17. Lyu PC, Gans PJ, & Kallenbach NR (1992) Energetic contribution of solvent-exposed ion pairs to alpha-helix structure. *J Mol Biol* 223(1):343-350.
18. Sivaramakrishnan S, Spink BJ, Sim AY, Doniach S, & Spudich JA (2008) Dynamic charge interactions create surprising rigidity in the ER/K alpha-helical protein motif. *Proc Natl Acad Sci U S A* 105(36):13356-13361.
19. Olson CA, Spek EJ, Shi Z, Vologodskii A, & Kallenbach NR (2001) Cooperative helix stabilization by complex Arg-Glu salt bridges. *Proteins* 44(2):123-132.
20. Spudich JA & Sivaramakrishnan S (2010) Myosin VI: an innovative motor that challenged the swinging lever arm hypothesis. *Nat Rev Mol Cell Biol* 11(2):128-137.
21. Wang CL*, et al.* (1991) A long helix from the central region of smooth muscle caldesmon. *J Biol Chem* 266(21):13958-13963.

22. Sivaramakrishnan S*, et al.* (2009) Combining single-molecule optical trapping and small-angle x-ray scattering measurements to compute the persistence length of a protein ER/K alpha-helix. *Biophys J* 97(11):2993-2999.
23. Bryan J*, et al.* (1989) Cloning and expression of a smooth muscle caldesmon. *J Biol Chem* 264(23):13873-13879.
24. Lash JA, Sellers JR, & Hathaway DR (1986) The effects of caldesmon on smooth muscle heavy actomeromyosin ATPase activity and binding of heavy meromyosin to actin. *J Biol Chem* 261(34):16155-16160.
25. Liu D, Yao H, Chen Y, Feng Y, & Wang J (2005) The N-terminal 26-residue fragment of human programmed cell death 5 protein can form a stable alpha-helix having unique electrostatic potential character. *Biochem J* 392(Pt 1):47-54.
26. Hoffman DW*, et al.* (1994) Crystal structure of prokaryotic ribosomal protein L9: a bi-lobed RNA-binding protein. *EMBO J* 13(1):205-212.
27. Gaspari Z, Suveges D, Perczel A, Nyitray L, & Toth G (2012) Charged single alpha-helices in proteomes revealed by a consensus prediction approach. *Biochim Biophys Acta* 1824(4):637-646.
28. Kuhlman B, Yang HY, Boice JA, Fairman R, & Raleigh DP (1997) An exceptionally stable helix from the ribosomal protein L9: implications for protein folding and stability. *J Mol Biol* 270(5):640-647.
29. Spink BJ, Sivaramakrishnan S, Lipfert J, Doniach S, & Spudich JA (2008) Long single alpha-helical tail domains bridge the gap between structure and function of myosin VI. *Nat Struct Mol Biol* 15(6):591-597.
30. Rock RS*, et al.* (2005) A flexible domain is essential for the large step size and processivity of myosin VI. *Mol Cell* 17(4):603-609.
31. Peckham M & Knight PJ (2009) When a predicted coiled coil is really a single [small alpha]-helix, in myosins and other proteins. *Soft Matter* 5(13):2493-2503.
32. Suveges D, Gaspari Z, Toth G, & Nyitray L (2009) Charged single alpha-helix: a versatile protein structural motif. *Proteins* 74(4):905-916.
33. Baboolal TG*, et al.* (2009) The SAH domain extends the functional length of the myosin lever. *Proc Natl Acad Sci U S A* 106(52):22193-22198.
34. Nagy S & Rock RS (2010) Structured post-IQ domain governs selectivity of myosin X for fascin-actin bundles. *J Biol Chem* 285(34):26608-26617.
35. Hariadi RF, Cale M, & Sivaramakrishnan S (2014) Myosin lever arm directs collective motion on cellular actin network. *Proc Natl Acad Sci U S A* 111(11):4091-4096.
36. Sivaramakrishnan S & Spudich JA (2011) Systematic control of protein interaction using a modular ER/K alpha-helix linker. *Proc Natl Acad Sci U S A* 108(51):20467-20472.
37. Robinson CR & Sauer RT (1998) Optimizing the stability of single-chain proteins by linker length and composition mutagenesis. *Proc Natl Acad Sci U S A* 95(11):5929-5934.
38. Zagrovic B, Jayachandran G, Millett IS, Doniach S, & Pande VS (2005) How large is an alpha-helix? Studies of the radii of gyration of helical peptides by small-angle X-ray scattering and molecular dynamics. *J Mol Biol* 353(2):232-241.
39. Ritt M, Guan JL, & Sivaramakrishnan S (2013) Visualizing and manipulating focal adhesion kinase regulation in live cells. *J Biol Chem* 288(13):8875-8886.
40. Malik RU*, et al.* (2013) Detection of G protein-selective G protein-coupled receptor (GPCR) conformations in live cells. *J Biol Chem* 288(24):17167-17178.
41. Swanson CJ*, et al.* (2014) Conserved Modular Domains Team Up to Latch-Open Active PKCalpha. *J Biol Chem*.

42. Kerppola TK (2008) Bimolecular fluorescence complementation (BiFC) analysis as a probe of protein interactions in living cells. *Annu Rev Biophys* 37:465-487.
43. Shekhawat SS & Ghosh I (2011) Split-protein systems: beyond binary protein-protein interactions. *Curr Opin Chem Biol* 15(6):789-797.
44. Zhou XX, Chung HK, Lam AJ, & Lin MZ (2012) Optical control of protein activity by fluorescent protein domains. *Science* 338(6108):810-814.

Appendix B: Supplemental to Chapter 3

B.1 Results:

Size exclusion chromatography

We started by assessing PKCα oligomerization by SEC. PKCα-mCit under EGTA buffered conditions ran as 1 prominent peak followed by several smaller degradation product peaks **(Fig. B.1 a)**. The MW of the prominent peak was determined to be $1.00*10^5 \pm 0.19*10^5$ dalton (mean and 1 standard deviation from Gaussian fit; anticipated MW of PKCα-mCit is $1.06*10^5$ dalton), and PKC-α was detected in the corresponding fraction by a monoclonal anti-PKCα antibody. When the mobile phase contained 300 μM free Ca^{2+} and the protein sample was pre-incubated with matched buffer for 3, 10 or 30 minutes prior to the chromatography run, the prominent peak was progressively quenched and no additional peak was observed. The column manufacturer states the exclusion limit of the resin (Superdex 200; for globular protein) as $1.3 * 10^6$ daltons (~10 fold increase in Mr of monomer assuming spherical particles). Interestingly, no oligomers within the range of 2 – 10 times the monomer size were resolved, except for a small peak in the void fraction after the shortest calcium incubation period. We conclude that in the presence of calcium the protein oligomerizes into particles larger than the exclusion limit of the column. We were surprised that oligomeric species could not be resolved in the range of $1.14*10^5$ - $1.3 * 10^6$ daltons (2 - 10 molecules/particle). To address specificity, we introduced the single point mutation D246N which is known to disrupt Ca^{2+} ion coordination to the C2 domain(1). We find that under EGTA buffered conditions the D246N point mutation has no observable effect on Mr compared to the native sequence **(Fig. B.1 b)**. However, when treated with Ca^{2+}, D246N runs exactly as in the EGTA buffered condition. This finding provides evidence that not only is Ca^{2+}

minimally sufficient to oligomerize PKCα, it does so specifically through the well-characterized Ca^{2+} binding pocket in the C2 domain.

Differential sedimentation

We chose centrifugation conditions such that the monomer (MW < 112.6 KDa) species would remain in the supernatant, while any aggregated/oligomeric species would be pelleted. We found that protein buffered with EGTA primarily remained in solution, while buffering with 200 μM free Ca^{2+} caused a significant pellet fraction to be observed. However, if the D246N mutation is present, the protein no longer forms pellets in a calcium-dependent manner (**Fig. B.1 c**). We designed an experiment in which the same protein sample was sequentially buffered with EGTA, fractionated, the soluble component buffered with free Ca^{2+}, re-fractionated, the pellet re-suspended in EGTA buffered solution and fractionated a 3rd time. Remarkably, we observed calcium to drive pelleting of the protein, but once the pellet was re-suspended in EGTA buffered solution the entire fraction remained in the soluble fraction **(Fig. 3.1 a)**. This experimental result suggests that oligomerization is reversible and dependent on calcium.

Dynamic Light Scattering

In order to get an estimate of the size of oligomers as well as confirm reversibility, we utilized dynamic light scattering (DLS). We initially investigated a modestly concentrated sample of PKCα-mCit (1 μM) buffered with EGTA so that the hydrodynamic radius between SEC and DLS experiments ($H_{R(SEC)}$, $H_{R(DLS)}$) could be compared. Using a regularization fit, it was found that PKCα-mCit was bi-model, with a peak with estimated H_R consistent with monomers (in all cases representing > 94% mass) as well as a peak with H_R ~100 fold larger than monomer (presumably aggregated protein) **(Fig. B.2)**. Not surprisingly, the monomeric peak is polydisperse, which is consistent with SEC data in which several degradation products were observed. When the $H_{R(DLS)}$ of the first peak (3.14 nm) is used to estimate a molar mass using the Stokes-Einstein relationship with an isotropic spheres model, the mean is 95.8 ± 16.3 KDa (mean and s.e.m. n = 65; compared with 100 KDa from SEC and 106 KDa estimate from primary sequence). We then sequentially added calcium and EGTA to the same sample with 15 min incubations in between. A dramatic shift in the autocorrelation data towards longer time occurred following calcium addition and partial recovery to shorter time with EGTA addition **(Fig. 3.1 b**

left). We used a cumulant fit to estimate an averaged diffusion constant and used an isotropic sphere model to calculate the MW of all species in the sample and normalized by the starting condition. The average mass sequentially increased by 13 fold and returned to 4 fold above the starting EGTA buffered condition **(Fig. 3.1 b right)**. The introduction of the D246N point mutation increased a modest 1.7 fold following introduction of calcium. These results are consistent with both the specificity and reversibility of the oligomerization phenomenon previously observed.

Fluorescence microscopy

Using non-specific adhesion to coverslips, PKCα-mCit formed large fluorescent punctae specifically and reversibly in the presence of free calcium **(Fig. 3.1 c)**. By quantifying the fluorescent images the relative number and intensity of particles could be distinguished. We initially aimed to do step-wise photobleaching of the punctae to estimate the # of molecules / punctae, however the intensity of punctae >> the intensity of individual fluorophores making this quantification unfeasible as punctae are saturated under imaging conditions resolving individual fluorophores. Instead, we quantified the total fraction of molecules in punctae **(Fig. 3.1 c right)** as well as the heterogeneity in punctae intensity. Further, these punctae are used to justify the isotropic models used in SEC and DLS analysis as they visually appear as isotropic spots as opposed to fibers. As a control, the occurrence of punctae as well as differential sedimentation was quantified as a function of free Ca^{2+} concentration **(Fig. 3.1 d)**. Both punctae formation and the degree of sedimentation were variable with the free calcium concentration and could be fit to a one phase binding curve (K_D = 1.6 ± 0.3 μM punctae formation, K_D = 320 ± 260 nM differential fractionation). Both fall in the range of reported C2·Ca^{2+} equilibrium coefficients (1-3). This assay was further used to explore additional axis of this phenomenon including time and protein concentration. We observed that both punctae number and the relative intensity of punctae increases as a function of time, and that higher PKCα concentration accelerates the growth of punctae **(Fig. B.3)**. These results suggest a mode of growth in which two processes occur: nucleation of an oligomer from monomers as well as the joining of oligomers into larger oligomers. Such a process is more commonly referred to as polymerization or self-assembly than oligomerization. Because the polymerization is strictly dependent on calcium we will refer to this

phenomenon as self-assembly. Together these data support our conclusion that self-assembly of PKCα is reversible and specific to calcium binding.

Hetero-FRET in C1a SPASM C2 sensor

Hetero-FRET in the C1a – SPASM- C2 sensor is expected to be detected when C1a and C2 domains (both intra- or inter-molecular) are within ~1.6 of R_o (mCer-mCit R_o = 5.4 nm; 8.6 nm < 9 nm mean end-to-end distance of 10 nm linker (4)). We found that hetero-FRET in C1a-10nmSPASM-C2 reversibly increased in the presence of calcium. Further, the calcium induced increase in hetero-FRET is dependent on linker length where longer lengths have attenuated responses even when the total concentration of C1a and C2 domains in solution is held fixed. The degree of attenuation in both hetero-FRET and coverslip assays is positively correlated with helix length (Appendix 2. 6a; linear fit r^2 = 0.936). Accordingly, the increase in hetero-FRET is concentration dependent, suggesting it is affected by inter-molecular interactions (**Fig. B.5 b**). The concentration dependent change in hetero-FRET is fit well by a Hill binding model providing a half-maximal value of 61.1 ± 1.2 nM (best fit and standard error), which serves as our best estimate of the free in solution equilibrium dissociation constant however, this output is a convolution of both intra- and inter-molecular contributions to hetero-FRET and should be considered only a coarse estimate (Appendix 2. 6 c). An additional benefit of this hetero-FRET output from the sensor is the ability to monitor kinetics of both association and dissociation. What we found was the initial phases of kinetics were faster than the time resolution of our recording (0.5 Hz). Together this line of enquiry provides orthogonal confirmation of our major findings.

B.2 materials and methods:

DNA constructs: Many constructs used in this study with human PKCα were previously reported (5). The pBiex1 (Novagen) plasmid vector was used for Sf9 expression and pcDNA/FRT (Invitrogen) was used for CHO expression. All constructs contained a C-terminal FLAG tag and $(Gly\text{-}Ser\text{-}Gly)_2$ linkers were inserted between each fusion element. The C1a – C2 biosensors (with three length SPASM linkers) were sub-cloned with restriction enzymes into the SPASM backbone as previously described. The C1a domain is defined as aa 32 – 100, C1b as aa 101 – 151, C2 aa 158 -292. Site- directed mutagenesis were performed with Pfu-turbo (Agilent).

Sf9 protein expression and purification: Sf9 expression and purification was performed as previously described (5). Briefly, Sf9 cells in suspension were transiently transfected with desired DNA constructs using Escort IV transfection reagent (Sigma-Aldrich) and harvested 60 h later. Protein was batch purified with anti-FLAG M2 Affinity gel (Sigma-Aldrich), eluted with FLAG peptide, and buffer-exchanged using Zeba Spin Desalting columns (Pierce) into the working buffer (20 mM HEPES, 0.5 mM EGTA, 5 mM $MgCl_2$, 2 mM DTT, pH 7.5). Protein was further diluted into this working buffer plus 0.1 mg/ml BSA for all experiments unless otherwise described. Prior to each experiment, de-salted protein was centrifuged (2.8 x 10^5 rcf , 10 min, 4° C) and the concentration was quantified using either an absorbance at 280 nm and a extinction coefficient calculated using ProtParam (http://web.expasy.org/ProtParam) or using mCitrine fluorescence fit to a standard curve (FluoroMax-4, Horiba Scientific). Protein batches were made fresh and experiments performed within 72 hours of Sf9 cell harvesting.

Size-exclusion chromatography: A Superdex 200 10/300 GL Size-exclusion column (GE) on a FPLC (BioRad) was pre-equilibrated with 3 column volumes of HEPES buffer, 100 mM $NaCl_2$, 500 µM EGTA (EGTA) or + 800 µM $CaCl_2$ (calcium condition). PKCα-mCit or PKCα(D246N)-mCit (9.5 µM) was incubated with matched buffer condition for indicated time and 100 µL was injected and flowed through the column. Fractions were collected (200 µL) in a black clear bottom 96 well plate (Grenier) and scanned for mCit fluorescence (SpectraMax M5e). Chromatography and pre-incubation of protein were all performed at 4° C. The column was pre-calibrated using known protein standards (Bio-Rad) to analytically determine protein size. Select fractions were run on SDS-PAGE gel and scanned for mCit fluorescence (Typhoon imager), and either probed with PKCα antibody or stained with Coomassie brilliant blue to verify fractions corresponded with anticipated molecular weights.

Fluorescence coverslip assay additional: For the experiment in Appendix fig 2. 3 b the concentration of PKCα-mCit-FLAG was held constant at 50 nM while the concentration of PKCα-FLAG was adjusted. For experiments where mCer and mCit were monitored a dual view module (Photometrics; 505 nm beam splitter, D480/30 nm and 535/40nm) designed to monitor mCer and mCit emission was used, and two images were sequentially taken with mCer excitation (custom filter cube 436/20 nm excitation, 455 nm LP) followed by mCit excitation (GFP cube). Only the mCer excitation – mCer emission and mCit excitation – mCit emission

channels were analyzed. Visual inspection of mCer-mCit and mCit-mCer channels showed negligible bleed-through and cross-excitation.

Spot identifier: Coverslip assays were quantified with custom Matlab code. Briefly, a background slide was subtracted and the image was median filtered. Spots were identified based on local intensity ratios (center pixel intensity $I_{center} > 1.12\,\langle I\rangle_{local}$ where $\langle I\rangle_{local}$ is the mean intensity of surrounding 21 x 21 pixels; only one pixel / neighborhood). Spot intensities were quantified as the sum of pixels with greater than half maximum difference in intensity:

$$I_{spot} = \sum_{x=-10}^{10}\sum_{y=-10}^{10} I'_{xy}$$

$$I'_{xy} = \begin{cases} I_{xy} : I_{xy} > \dfrac{I_{center} + \langle I\rangle_{local}}{2} \\ 0 : Otherwise \end{cases}$$

Kinase activity: Kinase activity was assessed as previously described (5). ATP consumption was measured using the Kinase-Glo Max Luminescence assay kit (Promega) measured in a white, opaque 96 well plate (Nunc) on a SpectraMax M5e (Molecular Devices). Reactions occurred in individual wells with starting concentrations of 100 µM ATP, 100 µM myelin basic protein peptide (4-14; Genscript), 100 nM PKCα-mCit-FLAG, 300 µM free Ca^{2+}, and 30 µM of the indicated liposomes. Reactions were initiated with the addition of ATP, and were arrested with addition of the Kinase-Glo substrate after 4 min at room temperature.

Liposome preparation: Liposomes were prepared fresh from chloroform stocks (Avanti) and mol % were calculated using manufacturer provided concentrations and molecular weights. The chloroform was dried with nitrogen and incubation under vacuum for 1 h. The lipids were brought to a working concentration of 1.27 mM with addition of working buffer and were allowed to hydrate at 60° C for 1 h with intermittent suspension by pipetting. Liposomes were generated by 10 rounds of sonication (10 s on 50 s off). Data presented in Fig. 4 are representative of multiple batches of liposome preparations, but were all performed with the same batch of lipid. For the time-resolved anisotropy measurements instead of sonication, the

liposome mixture was extruded using a 100 nm nitrocellulose membrane (Millipore) according to manufacturer's protocol (Avanti).

Steady-state fluorescence anisotropy plate reader: A SpectraMax M5e (Molecular Devices) was used to record fluorescence anisotropy. The instrument was calibrated with FITC (1 µM pH 8.0; excitation 483 nm, emission 515 nm) in solutions of water and 0, 10, 30, 50, 70 and 90% glycerol in a black clear bottom 96 well plate (n = 12; Grenier). The high and low ends are in good agreement with anticipated anisotropy values (0.046 ± 0.025 and 0.392 ± 0.020) and no correction factor was used (G-factor = 1). These same standards were applied to the microscope where a G-factor was applied (see below). For protein experiments mCit (excitation 485 nm, emission 515 nm) was monitored, and buffer blanks were subtracted before anisotropy calculation. mCit containing protein starting concentration is 200 nM in a 50 µL volume unless otherwise stated, and for sequential addition of calcium and EGTA was performed by addition of concentrated stocks at 2.5% of volume. For each condition 4 – 8 wells were monitored in triplicate. All experiments were performed at room temperature (22.0 ± 0.5° C).

Steady-state anisotropy optical set-up: A TiE microscope equipped with perfect focus, an automated filter wheel containing a polarizing filter, a separate ND4 filter (excitation path; Nikon), an EVOLVE 512 x 512 EMCCD camera (Photometrics), a polarized beam-splitting Dual-View filter (Photometrics), a mercury arc lamp, and a yellow GFP filter cube (Nikon). A 40X DIC M/N2 0.75 NA objective combined with the 1.5X optovar (Nikon) was used for imaging cells. FITC calibration samples were placed on glass bottom tissue culture plates (MatTek Corp.) and imaged with polarized excitation and the dual view polarized beam splitter. As with the plate reader, the instrument was calibrated with FITC (1 µM pH 8.0; excitation 483 nm, emission 515 nm) in solutions of water and 0, 10, 30, 50, 70 and 90% glycerol. Qualitatively, the relative anisotropy values matched those obtained from the fluorimeter, but with systematically lower absolute values. A G-factor was applied such that the 0% glycerol sample had an anisotropy value of 0.00 (i.e., equal emission in both polarized channels)(6). This G-factor (0.773) was applied to all additional anisotropy analysis and no further correction factor was used.

B.3 Table:

	Fluorescence lifetime (ns) τ	Correlation time 1 (ns) ϕ_1	Fraction correlation time 1 χ_1	Correlation time 2 (ns) ϕ_2
mCit-PKCα (EGTA) TCSPC	3.43 [3.42 to 3.45]	--	--	32.6 [30.0 to 35.9]
mCit-PKCα (Ca^{2+}) TCSPC	3.43 [3.41 to 3.45]	--	--	36.0 [32.6 to 40.1]
PKCα-mCit (EGTA) TCSPC	3.44 [3.42 to 3.46]	0.753 [0.343 to 1.529]	0.070 [0.048 to 0.114]	30.5 [25.9 to 41.4]
PKCα-mCit (Ca^{2+}) TCSPC	3.45 [3.42 to 3.46]	0.753 [0.0 to 0.93]	0.065 [0.055 to 0.076]	32.1 [29.0 to 35.9]
PKCα-mCit + liposome (EGTA) TCSPC	3.46 [3.44 to 3.48]	--	--	31.2 [28.5 to 36.0]
PKCα-mCit + liposome (Ca^{2+}) TCSPC	3.28 [3.26 to 3.29]	0.761 [0.372 to 1.34]	0.182 [0.127 to 0.283]	12.1 [9.84 to 17.4]
PKCα-mCit (EGTA) DWR	3.41 [3.39 to 3.43]	0.431 [0.0 to 0.692]	0.088 [0.065 to 0.097]	40.8 [31.8 to 50.7]
PKCα-mCit (Ca^{2+}) DWR	3.41 [3.39 to 3.43]	0.349 [0.0 to 0.577]	0.093 [0.071 to 0.102]	41.5 [32.1 to 51.1]
PKCα-mCit + liposome(EGTA) DWR	3.42 [3.40 to 3.44]	0.540 [0.217 to 0.760]	0.094 [0.0711 to 0.109]	43.5 [34.0 to 53.6]
PKCα-mCit + liposome (EGTA + Ca^{2+}) DWR	3.30 [3.28 to 3.32]	0.554 [0.428 to 0.685]	0.230 [0.208 to 0.254]	30.9 [25.5 to 40.4]
PKCα-mCit + liposome (EGTA + Ca^{2+} + EGTA) DWR	3.34 [3.32 to 3.36]	0.525 [0.342 to 0.746]	0.152 [0.131 to 0.177]	40.8 [32.6 to 52.2]
C1a-SPASM-C2 (EGTA) DWR	3.30 [3.28 to 3.33]	0.356 [0.178 to 0.563]	0.150 [0.130 to 0.175]	61.2 [43.4 to 110]
C1a-SPASM-C2 (Ca^{2+}) DWR	3.18 [3.15 to 3.20]	0.225 [0.063 to 0.349]	0.236 [0.208 to 0.259]	129.7 [62.2 to >1000]

Table B.1: Values from TCSPC and DWR analysis. Fluorescence lifetime of the sample obtained at the magic angle was fit by a single exponential function. The lifetime value was constrained as the anisotropy profile was fit to a 2 exponential function where the two correlation time parameters and the fractional contribution of the faster correlation time were co-estimated. Initial and final anisotropies were constrained to 0.4 and 0 respectively. For the conditions with only one reported correlation time, only a single correlation time was resolved by the fit (i.e., the fraction of the faster component was zero). Steady-state anisotropy was calculated as the fluorescence weighted average of the anisotropy decay given by the best-fit parameters. Standard errors of the fit (67% confidence interval) are listed in brackets.

B.4 Figures:

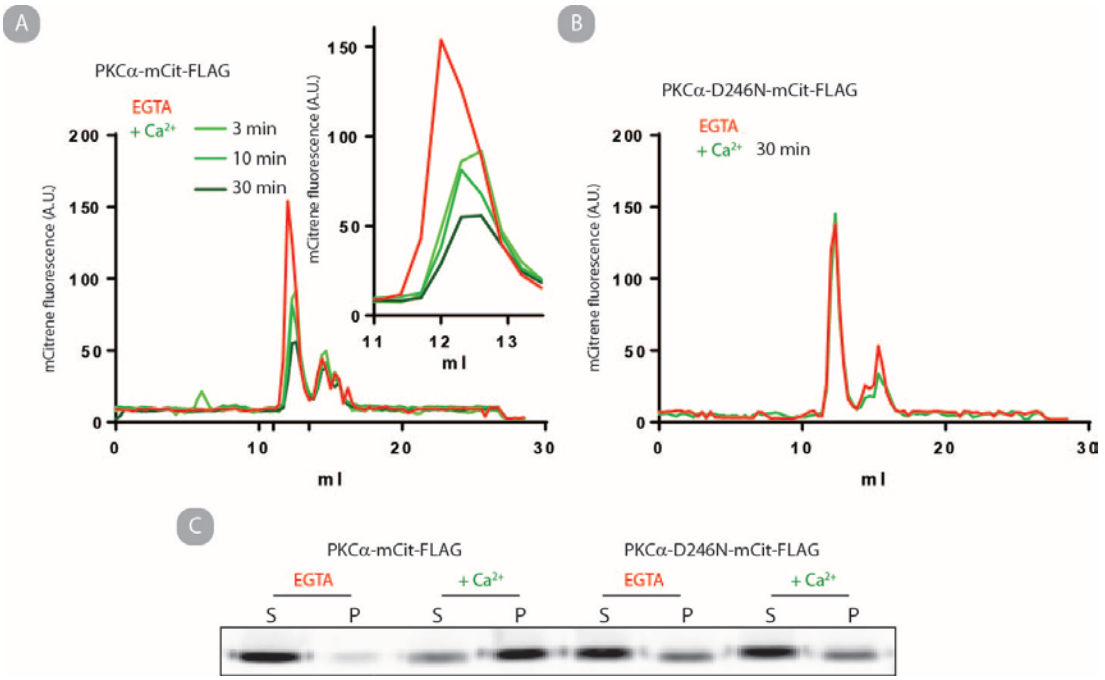

Figure B.1. D246N point mutation blocks calcium induced oligomerization of PKCα-mCit. Size exclusion chromatography elution profile of PKCα-mCit wild-type (**a**) or D246N (**b**) under indicated incubation conditions. (**c**) Differential fractionation of the same fusion proteins following a 30 min incubation with or without 300 μM free calcium. The soluble (S) and pelleted (P) fractions were run on an SDS-PAGE gel and imaged on a typhoon imager for mCit fluorescence.

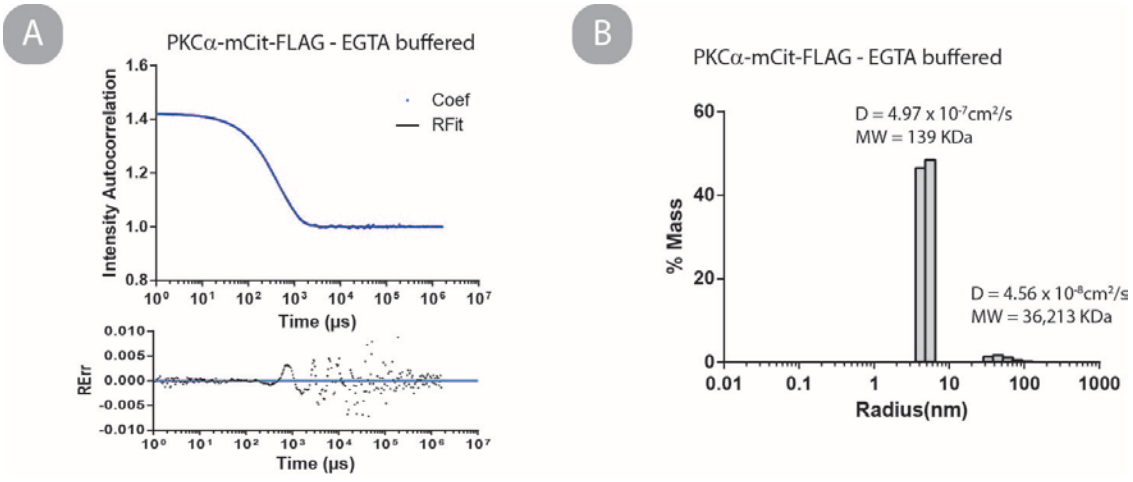

Figure B.2. Representative analysis of DLS data of PKCα-mCit in EGTA buffer. (**a**) The intensity autocorrelation data (blue dots) is fit by a regularization model (black line) with residuals in bottom panel. (**b**) An isotropic spheres model is applied to calculate the distribution of particle mass. This panel is representative of most experiments where two populations are observed, the predominant peak near the expected mass of particles, and a second peak of much larger particles that was not removed despite high-speed ultracentrifugation immediately prior to the measurement.

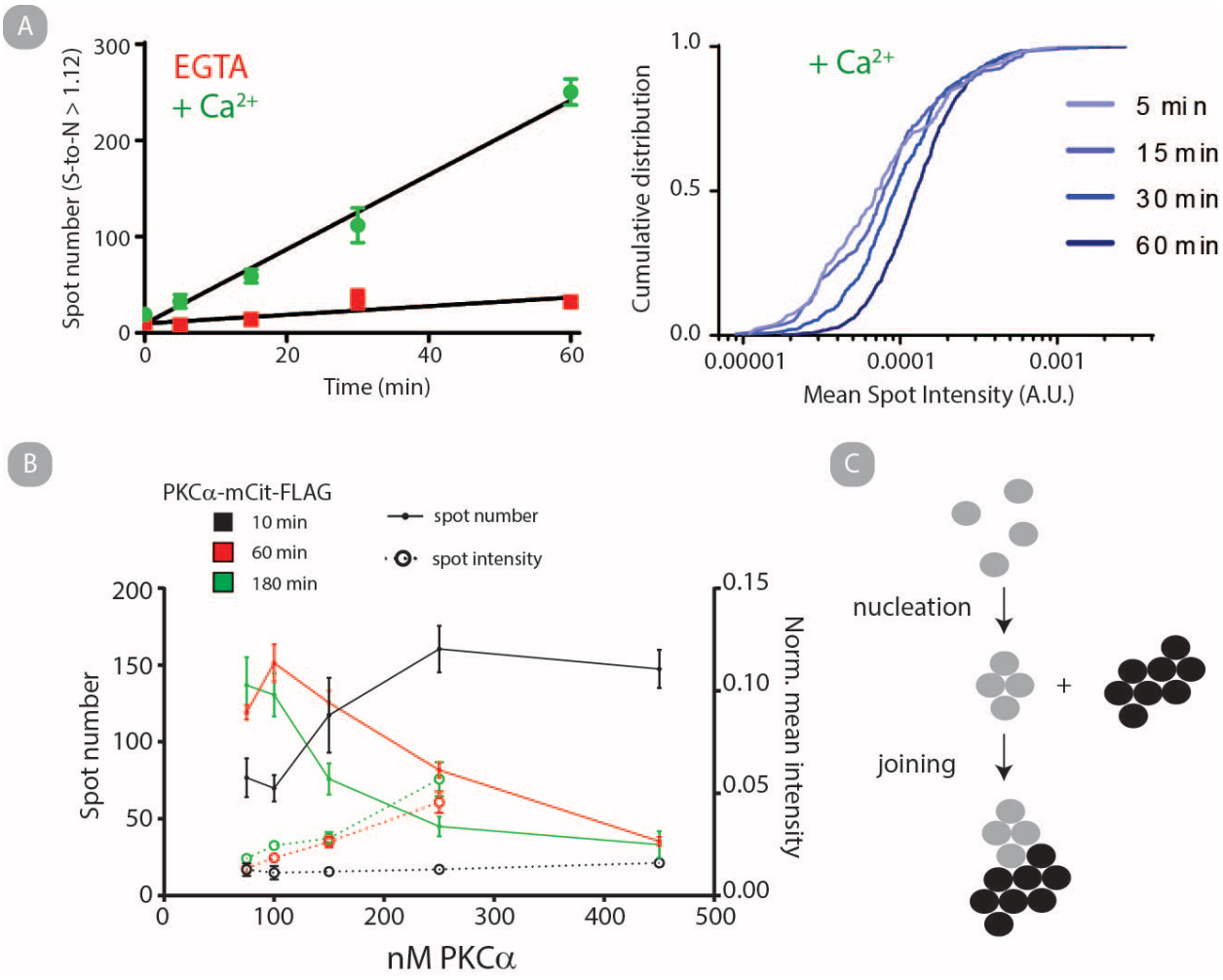

Figure B.3. Two step growth of PKC oligomers. (**a**) The number of identified spots on a coverslip of PKCα-mCit (100 nM) with and without free calcium was assessed at time points up to 60 minutes. The data are fit to a linear regression for visualization. The points represent mean and standard deviation of 4 images (left). A cumulative histogram of the mean intensity of each spot normalized to the total intensity of the image from the corresponding images (right). (**b**) The concentration of PKCα-mCit was held constant (50 nM) and unlabeled PKCα (0, 50, 100, 200, 400 nM) was added such that the concentration of PKCα (represented on the x-axis) is the sum of the two species. The mean spot number and the mean intensity with standard deviation (6 images) of all the spots are plotted at 3 time points after the addition of free calcium. The mean intensity of the 450 nM PKCα condition at the 60 and 180 minute time points are not reported due to saturation of spots in the imaging conditions. (**c**) A schematic depicting the two processes in PKC self-assembly observed. The initial increase in spot number is the result of nucleation events. The subsequent decrease in spot number as well as the increase in mean particles size is the result of smaller oligomers joining into larger oligomers.

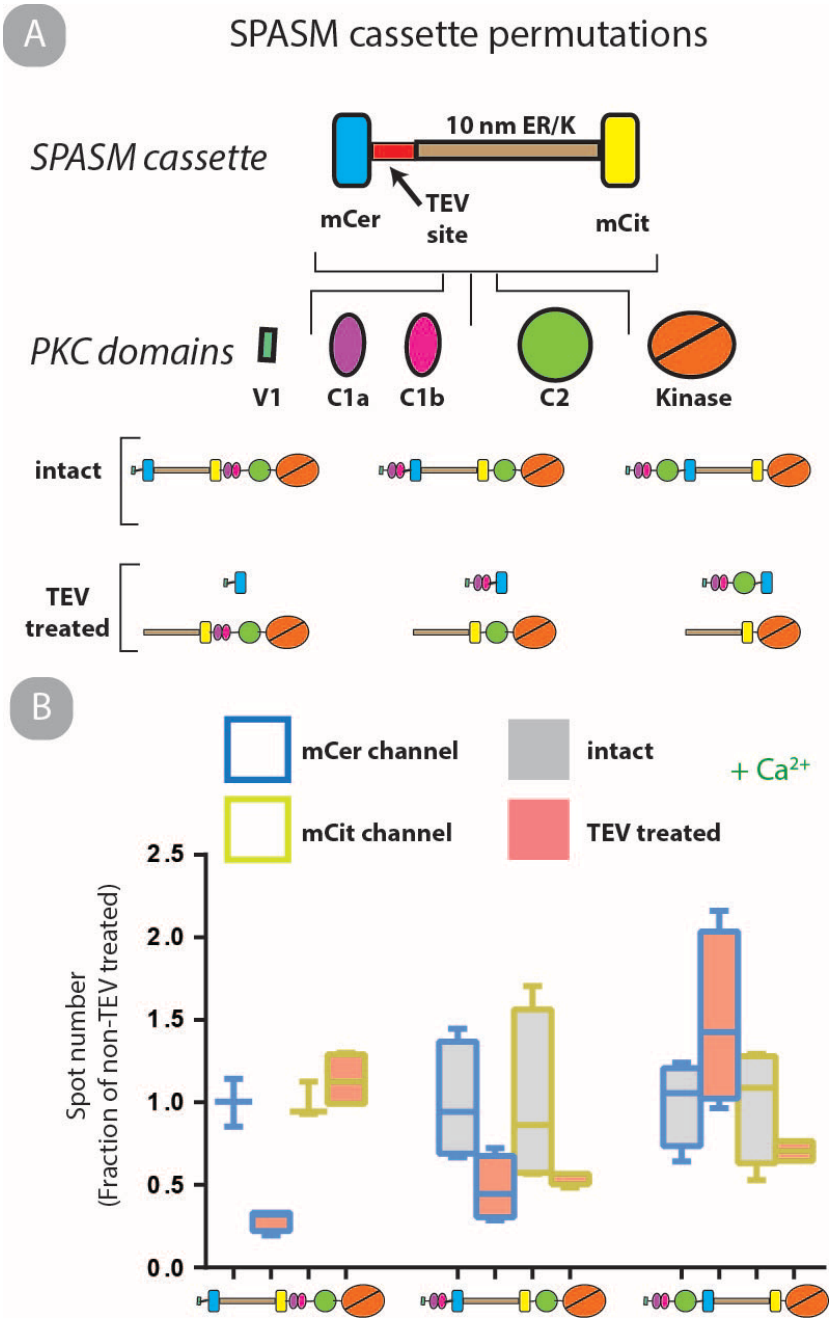

Figure B.4. Separating the C1 and C2 domains eliminates calcium clustering on coverslip. (**a**) A schematic shows the modular strategy by which we previously created 3 PKCα biosensors. All three biosensors specifically clustered in the presence of calcium. (**b**) We then used TEV protease to site specifically generate two peptide fragments, the N-terminus always containing the mCer, and the C-terminus the mCit fluorophore. We then took two images of each sample using a dual view emission splitter optimized for mCer and mCit, with two excitations optimized for mCer and mCit. In total 4 images of each field of view were obtained (mCer excitation: mCer emission; mCer excitation: mCit emission; mCit excitation: mCer emission; mCit excitation: mCit emission) of which we only analyzed the mCer excitation: mCer emission, and mCit excitation: mCit emission images which had negligible cross excitation and bleed through for the purposes of our spot identifier program. The spot numbers for both channels are depicted normalized to the mean number of spots in the corresponding non-TEV treated sample (4 images in each channel/ condition).

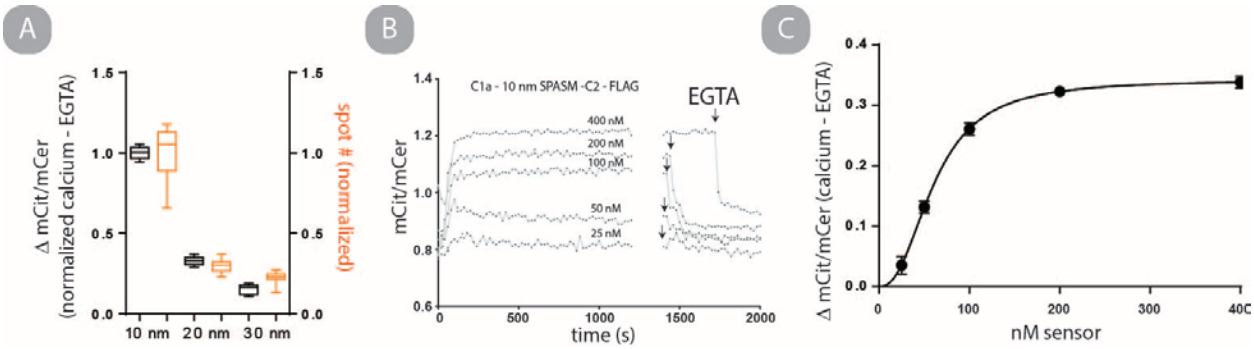

Figure B.5. Hetero-FRET of C1a – SPASM- C2 biosensors report on self-assembly. (**a**) The relative increase in hetero-FRET and the relative number of spots identified for the 10, 20 and 30 nm linker biosensors (as in Fig. 2 c) are plotted for side-by-side comparison. (**b**) Hetero-FRET provides a qualitative description of assembly and disassembly kinetics. (**c**) The change in mCit/mCer fluorescence ratio as a function of protein concentration is well described by a Hill binding function (black line) with a hill coefficient of 2.39 ± 0.09 and a half-maximum concentration of 61.1 ± 1.2 nM (best fit and standard error).

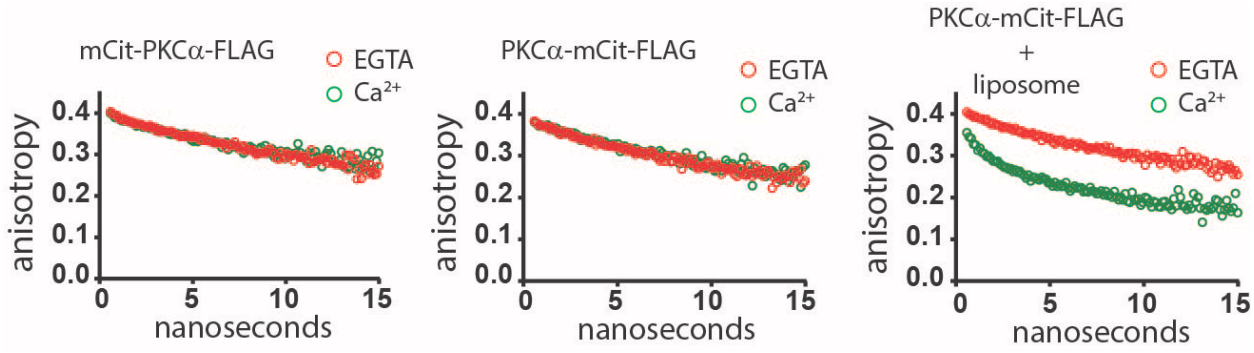

Figure B.6. Homo-FRET of full length PKCα only observed with liposomes and free calcium. Shown is representative TC-SPC data. Each condition has matched protein concentration (500 nM) incubation time (2 min) and buffering conditions. In each case the EGTA condition was obtained and free calcium was spiked into solution for the subsequent measurement, the right panel is the same as in Fig. 3 a, shown again here for comparison. Analysis of data is found in table B.1.

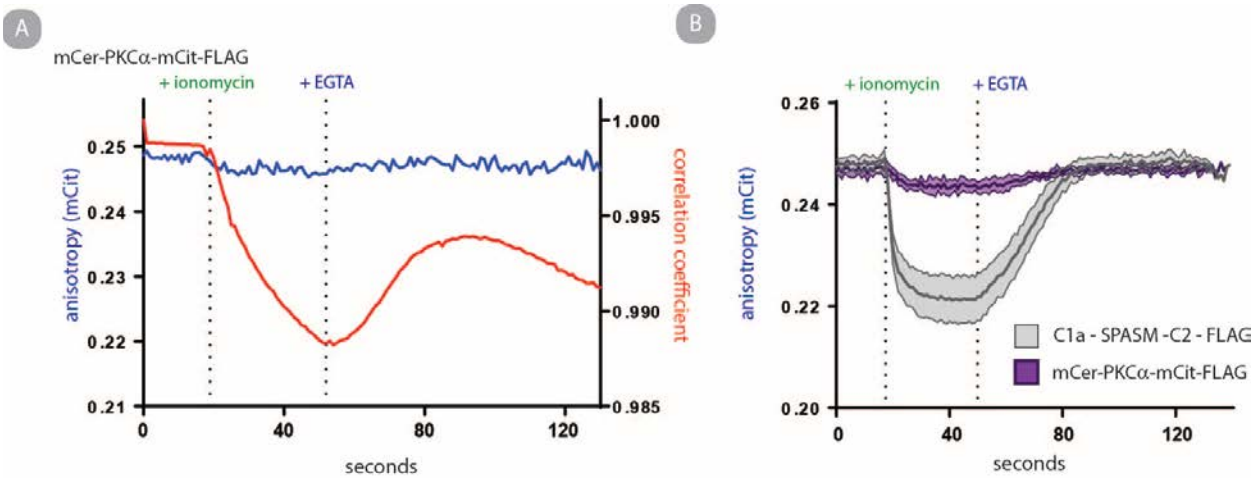

Figure B.7. CHO cell steady-state anisotropy: comparing mCer-PKCα-mCit and C1a-SPASM-C2 following ionomycin treatment. (**a**) Corresponding experiment to Fig. 3 b except in a cell transiently transfected with mCer-PKCα-mCit. Here is representative data translocation {correlation coefficient) and steady-state anisotropy. (**b**) The mean and s.e.m. of steady-state anisotropy of 3 independent experiments (1 cell each).

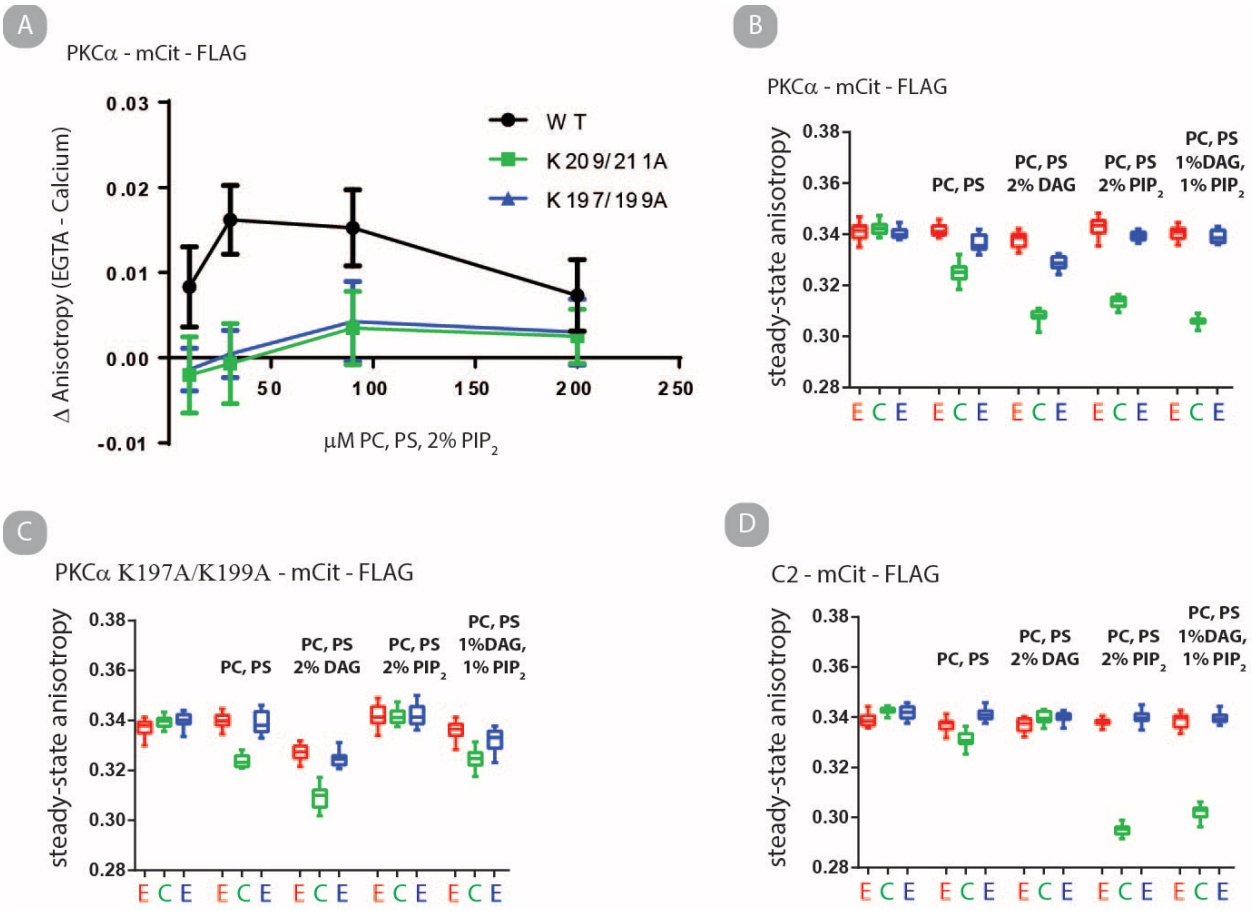

Figure B.8. PKCα clusters through two independent mechanisms, one PKC driven and one PI(4,5)P_2 driven. (**a**) To assess the relative lipid:protein concentration to use in these experiments we started with liposomes containing PI(4,5)P_2. We anticipate PI(4,5)P_2 clustering in the presence of calcium to serve as a positive control for PKCα-mCit homo-FRET, and that controls with disrupted PI(4,5)P_2 binding pockets (7)should have modest homo-FRET under identical condition. We chose a condition where liposome concentration was not limiting, or artificially crowding, but also not so dilute that interactions would be limited. We chose the condition where an 80:1 molar ratio of PS:PKCα where PS is 10% molar composition of liposome is maintained for the subsequent experiments. Under the given experimental conditions we anticipate all PKCα to be bound to the liposome. We subsequently monitored the sequential steady-state anisotropy of PKCα-mCit (**b**) PKCα K197A/K199A-mCit (**c**) and C2-mCit (**d**) under the indicated conditions.

B.5 References:

1. Medkova M & Cho W (1998) Mutagenesis of the C2 domain of protein kinase C-alpha. Differential roles of Ca2+ ligands and membrane binding residues. *J Biol Chem* 273(28):17544-17552.
2. Kohout SC, Corbalan-Garcia S, Torrecillas A, Gomez-Fernandez JC, & Falke JJ (2002) C2 domains of protein kinase C isoforms alpha, beta, and gamma: activation parameters and calcium stoichiometries of the membrane-bound state. *Biochemistry* 41(38):11411-11424.
3. Sanchez-Bautista S, Marin-Vicente C, Gomez-Fernandez JC, & Corbalan-Garcia S (2006) The C2 domain of PKCalpha is a Ca2+ -dependent PtdIns(4,5)P2 sensing domain: a new insight into an old pathway. *J Mol Biol* 362(5):901-914.
4. Sivaramakrishnan S & Spudich JA (2011) Systematic control of protein interaction using a modular ER/K alpha-helix linker. *Proc Natl Acad Sci U S A* 108(51):20467-20472.

5. Swanson CJ*, et al.* (2014) Conserved modular domains team up to latch-open active protein kinase Calpha. *J Biol Chem* 289(25):17812-17829.
6. Ghosh S, Saha S, Goswami D, Bilgrami S, & Mayor S (2012) Dynamic imaging of homo-FRET in live cells by fluorescence anisotropy microscopy. *Methods Enzymol* 505:291-327.
7. Evans JH, Murray D, Leslie CC, & Falke JJ (2006) Specific translocation of protein kinase Calpha to the plasma membrane requires both Ca2+ and PIP2 recognition by its C2 domain. *Molecular biology of the cell* 17(1):56-66.